2014

Numerical Experiments of Hurricane Impact on Vertical Mixing and De-Stratification of the Louisiana Shelf Waters

Mohammadnabi Allahdadi
Louisiana State University and Agricultural and Mechanical College

NUMERICAL EXPERIMENTS OF HURRICANE IMPACT ON VERTICAL MIXING AND DE-STRATIFICATION OF THE LOUISIANA SHELF WATERS

A Dissertation

Submitted to the Graduate Faculty of the
Louisiana State University and
Agricultural and Mechanical College
in partial fulfillment of the
requirements for the degree of
Doctor of Philosophy

in

The Department of Oceanography and Coastal Sciences

by
Mohammadnabi Allahdadi
B.S., Shiraz University, 1998
M.S., University of Tehran, 2001
May 2015

ACKNOWLEDGEMENTS

This dissertation would have been incomplete without the dedicated help from numerous people as listed below:

First, I would like to express my sincere gratitude to my adviser Dr. Chunyan Li, for his financial support during my studies and his great impact on my study in Oceanography through both courses and group meetings. I'm so much grateful for his patience and scientific comments that highly improved my dissertation.

I am also grateful to the other committee members, Drs. Nan Walker, Barry Keim, Nancy Rabalais and Laura Ikuma, for suggestions which improved this dissertation substantially.

I would like to thank Dr. Changsheng Chen (University of Massachusetts-Dartmouth) for his kindness in sharing the FVCOM code.

I would like to acknowledge the former WAVCIS colleagues Dr. Seyed Mostafa Siadat Mousavi and Dr. Felix Jose and the former CSI Ph.D. student Dr. Clint Edrington for their kind suggestions and help during and after their presence at LSU. Also, I always appreciate and remember the great help and kindness of my former advisor, Dr. Gregory W. Stone (late).

Lastly, the seemingly endless patience and support of my wife must also be recognized.

TABLE OF CONTENTS

ABSTRACT

The numerical model FVCOM (Finite Volume Community Ocean Model) was applied to study the effects of Hurricane Katrina on the vertical mixing over the Louisiana shelf and the process of post-storm re-stratification. Wind field from Hurricane Katrina was generated using a single vortex analytical model and was evaluated using available wind measurements over the shelf. Simulations of shelf circulation under Hurricane Katrina were done through several numerical tests to find the best approach for treating vertical eddy viscosity. Model results for the shelf during Katrina demonstrated opposite currents between surface and bottom for most of the shelf area. Results also show current intensification between the eye and the Birds-foot delta, where current speed reached ~ 3.5 m/s at one time.

Shelf-wide mixing and re-stratification during and after Katrina were studied by examining the salt and heat transports. Climatological salinity and temperature profiles for August from NOAA were used as the initial conditions. Model performance in simulating water temperature was evaluated using the cloud transparent microwave band SST data (OI-MW) along the shelf break. Model was also evaluated for the mixed layer depth (MLD) calculated from model results which were compared with that from the OI-MW SST data and a theoretical model.

During Katrina, the SST decreased up to 1C for areas outside of the 1-1.5 Radius of maximum wind (RMW), while inside the RMW and west of the Birds-foot delta 2-3.5 C. Consequently, the mixed layer depth (MLD) left of the 1-1.5 RMW region was smaller than 10 meter. Inside this region the MLD was up to 40 meters. By inspecting the mixing and re-stratification pattern using the model outputs, conceptual models for water column mixing during the hurricane and re-stratification were proposed. It was concluded that the complete recovery of the water column temperature was not achieved even after 14 days following the landfall and it is likely that the effect of solar radiation may qualitatively change the conclusion. Hence, the effect of solar insolation on the shelf heating was simulated separately for non-hurricane summertime conditions. This simulation demonstrated the significant effect of solar insolation on the shelf heating and stratification of the water column.

CHAPTER 1: INTRODUCTION AND BACKGROUND INFORMATION

1.1 Introduction

Water column stratification is common in oceanic, shelf, and estuarine waters. Stratification modulates bio-geochemical processes across the water column and affects concentration of different chemicals (Katsev et al., 2010, Chaichitehrani at al., 2013, Chaichitehrani et al., 2014). The stratification can be destroyed by mixing, which can be caused by winds, waves, and tides. Water column stratification occurs when mixing declines and buoyancy input on the surface increases (usually as a result of increasing river discharge or precipitation or surface heating in summer). The stratified water column prevents oxygen from penetrating through the water and the stratification acts as a barrier of vertical exchange in the bottom layer (Wiseman et al., 1997) (Figure1.1), which can have biological and ecological consequences such as hypoxia.

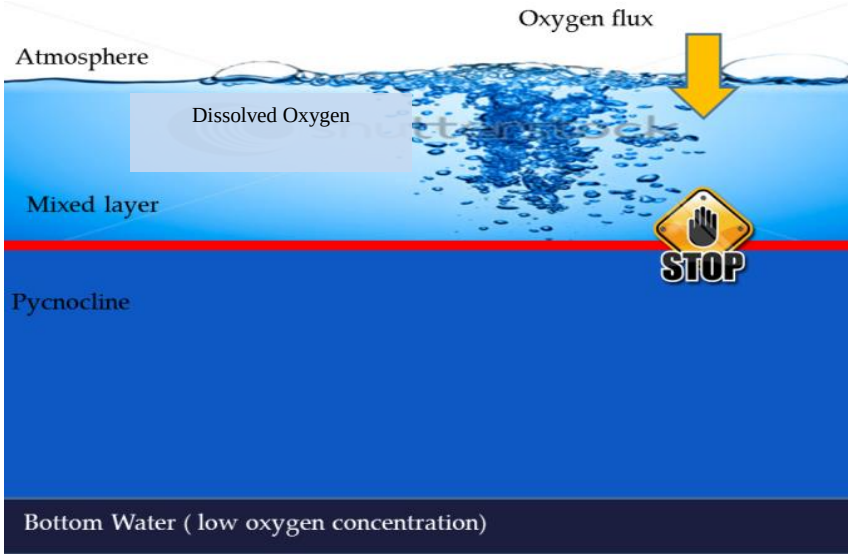

Figure 1.1: Schematic of water column stratification and corresponding dissolved oxygen.

1.2 Background and Literature Review

Oceanic, shelf and coastal waters are affected by stratification and mixing due to buoyancy input and turbulence forces. Turbulence results from wind, waves, and ambient currents. The Richardson number is often used for the examination of turbulence formation (Lyons et al., 1964):

$$R_i = \frac{N^2}{\left(\frac{\partial u}{\partial z}\right)^2 + \left(\frac{\partial v}{\partial z}\right)^2}, \quad N^2 = \frac{g}{\rho}\frac{\partial \rho}{\partial z} \tag{1.1}$$

where R_i is the Richardson number, N the Brunt-Vaisala or buoyancy frequency (in s^{-1}), ρ the density of water, and g acceleration due to gravity. Small Richardson number values correspond to large velocity shear across the water column, under which condition, turbulence forces may overwhelm stratification. Increasing the value of the Richardson number above a threshold (0.2–0.25) suppresses turbulence. Large buoyancy shown by a large vertical density gradient gives a large R_i: when it is greater than 1, it means a stable stratification (Lyons, et al., 1964; Turner, 1973; Galperin et al., 2007). As mentioned above, velocity shear and turbulence can be produced by winds, waves, and currents. However, wind is considered the main mixing force over many oceanic and shelf waters (Goodrich, 1987), especially in the absence of strong tidal mixing (Goodrich et al., 1987).

The effect of wind on mixing in coastal and shelf waters has been studied for several decades. Voorhis et al. (1976) measured horizontal and vertical variations of current speed as well as temperature and salinity across water column in New England shelf waters to determine the mechanisms contributing to the vertical mixing. They found that the water layers were affected by shear force on a time scale of 1-3 days for temperature and salinity variations. Based on observations at two stations west of the Florida continental shelf, Price et al. (1978) studied the deepening of mixed layer during storms. The main finding was that velocity shear contributes to the deepening of the mixed layer, not the wind friction velocity (U_*) as previously believed. In the northeastern Pacific, upper-ocean response (including currents and mixing processes) to atmospheric forcing was observed at two mooring sites during the mixed layer experiment (MILE) in 1977 (Davis et al., 1981). The one-dimensional heat budget and wind variabilities were examined and a qualitative agreement was found between low-frequency wind and upper ocean transport. Washburn and Gibson (1984) studied the horizontal temperature microstructures in the base of the mixed layer using MILE observations. They found an intermittent behavior of temperature seasonal variability with a horizontal scale of 10 meters.

The combined effect of wind, solar heating and tidal currents on mixing and thermocline dynamics in the North Sea was studied by Haren (2000). Mooring data in a point with total water depth of 45 meters were analyzed assuming harmonic-exponential functions for horizontal oscillatory currents. He showed that the inertial shear was the dominant forcing within the mixed layer after the strong winds and also during calm weather when a thick mixed layer existed. Another study by Rippeth (2005) discussed the mixing processes in seasonally stratified regions of the north western European shelf seas. It was found that shear instability and internal wave breaking were the main contributors in thermocline mixing.

Wind induced mixing has also been studied for many marginal seas, inland waters and estuarine-river systems. In Chesapeake Bay, for instance, several studies addressed mixing processes, especially those related to wind-induced mixing. Goodrich et al. (1987) studied wind-induced de-stratification using weather data and oceanographic data from hydrographic surveys and moored current meters, and salinity and temperature sensors. The observations indicated that frequent wind-induced de-stratification occurred between fall and mid-spring. The events started

near the autumnal equinox, breaking down the strong summertime stratification. The effect of surface cooling was found important but secondary in water column mixing. Horizontal velocity shear was confirmed as the main mixing mechanism, which is in agreement with Price et al. (1978). Analysis of 30 month mooring and transect data of salinity in Mobile bay along with hourly wind data recorded at Dauphin Island and river discharges to the Bay demonstrated the effect of wind in de-stratifying the water column in this shallow bay (Schroeder et al., 1990).

Simpson and Rippeth (1993) investigated wind and thermal induced mixing in the Clyde Sea, a deep partially enclosed sea in the west of Scotland by analyzing available mooring data in the deep water in November 1990. The water column was completely mixed for water depths as large as 100 meters as a result of surface cooling and wind stirring. Current velocities resulted from an ADCP measurement before and after breaking down the stratification demonstrated the modification effect of vertical mixing on circulation. Inspection of historical data showed that the buoyancy driven stratification is produced by both riverine freshwater discharge and surface heating.

Study of mixing and stratification in Lake Erie was implemented by analyzing current and temperature data from instruments installed at four different stations in the west of the lake for two months (Loewen et al., 2007). Their study demonstrated the effects of surface cooling and wind forcing in mixing the water column, In this regard, when wind speeds were greater than 7 m/s and air was colder than the water, a well-mixed condition resulted in the water column.

Analytical and numerical models have been developed and applied throughout the years. Analytical models can provide simplified but useful solutions while the sophisticated 3-dimensional numerical models deal with more complexities and realistic conditions. One of the earliest models for simulation of ocean mixing was the model suggested by Munk and Anderson (1948).

A similar model including an analytical solution of one-dimensional unsteady equations of motion were proposed by Mellor and Durbin (1975) with some modification in Richardson number-dependent stability functions. Compared to Munk and Anderson (1948), they combined different elements including more realistic turbulence and heat flux as well as Richardson number criteria. Figure 1.2 shows an example of mixed layer time evolution from this model. An analytical model given by Roisin (1981) was based on a two layer fluid system. The model was one-dimensional, frictionless and thus neglected the turbulence produced internally by mean flow shear in the thermocline.

The energy required for the mixed layer deepening was provided by surface turbulence (including wind energy) penetrating down the water column; hence it is a type of turbulent erosion model. An analytical solution was found assuming a well-mixed layer overlaying a sharp thermocline. The model is valid only for the mixing events during which the gradient Richardson number is much higher than unity. A schematic of the proposed model is shown in Figure 1.2. Analytical models were very useful in developing the understanding the mixing mechanisms and

contributing factors. However, the assumptions and simplifications often used for analytic models about the dimensions, geometry, Richardson number range and turbulence limited their applications to only some specific cases. The numerical models offered more advantages in studying mixing related phenomena. There are a number of studies conducted by applying 2-D laterally averaged models (e.g., Blumberg, 1977; Hamilton, 1975). These models provided insights about the circulation and mixing especially for estuaries and lakes. However, in the case of significant lateral variations, the method is problematic. A popular 2-D Model for simulation of hydrodynamics, mixing and water quality in lakes and estuaries is CE-QUAL-W2. Recently this model was applied to wind-induced mixing and oxygen dynamics in Lake Erie (Boegman et al., 2008).

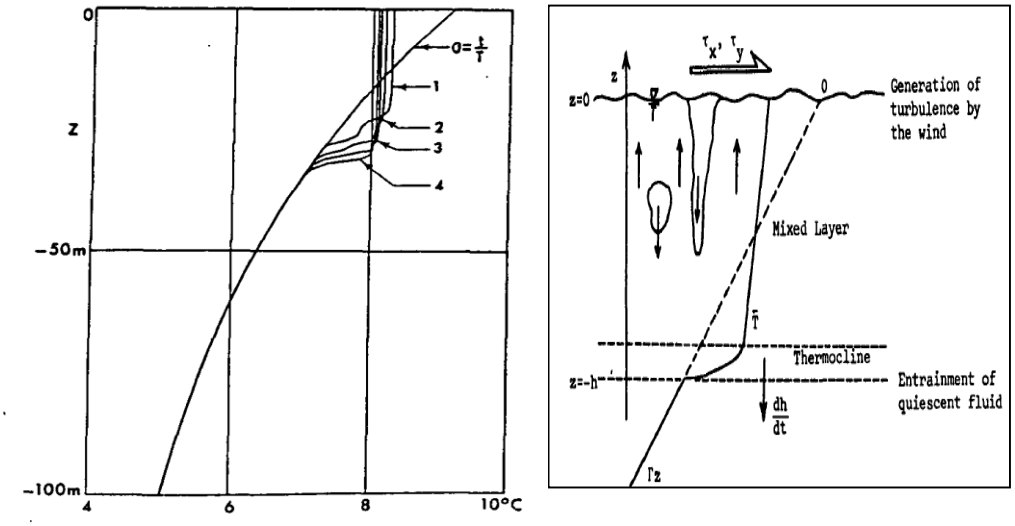

Figure 1. 2: Left) time evolution of mixed layer for a test case resulted from Mellor and Durbin (1975), Right) A schematic of the proposed model proposed by Roisin (1981).

3-D simulation of hydrodynamics and mixing would be ideal for the study of wind-induced mixing. The modeling study of Blumberg and Goodrich (1990) of wind-induced mixing in Chesapeake Bay was one of the pioneer applications of a 3-D model with enhanced vertical turbulence parameterization. The model was developed by Blumberg and Mellor (1983) assuming hydrostatic pressure with the Boussinesq approximation. The horizontal momentum and salt diffusivities were assumed $10 m^2/s$ based on some prognostic simulations, while a value of $0.0001\ m^2/s$ was obtained for vertical eddy diffusivity based on a calibration process. Model results were validated with field measurements of currents, temperature, and salinity from 1983. Model results were consistent with the field data (Goodrich et al., 1987) and the dominant effect of horizontal velocity shear forces on deepening the mixed layer was concluded. Figure 1.3 shows the modeling area and the computational grid for this study. A more recent modeling study for Chesapeake Bay was implemented by Li et al. (2007) aiming at studying hurricane-induced de-stratification. The Regional Ocean Modeling System (ROMS) coupled with a nested-

grid (4/12/36 km) version of the MM5 based on a regional atmospheric model for the Middle Atlantic Region was applied for simulation of de-stratification and the preceding re-stratification induced by Hurricane Isabel in the Bay (Figure 1.3).

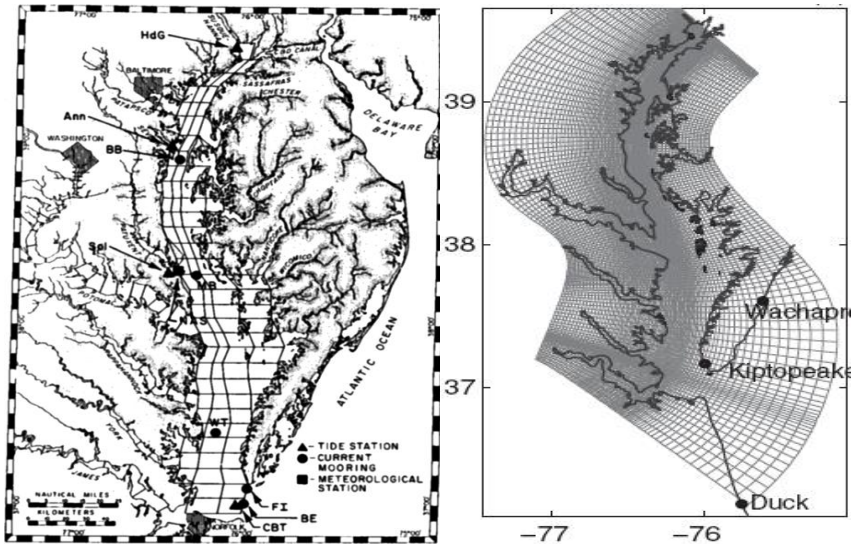

Figure 1.3: Left) Computational mesh over the Chesapeake Bay used by Blumberg and Goodrich (1990), Right) Computational grid used by Li et al. (2007).

In the northern Gulf of Mexico, cold fronts are the main atmospheric force for breaking down the summertime stratification (Wiseman et al., 1997). However, hurricanes cande-stratify the water column and increase the oxygen concentration in theatercolumn (Li et al., 2007). Wind, waves, and currents during hurricanes can deepen the mixed layer.

The effect of hurricanes on the mixed layer has been the focus of many studies. Jacob et al. (2000) studied the response of the mixed layer to Hurricane Gilbert in the western Gulf of Mexico. They used AXBT and AXCP temperature measurements to quantify heat, mass, and mixed layer processes before, during, and after hurricane passage. This study showed that after the passage of the storm, for up to three days, the main contributor to the mixed layer dynamics was the near-inertial oscillation induced by the hurricane. Korty et al. (2007) applied the MIT ocean circulation model coupled with a zonal atmospheric model to study the effect of the mixed layer on the climate under the influence of tropical storms. Results were significantly different from former studies that considered a uniform mixed layer. Mayer (1981) summarized the mixed layer response to hurricanes. He pointed out that there are three different mechanisms causing turbulent mixing by atmospheric forcing: 1) shear induced by wind at the water surface; 2) shear produced at the base of the mixed layer as a result of near-inertial oscillation; and 3) motion induced by convection of heat and salt. Storm-induced shear currents dominate during the hurricane passage, while the inertial motions come to effect after hurricane's passage.

There are some modeling studies addressing wind induced mixing over the Louisiana shelf. The modeling study implemented by Wang and Justic (2009) is one of the most relevant studies. They used the Finite Volume Community Ocean Model (FVCOM) to simulate the shelf hydrodynamics resolving the temperature and salinity distributions that affect seasonal hypoxia. The modeling area comprised of coastal and shelf waters from the west of the Mobile Bay to the east of Galveston-Texas. They used currents and water levels at two WAVCIS (Wave-Current-Surge Information System) stations to validate the hydrodynamics model. Simulated salinity and temperature were also compared with CTD data along two transects over the shelf area (Figure 1.4). Buoyancy frequency and Richardson number were used as criteria for detecting the strength of stratification and mixing. The study demonstrated the effect of cold fronts in breaking down the persistent summertime stratification over the Louisiana shelf.

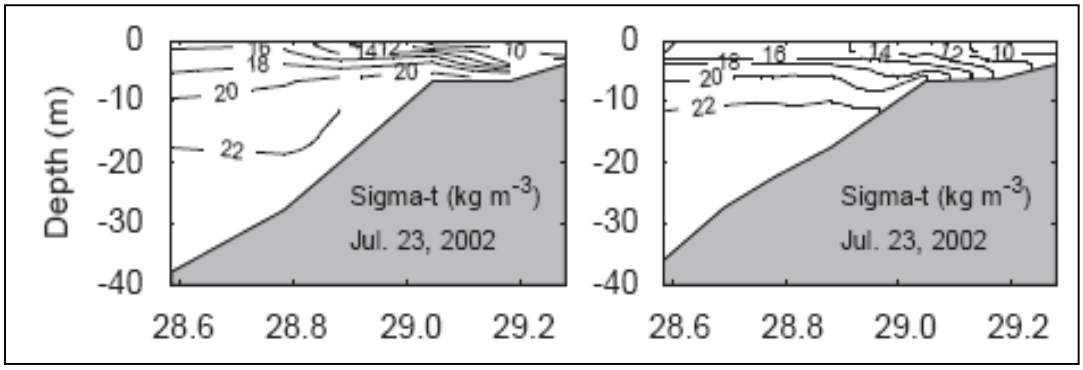

Figure 1.4: A sample of comparison between, Left) observed, and Right) simulated cross-shelf distributions of salinity (psu) along a transect off-Atchafalaya Bay (Wang and Justic, 2009).

Most recently, Hetland and DiMarco (2012) conducted an integrated modeling study of temperature and salinity and thereby stratification (Figure 1.5). The study didn't address the details about the mixing processes induced by wind events and preceding stratification. The main focus of the study was skill assessment of simulated transport quantities. They applied the ROMS model over a modeling area similar to that of Wang and Justic but from 1992 to 1994 covering the time period of the Louisiana–Texas Shelf Circulation and Transport Processes Study. The results were included in reports, regulations, and books addressing mixing and hypoxia over the LATEX shelf (for example EPA-SAB-08-003, 2007). Although they have mentioned Mellor-Yamada level 2.5 as the approach for resolving vertical eddy viscosity, the value of background eddy viscosity for which simulated temperature and salinity were validated was not presented.

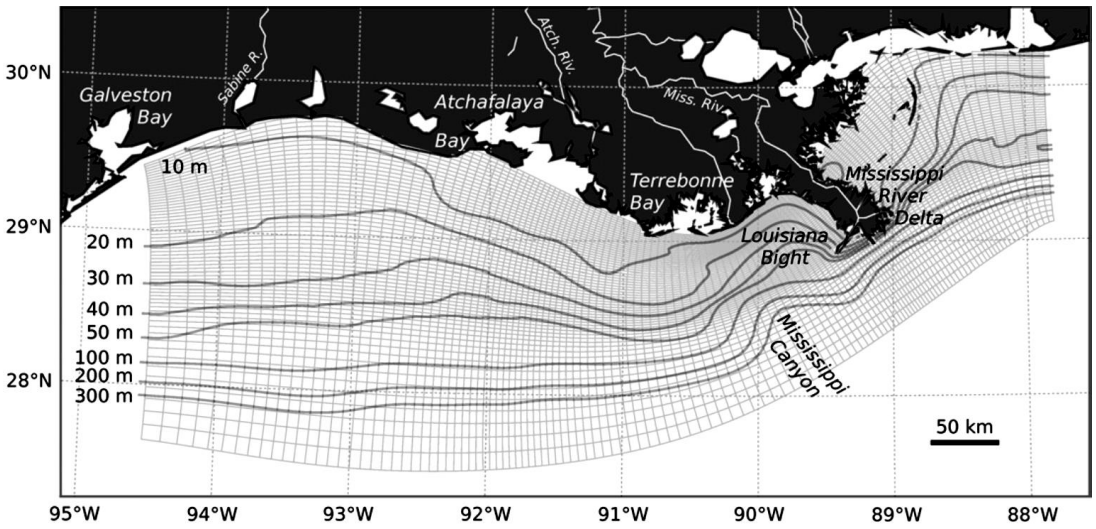

Figure 1.5: Modeling area and computational grid for modeling study of Hetland and DiMarco (2012).

Hetland and DiMarco (2012) showed a significant effect of vertical eddy diffusivity on circulation. They pointed out that it is not possible to get high skills for temperature/salinity and current velocity at the same time. Hence, the high skill presented in the paper for simulation of temperature and salinity led to a poor skill for circulation. The effect of vertical eddy viscosity on circulation has been reported by other researchers including Blumberg and Goodrich (1987) and Zhang and Steele (2007).

1.3 Objectives

In view of the above literature review of studies on wind-induced mixing, especially for the northern Gulf of Mexico (GoM), more studies need to be done. The present study addresses the questions in the GoM region as follows:

1) The nature and mechanism of wind-induced de-stratification.
2) High resolution water temperature variations during a hurricane.
3) Re-stratification mechanisms and characteristics after hurricanes.
4) Mixed layer depth calculations for different times during and after a hurricane.
5) Background mixing coefficient for model simulation.

1.4 Approach

In view of the objectives described above, the following approach is used:

Numerical Simulation: Due to the lack of data, especially during hurricane conditions, not all intended scenarios for wind induced mixing can be examined with observations. Hence, using a skill assessed numerical model, hypotheses can be examined. For this study the state of the art model FVCOM is used.

Field data analysis: Although field data analysis is not the main focus of this study, field data are required for developing the simulation scenarios as well as to skill assess simulated circulation and temperature/salinity fields.

1.5 Organization of Dissertation

This dissertation contains 6 chapters:

Chapter 1 includes an introduction and motivations for this research, a literature review and the objectives of this study.

Chapter 2 addresses seasonal characteristics of stratification and mixing over the Louisiana shelf using field measurements of currents.

Chapter 3 discusses the implementation of hydrodynamics model using FVCOM including model verification for different scenarios and simulation of the hydrodynamics under Hurricane Katrina over the Louisiana shelf.

In Chapter 4, Katrina-induced mixing and temperature responses of the Louisiana shelf is discussed. These responses were studied using various model outputs including maps of sea surface temperature (SST), time series of temperature across the water column and along longitudinal and latitudinal transects.

Chapter 5 presents results of simulation for stratification produced by summertime solar insolation (non-hurricane time).

Chapter 6 summarizes all results presented in the previous chapters and presents suggestions for future studies.

CHAPTER 2: INVESTIGATION OF SEASONAL MIXING ALONG THE LOUISIANA COAST USING HYDRODYNAMICS DATA[1]

2.1 Introduction

Although the ultimate goal of this dissertation is to determine hurricane induced mixing over the Louisiana shelf, an understanding of the "normal" seasonal mixing and stratification is needed for the background or pre-storm conditions. This is needed for a proper interpretation of model results in view of the fair weather conditions.

Mixing produced by velocity shear plays an important role on bio-geochemical processes over the Louisiana shelf (Wiseman et al., 1997; Belabbasi, 2006). Hence it is imperative to study hydrodynamics of seasonal currents in relation to the seasonal mixing. Wiseman et al. (2004) studied the flow characteristics west of the Birds-foot delta, using data from an acoustic Doppler current profiler (ADCP) for March–November 2002. The data revealed a weak vertical shear of horizontal velocity for the majority of this time period. Simultaneous measurements of density demonstrated the effect of shear on water column mixing (Wiseman et al., 2004).

This chapter addresses the seasonal mixing and stratification of the Louisiana shelf based on field data of currents and winds. The objective of this study is to determine seasonal flow structure and its spatiotemporal variability for the east and west of the Birds-foot delta, around the deltaic morphological feature along the Louisiana coast. The time series of 3D velocity profiles, measured by ADCPs at three WAVCIS stations, along with wind data, were analyzed.

2.2 Data and Methods

WAVCIS started back in 1998 (Stone et al., 2009; Zhang, 2003) and it was evolved over the years. It collects a wide array of met-ocean real time data from fixed oil and gas production units along the Louisiana coast (Figure 2.1). The real time data are reported to the National Data Buoy Center (NDBC) through the Gulf Coast Ocean Observing System (GCOOS) and WAVCIS web pages (www.wavcis.lsu.edu).

Hourly observations of directional waves, vertical current profiles, tide, wind speed and direction, sea surface temperature, pressure, etc. from individual stations are transmitted via satellite and cellular communications to the WAVCIS Lab at the Louisiana State University. Teledyne RDI ADCPs are used for wave and current measurements with vertical bins of 35–50 cm. More details on the offshore instrumentation, data processing, and communication protocol implemented for WAVCIS can be found in Zhang (2003).

---

[1] This chapter previously appeared as Allahdadi, M. N., Jose, F. and Patin, C. 2013. Seasonal Hydrodynamics along the Louisiana Coast: Implications for Hypoxia Spreading, *Journal of Coastal Research*, 29, 1092-1100. It is reprinted by permission of the JCR President and Executive director.

Here, we use the current and wind data collected in 2009 from stations CSI-6 and CSI-9 west of the Birds-foot delta inside the seasonal hypoxia zone, and CSI-16, east of the delta, which is relatively new (installed in August 2008).

Due to the maintenance and technical problems especially during hurricanes and the 2010 oil spill, significant gaps exist in the data. The most complete simultaneous dataset, covering both summer and fall for all three stations, was from the year 2009. The mean water depths at CSI-6, CSI-9, and CSI-16 are 21, 19, and 13 m, respectively. Standard QA/QC was performed to eliminate bad data near the sea surface. The measurement period in 2009 was divided into summer (June–August) and fall (September–November). Other non-summer months were not included in the study because no data were available for CSI-6 from January to mid-June and also for CSI-16 from January to March. Wind data from the same stations and period in 2009 were used to calculate wind stress.

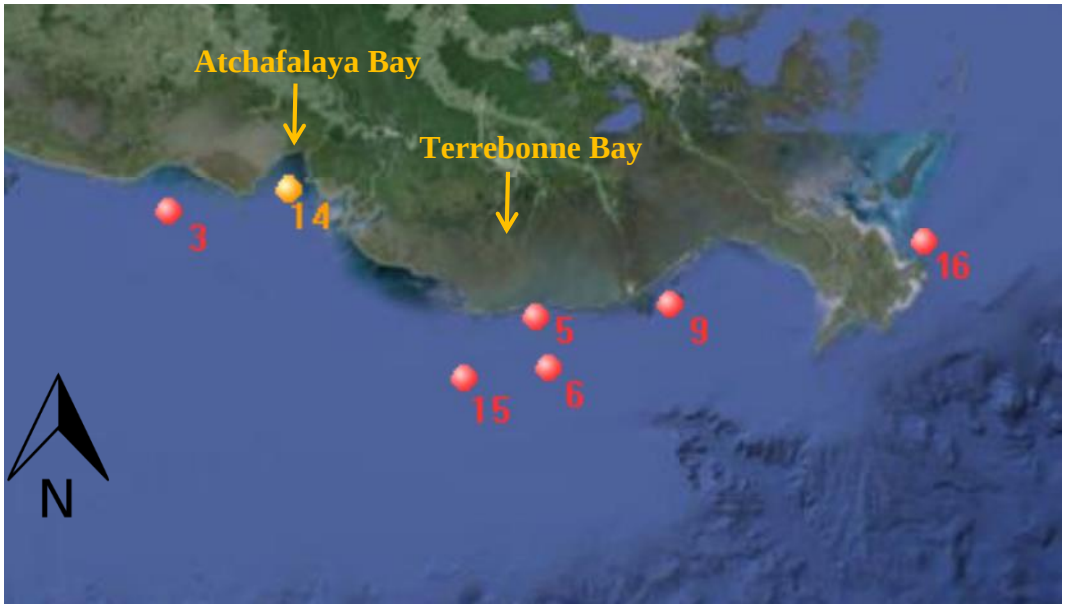

Figure 2.1: Study area and the locations of WAVCIS stations.

2.3 Results

2.3.1 Summer and Fall Current Pattern

Surface currents at CSI-6 during summer (Figure 2.2, a.) showed a disorganized pattern that is in agreement with previous studies (e.g., Crout et al., 1984). During June and July, the directions of the flow changed frequently in response to changing wind direction from south/southeast to west, whereas from mid-August, persistent northerly winds resulted in a southward current component. Current vectors during fall months at CSI-6 (Figure 2.2, b.) were more organized and were consistent with the patterns presented by Crout et al. (1984). During this period, especially from mid-October, the area was affected by frequent cold fronts,

generating southeastward and southwestward velocities. Currents at CSI-9 (Figure 2.2, c. for summer and Figure 2.2, d. for fall), located off the mouth of Barataria Bay (Figure 2.1), were obviously sluggish compared with those at CSI-6. Again, the current time series during summer was disorganized, whereas in the fall they showed more persistent patterns. The net current direction was northeastward, as the station is located inside a seasonal gyre, west of the Birds-foot delta (Rouse, 1998; Rouse and Coleman, 1976; Walker, 1996; Walker et al., 2005; Wiseman et al., 1976). The disorganized pattern of summer currents was less pronounced at CSI-16 than at CSI-6 and CSI-9. Regular occurrences of northeastward and southwestward currents were observed at CSI-16 and were more persistent in the summer (Figure 2.2, e.); whereas frequent shifts in current directions to the southwest occurred during the fall cold fronts (Figure 2.2, f.; see also Walker, 2005).

As forcing for the seasonal coastal currents, wind stress time series are computed using wind data from CSI-6 (Figure 2.3). Wind stress time series for CSI-9 and CSI-16 were similar. Although there were discrete events associated with high wind stress in June–August, in general, summer wind stress values were smaller than that of fall.

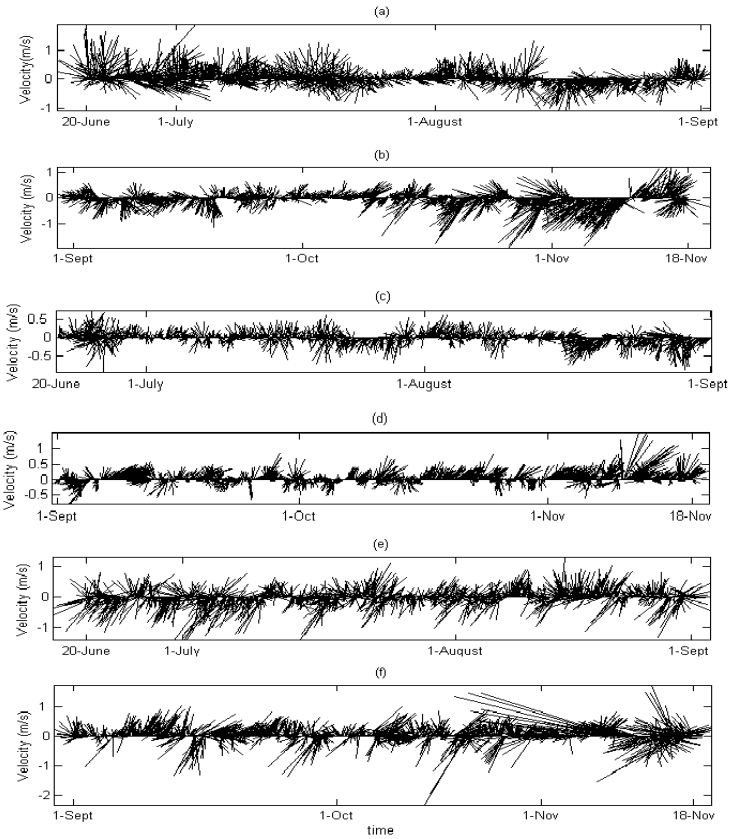

Figure 2.2: Time series measurements of surface currents from three WAVCIS stations, corresponding to summer and fall 2009; a and b: CSI-6, c and d: CSI-9, e and f: CSI-16.

A significant increase in wind stress, because of the passage of cold fronts, was obvious in the fall (September–November). Two discrete events, one during summer and the other in the fall, were selected for studying the response of current profiles at the three stations during these time periods. There were a number of additional wind events, especially in the fall. However, these two events were selected as examples to address the effect of wind on the velocity profiles during summer and fall, respectively. During event 1 (Table 2.1), the average wind speed at the three stations was 7 m/s. Wind direction for both CSI-6 and CSI-16 was southwesterly. At CSI-9, wind direction was northwesterly. Event 2 was a severe storm with wind speeds reaching 11 m/s at CSI-6 and 24 m/s at CSI-16. Wind direction was northwesterly for both CSI-6 and CSI-9 and north-to-northeasterly for CSI-16.

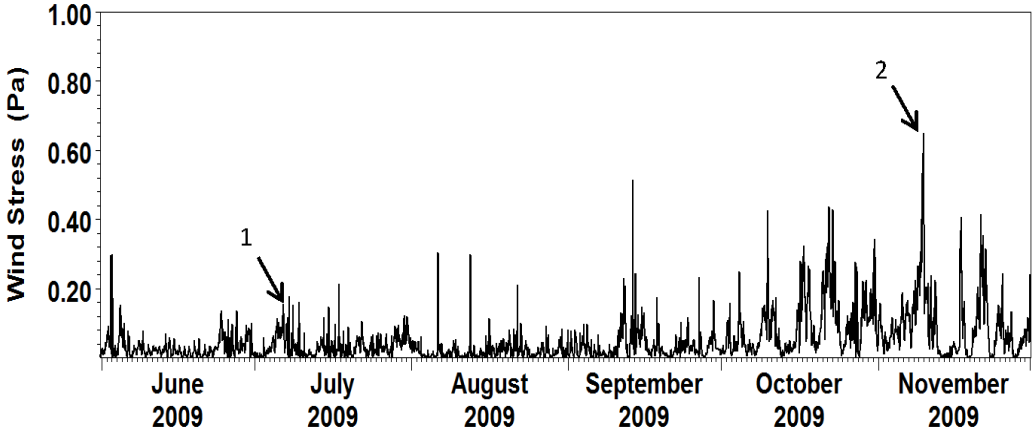

Figure 2.3: Variations of wind stress based on wind speed measurements at CSI-6 during the study period. Events 1 and 2 are discussed in the text (wind stress was calculated using equations 3.17 and 3.18).

Velocity components are expressed by u and v for east and north components, respectively (Figure 2.4). During event 1, for the u component of the water velocity, dominant southwesterly wind generated an eastward component of surface current at CSI- 6, but currents below the surface were directed westward. Likewise, for the v component of the velocity, it had a southward flow component on the surface with a northward flow underneath. Vertical profiles of horizontal flow components showed a small gradient, which was the same as CSI-9. At both stations, the magnitudes of velocity components were small (0.1 m/s or less except the surface u component at CSI-6). CSI-16 showed higher vertical gradients for both velocity components. Current velocities at the surface reached 0.4 m/s. Event 2 corresponds to the passage of a severe cold front in the fall with high current speeds for all stations.

The northwesterly winds produced southwestward flows of more than 0.5 m/s at CSI-6, with small vertical gradients. At CSI-9, currents were directed to the northeast, with higher vertical gradient compared to that of CSI-6. Magnitude of current velocities at CSI-16 occasionally reached 1.5 m/s, with significant vertical gradient for the v component

(quantification of shear gradient at all three stations for average seasonal conditions is presented in section 2.4).

Table 2.1: wind parameters for events 1 and 2.

Event	CSI-6		CSI-9		CSI-16	
	Speed (m/s)	Direction (degree)	Speed (m/s)	Direction (degree)	Speed (m/s)	Direction (degree)
1	7.5	264	6.5	322	6.5	274
2	11	341	15	344	24	10

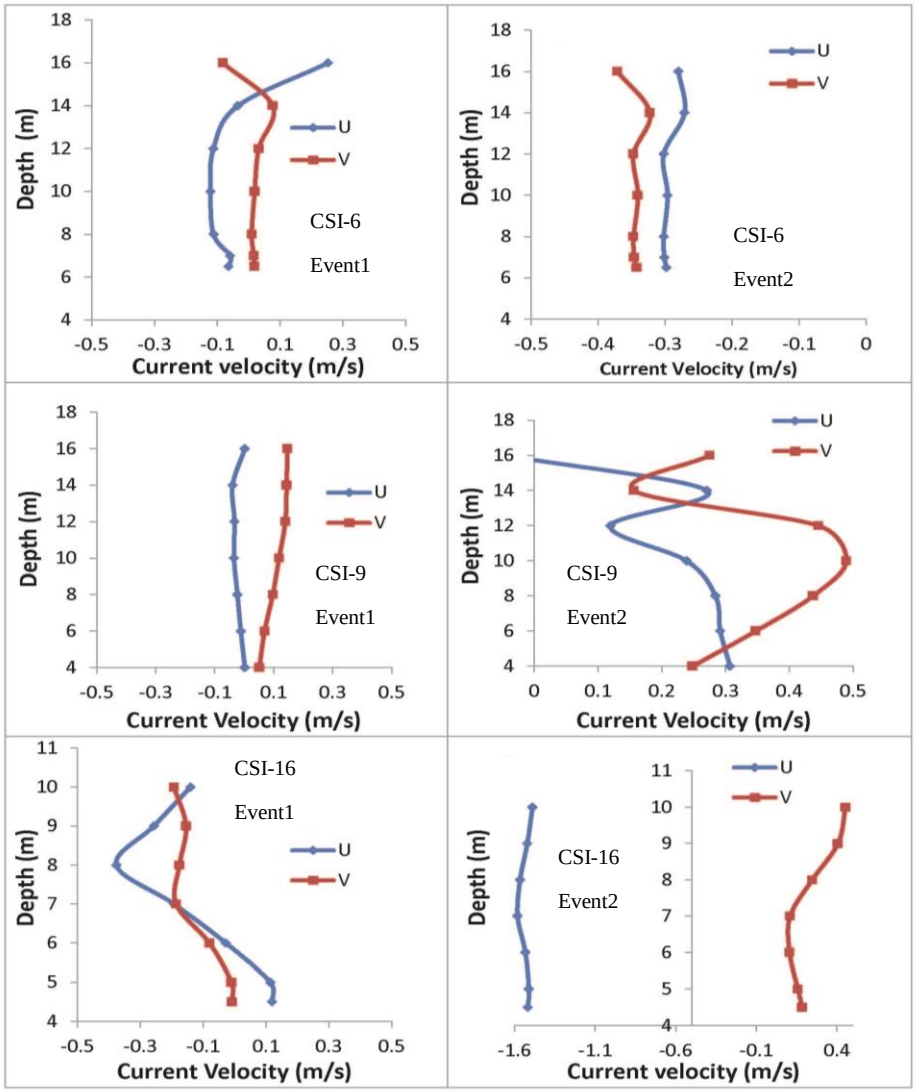

Figure 2.4: Vertical profiles of u & v velocity components for the three stations corresponding to events 1 and 2.

2.3.2 Current Profiles

Because the vertical gradient of horizontal current is one of the critical factors affecting water column mixing (Turner, 1973), vertical profiles of both velocity components for all three stations were examined (Figures 2.5 and 2.6). There were small velocity shears (see Table 2.2 for quantifications) for both components for CSI-6 and CSI-9, compared with CSI- 16, especially during summertime. Velocity and velocity shear increased from mid-August to mid-September as a result of energetic storms breaking down the summertime stratification. During November, cold fronts and their associated storms were more frequent and strong enough to mix the entire water column. The velocity at CSI-16 was entirely different with those of CSI-6 and CSI-9. July and August profiles of the u component had significant variations across the water column, but more uniform from late August to the end of November. The summertime velocity shear was more pronounced for the v component. A high-velocity core was seen in the distances 6–9 m above the seabed. This high-velocity core could cause significant mixing to both the upper and lower water columns. A similar core was also detected in the u component but with smaller magnitude. The velocity shear across the water column was persistent during the entire summer, especially for the u component, whereas strong velocity shears at CSI-6 and CSI-9 were ephemeral.

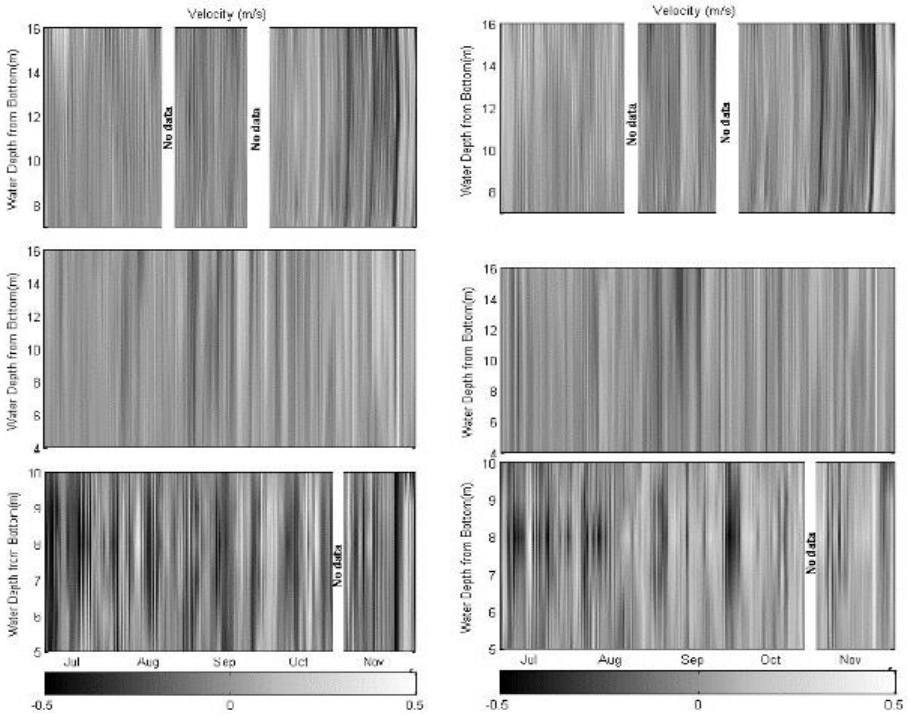

Figure 2.5: Vertical profile of u velocity component (left panel) and v velocity component (right panel) for three stations during the study period (Upper: CSI-6, middle: CSI-9, and lower: CSI-16).

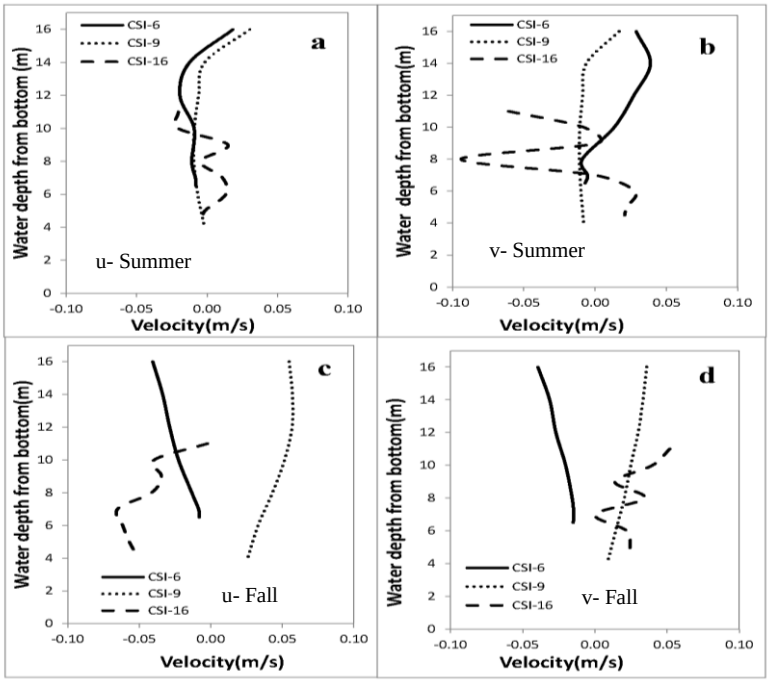

Figure 2.6: Seasonal time-averaged u and v velocities from three stations.

2.4 Hydrodynamics and Hypoxia

Water column stratification during summer is identified to be one of the main factors in determining the seasonal hypoxia (Hagy and Murrell, 2007). A stratified water column with at least 6 kg/m^3 surface to bottom density difference in the northern Gulf of Mexico is found to be a necessary condition for hypoxia (Walker and Rabalais, 2006). Considering the characteristics of the current velocity profiles discussed in the previous section, a smaller shear effect was expected for both stations west of the Birds-foot delta (CSI-6 and CSI-9) compared to CSI-16 east of the Birds-foot delta. Table 2.2 presents the average values of the denominator of the Richardson number for all three stations during both summer and fall.

Table 2.2: Mean values of denominator in Richardson number relationship$[(\frac{\partial u}{\partial z})^2 + (\frac{\partial v}{\partial z})^2]$, based on measured currents from each station.

Station	Summer	Non-Summer
CSI-6	0.0011	0.0015
CSI-9	0.0002	0.0007
CSI- 16	0.0100	0.0036

A much larger denominator at CSI-16, especially during summertime, was shown. The denominator in this station in the summer was higher than that in the fall. In the summertime, it was one order of magnitude greater than that of CSI-6 and two orders of magnitude greater than that of CSI-9. During the fall, it was more than two times greater than that of CSI-6 and seven times greater than that of CSI-9. Therefore, even if the buoyancy effect (the numerator of the Richardson number) is the same for all stations, CSI-16 would have a smaller Richardson number, accounting for less stratification. Furthermore, it has been reported that the Mississippi River discharge to the eastern side of the Birds-foot delta is 15% less than that of the western side (Rego et al., 2008); therefore, less buoyancy effect would be expected for the eastern side, resulting in less stratification, reducing the hypoxia potential for the CSI-16 region.

2.5 Summary and Conclusions

Summer and fall flow characteristics from locations west and east of the Mississippi Birds-foot delta at CSI-6, CSI-9, and CSI-16 were analyzed and discussed using current and wind data from three WAVCIS stations off the Louisiana coast. Current profiles from CSI-16 exhibited larger vertical gradients during the summer compared with the other two stations located on the western side of the Mississippi River. This higher velocity gradient translated to smaller Richardson numbers, showed a higher degree of mixing for the eastern station. The contrasting hydrodynamic data from different locations east and west of the Birds-foot delta has significant implications of the importance of the physical processes in the formation and evolution of the seasonal hypoxia in the northern Gulf of Mexico.

CHAPTER 3: NUMERICAL SIMULATION OF LOUISIANA SHELF CIRCULATION UNDER HURRICANE KATRINA FORCES

3.1 Introduction

To simulate the impact of a hurricane on water column mixing, a reliable circulation model is needed. The vertical variations of currents are related to the vertical turbulent diffusion responsible for the deepening of the mixed layer. Such a circulation model applied to Hurricane Katrina is presented in this chapter. The chapter describes the details about the numerical model and its setup including the hurricane wind field. Model calibration and verification for different cases were discussed before simulation results were presented and discussed.

3.2 Background

Hurricanes are energetic atmospheric events impacting the ocean including continental shelf hydrodynamics. They can produce large waves, surges, and circulations much greater than normal. Waves generated by hurricanes can damage offshore structures (including oil rigs), and coastal facilities (Cooper and Thompson, 1989a). Large hurricane storm surges are a serious threat to the coastal properties and residents, especially in the vicinity of landfall (Chen et al., 2009). Hurricane-induced currents, may cause significant coastal erosion and deposition, associated with sediment transport over the shelf. Hurricanes can significantly mix shelf waters and redistribute biogeochemical substances. Furthermore, the strong horizontal shear produced by currents along with the effect of large waves mixes the water column and break down the stratification. This mixing has a significant implication to the gas exchange that affects dissolved oxygen concentration in the water column (Wiseman et al., 1997, Allahdadi et al., 2013).

The shallow shelf in the northern Gulf of Mexico (NGoM) is frequently affected by hurricanes. It is imperative to understand how hurricanes affect the circulation, and mixing in this area. The fair weather conditions have been studied in Chapter 2 demonstrating the significant role of the velocity field and its vertical shear in the mixing of the water column.

Previous studies have examined the hydrodynamic response to hurricanes in the NGoM, such as Rego and Li (2009, 2010), and Cardone et al. (2007). Rego and Li (2010) studied the storm surge produced by Hurricane Rita in Galveston Bay by applying the Finite Volume Community Ocean Model (FVCOM). The model was calibrated using observed water levels from USGS at several locations along the coast. Siadatmousavi et al. (2012) used the SWAN model to simulate the wave field generated by Hurricane Dennis in the Gulf of Mexico. The model was skill assessed using wave measurements from a number of NDBC stations and from WAVCIS stations on the Louisiana shelf. Currents induced by hurricanes in the NGoM have been studied based on both observations and numerical modeling (for example, Keen and Glenn, 1999; Ly, 1994; Teague et al., 2007; Mitchel et al., 2005; Cooper and Thompson, 1989a, b). Ly (1994) studied water levels and currents induced by Hurricane Fredric by applying a 3-D finite

difference ocean model with sigma coordinate in the vertical. Hurricane Fredric made its landfall on Dauphine Island, Alabama on 13 September 1979, producing currents as large as 2 m/s as well as inertial motions on the shelf in the NGoM. Hurricane Ivan passed over an array of 14 ADCPs deployed over the edge of continental shelf off the Mobile, Alabama in September 2004, providing a unique opportunity to study the response of inner and outer shelf water in this area to a hurricane (Teague et al., 2007; Mitchel et al., 2005). Analysis of time series water level and current profiles obtained from the measurements demonstrated that the outer-shelf response to the hurricane was consistent with the four different stages suggested by different researchers (Pedlosky, 1979; Price et al., 1994). Current velocity greater than 2 m/s was observed during the hurricane passage. On the shelf edge, the largest currents were recorded by the current meters left of the storm eye, while on the outer-shelf the largest current was measured on the right side of the hurricane track. The near-bottom currents were large enough that along with the surface waves caused substantial scours on the seabed at 90 meter water depth. The effect of stratification on the currents in the shallow Louisiana water during Hurricane Andrew was studied by Timothy and Scott (1999) using a combination of the Princeton Ocean Model and field measurements. Their study demonstrated a significant impact of stratification on both baroclinic and barotropic responses to the hurricane.

Hurricane Katrina was one of the most devastating hurricanes in U.S. history with respect to its damages. It impacted both the east and west of the Birds-foot delta. Many modeling studies examined the storm surge and waves generated by Katrina (Cardone et al., 2007; Chen et al., 2008; Wang and Oey, 2008; Chen and Wang, 2009; Dietrich et al., 2011). However, few studies focused on the circulation and velocity field induced by Katrina. Wang and Oey (2008) applied the Princeton Ocean Model (POM) and the National Centers for Environmental Prediction (NCEP) Wave Watch III (WW3) model for currents and waves generated by Hurricane Katrina in the Gulf of Mexico. The models were forced by Katrina's wind fields derived from a database obtained from a blend of winds simulated by NCEP Global Forecast System and National Oceanic and Atmospheric Administration (NOAA) Hurricane Research Division high resolution analyzed winds. The wave model was calibrated against the time series of wave parameters obtained from several NDBC buoys as well as satellite altimetry data. Apparently, no current data were publicly available during Hurricane Katrina in the Gulf of Mexico; hence, no verification could be done on the currents. Cardone et al. (2007) carried out a study for hindcasting wind, waves, and currents in the northern Gulf of Mexico during Hurricanes Katrina and Rita of 2005. They combined the wind field from a planetary boundary layer (PBL) with the hurricane wind field provided by the NOAA HRD H-Wind snapshots to obtain a high resolution wind field for both hurricanes. Depth-averaged currents were simulated using the ADCIRC-2D model, although there were no current data used for model calibration. To simulate the vertical current structure, a 1-D mixed layer model for water depth greater than 75 meters was used. The model was verified using some velocity data measured during Hurricane Katrina offshore of the Mississippi Delta. Detailed studies using 3D models are rare for high resolution circulation with good accuracy over the shelf during Hurricane Katrina. In this study the 3D FVCOM was

applied for the hydrodynamics, focusing on the current velocity structure and characteristics induced by Hurricane Katrina over the Louisiana shelf.

3.3 Hurricane Katrina

Starting as a tropical depression over the Bahamas on 23 August 2005 (Knabb et al., 2005), Katrina turned to a Category 5 Hurricane on 28 August after passing over the warm waters associated with the Loop Current (Shen et al., 2006). The hurricane degraded to some extent as it approached the Louisiana shelf. In the early morning (GMT time) on 29 August, as a Category 3 hurricane it made its first landfall between the Grand Isle LA and the Mississippi River mouth, near Buras, LA. Figure 3.1 shows the track of Hurricane Katrina as it traveled in the NGoM. Hurricane Katrina impacted both shelves east and west of the Mississippi Birds-foot delta. The Louisiana shelf west of the delta was profoundly affected by Hurricane Katrina (Chen and Wang, 2008).

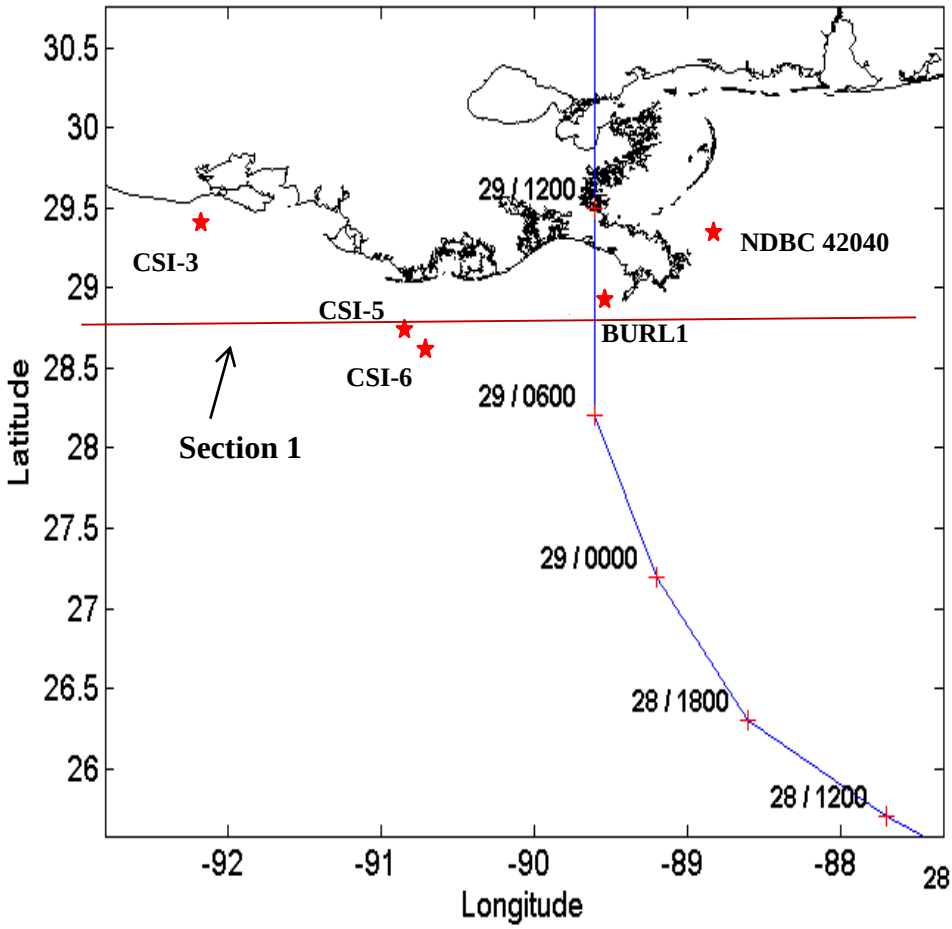

Figure 3.1: Track of Hurricane Katrina in the Northern Gulf of Mexico at different dates and times (asterisks show the locations of wind and current measurements, where simulated time series of current were also presented).

3.4 The Circulation Model

3.4.1 Governing Equations

In the present study, simulations of current and salt/heat transport were done using FVCOM which is a prognostic, unstructured-grid, finite-volume, free-surface, three-dimensional (3-D) primitive equation ocean model. The model was developed by Chen et al. (2003). The main equations solved by the model, include the momentum balance, continuity, energy conservation (for solving temperature), and mass conservation (for solving salinity):

$$\frac{\partial u}{\partial t} + u\frac{\partial u}{\partial x} + v\frac{\partial u}{\partial y} + w\frac{\partial u}{\partial z} - fv = -\frac{1}{\rho_0}\frac{\partial P}{\partial x} + \frac{\partial}{\partial z}\left(K_m\frac{\partial u}{\partial z}\right) + F_u \quad (3.1)$$

$$\frac{\partial v}{\partial t} + u\frac{\partial v}{\partial x} + v\frac{\partial v}{\partial y} + w\frac{\partial v}{\partial z} + fu = -\frac{1}{\rho_0}\frac{\partial P}{\partial y} + \frac{\partial}{\partial z}\left(K_m\frac{\partial v}{\partial z}\right) + F_v \quad (3.2)$$

$$\frac{\partial P}{\partial z} = -\rho g \quad (3.3)$$

$$\frac{\partial u}{\partial x} + \frac{\partial v}{\partial y} + \frac{\partial w}{\partial z} = 0 \quad (3.4)$$

$$\frac{\partial T}{\partial t} + u\frac{\partial T}{\partial x} + v\frac{\partial T}{\partial y} + w\frac{\partial T}{\partial z} = \frac{\partial}{\partial z}\left(K_h\frac{\partial T}{\partial z}\right) + F_T \quad (3.5)$$

$$\frac{\partial S}{\partial t} + u\frac{\partial S}{\partial x} + v\frac{\partial S}{\partial y} + w\frac{\partial S}{\partial z} = \frac{\partial}{\partial z}\left(K_h\frac{\partial S}{\partial z}\right) + F_s \quad (3.6)$$

$$\rho = \rho(T, S) \quad (3.7)$$

In the above equations, parameters are defined as follows:

$x, y,$ and z: east-west, north-south, and vertical Cartesian coordinate axes respectively

u: current velocity component in x-direction

v: current velocity component in y-direction

w: current velocity component in z-direction

t: time , f: Coriolis parameter , P: pressure , g: acceleration of gravity

ρ : water density , t: temperature, S: Salinity

K_m: vertical eddy viscosity coefficient

K_h: thermal vertical eddy diffusion coefficient

F_u, F_v, F_T, and F_s: horizontal momentum, thermal , and salt diffusion terms

The formulation assumes a hydrostatic pressure balance in the water column. The Boussinesq approximation was used on the momentum equation to deal with the variations of density. This is a reasonable assumption for most oceanic, coastal, and estuarine waters. To close the system of equations, horizontal momentum, thermal and salt diffusion terms, vertical eddy viscosity coefficient, and thermal vertical eddy diffusion coefficient should be provided or

calculated. Horizontal diffusive terms (F_u, F_v, F_T, and F_s) are obtained based on the Smagorinsky turbulent closure scheme for horizontal mixing. The Smagorinsky horizontal diffusion for the momentum is given as:

$$A_h = \frac{0.5C\Omega^{\zeta}}{P_r}\sqrt{(\frac{\partial u}{\partial x})^2 + 0.5(\frac{\partial v}{\partial x} + \frac{\partial u}{\partial y})^2 + (\frac{\partial v}{\partial y})^2} \quad (3.8)$$

where C is a constant and Ω the area of the individual momentum control element.

The vertical eddy viscosity and diffusivity parameters are estimated using the Mellor-Yamada level 2.5 turbulence closures. The equations for K_m (vertical eddy viscosity for momentum), K_h (vertical eddy diffusivity for temperature and salinity), and K_p are:

$$K_m = lqS_m\ ,\ K_h = lqS_h, K_q = 0.2\ lq \quad (3.9)$$

in which $0.5q^2$ is the turbulent kinetic energy, l the turbulent macroscale, and $S_m$and S_h stability functions. Parameters q and l are calculated by solving the following set of differential equations:

$$\frac{\partial q^2}{\partial t} + u\frac{\partial q^2}{\partial x} + v\frac{\partial q^2}{\partial y} + w\frac{\partial q^2}{\partial z} = 2(P_s + P_b - \varepsilon) + \frac{\partial}{\partial z}\left(K_q\ \frac{\partial q^2}{\partial z}\right) + F_q \quad (3.10)$$

$$\frac{\partial q^2 l}{\partial t} + u\frac{\partial q^2 l}{\partial x} + v\frac{\partial q^2 l}{\partial y} + w\frac{\partial q^2 l}{\partial z} = lE_1(P_s + P_b - \frac{\widetilde{W}}{E_1}\varepsilon) + \frac{\partial}{\partial z}\left(K_q\ \frac{\partial q^2 l}{\partial z}\right) + F_l \quad (3.11)$$

S_m and S_h are defined as:

$$S_m = \frac{0.4275 - 3.354G_h}{(1 - 34.676G_h)(1 - 6.127G_{h)}}\ and\ S_h = \frac{0.494}{1 - 34.676G_h} \quad (3.12)$$

$$G_h = \frac{l^2 g}{q^2 \rho_0}\rho_z \quad (3.13)$$

3.4.2 Model Setup

3.4.2.1 Modeling Area/Computational Mesh

The modeling area is fan shaped and centered at Terrebonne Bay including the coastal, shelf and deep ocean regions covering the coastal areas of Mobile-Alabama to Galveston-Texas. The computational meshes are triangular (Figure 3.2).

3.4.2.2 Boundary Condition

Numerical artifacts can cause reflection of waves from the model open boundary which can lead to instabilities inside the modeling area. Hence, the open boundary should be treated appropriately to damp the waves reflected into the modeling area. FVCOM includes a number of approaches to deal with this open boundary effect.

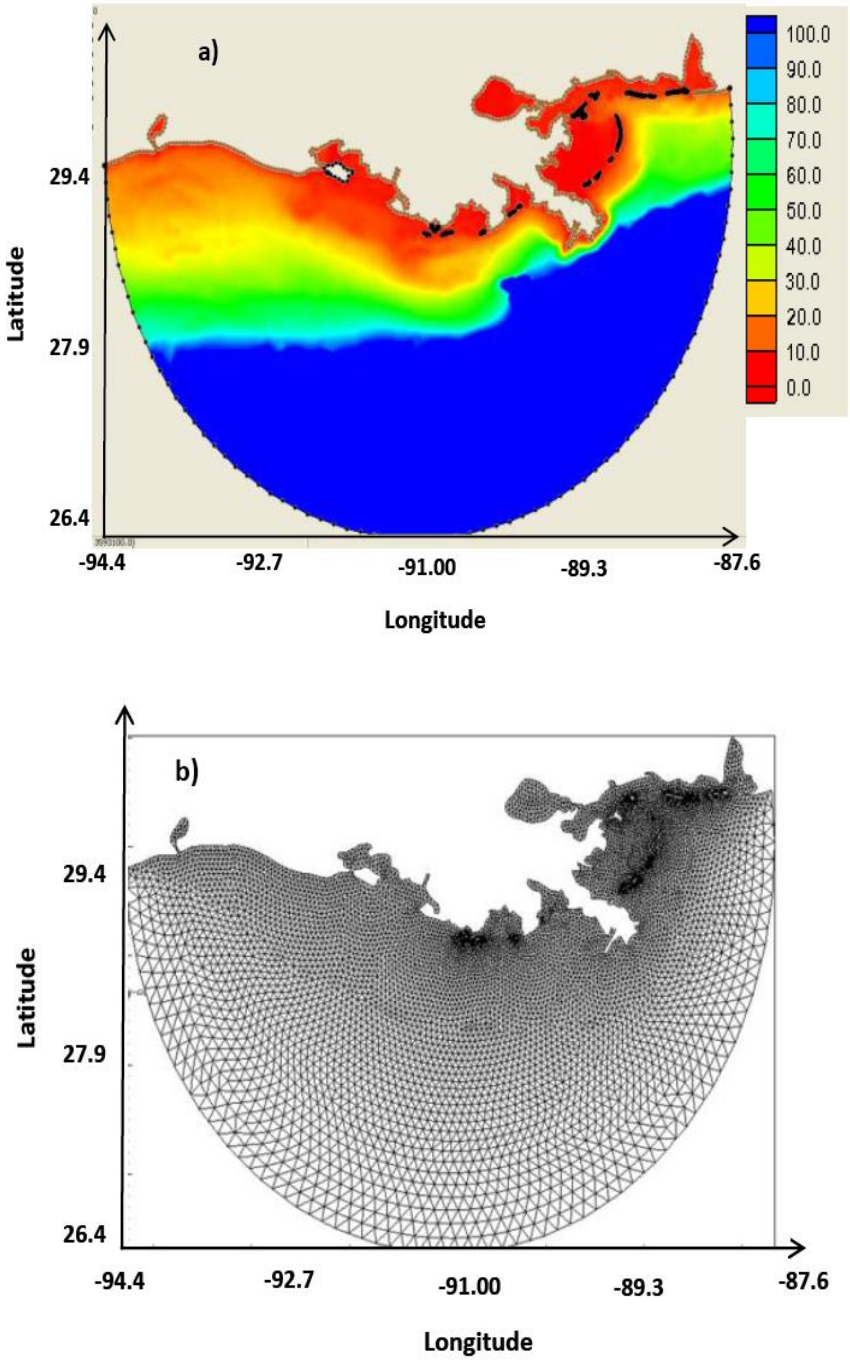

Figure 3.2: a) Modeling area and bathymetry, b) Computational mesh.

To damp the radiated waves and suppress the disturbances, a series of sponge layers are considered with defined damping factors. In the present modeling for Hurricane Katrina, boundary condition type 5 which is the Explicit Orlanski Radiation (ORE) along with the appropriate sponge layer has been used. These include specifying the water level along the boundary and radiation boundary conditions (Table 3.1).

Table 3.1: Different types of open boundary treatment included in FVCOM model (Chen et al., 2003).

Type1	Active(ASL) The sea level is specified at the OB. For example, tidal amplitude and phases (optional FVCOM setup)
Type2	Clamped(ASL-CLP) (Berdsley and Haidvogel, 1981) $\xi = 0$ at OBC
Type3	Implicit Gravity Wave Radiation(GWI) (Chapman, 1985) $\xi_t + C_0\xi_n$=0 , $C_{0=}\sqrt{gH}$, n is the normal direction to the OB
Type 4	Partial Clamped Gravity Wave Radiation (BKI) (Blumberg and Kantha,1985) $\xi_t + C_0\xi_n = -\xi/T_f$, $C_{0=}\sqrt{gH}$ T_f: User-specified frictional timescale
	Explicit Orlanski Radiation (ORE) (Orlanski,1976; Chapman, 1985)
Type 5	$\xi_t + C_0\xi_n$=0 ; $C_0 = \frac{\Delta n}{\Delta t}$ if $-\frac{\xi_t}{\xi_n} \geq \frac{\Delta n}{\Delta t}$ $-\frac{\xi_t}{\xi_n}$ if $-\frac{\xi_t}{\xi_n} < \frac{\Delta n}{\Delta t}$ 0 if $-\frac{\xi_t}{\xi_n} \leq 0$

3.5 Preparation of Input Wind

3.5.1 Hurricane Wind Field Generation

A parametric model suggested by Holland (1980) was applied for the wind field of Hurricane Katrina. This model has been successfully used for hurricane-induced current, waves, and storm surges (e.g. Young and Sobey, 1981; Phadke et al., 2003; Rego and Li, 2009; Rego and Li, 2010).

This is a single vortex model that uses some parameters associated with the hurricane to re-construct the spatial distribution of wind and air pressure fields. Using $V_g(r)$ and $p(r)$ to denote the wind speed and air pressure, respectively:

$$V_g(r) = \sqrt{(p_n - p_c)\frac{B}{\rho_A}\left(\frac{R_{mw}}{r}\right)^B \exp\left(-\frac{R_{mw}}{r}\right)^B + \left(\frac{r.f}{2}\right)^2} - \frac{r|f|}{2} \quad (3.14)$$

$$p(r) = p_c + (p_n - p_c)exp\left(-\frac{R_{mw}}{r}\right)^B \quad (3.15)$$

$$B = 2.0 - (p_c - 900)/160 \quad (3.16)$$

in which P_n, P_c R_{mw}, r, f, ρ_A denote the neutral air pressure, pressure at the center of hurricane, the radius of maximum wind, radial distance from the center of the hurricane, Coriolis parameter, and air density, respectively.

The pressure data at 6-hour intervals at the center of the hurricane were obtained from the National Hurricane Center advisories and the neutral air pressure data were obtained from pressure map data at the same time. Selecting the radius of maximum wind is challenging. Based on the literature (for example Hsu and Yan, 1998), it can be 40 km. In this study, only for the times that Hurricane Katrina is passing the outer Louisiana shelf, this assumption was used, but over the Louisiana shelf, observations of wind speed and direction were used to tune the radius of maximum wind. The resulted values were between 30 to 35 km.

The simulation of Katrina's wind field was for 180 hours starting from 18:00:00 UTC, 23 August 2005, the approximate time that Katrina entered GoM, to 06:00:00 UTC, 31 August 2005, almost two days after the final landfall. Table 3.2 lists the hurricane parameters used for the wind field at different times.

Table 3.2: Hurricane parameters for the wind field at different times (Source: National Hurricane Center).

Date	Elapsed time (hour)	Longitude	Latitude	Pc (hp)	Pn (hp)	B	Rmw (km)
8/23/2005 18:00	0	-75.1	23.1	1008	1012	1.3	27
8/24/2005 00:00	6	-75.7	23.4	1007	1012	1.3	27
8/24/2005 06:00	12	-76.2	23.8	1007	1012	1.3	27
8/24/2005 12:00	18	-76.5	24.5	1006	1012	1.3	27
8/24/2005 18:00	24	-76.9	25.4	1003	1012	1.3	27
8/25/2005 00:00	30	-77.7	26	1000	1012	1.3	27

(Table 3.2 continued)

Date	Elapsed time (hour)	Longitude	Latitude	Pc (hp)	Pn (hp)	B	Rmw (km)
8/25/2005 12:00	42	-79	26.2	994	1012	1.4	27
8/25/2005 18:00	48	-79.6	26.2	988	1012	1.4	27
8/26/2005 00:00	54	-80.3	25.9	983	1012	1.5	27
8/26/2005 06:00	60	-81.3	25.4	987	1012	1.4	27
8/26/2005 12:00	66	-82	25.1	979	1012	1.5	27
8/26/2005 18:00	72	-82.6	24.9	968	1012	1.5	27
8/27/2005 00:00	78	-83.3	24.6	959	1012	1.6	27
8/27/2005 06:00	84	-84	24.4	950	1012	1.7	27
8/27/2005 12:00	90	-84.7	24.4	942	1012	1.7	27
8/27/2005 18:00	96	-85.3	24.5	948	1012	1.8	35
8/28/2005 00:00	102	-85.9	24.8	941	1012	1.8	35
8/28/2005 06:00	108	-86.7	25.2	930	1012	1.9	35
8/28/2005 12:00	114	-87.7	25.7	909	1012	2	35
8/28/2005 18:00	120	-88.6	26.3	902	1012	2	35
8/29/2005 00:00	126	-89.2	27.2	905	1012	2	35
8/29/2005 06:00	132	-89.6	28.2	913	1012	2	35
8/29/2005 12:00	138	-89.6	29.5	923	1012	1.8	20
8/29/2005 18:00	144	-89.6	31.1	948	1012	1.7	20
8/30/2005 00:00	150	-89.1	32.6	961	1012	1.6	20
8/30/2005 06:00	156	-88.6	34.1	978	1012	1.5	35
8/30/2005 12:00	162	-88	35.6	985	1012	1.4	35
8/30/2005 18:00	168	-87	37	990	1012	1.4	35
8/31/2005 00:00	174	-85.3	38.6	994	1012	1.4	35
8/31/2005 06:00	180	-82.9	40.1	996	1012	1.4	35

As mentioned, the radius of maximum wind was adjusted through a calibration process based on available wind data over the shelf. Figure 3.1 shows locations at which wind data were available over the shelf during Katrina (stations CSI-6, CSI-5, BURL1, and NDBC 42040). CSI-6 and CSI-5 are both located west of the Birds-foot delta. CSI-5 is adjacent to the mouth of Terrebonne Bay, while CSI-6 is positioned further offshore. During the time that Hurricane Katrina passed over the Louisiana inner shelf, the anemometer at CSI-6 stopped working. Hence the measurement did not catch the peak hurricane wind. The peak was however captured by CSI-5. Station BURL1 located on the South Pass offers reliable measurements of wind parameters and was employed in several studies (for example Wang and Justic, 2009; Hetland and DiMarco, 2012). Similar to CSI-6, measurements at BURL1 were available only up to several hours prior to the peak wind speed. To evaluate the accuracy of the model wind field on the shelf east of the Birds-foot delta, wind data from NOAA's station 42040 were used. Wind vectors generated by

the Holland (1980) model were compared to that of measurements. We obtained the best match by changing the radius of maximum wind (Figure 3.3). As mentioned before, no wind data were measured at stations CSI-6 and BURL1 from several hours before the peak hurricane wind. However, the available data showed very good agreement with the calibrated wind speed from the model. Simulated wind directions were also compared with measurements demonstrating a good agreement. Examples of this wind field for different times, as the hurricane's eye passed over the southwest of the Birds-foot delta is presented in Figure 3.4. With calibrated radius of maximum wind, the model wind was applied to simulate the ocean's response to Katrina.

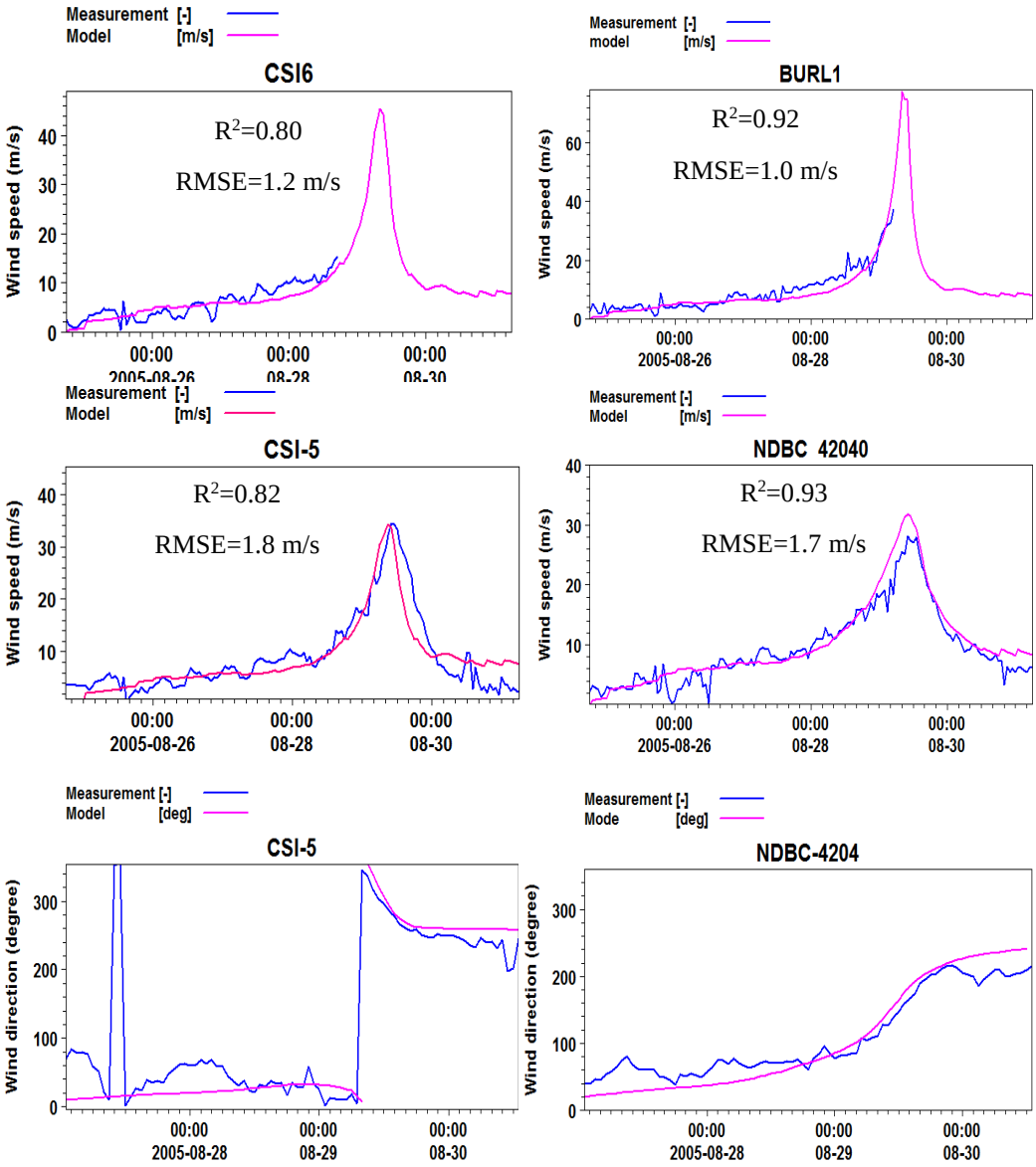

Figure 3.3: Comparison between the generated and measured wind speeds and directions over the Louisiana shelf.

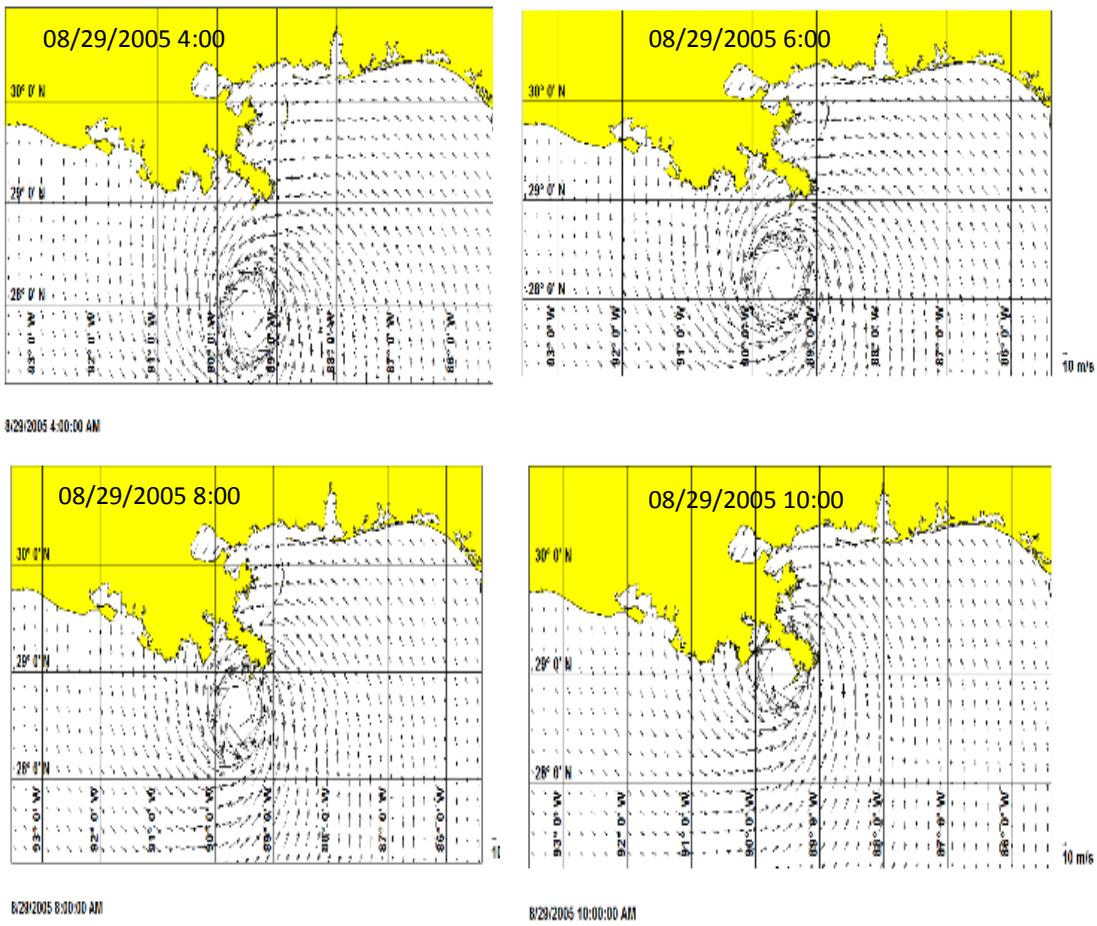

Figure 3.4: Model-generated Katrina's wind field over the Louisiana shelf at different times.

3.5.2 Wind Friction Coefficient

Wind energy is transferred to the water surface through the shear stress between the air and water. This stress is calculated by the quadratic law:

$$\tau = C_d \rho_a U^2 \tag{3.17}$$

where C_d is the drag coefficient, ρ_a air density, and U wind speed. The drag coefficient is assumed to be dependent on wind speed. Large and Pond (1981) suggested that the drag coefficient increases linearly with wind speed for wind speed between 11 m/s and 25 m/s. For wind speeds greater than 25 m/s, the coefficient was considered constant:

$$C_d^{srf} \times 10^3 = \begin{cases} 1.2 & \left|\overrightarrow{V_w}\right| \le 11.0 m/s \\ 0.49 + 0.65\left|\overrightarrow{V_w}\right| & 11.0 \le \left|\overrightarrow{V_w}\right| \le 25.0 m/s \\ 0.49 + 0.065 \times 25 & \left|\overrightarrow{V_w}\right| \ge 25.0 m/s \end{cases} \tag{3.18}$$

in which V_w is wind speed.

Although this approach was used in many studies and had acceptable results, further studies on air-sea interaction and wind-wave boundary layer showed that the rate of energy transfer from wind to the water surface decreases for wind speeds greater than a specific threshold (25-32 m/s) (Makin, 2003 and 2005).

It was shown that when the wind speed was greater than the threshold, the white caps produced at the sea surface prevented further transfer of wind energy to the water surface. Based on this finding, a modified relationship between the drag coefficient and wind speed was defined and was used in the present study. The resulting drag coefficient was compared with that of Large and Pond (1981) for different wind speeds in Figure 3.5.

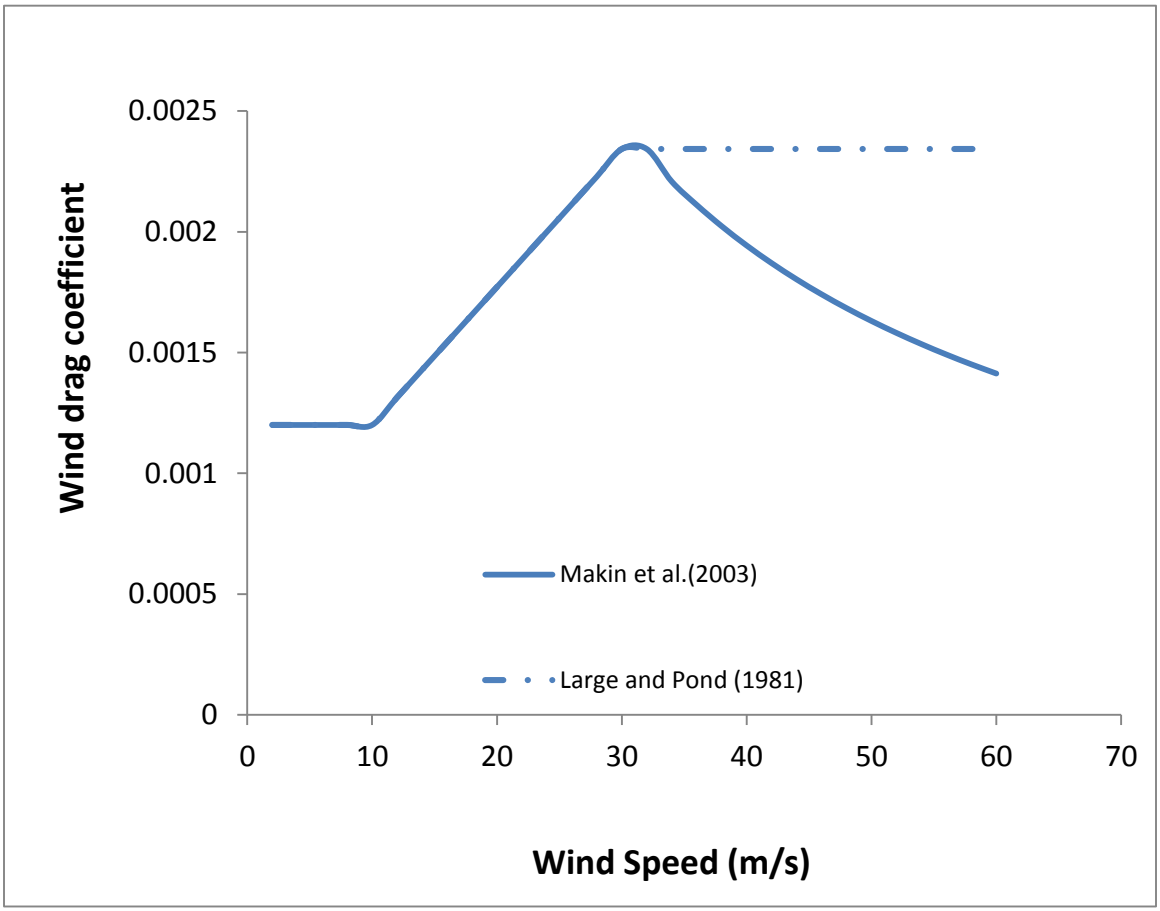

Figure 3.5: Wind drag coefficient as a function of wind speed based on two different approaches.

3.6 Current Verification

3.6.1 Evaluation for Tidal Currents

Although studying the tidal hydrodynamics is not the goal of the present study, it is useful to evaluate model performance in simulation of tide propagating from the open boundary

to the shelf area. This will provide more confidence about the model performance. For implementing a tidal simulation, the model open boundary was forced by spatially varying water level extracted from the ADCIRC model tidal database (Mukai et al., 2002). Variations of water level at the middle of the model boundary (off Terrebonne Bay) during a one month period (March 2005) are shown in Figure 3.6. Results for the water level were evaluated using NOAA's predicted tide at some coastal stations.

Comparison for several stations revealed two types of discrepancies between the model results and predictions. First, there was a level shift of 10-25 centimeters between modeled and predicted tides which may be due to the difference in reference level. This problem was solved by changing the datum for tidal level predictions to get the best match up comparisons l. The second problem was that the model produced tidal range was larger than that of predictions. Increasing the bed resistance did not help, even for coastal stations of small depths.

According to the technical report of ADCIRC tidal modeling (Mukai et al., 2002), tidal amplitude for the dominant diurnal constituents over the Louisiana shelf area were overestimated by 15-20 % (Figure 3.7).

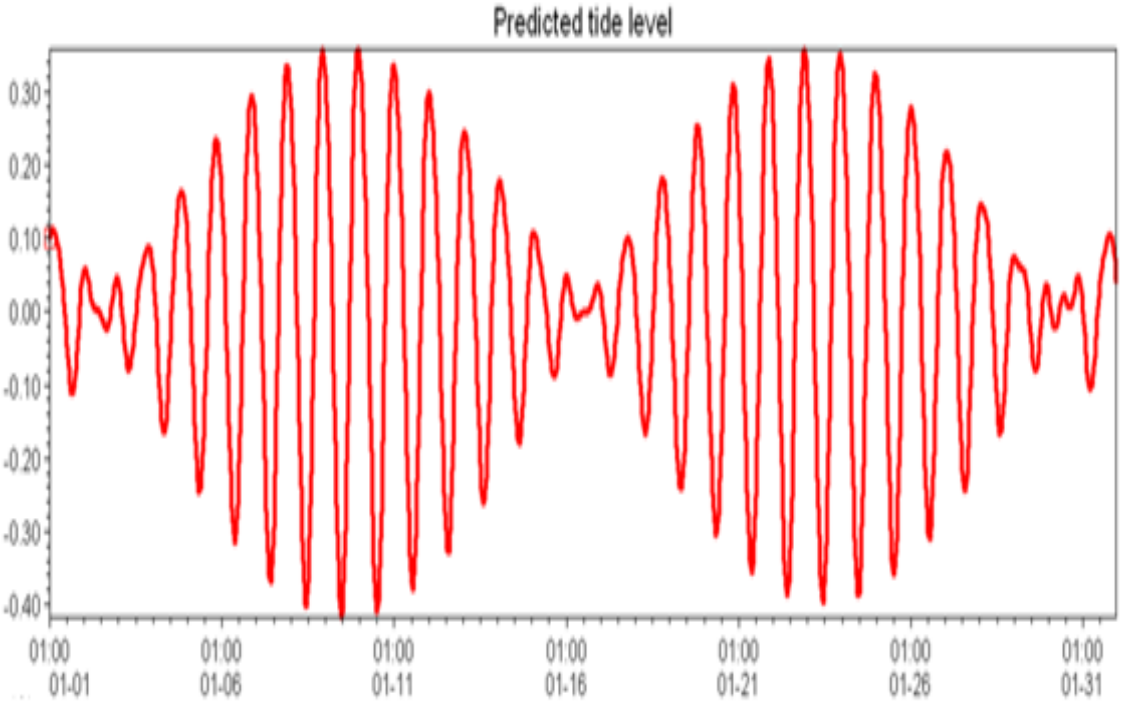

Figure 3.6: One month (March 2005) ADCIRC-derived timeseris of tidal level for a point at the middle of the model boundary (water level is in meter and was reduced to the mean sea level).

Therefore, in correcting the problem, we reduced the tidal levels along the model boundary by 20 %, producing improved results. Examples of comparisons for a station inside the Atchafalaya Bay and a station at the Southwest Pass (see Figure 3.8 for location) are presented in Figures 3.9 and 3.10.

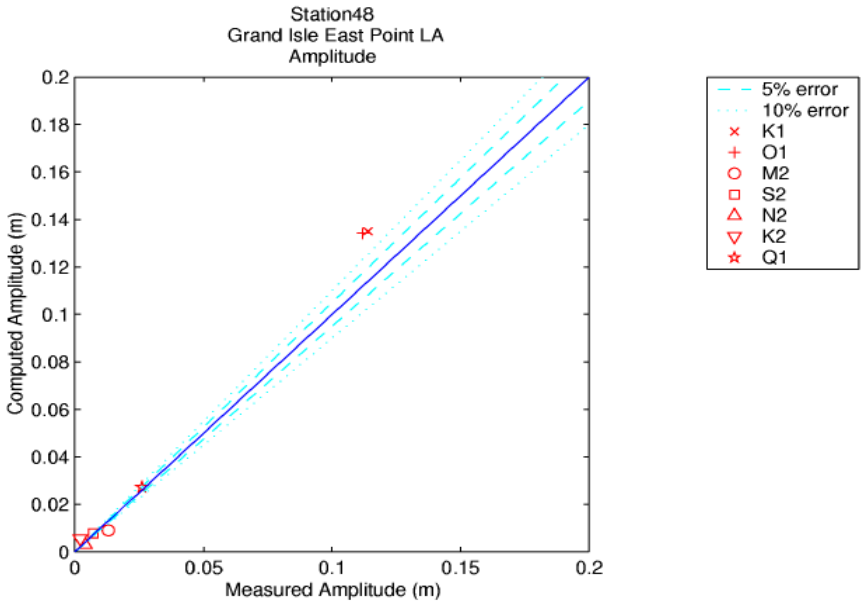

Figure 3.7: Overestimation of K1 and O1 tidal constituents along the Louisiana coast by ADCIRC model.

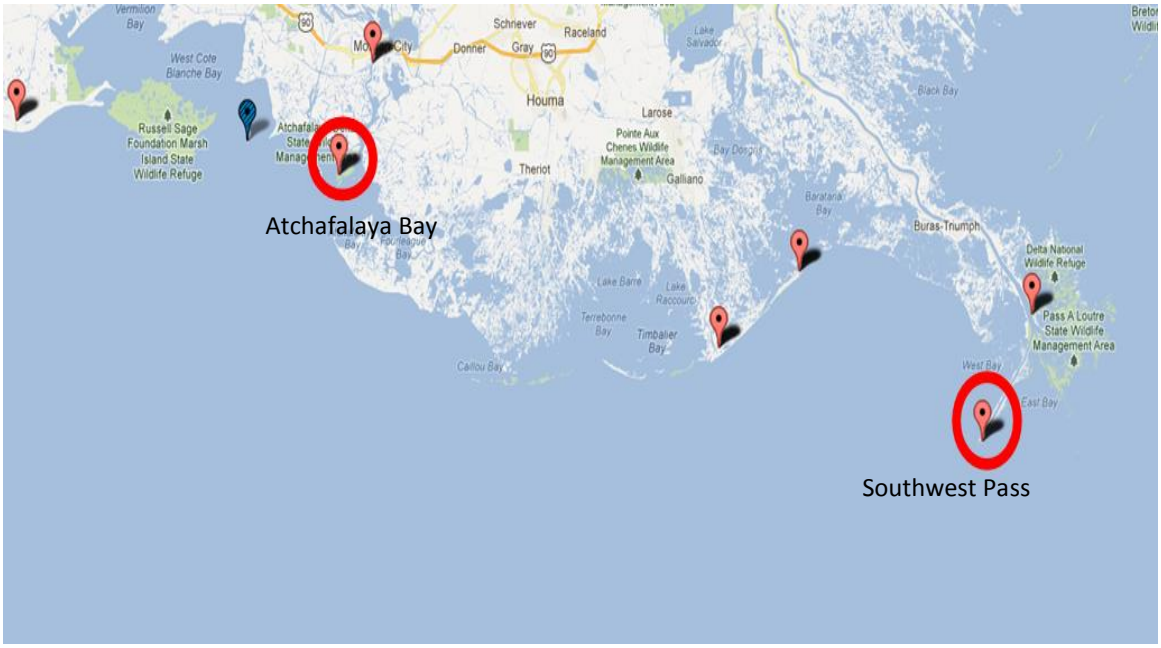

Figure 3.8: Stations used for tidal level comparison (red circles).

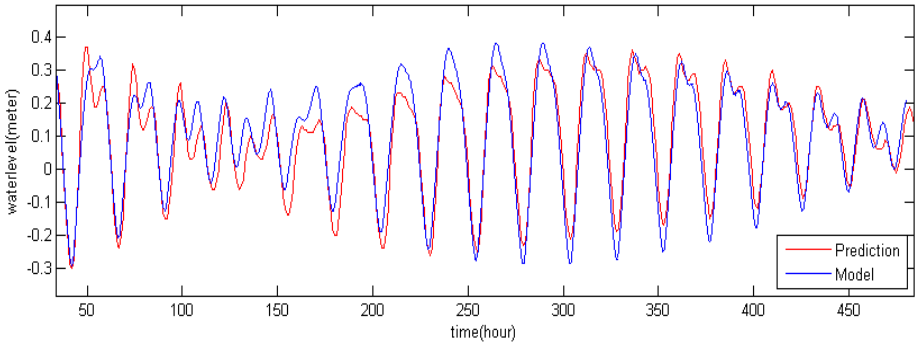

Figure 3.9: Comparison between simulated and predicted tidal level at the station inside the Atchafalaya Bay.

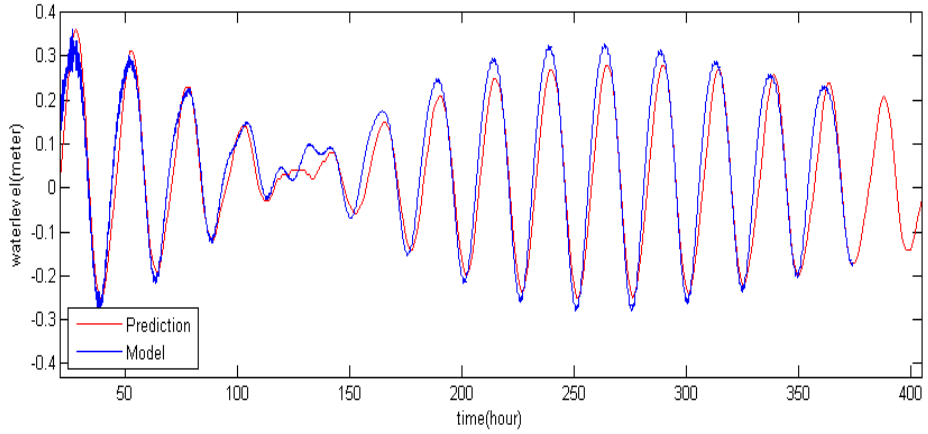

Figure 3.10: Comparison between simulated and predicted tidal level at the station in front of the Mississippi River Southwest Pass.

3.6.2 Evaluation of Hydrodynamics under both Wind and Tide

In evaluating the FVCOM model for the total currents, velocities at two of the WAVCIS stations, CSI-3 and CSI-6, were compared with the model results. When the default input coefficients for wind friction, bed friction, and background vertical eddy viscosity were used, the FVCOM results and measurements showed significant differences (Figures 3.11-3.14, upper panels). The main modification in modeling parameters was then using a constant value for the vertical eddy viscosity ($0.005 m^2/s$), as done in a former simulation using Mike3 (Allahdadi et al., 2011). This modification resulted in increased current velocity.

This is consistent with former studies pointing out the substantial effect of vertical eddy viscosity on circulation (Goodrich et al., 1987; Zhang and Steele, 2007). The results including the above mentioned modification are presented in Figures 3.11 to 3.14 (lower panels).

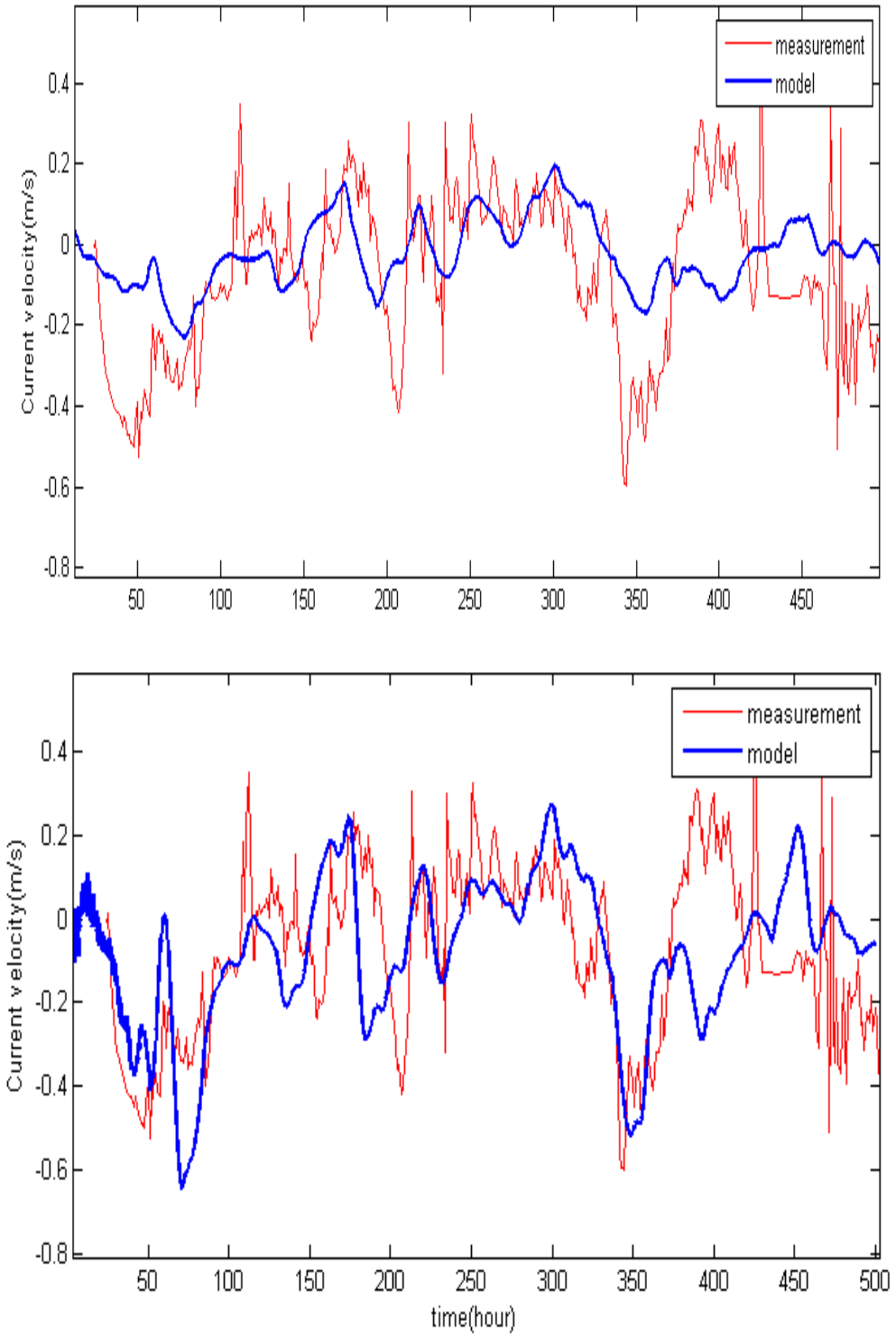

Figure 3.11: Model and measurement comparison for the east velocity component at CSI3. upper panel: using default setup, lower panel: with modifications.

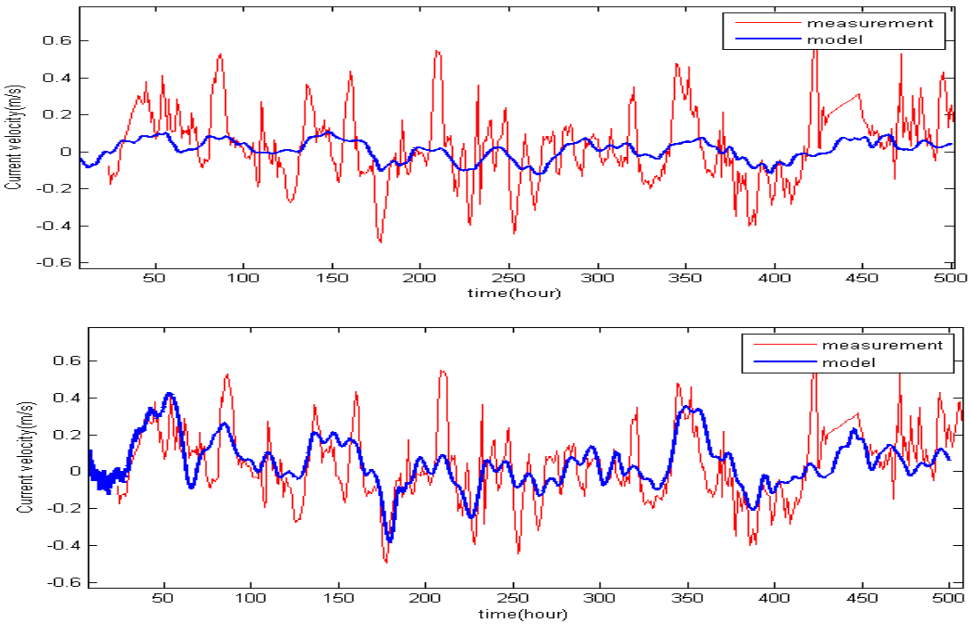

Figure 3.12: Model and measurement comparison for the north velocity component at CSI3. upper panel: with default setup, lower panel: with modifications.

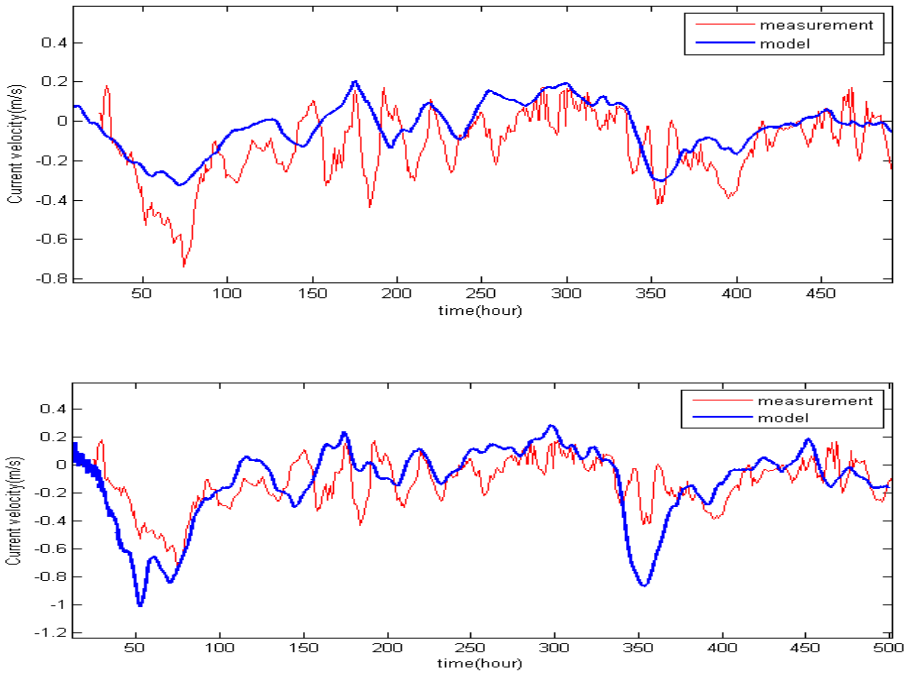

Figure 3.13: Model and measurement comparison for the east velocity component at CSI6. upper panel: with the default setup, lower panel: with modifications.

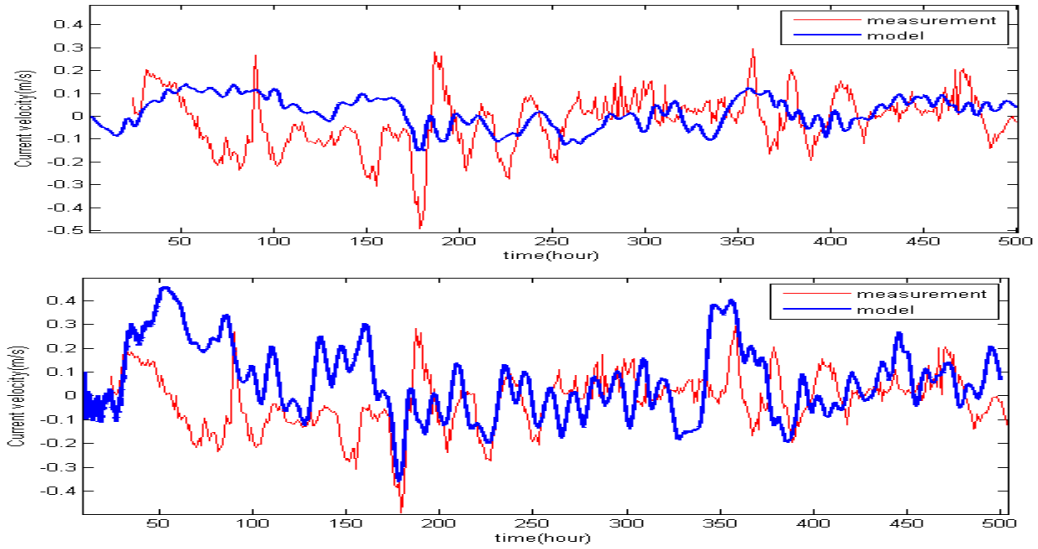

Figure 3.14: Model and measurement comparison for the north velocity component at CSI6. upper panel: with the default setup, lower panel: with modifications.

A sample of model results for simulated currents over the Louisiana shelf produced by northerly wind with speed of 12 m/s after 12 hours of simulation is presented in Figure 3.15.

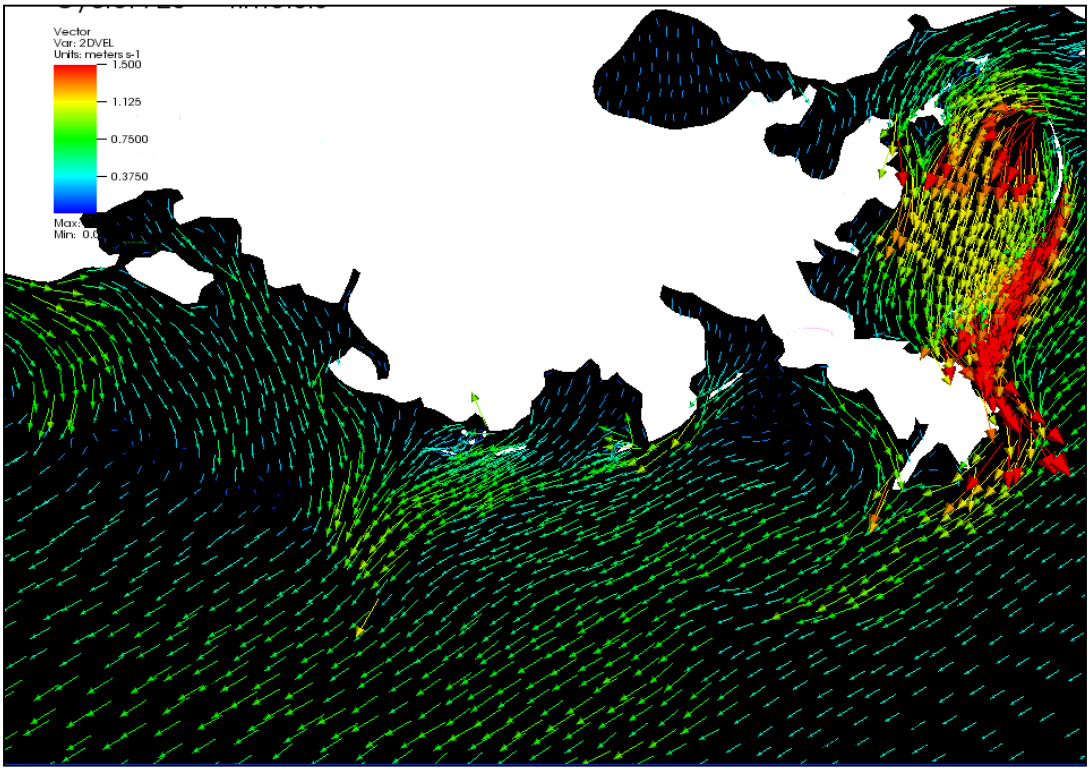

Figure 3.15: Simulated current field over the Louisiana shelf for northerly wind with speed of 12 m/s after 12 hours of simulation.

3.6.3 Evaluation for Katrina Induced Currents

3.6.3.1 Available Hydrodynamics Field Data during Katrina

During the hurricane, a number of WAVCIS (CSI) stations were operational for some time but most of them failed to measure currents when Katrina passed over the shelf. Only stations CSI-3 and CSI-6 (see Figure3.1 for locations) measured current data for several days before the hurricane reached the shallow Louisiana shelf and for several hours when Katrina was on the shelf. Water level data during Katrina were obtained at CSI-5 (Figure 3.1).

Figure 3.16 shows the vertical profile of measured current velocity components at CSI-6 during a six day time period before Katrina's eye reached the shelf. This station is located off the Terrebonne Bay where water depth is about 20 meters. The time series also contained several hours of currents when the shelf area was affected by Katrina. Currents were de-tided using tidal constituent analysis and results are presented for both east and north components. As shown, before the hurricane reached the shelf area (before 29 August), water column responded to the local forcing in two different ways. In many cases current velocities in the water column have approximately the same directions. However, there were several cases showing opposite flow directions between the upper and lower parts of the water column (black lines in Figure 3.16 for both velocity components). The measured velocity components at CSI-6 for different depths when the hurricane was over the shelf are shown in Figure 3.17.

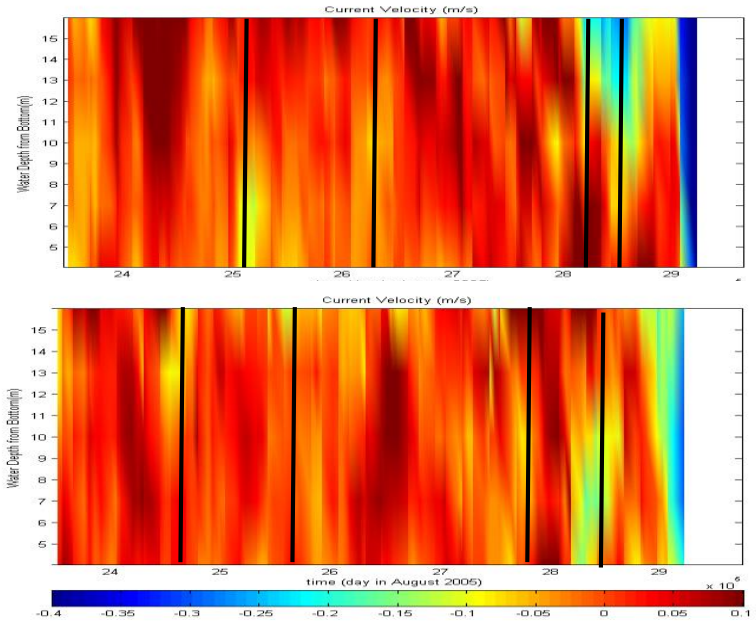

Figure 3.16: Vertical profiles of de-tided velocity components from CSI-6 before and during Hurricane Katrina. Upper panel: east component, lower panel: north component (black lines show cases with opposite directions between the surface and bottom currents).

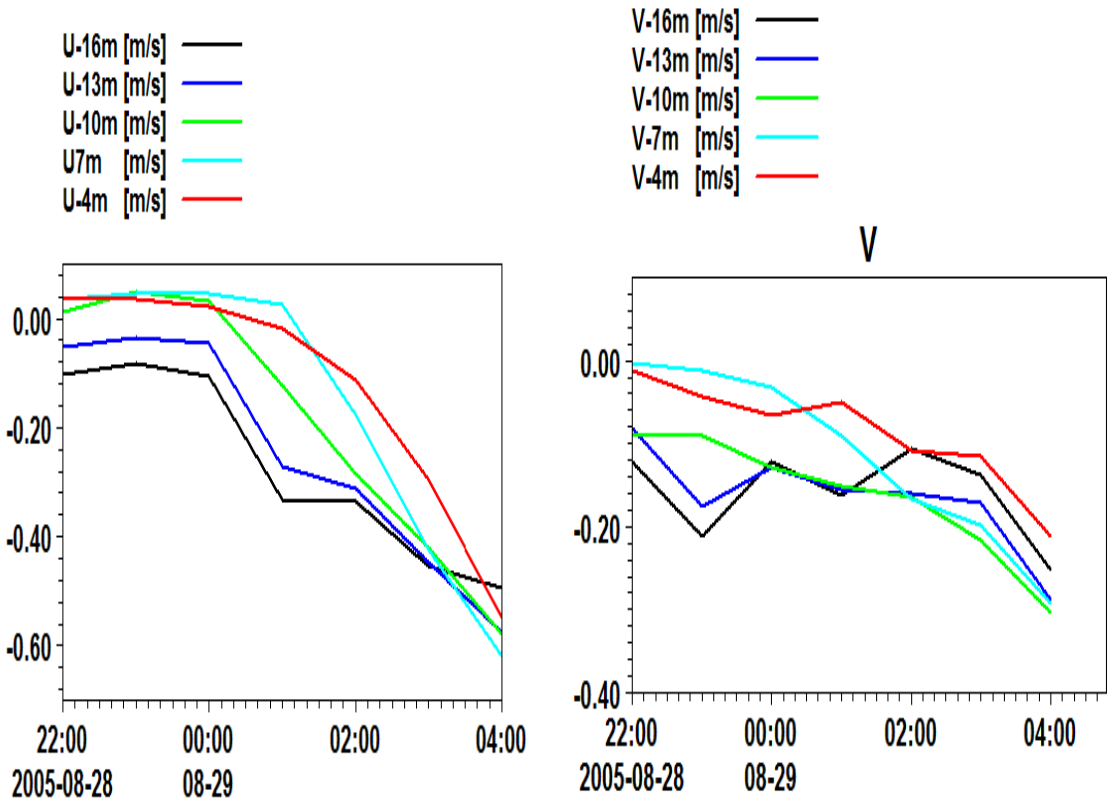

Figure 3.17: Time series of de-tided velocity components at different depths from CSI-6 when Katrina approached the Louisiana shelf.

3.6.3.2 Calibration Runs

As pointed out in section 3.6.2, the treatment of vertical eddy viscosity plays an important role in simulation of shelf hydrodynamics. This parameter controls the amount of energy redistribution to the water column for mixing. Several modeling studies addressed the effect of stratification on vertical turbulence (for example, Goodrich et al., 1987; Ly and Kantha, 1993; Keen and Glen, 1999, Zhang and Steele, 2007, Allahdadi et al., 2011). In addition to treating vertical eddy viscosity, parameters representing energy transfer rates also affect the model results. In the present study, three different scenarios were considered to examine the flow field produced by Hurricane Katrina:

A: simulation using an initially stratified water column and a constant value for the vertical eddy viscosity.

B: simulation using an initially stratified water column, but applying a turbulent closure (MY2.5) to calculate the vertical eddy viscosity.

C: simulation assuming no initial stratification, thereby constant temperature and salinity were assumed in water column (T=25 C, S=30 psu). Mellor-Yamada turbulent closure was used.

Not all of the above three simulations are realistic. For instance, ignoring water column stratification is contrary to the presence of a permanent thermocline in the deep ocean. Even over the shallow shelf this assumption is only valid when the hurricane eye is close (Keen and Glen, 1999). However, examining such scenarios can assist for a better understanding of stratification-turbulence interaction.For each case, different parameters were tried to obtain the best agreement with available measurements at CSI-5 and CSI-6. For case A, different values for the constant vertical eddy viscosity ranging from 0.003 m^2/s to 0 .05 were examined. The best match with field data was with 0.02 m^2/s. For case B, background eddy viscosity was used as the primary calibration parameter, which was varied between $0.001 m^2/s$ and $0.000001 m^2/s$. The surface currents were always smaller than data. It meant that the transfer rate of kinetic energy in water column was larger than reality. The rate of kinetic energy dissipation in the Mellor-Yamada closure is controlled by the following relationship:

$$\varepsilon = q^3/(B_1 l) \tag{3.19}$$

where ε is the rated of kinetic energy dissipation, and *B1* a coefficient between 12 and 25 (Keen and Glenn, 1998). However, the value had to be taken as low as 8 to agree with the measurements for the surface currents. Best turbulence model parameters for each case are summarized in Table 3.3.

Table 3.3: best fit model parameters.

Simulation Case	Approach for Vertical eddy Viscosity	Background/constant viscosity (m2/s)	B1
A	Constant value	0.02	-
B	Closure (MY2.5)	0.00001	8.00
C	Closure (MY2.5)	0.00001	8.00

With the limited available field data, the best agreement was obtained for the case assuming a pre-stratified water column along with a turbulent closure for treating vertical eddy viscosity (case B). Figure 3.18 shows the comparison between the model and measured water level and velocity at CSI-5, CSI-6, and CSI-3. Simulated water level at CSI-5 reproduced the 0.7 m water level drop induced by the hurricane at this location. Model results at CSI-6 were satisfactory with a similar trend, and while at CSI-3, some significant differences were seen. The main reason is probably due to the shallowness of the station (~5m) and the fact that CSI-3 is far from the hurricane center (about 250 km): currents at this location can be affected by local winds fluctuations which were not included in the single vortex hurricane wind model.

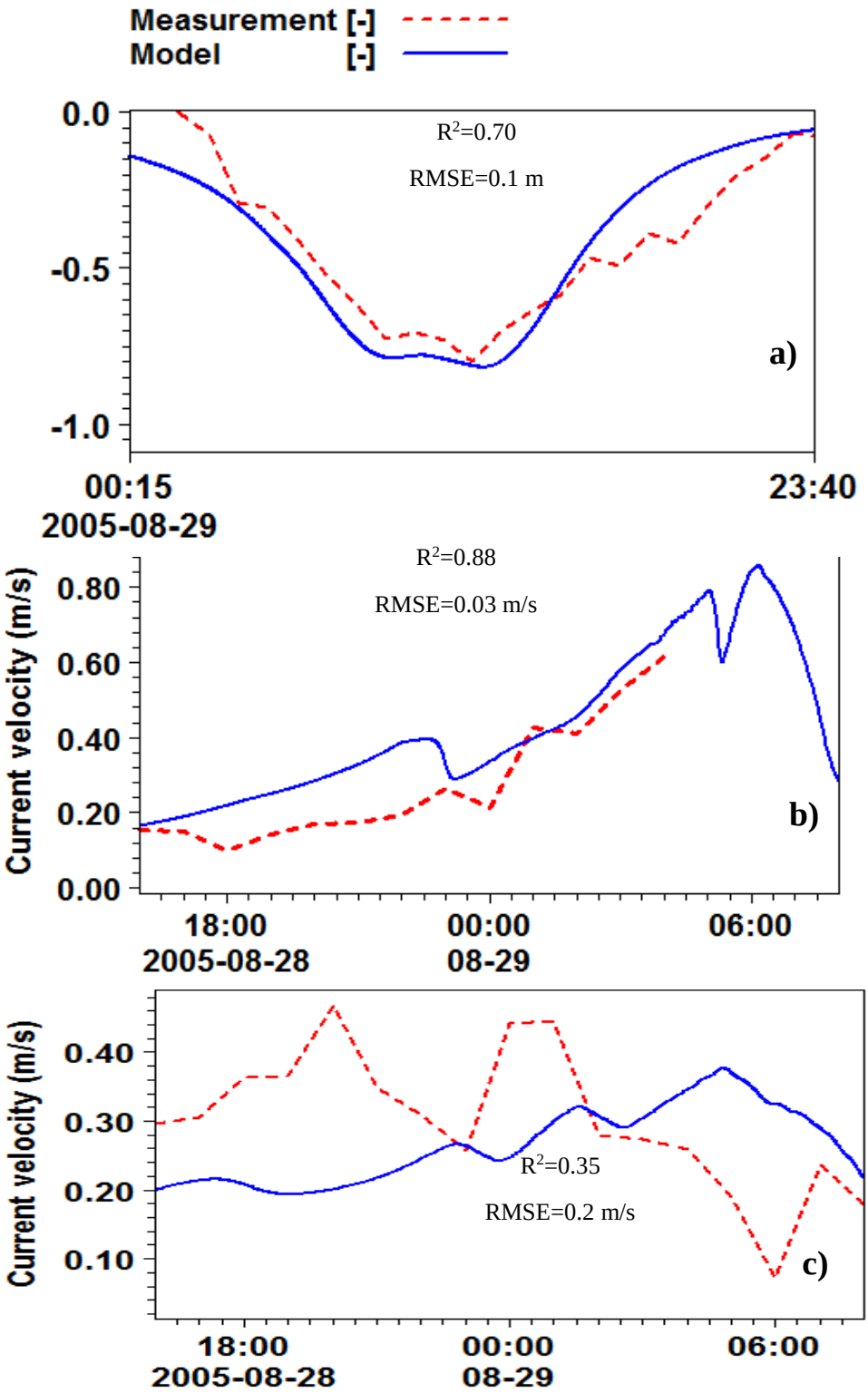

Figure 3.18: Comparison between model and data for a) water level at CSI-5, b) current speed at CSI-6, and c) current speed at CSI-3.

3.7 Simulation Results for Case B

3.7.1 Current Pattern

The simulated near-surface velocity vectors for case B are presented in Figure 3.19 for different times in the morning of 29 August 2005 (UTC time) when Hurricane Katrina was approaching the Birds-foot delta and subsequently made its landfall. Results showed that at 7:00, the surface currents over the deep water south of the Birds-foot delta followed a spatial pattern similar to that of the hurricane wind. A cyclonic gyre was created under the hurricane with northward currents in the east of the track and southward currents in the west, implying the predominant effect of wind stress on near-surface currents.

The strongest currents were observed at locations east of the hurricane track, consistent with the right-front side intensification due to the forward movement of the hurricane (e.g., Sanford et al., 1987; Church et al., 1989; Price et al., 1994). As a category 4 hurricane at this time, it strongly affected the surface currents over the shallow Louisiana shelf including areas off Barataria and Terrebonne Bays where southwestward to southward currents reached 1 m/s.

The shelf was located on the left-side of Katrina's track at this time and prior to the final landfall in the northern Gulf of Mexico. Hence, as a result of persistent northerly to northeasterly hurricane winds, southward to southwestward currents were dominant over the shelf during the hours that Katrina translated the outer and inner shelves.

The shallow shelf east of the delta was also affected by the strong easterly hurricane winds and at this time, the entire area between Chandeleur Island and the Birds-foot delta experienced relatively strong westward currents. As Katrina progressed northward within the next two hours, it was about to degrade to a category 3 hurricane and the current speeds generally decreased.

At 9:00 when the eye was located just south-west of the Birds-foot delta, strong northwestward currents with speeds up to 1.5 m/s were produced along the western side of the delta. In the next two hours, the direction of current changed to westward and then southwestward following the hurricane's wind field structure while the maximum velocity decreased to less than 1 m/s. Offshore of the Terrebonne Bay, a wake of this current joined the southward current leaving the Bay.

At the time of the first landfall at the Grand Isle LA, the response of the shelf west of the delta was a cyclonic gyre exhibiting stronger currents at the western limb. At the same time northwestward currents (parallel to the Birds-foot delta) appeared east of the delta and were extended over the entire eastern shelf one hour later. At the landfall over the Birds-foot delta and later over the mainland (at 11:00 and 12:00, respectively), the modeled wind was eastward and the currents were southeastward over the Louisiana shelf which were affected by the local bathymetry and geometry. At 11:00, the surface currents at the mouth of Terrebonne Bay and further offshore veered southeast as a result of the wind direction change as the hurricane moved,

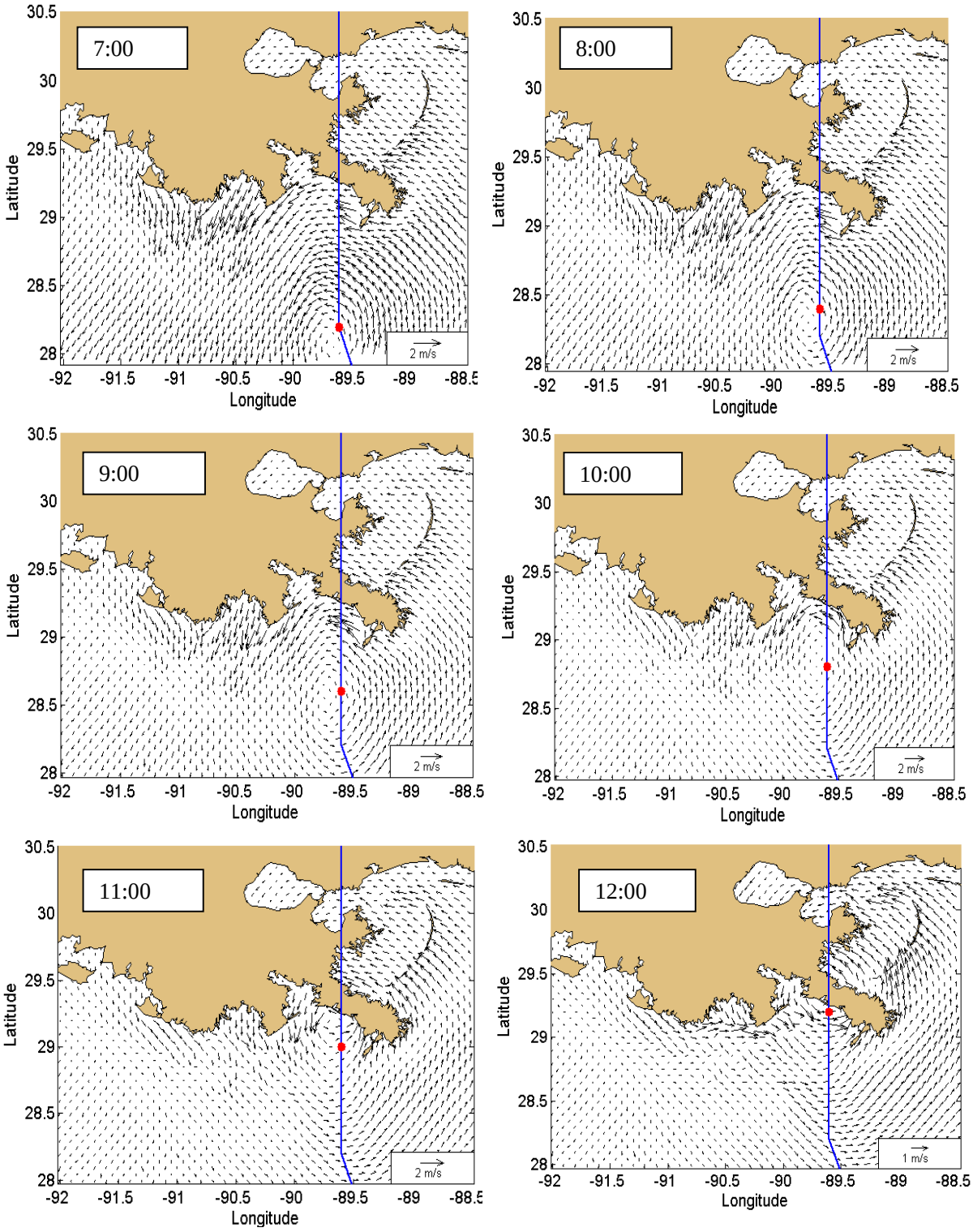

Figure 3.19: Simulated near-surface currents induced by Hurricane Katrina for case B and different hours on 29 August 2005 (the solid line represents hurricane track and the circle shows the location of hurricane's eye).

while currents off Barataria Bay remained southward due to its proximity to the hurricane track. At 12:00, the surface currents in front of the Terrebonne Bay turned to the east while off Barataria, the surface currents changed directions to the east and southeast. The near-bottom flow field in the area (Figure 3.20) is compared with the near-surface currents (Figure 3.19).

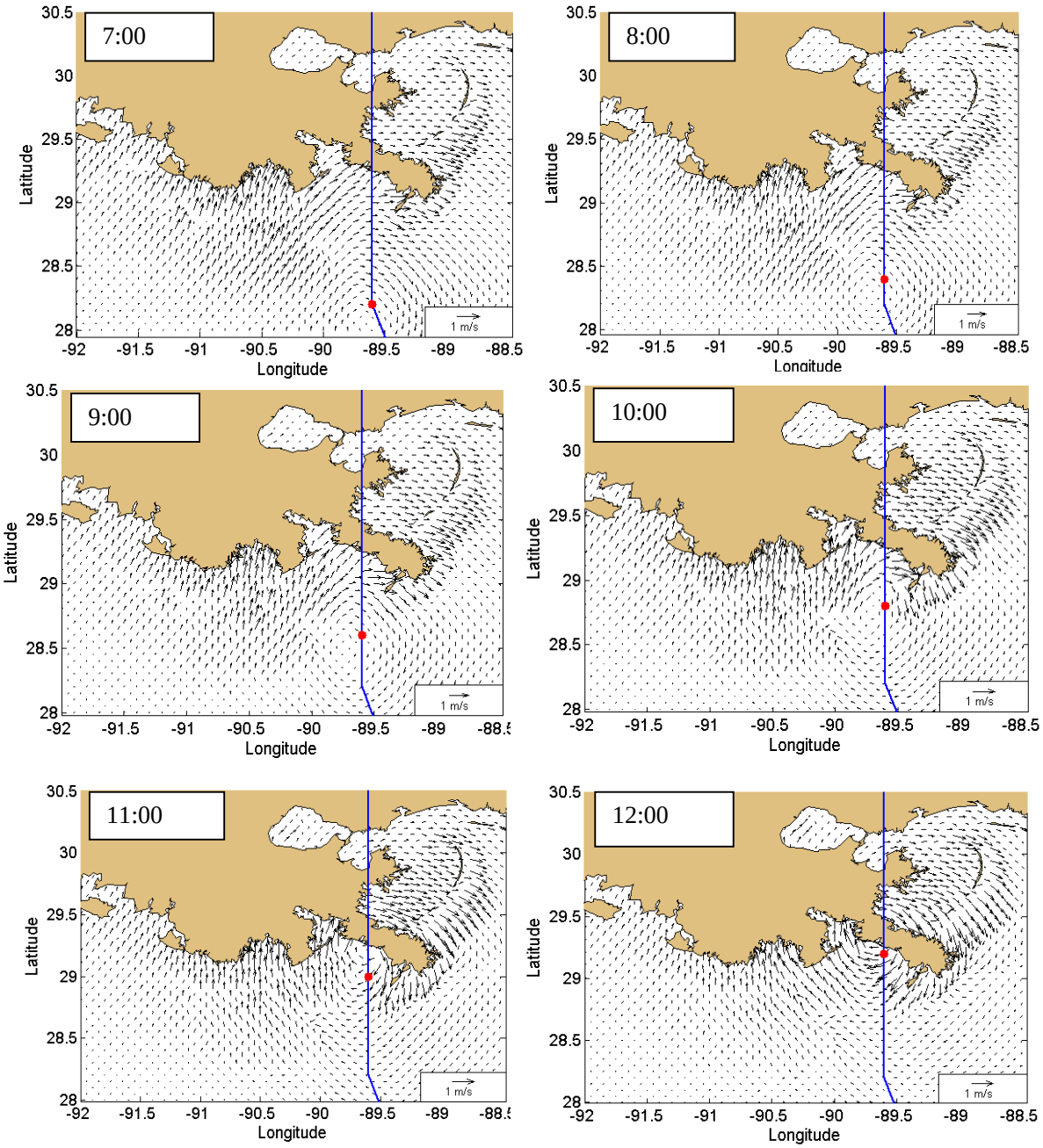

Figure 3.20: Simulated currents along the bottom sigma layer induced by Hurricane Katrina for case B and different hours on 29 August 2005 (11:00 UTC is the landfall time over the Birds-foot delta).

Contrary to the surface currents that generally follow the hurricane wind pattern, the bottom currents were less consistent with the wind field, both temporally and spatially. Over both inner and outer shelves, the bottom/deep water currents showed opposite directions in comparison to the surface currents.

At 7:00, the deep water response to the cyclonic near-surface gyre (thereby to the hurricane wind field) generated offshore of the Birds-foot delta, was an anti-cyclonic gyre with larger currents at the eastern side. Over the Louisiana shelf and at the shelf break, currents were generally northward with a maximum current speeds of about 0.8 m/s at the Terrebonne Bay's entrance.

Offshore of the Barataria Bay, currents veered northeast and became a part of the western limb of an anti-cyclonic gyre over the shelf west of the Birds-foot delta, while a maximum current speed over the western limb reached 0.4 m/s.

The Louisiana shelf west of the Birds-foot delta was not the only inner-shelf area exhibiting opposite directions for surface and bottom currents. Bottom currents over the shallow shelf east of the delta also showed reverse currents.

At 11:00, when the hurricane's eye was located approximately 20 km west of the southwest pass, coastal and offshore bottom currents at the Barataraia and Terrebonne Bays and further west to the Atchafalaya Bay completely turned to the north. The anti-cyclonic gyre previously formed west of the Birds-foot delta, was substantially decreased in size and was confined between the delta, shelf break, and the northward current flowing toward the Barataria Bay.

The gyre almost disappeared at 12:00, the time of the final landfall. Southwestward deep water currents up to 0.8 m/s were produced along the delta at this time. The response of bottom currents offshore of Barataria Bay to the hurricane wind at this time was northwestward, reaching the maximum speed of 0.5 m/s, while currents over the Terrebonne Bay and its offshore areas did not change much.

The bottom currents generated over the shallow eastern shelf at this time were mostly southeastward to southward. Along with the southwestward current at the delta, and the northwestward current at the mouth of the Barataria Bay, the current over the eastern shelf showed as an anti-cyclonic gyre whose eastern and western limbs were separated by the Birds-foot delta.

For two different times when the hurricane's eye was present over the outer and inner shelves, the average direction of surface and bottom currents over different regions of the inner-shelf are compared in Table 3.4.

Table 3.4: Average direction of surface and bottom currents over different regions on the Louisiana shelf for two different locations of Katrina.

29 August 7:00 (UTC)		
Region	Surface	Bottom
Off the Atchafalaya Bay	South	Northeast
Off the Terrebonne Bay	South to Southwest	North to Northeast
Off the Barataria Bay	Southwest	Northeast
Off the Birds-foot delta	Northwest	Southeast
West of the Birds-foot delta	West	East
29 August 11:00 (UTC)		
Region	Surface	Bottom
Off the Atchafalaya Bay	Southeast	North
Off the Terrebonne Bay	South	North
Off the Barataria Bay	Southwest	North
Off the Birds-foot delta	North	South

3.7.2 Temporal Variations of Currents

To examine the temporal variations of currents induced by Katrina over the Louisiana shelf, time series of simulated surface currents are analyzed at several locations (Figure 3.21).

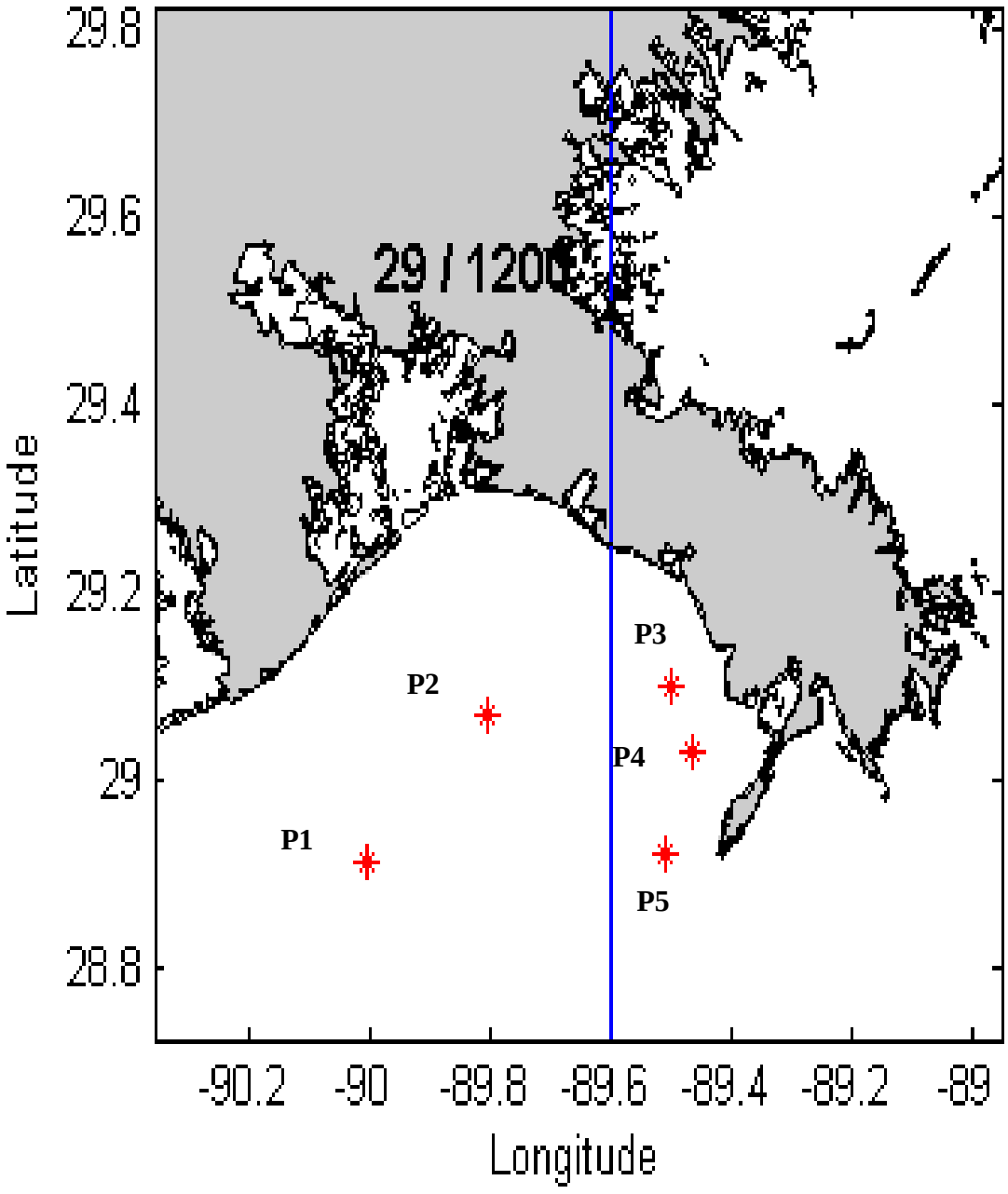

Figure 3.21: Locations of surface current time series.

These locations are selected from both sides of the hurricane track: two on the left and three on the right (Figures 3.22a and 3.22b). Results examined were from almost an 80 hour time period, including 55 hours prior to the time the hurricane's passage and about 25 hours thereafter (negative values on the time axes represent times before hurricane's eye reached this location and positive values show times after this position). Station P1 is located off the Barataria Bay about 45 km (1.2 RMW) west of the track and the water depth is about 33 meters. At time -50 hours (more than two days before the hurricane's eye reached the Louisiana shelf), there was only small southwestward currents. Current speed increased gradually for several hours before time zero, when a significant increase in current speed up to 0.85 m/s occurred.

Current speed decreased as hurricane's eye traveled further northward and its distance from P1 increased. Current speed reached another peak two hours after the main peak which was more likely due to the eastward current produced over the shelf during and after the landfall over the Birds-foot delta. All the variations in current speed were associated with a counterclockwise rotation of the flow. The hurricane induced currents at this location almost disappeared at Hour 25. For station P2 located on the left side of the track and south of the Barataria Pass (depth ~30 meter), the overall temporal variation of velocity was similar to that at station P1, i.e. showing a counterclockwise rotation of the flow and a peak in current speed almost at the time that the eye is closest to the station. The maximum velocity of about 0.7 m/s is smaller than that at station P1, which can be attributed to its location being at the distance of 0.6Rmw from the eye. The velocity variations on the right side of the track are significantly different in magnitude.

The maximum current speed at station P3 is about 2 m/s (Figure 3.22a). This station is located on the right side of the track mid-way between the Birds-foot delta at a distance of about 10 km from the track (water depth is about 12 meters). The current speed increased from 0.5 m/s at Hour -10 to about 2 m/s at time zero and decreased to very small values by Hour 20. Unlike the left side of the hurricane track, the velocity vector rotates in the clockwise direction. A similar pattern was observed for variations of currents at P4 located northwest of the Southwest pass with water depth of 16 meters.

The maximum current speed at this station was more than 3 m/s. There are two reasons for the increased velocity at stations located on the right side of the track: first, the rightward – bias as a result of the superposition of clockwise wind vector on the right side of the eye combined with the movement of the hurricane; second, the effect of the Birds-foot delta as a confining boundary.

The effect of the delta for the intensification of current velocities can be further investigated by examining the modeled velocity at a location on the right side of the track, but at the south of station P4 where the effect of the delta cannot be significant (station P5). As Figure 3.22b shows, the maximum current speed at this station was about 1 m/s, while the rotation of the flow field was the same as stations P3 and P4. The temporal variations of simulated velocity at all the above stations are shown in Figure 3.22b.

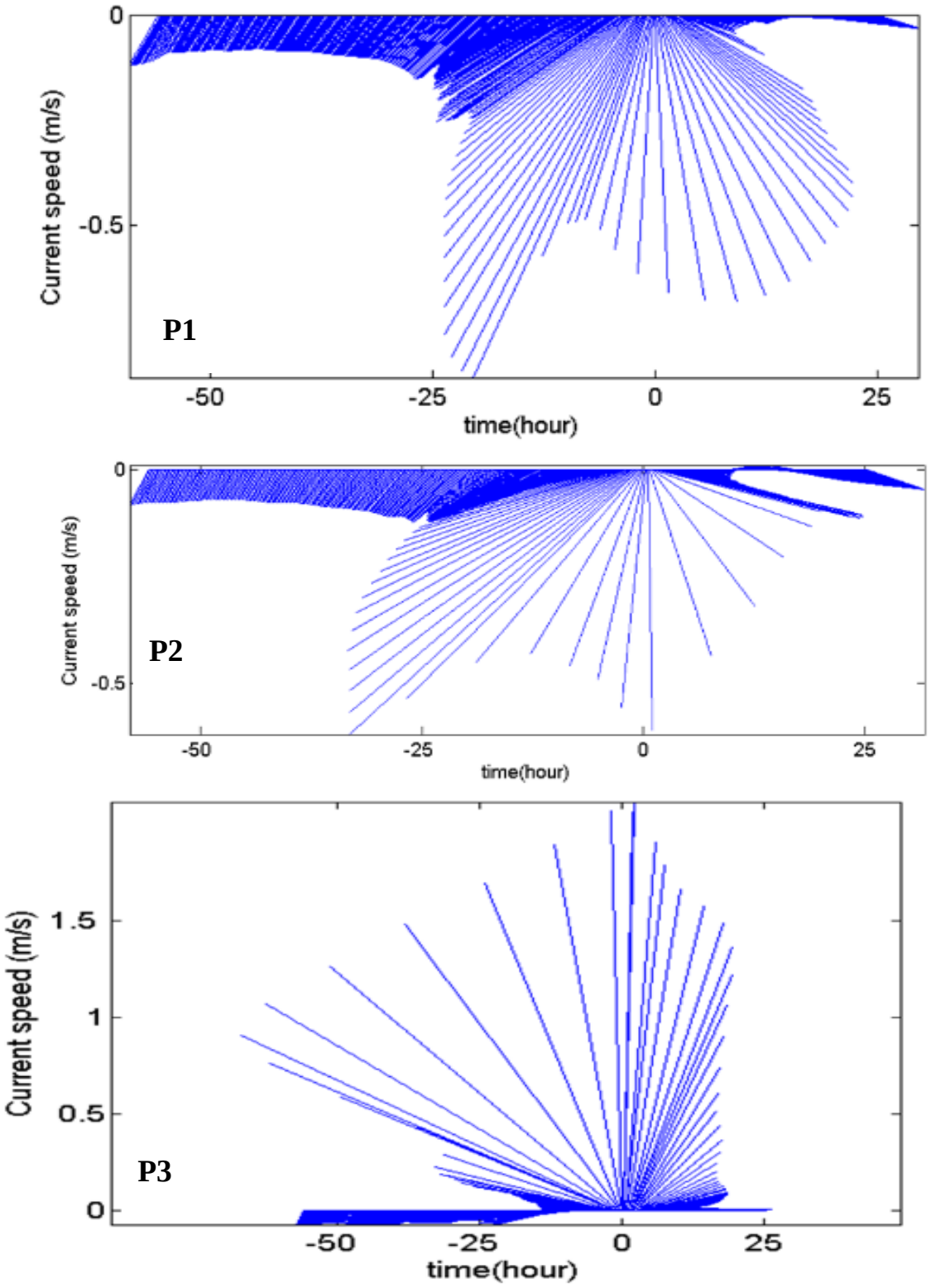

Figure 3.22a: Time series of simulated currents at stations at different stations.

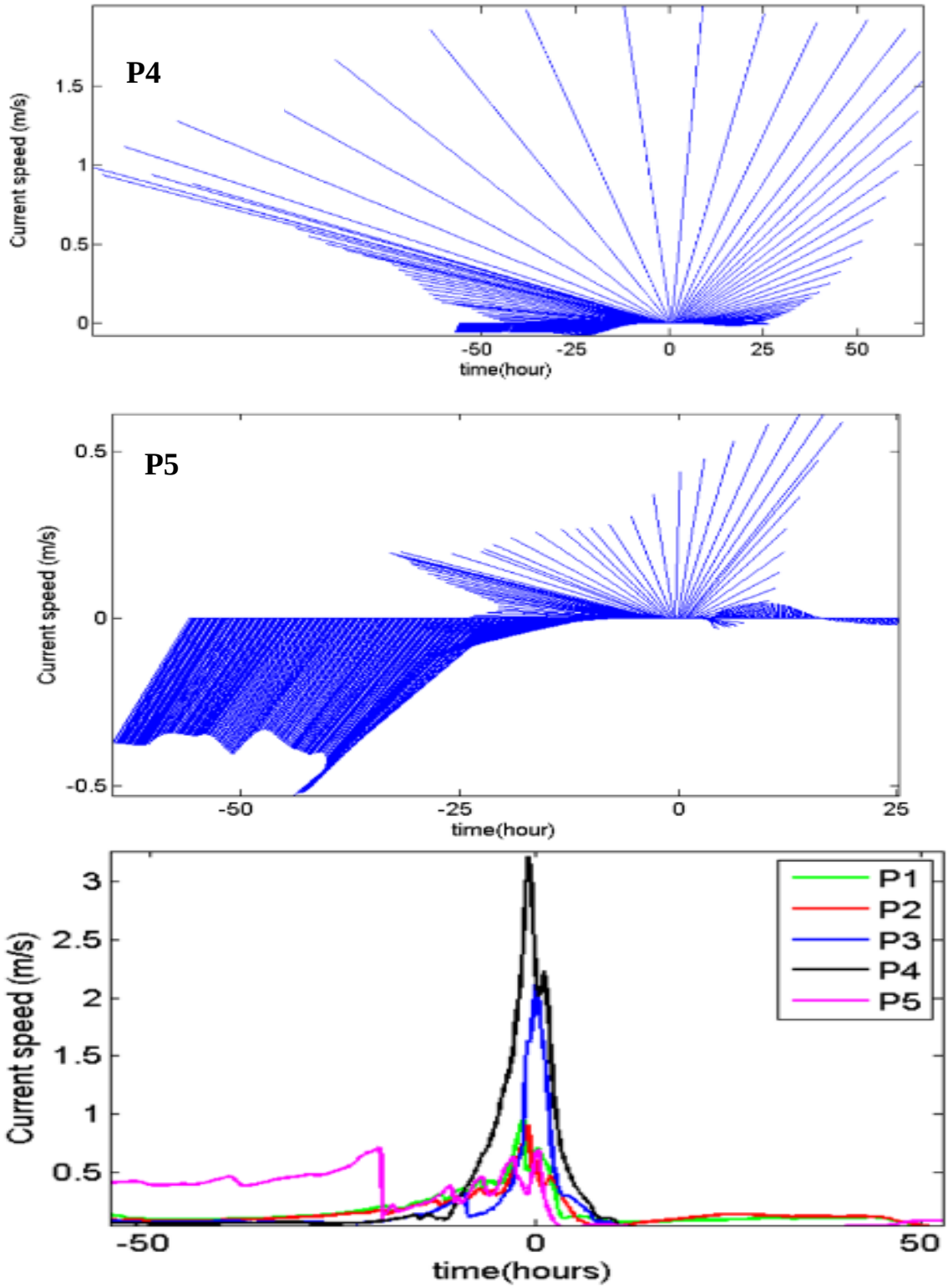

Figure 3.22b: Time series of simulated currents at stations at different stations.

3.7.3 Vertical Current Structure

The vertical profiles of temperature, salinity, and currents determine the gradient Richardson number as a criterion defining the strength of water column stratification. To investigate the response of the water column over the Louisiana shelf to Hurricane Katrina, four north-south transects were considered as shown in Figure 3.23. Transect A has the largest distance from the hurricane track west of the Birds-foot delta, while transect D is right in front of the Barataria Bay experiencing largest wind speeds among all transects. For each transect the currents are presented when the current reached its peak during Katrina.

Vertical current structure along Transect A over the shallow shelf in front of the Atchafalaya Bay is shown in Figure 3.24. Although the snapshot has been taken at the time of the maximum current speed, the current speed was only ~ 0.25-0.5 m/s over the depth less than 10 meter and smaller than 0.1 m/s over the deeper waters due to the distance from the hurricane track (over 200 km). The velocity shear was small. However, over the smaller water depths (5-10 meters) an abrupt change in current direction occurred in the mid-depth. While surface currents were toward offshore, mid-depth and bottom currents flowed shoreward. This created large horizontal shear at the level of direction change.

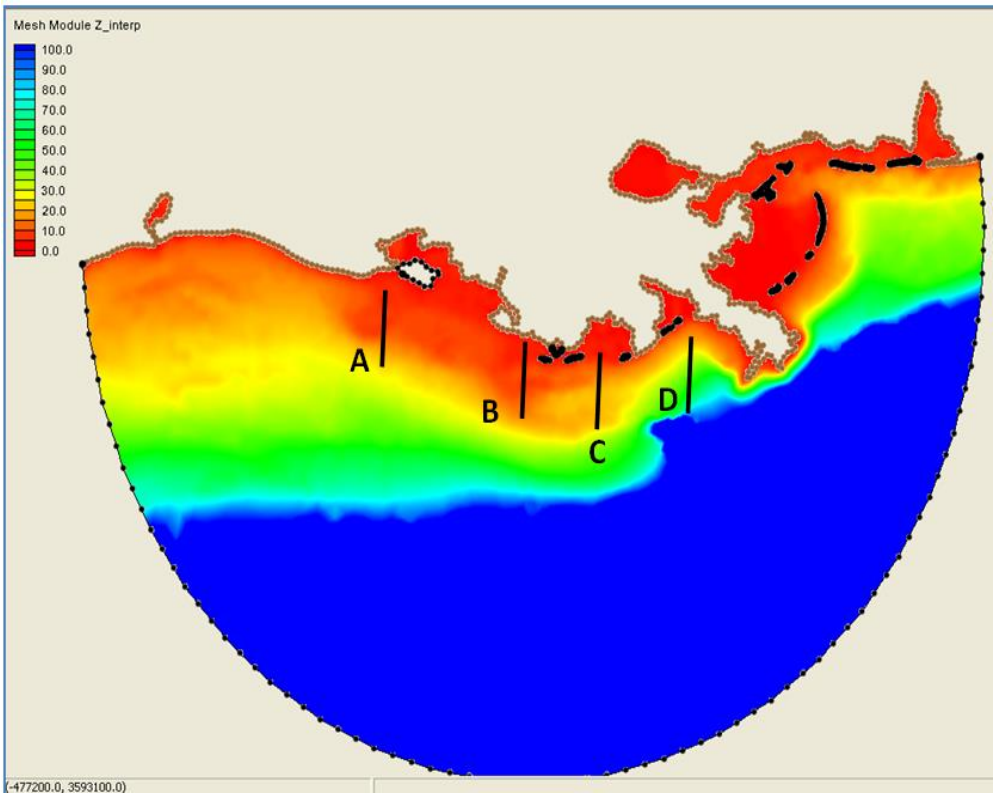

Figure 3.23: Location of transects to examine vertical current structure over the Louisiana shelf.

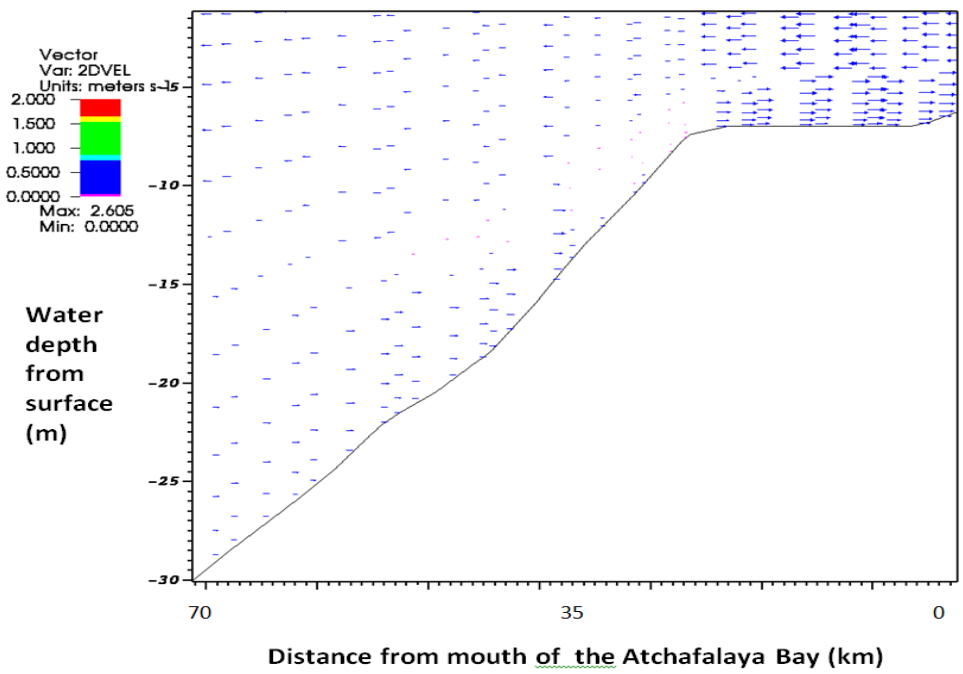

Figure 3.24: Simulated currents across transect A at 11:00UTCon 29 August 2005.

Current speeds corresponding to the peak of Katrina over the shelf, across transect B, located between the Atchafalaya and Terrebonne Bays, were 0.5-1.5 m/s over water depths smaller than 20 meter and less than 0.5 m/s for greater water depths (Figure 3.25). While current direction was toward offshore across the whole water column for water depth less than 7 meter, flow direction was reversed almost in the mid-depths for water depths 7-25 meters. The vertical shear of horizontal currents was not significant except close to the depth where the flow changed direction (almost at the mid-depth). The vertical current structure for transect C (Figure 3.26) extending from the mouth of the Terrebonne Bay to 60 meter waters showed opposite flow directions all along the transect and there were levels of flow reversal at all points along the transect. This is consistent with Figure 3.16 showing a similar response of water column in station CSI-6 at water depth 20 meter along this transect from measurements.

As demonstrated based on simulation results, the response of the water column over the Louisiana shelf to Hurricane Katrina had strong vertical shears, different from some other studies (Keen and Glen, 1998; Keen and Glen, 1999). Comparison of response to Hurricane Katrina and Andrew suggests that the main reason for the difference in behavior would be the track of Hurricane Andrew being crossing the middle of the Louisiana shelf. Hence, the shallow areas over the shelf experienced large wind stress in the vicinity of the hurricane eye wall and the water column responded with a uniform velocity profile. In contrast to Andrew, Hurricane Katrina affected deeper areas close to the Mississippi Birds-foot delta and the wind was not strong enough to move the entire water column together and produce a uniform response.

Flow reversal for transect D (Figure 3.27) in front of the Barataria Bay was at 12-20 meter, similar to transect C. Across this transect, currents peaked at 11:00 when the hurricane was in closest to the transect, when the flow speed reached 3 m/s.

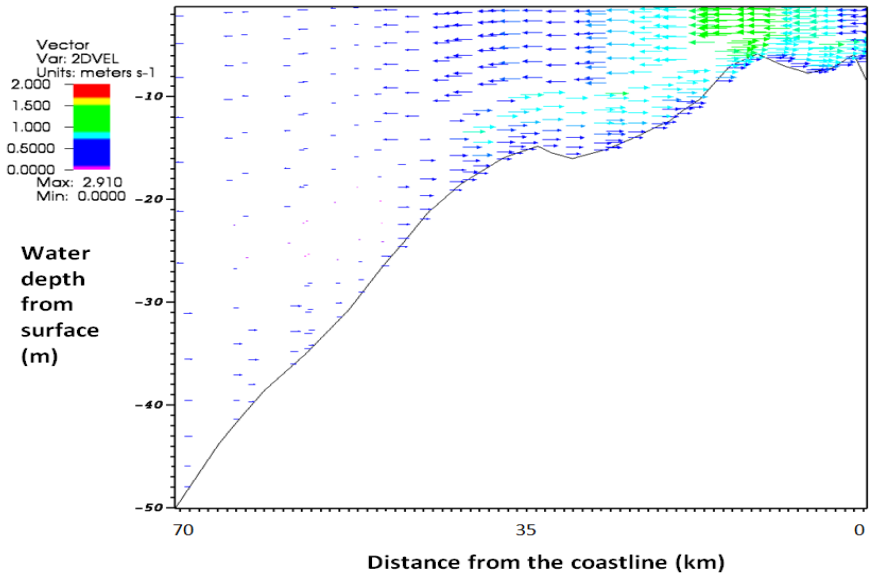

Figure 3.25: Simulated currents across B at 6:00 UTC on 29 August 2005.

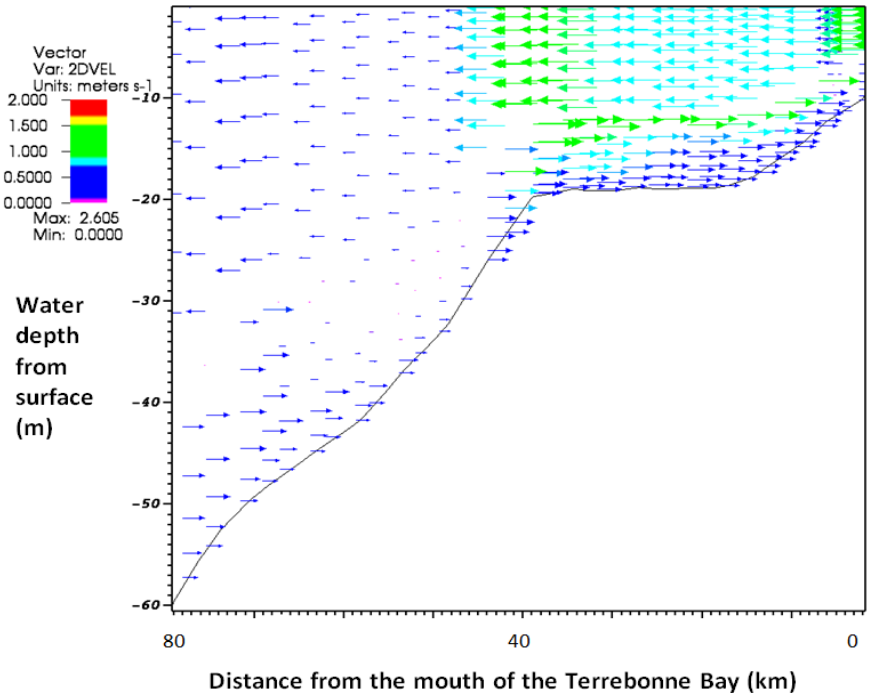

Figure 3.26: Simulated currents across C at 6:00 UTC on 29 August 2005.

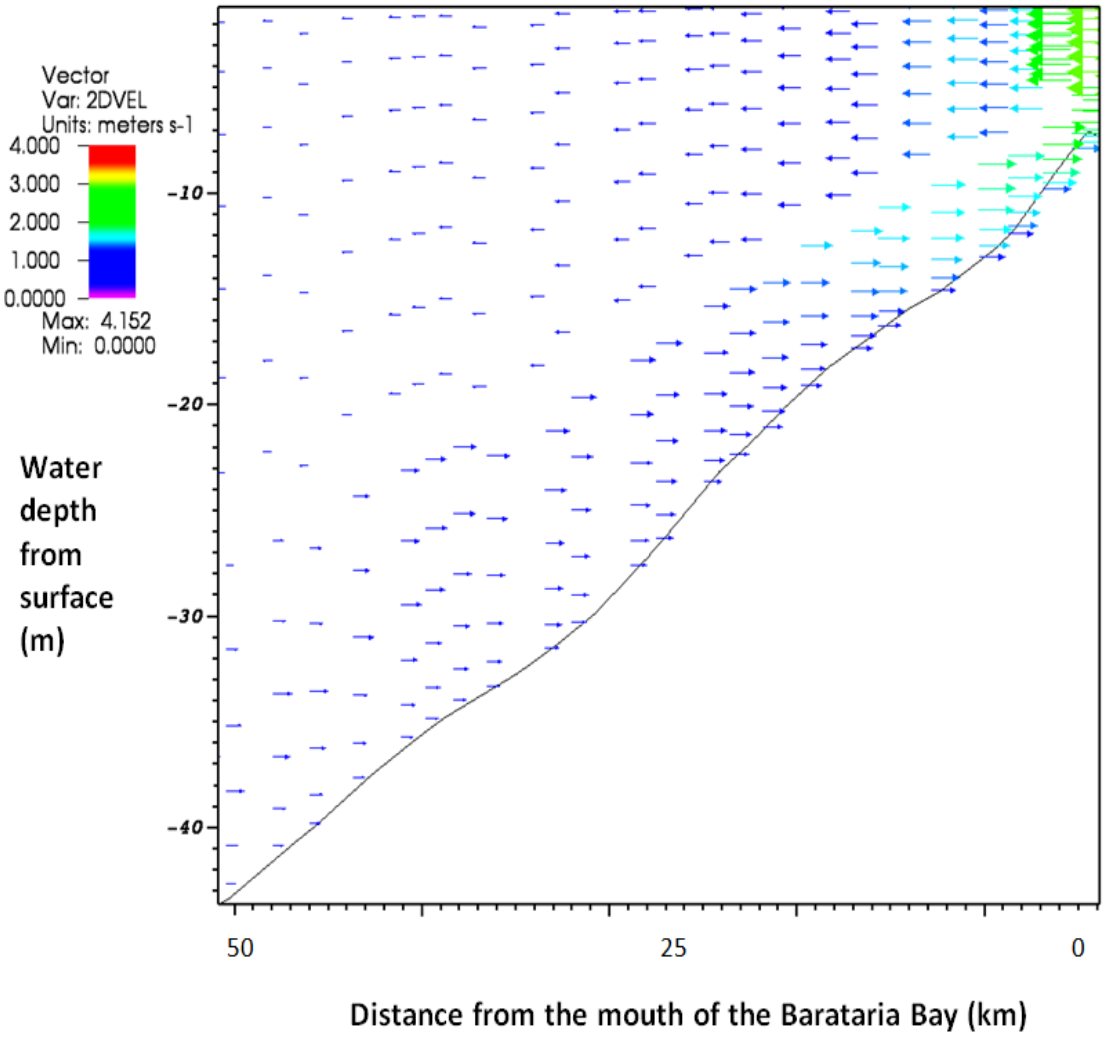

Figure 3.27: Simulated currents across D at 6:00 UTC on 29 August 2005.

3.8 Discussion

Hydrodynamic responses of shelf waters are quite complicated during a hurricane (Ly, 1994; Mitchel et al., 2005). The response is a function of hurricane's eye position on the shelf as well as its forward speed and the maximum sustained wind speed (Mitchel et al., 2005; Wang and Oey, 2008). All three parameters (eye's position, forward speed, and the maximum sustained wind speed) affect the stratification (Keen and Glenn, 1999). The effect of stratification on the flow pattern was optimized by examining different scenarios for shelf stratifications and different variables for parameterizing vertical mixing through the calibration procedure (section 3.6.3.2). The non-uniform response of deep water currents (which corresponds to the reverse current directions at the surface and bottom) to Hurricane Katrina as a result from the present numerical experiment is consistent with the previous findings about the water column response in deep

regions to a moving hurricane (Cooper and Thompson, 1989a; Cooper and Thompson, 1989b; Mitchel et al., 2005; Teague et al., 2007). The response of shelf-break and shallow shelf regions can be either uniform or non-uniform depending on the intensity of the hurricane and the location of eye (Cooper and Thompson, 1989b; Mitchel et al., 2005; Teague et al., 2007). For several category 4 and 5 hurricanes, it was reported that the region within 1 R_{mw} from the center of hurricane showed a vertical uniform response over the mid-depth and shallow waters (Keen and Scott, 1999; Teague et al., 2007).

The intense hurricane wind stress mixes water column and completely destroys the stratification. As a result, surface Ekman layer is coupled to the bottom boundary layer causing a uniform response (Mitchel et al., 2005). Outside of this interior region, mixing weakens and stronger stratification prevents a mixing all the way to the bottom. During the time that Hurricane Katrina was present over the Louisiana shelf until the landfall, most regions over the shelf were out of the interior mixed region. The regions offshore of the west side of the Barataria Bay were within 1.2-1.5 R_{mw} distance from the hurricane center, while for Terrebonne Bay and its offshore regions this distance was 2.5-5 R_{mw}. Over these regions especially Terrebonne Bay, the wind speed and the associated mixing decreased significantly (Figure 3.28). Hence, the stronger shelf stratification decoupled the surface and bottom Ekman layers. The non-uniform response of water column at CSI-6, off the Terrebonne Bay was also illustrated in Figure 3.16 during several days before Katrina reached the inner-shelf when fair weather condition was dominant and mixing over the shelf was weak. Shelf behavior during the small hurricane winds is similar. Although for regions just east and west of the hurricane track a uniform response was expected, the larger depths compared to the shallower Louisiana shelf and degrading Katrina to a Category 3 hurricane caused a non-uniform response in the water column. The reversal of flow directions between the surface and bottom over the shallow shelf east of the Birds-foot delta can be described in a similar way.

The flow velocity is also affected by vertical eddy viscosity (Zhang et al., 2007). Although appropriate parameters representing Mellor-Yamada turbulent closure were selected based on the limited available field data, model performance for the simulation of maximum speed is dubious. Applying the turbulent closure is more reasonable in including the 3-D variations of vertical eddy viscosity. However, our sensitivity simulations showed an underestimation of the peak velocity due to large rates of surface energy dissipation associated with the closure scheme. Simulation with constant values of vertical eddy viscosity can result in current speed twice as large as those from the turbulence closure approach (Figure 3.29).

In addition to the vertical stratification, the inhomogeneous cooling caused by a hurricane can contribute to the non-uniform shelf response during Katrina. The vorticity field caused by a baroclinic pressure gradient thus produced can form anti-cyclonic gyres beneath the mixed layer after the hurricane is dissipated (Pan and Sun, 2005). This can explain a part of the non-uniform response of the Louisiana shelf during Katrina.

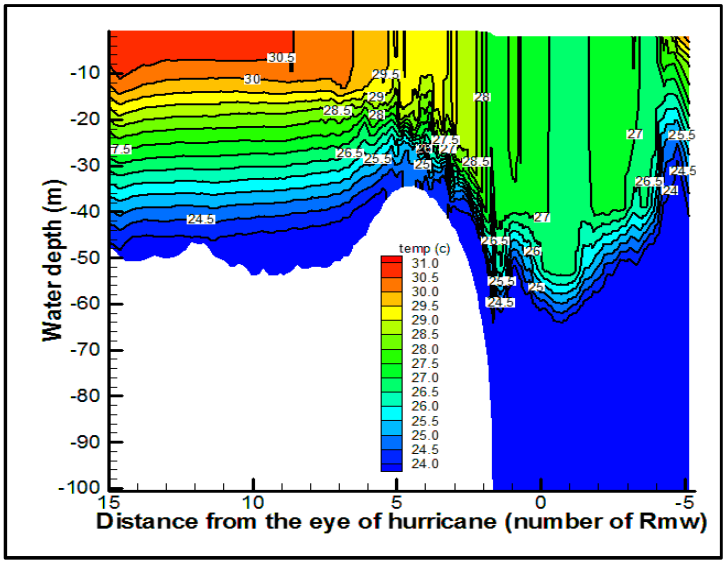

Figure 3.28: Vertical temperature structure across an east-west section over the Louisiana shelf at 10:00 UTC on 29 August 2005 (section 1 in Figure 3.1).

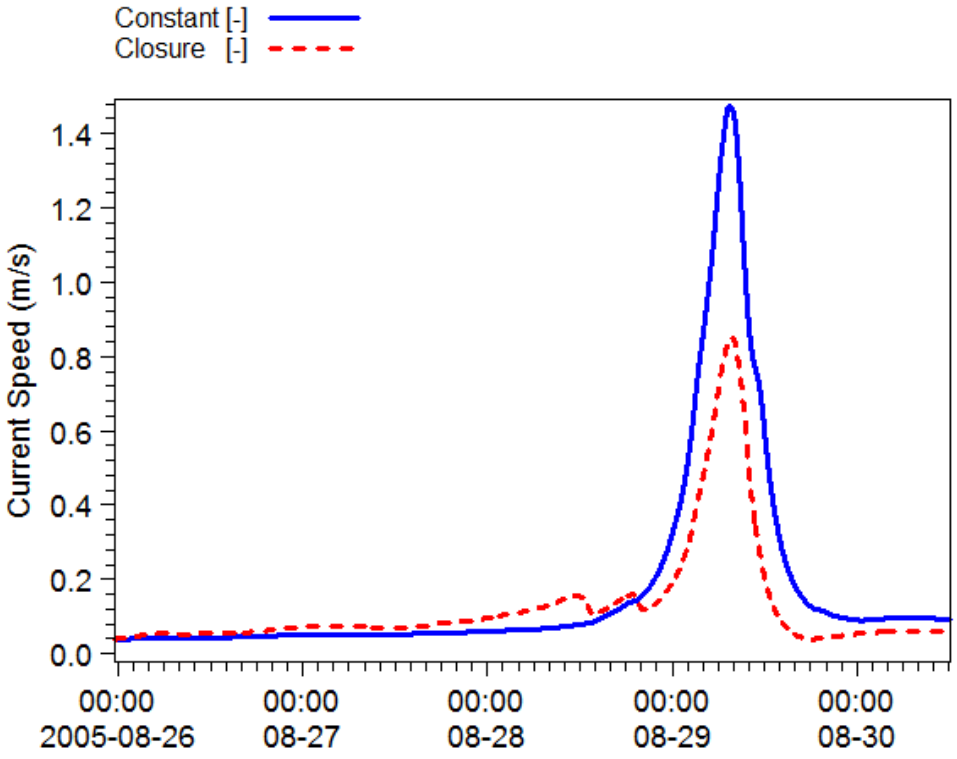

Figure 3.29: Time series of the simulated current speed at CSI-6 using two different approaches for treating vertical eddy viscosity.

Figure 3.30 shows spatial variation of the simulated sea surface temperature (SST) over the Louisiana shelf and the deep outer shelf for two different time instances as Katrina was on the inner shelf. There are substantial horizontal variations of SST which can introduce baroclinicity to the shelf waters.

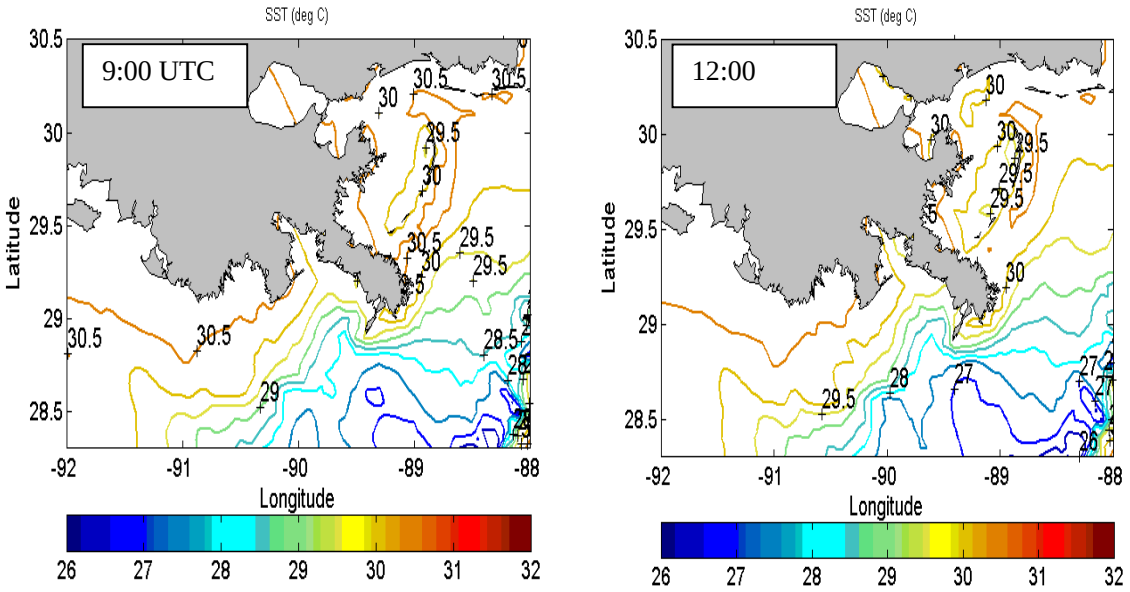

Figure 3.30: Simulated SST over the Louisiana shelf for two different position of Katrina on the shelf on 29 August 2009.

3.9 Summary and Conclusions

In this paper, the hydrodynamic response to Hurricane Katrina over the Louisiana inner shelf and a part of the outer shelf area was examined using a hydrodynamic model (FVCOM). The model was forced by parametric single vortex wind model. Wind speed and direction generated by this model were tuned by changing the radius of maximum wind based on available wind over the Louisiana shelf. Different cases with different types of stratification and vertical eddy viscosity were considered. By comparing with the limited available *in situ* current data, the best agreement was obtained for case B considering an initially stratified water column with the Mellor-Yamada level 2.5 for turbulence closure. Over the Louisiana shelf and adjacent outer shelf, the near-surface currents were consistent with the hurricane wind field (cyclone). The bottom water had reverse flows (anti-cyclone). This non-uniform response was produced because the distance of the Hurricane to the major parts of the Louisiana shelf was greater than $1R_{mw}$. As a result of this large distance, mixing was not strong enough over the western shelf to destroy stratification and make surface and bottom layers coupled. Furthermore, the spatial variations of surface cooling induced by hurricane can produce a horizontal pressure gradient that forced an anti-cyclonic gyres beneath the mixed layer.

CHAPTER 4: HURRICANE INDUCED MIXING AND POST-STORM RE-STRATIFICATION OVER THE LOUISIANA SHELF

4.1 Introduction

Hurricanes can provide energetic mixing over the shelf often in summer when wind is normally rather weak (Chapter 2). This chapter is aimed at addressing the characteristics of the mixing produced by hurricanes over the Louisiana shelf.

A tropical storm can cause surface cooling, turbulent mixing and inertial motions as addressed by many studies in the last few decades. Field and satellite observations have been used extensively (Leipper, 1967; Jacob et al., 2000; Zedler et al., 2002, Pan and Sun, 2013; Black et al., 2007) and numerical models (Elsberry, 1976; Price, 1981; Martin, 1982; Bender et al., 1993; Ginis, 2002; Zedler et al., 2002, Jacob and Shay, 2003, Richards et al., 2009). Heat loss to the storm, entrainment by turbulent mixing, and advection all contribute to the mixed layer heat budget (Price, 1981). During the forcing stage of the hurricane over a region, entrainment causes a deepening of the mixed layer (Price, 1981; Bender, 1993). Within the radius of the maximum wind (Rmw), the surface divergence caused by the cyclonic wind enhances upwelling, reducing the mixed layer depth (MLD) compared to the outer region. The maximum MLD deepening occurs just beyond the radius of maximum wind where storm induced stress and heat loss to the storm reach the maximum values (Elsberry et al., 1976).

At any given time, the MLD decreases as the radial distance increases from 1 Rmw, where surface convergence produces downwelling (Elsberry et al., 1976). It was observed that the maximum cooling occurs on the right side of the hurricane's track for most hurricanes (Price, 1981; Bender, 1993; Ginis, 2002). Price (1981) described this rightward bias as due to the clockwise rotation of the wind vector on the right side of the track working in near-resonanted with the wind-driven near-inertial motion. The maximum cooling is a function of hurricane's forward speed. A larger response is produced by a slower moving hurricane, given other conditions unchanged. The cooling of surface water decreases as hurricane forward speed increases (Price, 1981; Bender, 1993; Ginis, 2002, Walker, 2005). In coastal waters, even though results are similar in terms of strong surface cooling, right-ward bias, and subsurface upwelling and cooling in the interior region (Chu et al., 2000), the bottom water topography and the coastal boundary can be more important than that in deeper water (Mayer et al., 1981). Near-inertial oscillations in the post-storm stage are mostly present in water depth greater than 70 meter. Over the shelf with water depth ~ 50 m, they are significantly damped as a result of bottom friction (Xie et al., 1998).

Temperature and salinity variations in shallow water during hurricanes have been less studied. Several studies examined the sea surface temperature for the shelf response to hurricanes (Bingham, 2007; Spekhart, 2004; Hu et al., 2007). Spekhart (2004) used field measurements of wind, current, temperature, and salinity to study the response of water in the Onslow Bay, NC to

three consecutive Hurricanes Dennis, Floyd, and Irene within a two month period in the fall of 1999. Analysis showed that a strong inertial oscillations associated with the hurricanes in deep water, was significantly damped in shallow water. The strong shear induced by Hurricane Dennis lasting an extended amount of time, caused the sea surface temperature to drop by about 3 degrees, producing a completely mixed water column. Consequently, the water appeared as barotropic during the time that Dennis was translating along the coast even at water deeper than 70 m.Modeling studies of mixing induced by hurricanes over shallow and estuarine waters are scant (Xie et al., 1998; Li et al., 2007). Li et al. (2007) applied a high resolution ROMS model coupled with the atmospheric model MM5 to simulate the temporal and spatial response of temperature and salinity in the Chesapeake Bay to Hurricane Isabel which made its landfall southeast of the Bay in September 2003. Results showed that the pre-storm strong salinity stratification was completely destroyed as a result of the hurricane-induced current shear and vertical turbulence.

Hence, a complete mixing was dominant along the axis of the Bay, even at water depth as greater as 25 m. The simulated salinity across the water column showed that the fully-mixed state lasted for several hours after the peak of the hurricane. The salinity stratification started to rebound several hours after the hurricane (reaching a significant stratification after 1 day) as a result of large density gradient within the estuary.

However, the understanding of the detailed behavior of the temperature and salinity response of the shelf/estuarine waters to a hurricane still needs significant amount of effort, especially the re-stratification after the hurricane. A 3-D dynamics of the response within an appropriate timescale needs to be fully described. The present study represents such an extension of work on this subject of response of the stratified Louisiana shelf to Hurricane Katrina.

4.2 Model setup for modeling that resolves temperature and salinity

The FVCOM (Chen et al., 2006) as described in chapter 3 was used for simulating the 3-D response of the Louisiana shelf to Hurricane Katrina. The model within the given area (Figure 3.2) was forced by a hurricane wind for Katrina using Holland et al. (1980) described in section 3.5. The heat exchange between the hurricane and water surface was not included, because the major contribution to mixed layer deepening is turbulent entrainment (Elsberry et al., 1976; Price, 1981). The pre-storm oceanic heat and salt content are prescribed by initial vertical profiles of temperature and salinity. Selecting appropriate distributions for these profiles is crucial to correctly calculating the response of the water column to the hurricane, since it defines the gradients across the thermocline that affects the deepening rate of the mixed layer (Elsberry et al., 1976). However, data over the Louisiana inner and outer shelves are scarce.

Hence, the climatological profiles of temperature and salinity from the National Oceanic and Atmospheric Association (NOAA) for August 2005 were selected as the initial condition (http://www.nodc.noaa.gov/access/allproducts.html). Both temperature and salinity profiles are

available for eight points over the northern Gulf of Mexico (Figure 4.1). Temperature profiles at different locations over the modeling area for the month that Hurricane Katrina translated GoM were presented (Figure 4.2). The profiles show average conditions in August for each station. Temperature profiles over the Louisiana inner shelf were modified using measured water temperature at CSI-6 (see Figure 3.1 for location) at two different depths (mid-depth and near bottom, Figure 4.3) and satellite-derived SST maps of AVHRR (Earth Scan Lab, Louisiana State University, www.esl.lsu.edu, Figures 4.4).

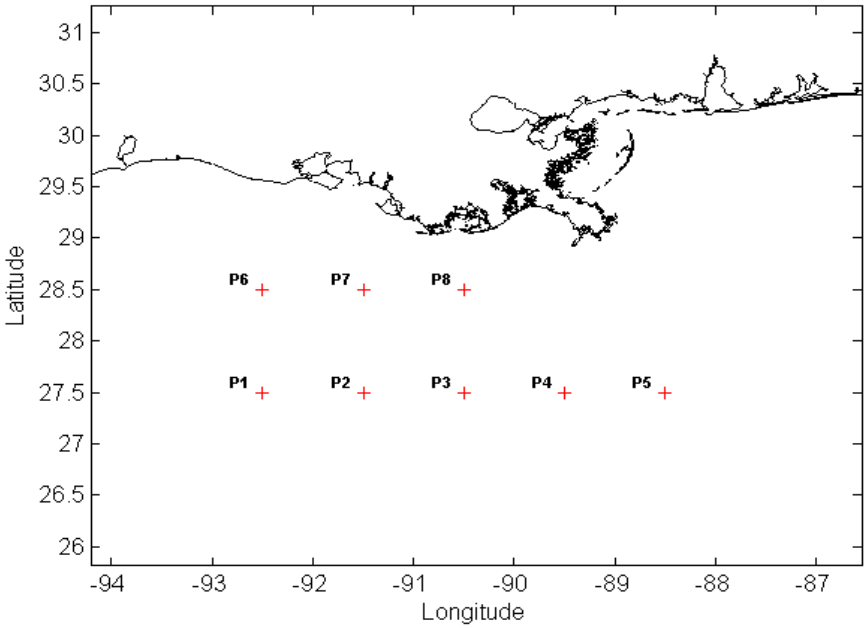

Figure 4.1: Locations of points containing climatological temperature and salinity profiles in the northern GoM based on NOAA database.

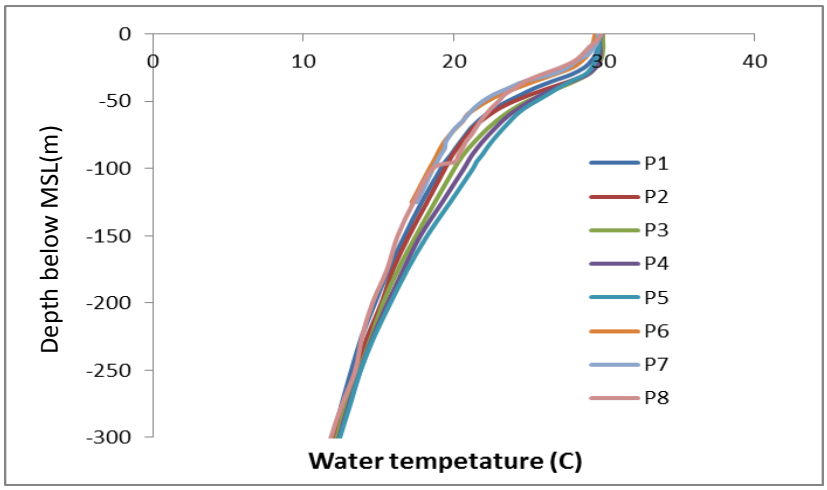

Figure 4.2: Temperature profiles of points shown in Figure 4.1.

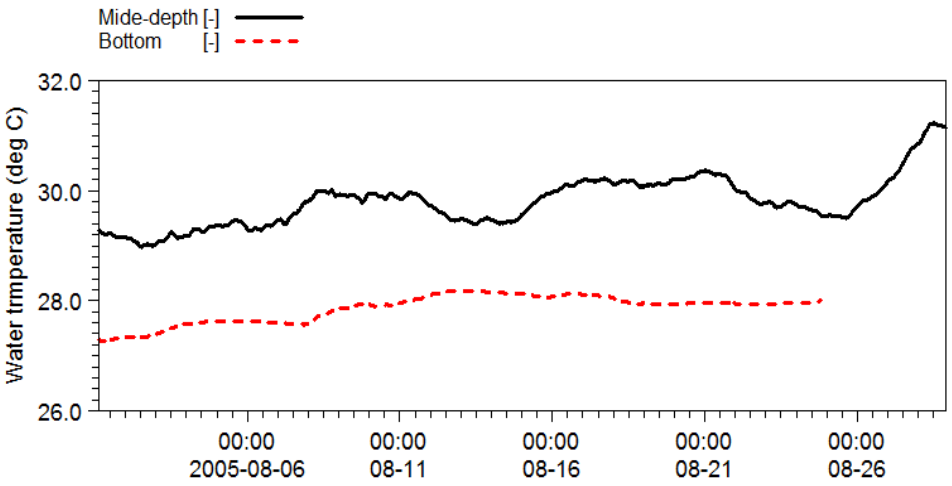

Figure 4.3: Time series 6 hours low-pass filtered measured water temperature at CSI-6 in August 2005.

Available temperature data were used to modify the climatological temperature profile for the initial temperature profile: the climatological temperatures at the surface, 10 meter, and 20 meters were replaced by the measured values. A smooth curve was used to determine the profile (Figure 4.5).

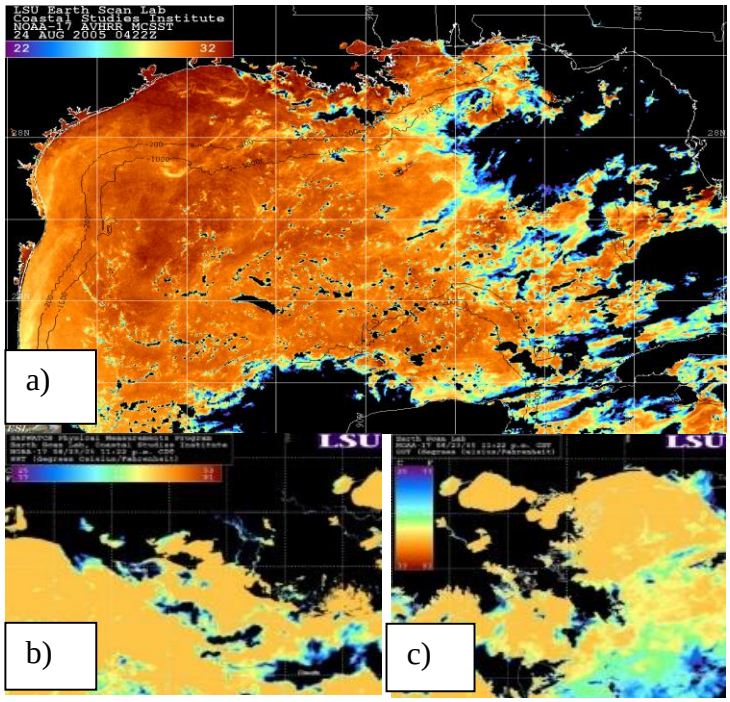

Figure 4.4: a) A snapshot of sea surface temperature in the GoM in 24 August 2005 at 04:22 UTC derived from AVHRR data, b) close view for the shelf offshore of the Atchafalaya Bay, c) Birds-foot delta and the shelves to the east and west.

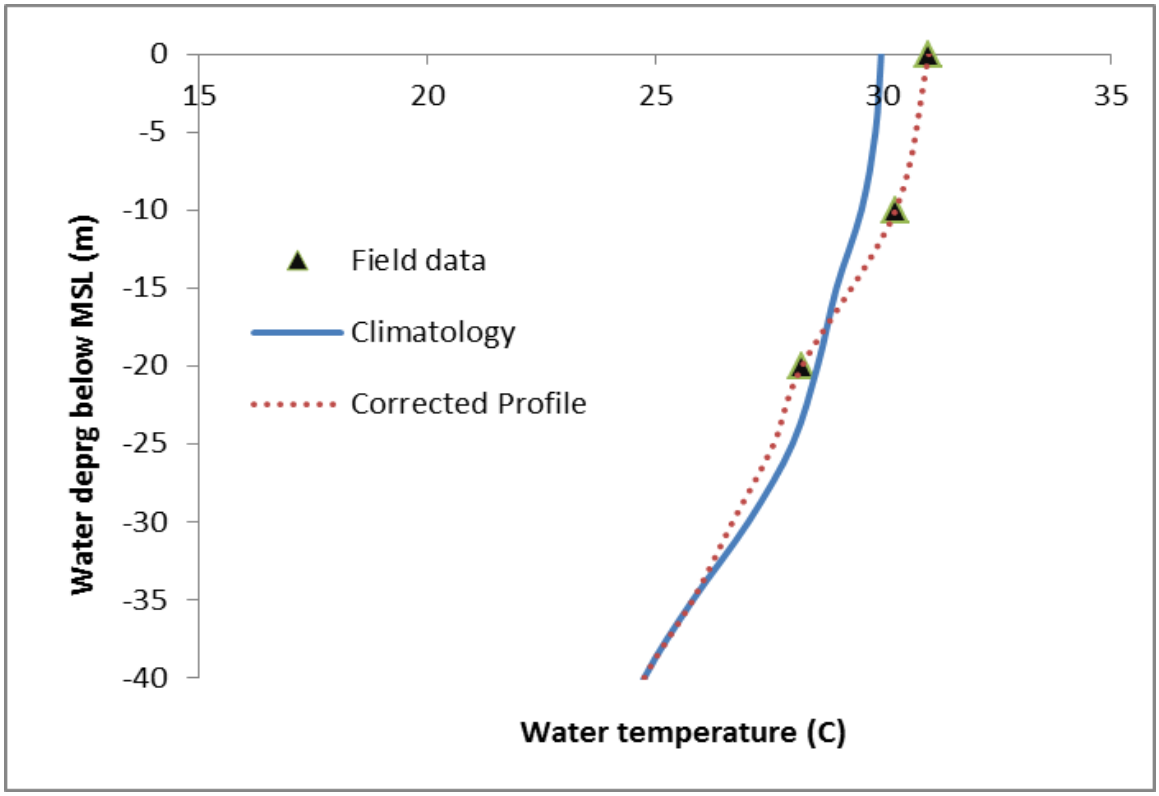

Figure 4.5: Modified temperature profile for the location of CSI-6 on the Louisiana shelf.

4.3 Verification of model

Water temperature profiles are controlled by the vertical turbulent mixing. Vertical turbulence in the model is resolved using the Mellor-Yamada level 2.5 turbulent closure. Two associated parameters including the background vertical eddy viscosity and energy dissipation coefficient quantify the vertical turbulent flux in the model. These parameters should be determined based on a calibration procedure. However, there is a lack of data during Hurricane Katrina. Furthermore, the extensive cloud coverage during this time period contaminated satellite measurements of SST from MODIS and AVHRR as the measurements are based on Infrared and mid-Infrared wavelength bands.

These wavelengths are absorbed by atmospheric water vapor. Since water vapor is transparent to microwave band, SST derived microwave band can be used for the hurricane period. The Microwave Optimally Interpolated (MW-OI) SST is reliable for model evaluation (Reynolds and Smith 1994; Pan and Sun, 2012).

Data are accessible from the Remote Sensing Systems website, www.remss.com. (Figure 4.6 for MW-OI SST maps during Katrina). SST data from MW-OI are available daily at about 8:30 (UTC time) over the GoM. The cooler areas on the right side of Katrina's track suggest rightward bias. As shown, data are only available over the offshore area extended roughly to the shelf break in the northern GoM.

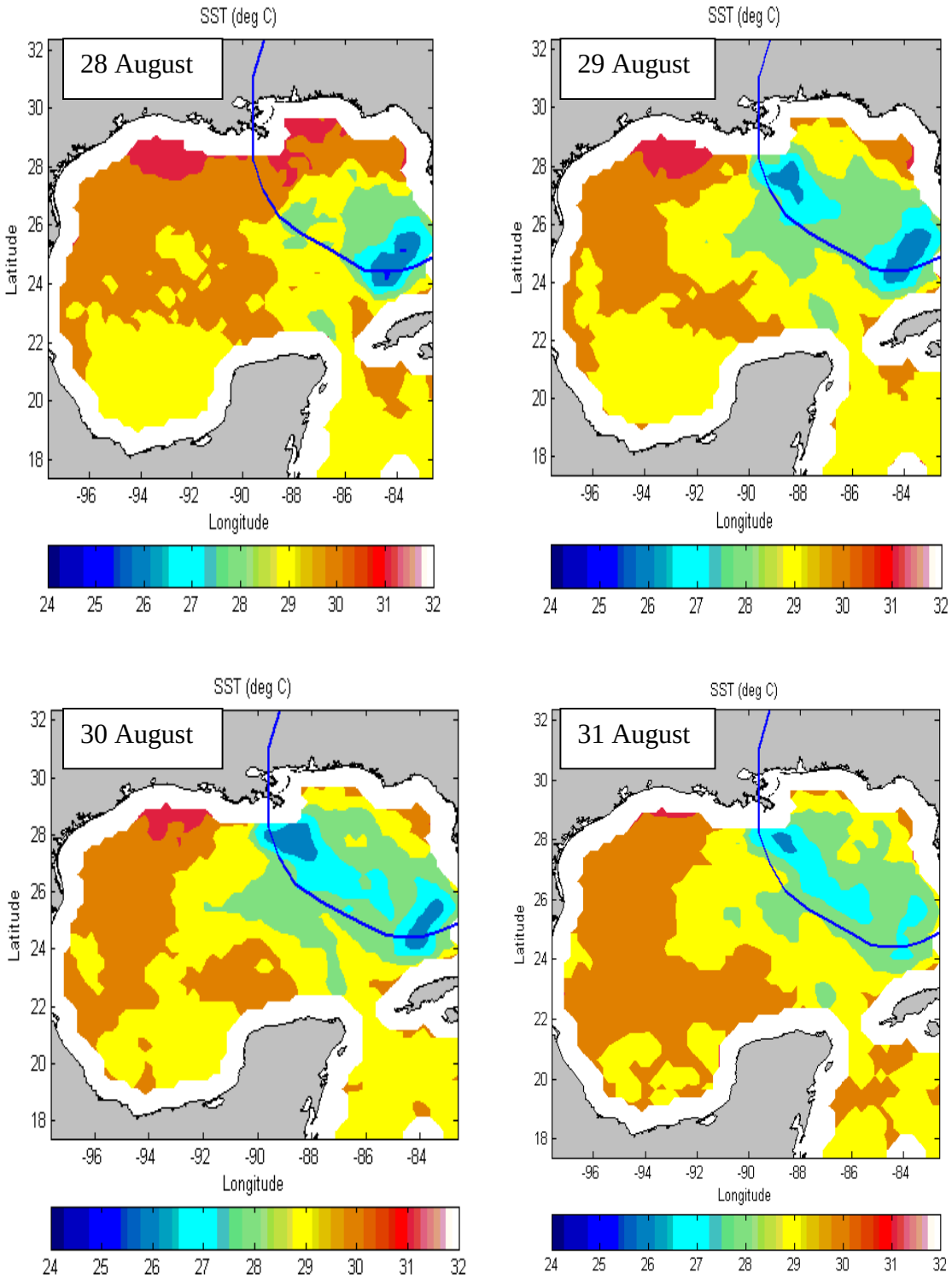

Figure 4.6: Satellite-derived (Microwave Optimally Interpolated (MWOI)) SST maps for different days (all measured at 8:30 UTC time) over the GoM during Hurricane Katrina (solid line shows Katrina's track).

The data closest to the inner shelf were used for model calibration/evaluation. Several sets of background vertical eddy viscosity (UMOL) and energy dissipation coefficient (B1) were considered to obtain the best match with SST data. Values for UMOL were within the range of 0.01 to 0.000001, while B1 values ranged from 6 to 25. Some representative simulations are listed in Table 4.1. Comparison of simulated SST with that from MW-OI data for several days after the hurricane showed that the parameters for run1 of Table 4.1 (UMOL=0.00001 and B1=8) resulted the best match.

Table 4.1: Some representative simulation cases with different combination of UMOL and B1.

Simulation case	UMOL	B1
run1	0.00001	8
run2	0.001	8
run3	0.001	20
run4	0.01	20
run5	0.005	20

Figure 4.7 shows an example of comparison between MW-OI-derived temperatures for the shelf break region with similar quantities from three different simulations. Also, the SST resulted from run1 is compared with AVHRR-derived SST (SST data are available from AVHRR at this time as after the hurricane the sky cleared up) for day 10 after Katrina's landfall in Figure 4.8. To evaluate the performance of the model, simulated temperature and salinity profiles and MLD values should be compared with field data.

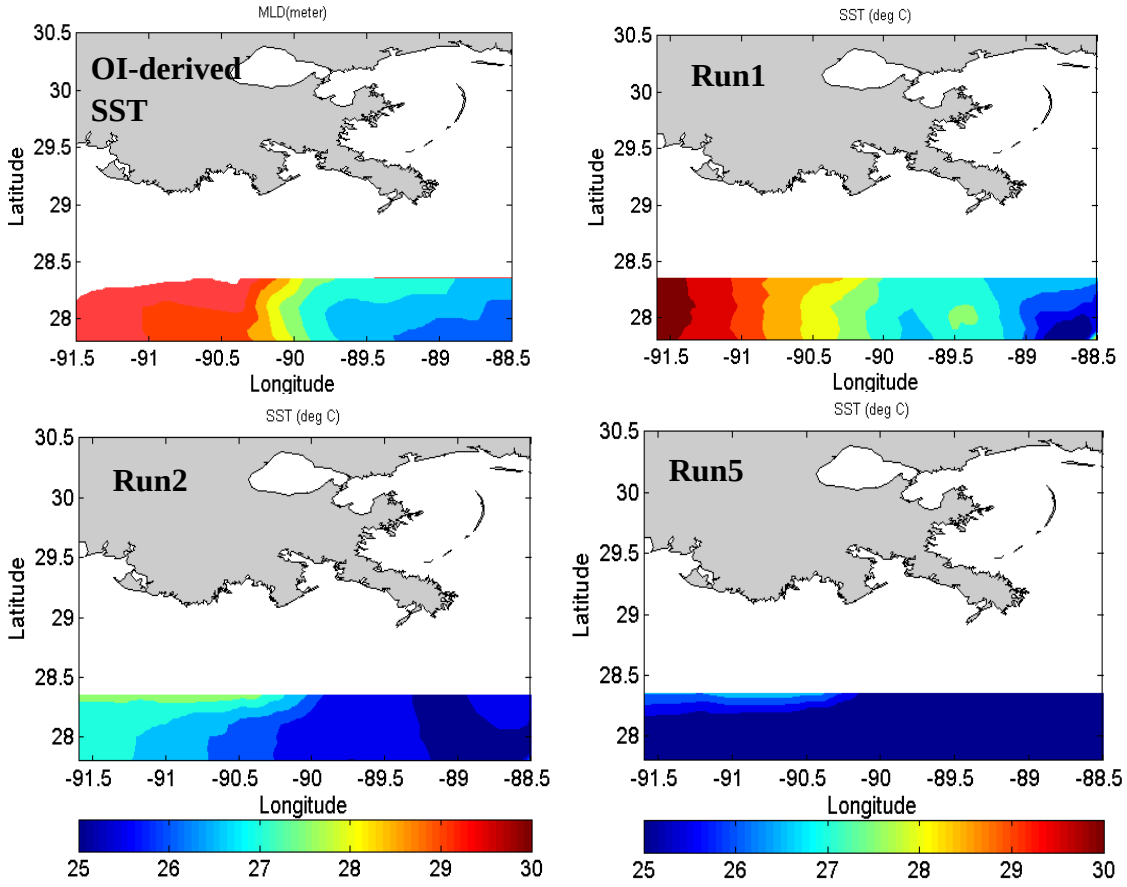

Figure 4.7: OI-derived SST in vicinity of the Louisiana shelf break at 8:30 UTC on 30 August 2005, almost 20 hours after Katrina's landfall in comparison with results from different simulation runs.

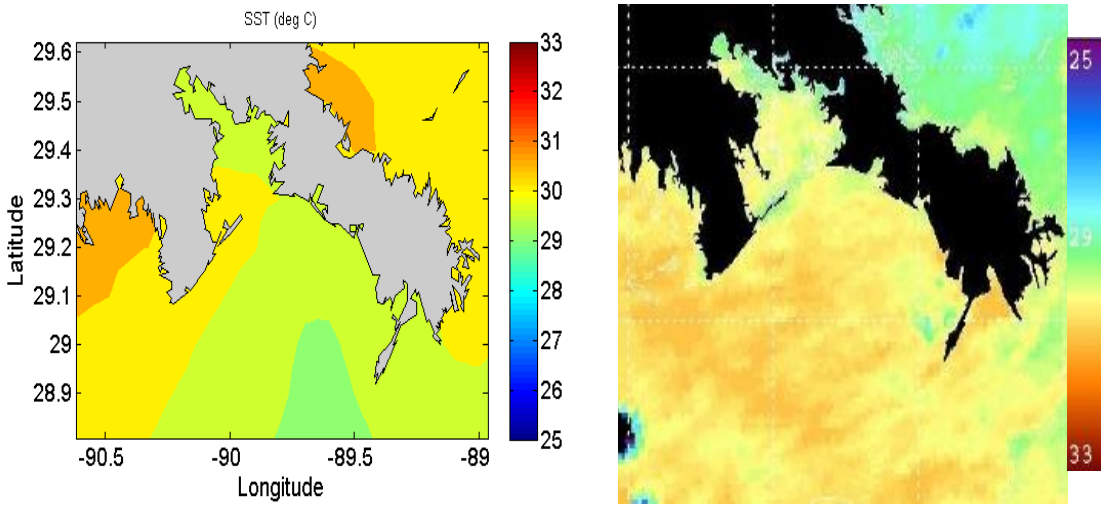

Figure 4.8: left) Simulated SST over the shelf west of the Birds-foot delta 10 days after Katrina's landfall, right) AVHRR-derived SST at the same time.

With a lack of field measurements over the Louisiana shelf during Hurricane Katrina, the MLD values were calculated using an MW-OI-derived SST data based on an approach suggested by Pan and Sun (2012). They assumed that the turbulence entrainment at the base of the mixed layer accounts for most of the mixed layer heat budget and the effect of advection and surface heat flux is minor (Price,1981; Ginis and Dikinov, 1989; Jacob and Shay, 2003; Zedler et al., 2002). A relationship for estimating MLD is thus proposed:

$$T = \frac{1}{D}\int_{-D}^{0} T_0\,(z)dz \qquad (4.1)$$

in which T is the current mixed layer temperature which is the same as the satellite-derived SST at the time of interest (e.g. a time after the hurricane passed), D is mixed layer depth, $T_0(z)$ is the pre-storm temperature at depth z (Figure 4.9). Equation (4.1) was used for finding the mixed layer depth (MLD or D) by using the modified temperature profile presented in section 4.2 as T_0. With this model, the MLD is roughly inversely proportional to SST (Figure 4.10).

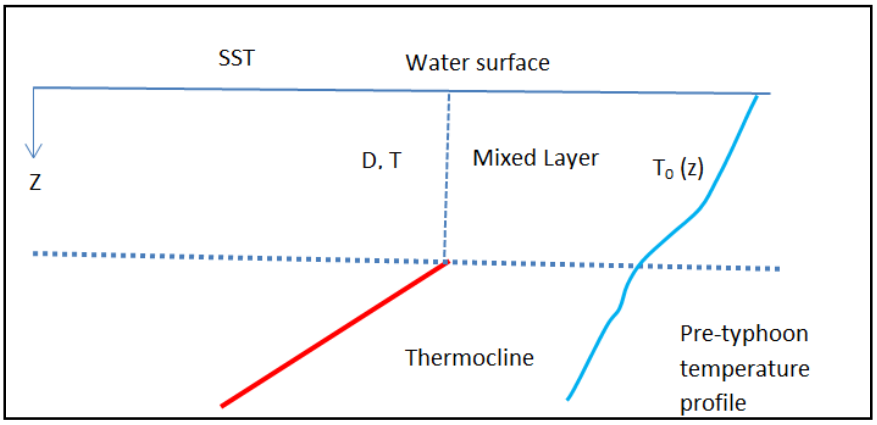

Figure 4.9: Schematic for MLD calculation using SST data.

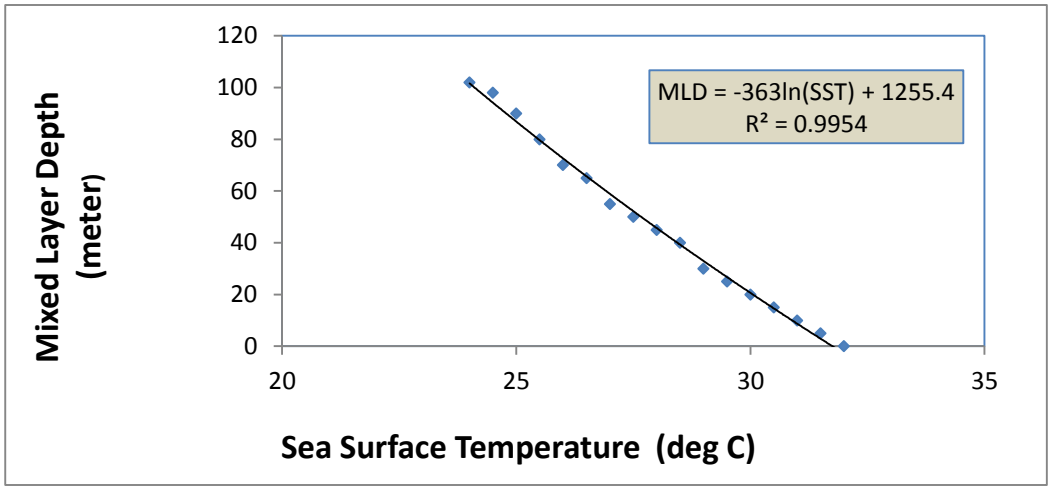

Figure 4.10: Relationship between MLD and SST following Pan and Sun (2012).

This model was applied to the MW-OI derived SST data producing the MLD maps for four different days during Hurricane Katrina (Figure 4.11). As expected, the maximum MLD values are along the hurricane's track, with a bias on the right hand side. However, it should be noted that the MLD values within the upwelling area (about 1 Rmw from the hurricane's track) are not reliable from this method (Ginis, 2001). The simulated MLDs for run1, run2, and run5 (Table 4.1) in the vicinity of the shelf break and offshore of the Birds-foot delta are compared with the calculated MLDs using equation 4.1 at 8:30, August 30, UTC (Figure 4.12).

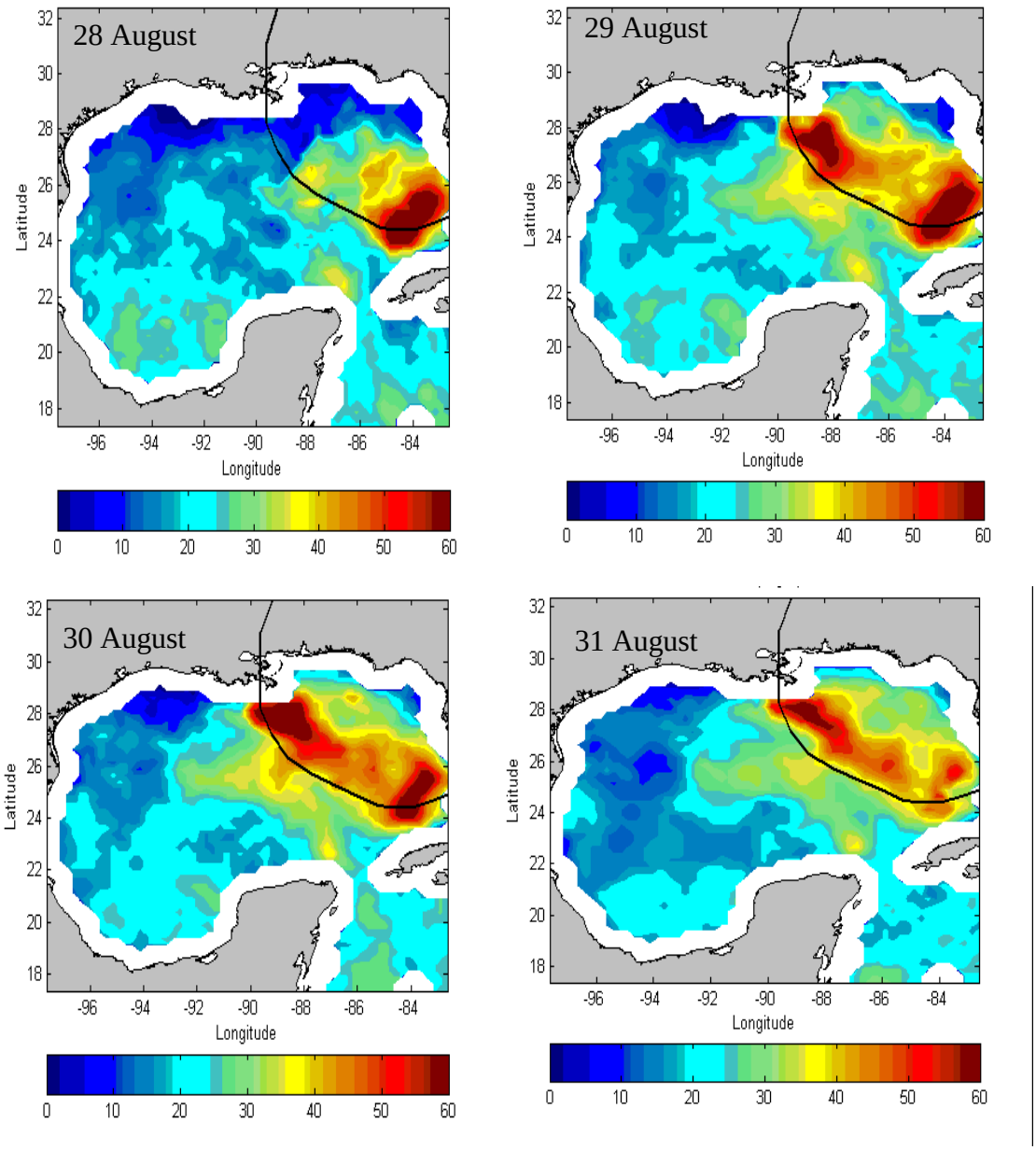

Figure 4.11: MLD maps over the GoM for four different days during Hurricane Katrina using Equation 4.1. All maps are snapshots at 8:30 UTC.

The simulated MLD values are shown only for latitudes smaller than 28.3 to make it consistent with the map of MLDs from Equation 4.1. The best agreement resulted from run1. Other cases (run2 and run5) overestimated the MLDs due to larger values of background eddy viscosity. The discrepancies between MLD's from run1 and calculations using Equation 4.1 can be attributed to the differences between the climatological temperature profile (used as the initial condition) with the real profile. Errors of the analytical model in calculating MLD from SST can also lead to some differences (Ginis, 2001; Pan and Sun, 2012).

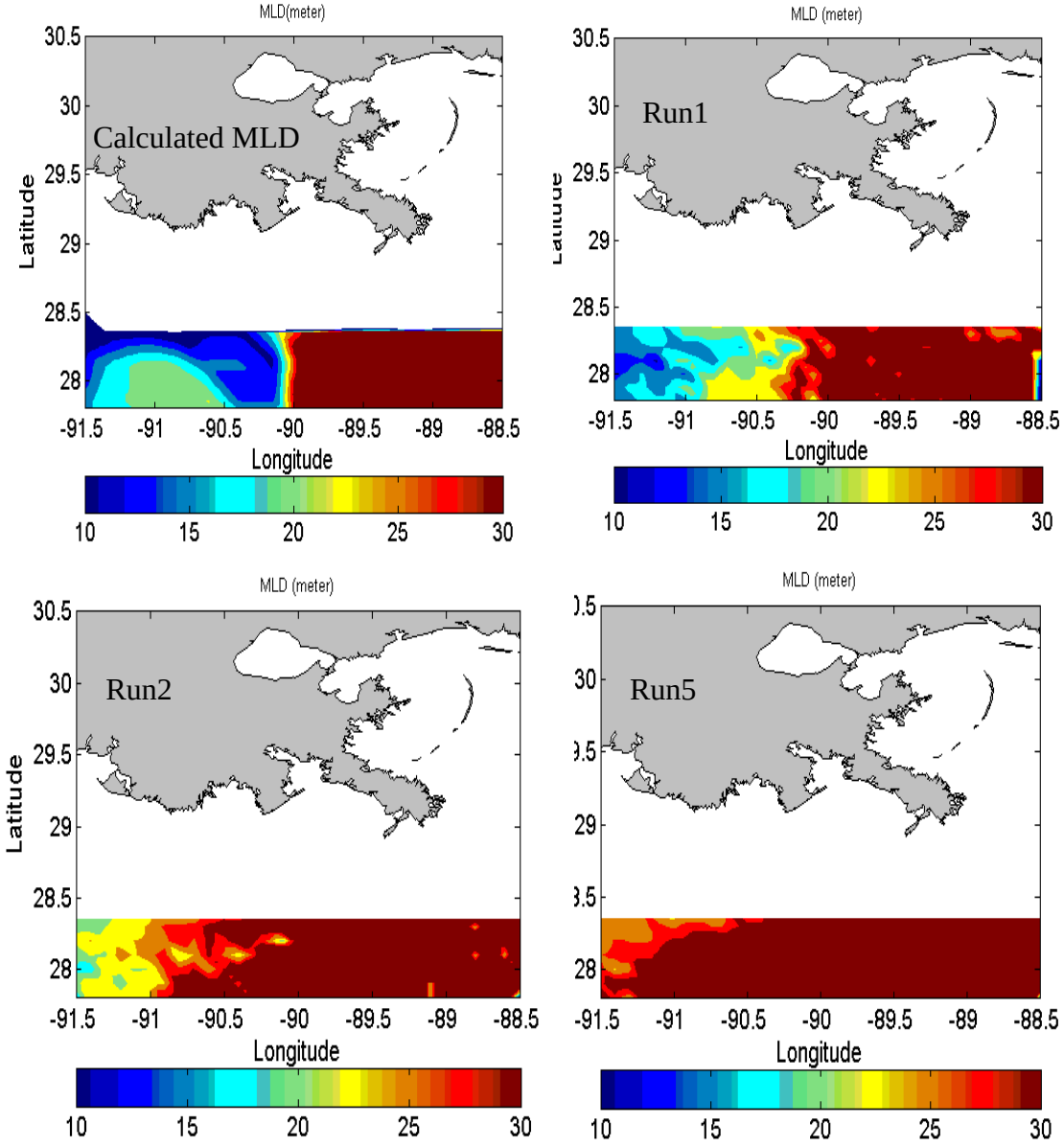

Figure 4.12: MLD at 8:30 UTC time on 30 August 2005, almost 20 hours after Katrina's landfall resulted from calculation from Pan and Sun (2012) model and different simulations runs.

4.4 Model Results

Model experiments were done using the parameters described in section 4.3 (run1). The model runs included about 10 pre-storm days until 10 days after the hurricane landed. This section discusses the distributions of temperature and salinity affected by the hurricane. Since the response of temperature and salinity to the hurricane is similar (Price, 1981; Ginis and dikinov, 2001), salinity response will not be discussed separately.

4.4.1 Sea Surface Temperature from the Simulations

In this section, the simulated SST variations are presented and discussed (Figures 4.13a-4.15). The time origin for these figures is the landfall time over the Birds-foot delta. Hence, all times before the landfall are negative and times after the landfall are positive.

The SST maps over the Louisiana shelf are obtained between the pre-landfall hours to about 8 days after the landfall of Hurricane Katrina. At 6:00 (UTC) on 29 August 2005, about 6 hours before Katrina's landfall (hour -6) the eye was located about 120 km southwest of the delta. Over the deep water region, the category 4 hurricane caused substantial surface cooling (up to 5 C) on both sides of the track with a larger cooling area to the right side (Figure 4.13a). The maximum cooling occurred as far as 1-1.5Rmw from the hurricane's eye.

The surface cooling along the Louisiana shelf break was 1.5-2 C, but no obvious cooling over the inner-shelves on both sides of the delta. As the hurricane progressed northward, the surface temperature along the shelf break off the Barataria Bay decreased from about 29 C (when the hurricane's eye was offshore) to about 27 C (at landfall).

The gradient of isotherms along the shelf break was greater south of the delta and westward to the deep water off the Terrebonne Bay. This shows that the shelf break was a transition zone separating the oceanic waters of a greater surface cooling from the inner-shelf waters of less cooling. After the landfall over the Birds-foot delta (Figure 4.13a), SST over the Mississippi Bight reached 28.5 C to 30 C, exhibiting 1-2.5 C of cooling.

For the shelf areas west of the Barataria Bay, sea surface cooling was less (1 C or less). During the next 6 hours, the SSTs had little variation in the deep water and on the shelf. However, due to the southerly hurricane winds, 6 hours after the landfall over the delta, the SST on the shelf east of the delta decreased by 0.5 C (Figure 4.13b). A day after the landfall (Figure 4.13b), the smoother shelf-wide isotherms over the delta area showed that the post-storm relaxation of SST had already started. At this time, the average SST over the Mississippi Bight increased by about 0.5 C, while over the deeper water, the distribution of SST was similar to the landfall time, probably due to the buffer effect of the large pool of cold, upwelled water by the hurricane. Within the next 2-3 days after the landfall (Figure 4.13b), SST over the inner-shelf continued the post-storm recovery. The SST values over the shelf break and deep water were

generally undergoing much smaller changes. Slightly reduced horizontal temperature gradient suggests the onset of SST recovery over this area.

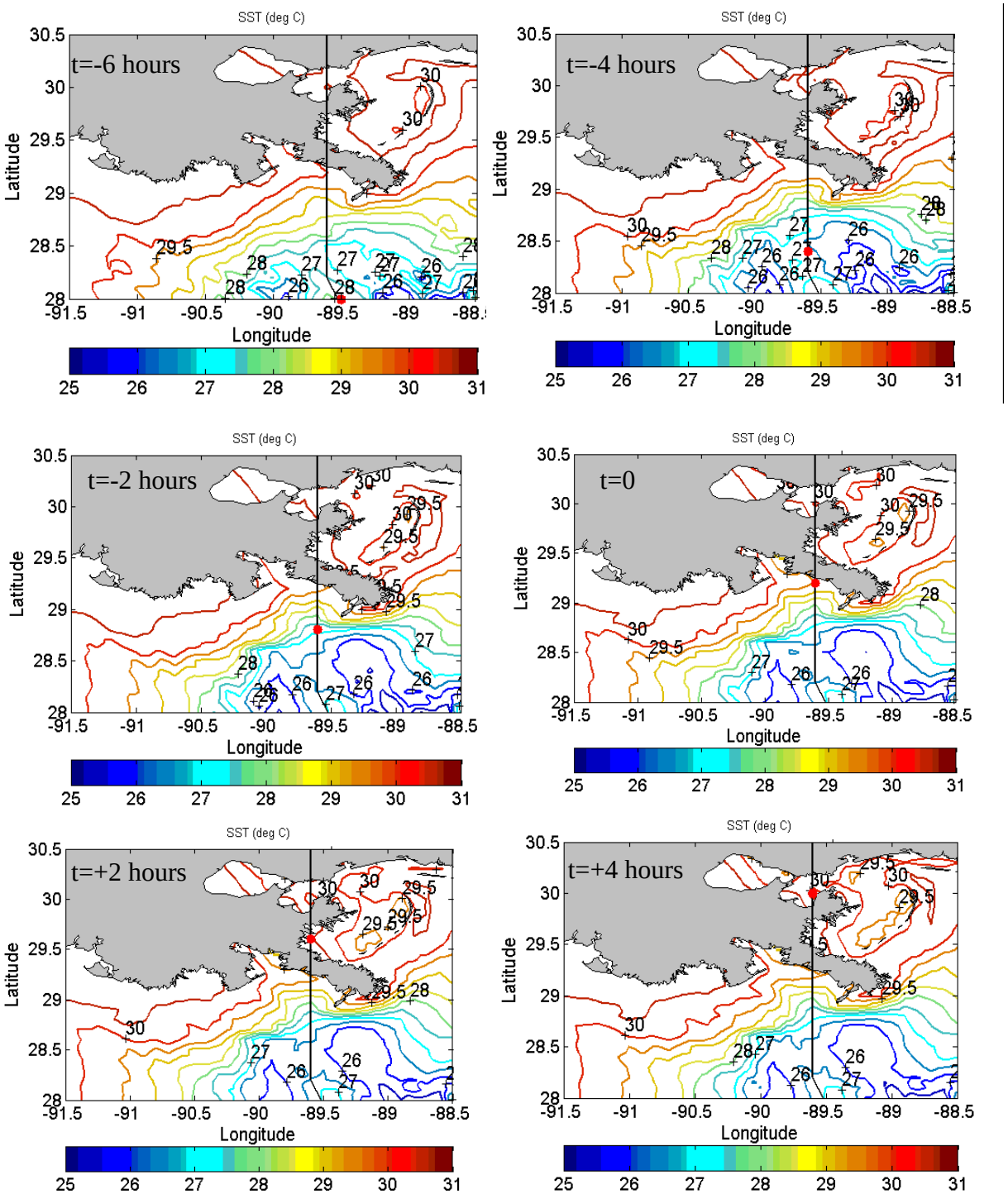

Figure 4.13a: Maps of simulated SST over the Louisiana shelf for different times relative to the time of Katrina's landfall over the Birds-foot delta.

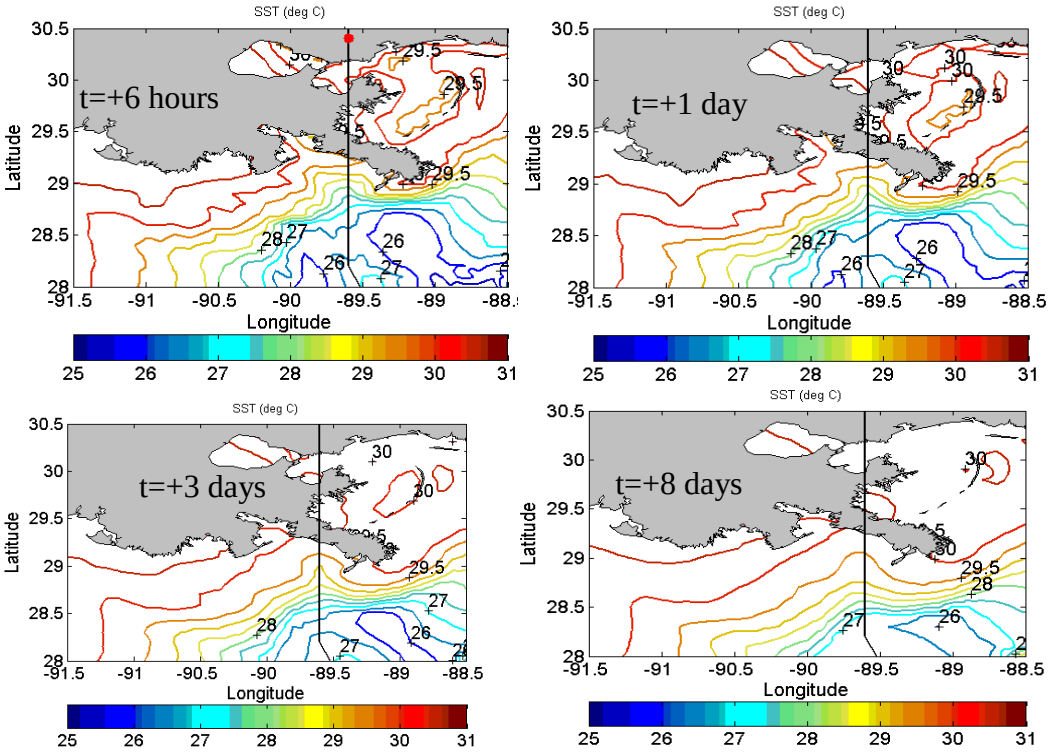

Figure 4.13b: Maps of simulated SST over the Louisiana shelf for different times relative to the time of Katrina's landfall over the Birds-foot delta.

By the 8th day after the landfall, SST over the Louisiana shelf was almost uniform (Figure 4.13b), but with a smaller magnitude compared to the initial SST. The high gradient of SST along the shelf break almost disappeared and the SST values increased to about 29-29.5 C. The offshore region of lower SST decreased in size on both sides of the track, while the SST on the left side of the track within the radius of maximum wind increased by about 1 C.

Figure 4.14 shows the calculated temperature cooling induced by Hurricane Katrina over the inner and outer Louisiana shelves at different times. About 4 hours before landfall over the Birds-foot delta (hour -4) the eye was located almost 80 km southwest of the Birds-foot delta (4 hours before the landfall over the delta), the category 4 hurricane produced substantial amounts of cooling over the outer shelf. Surface cooling as large as 6 C occurred along the track with significantly larger cooling areas on the right side of the track. At the edge of the shelf break off the Barataria Bay and the Terrebonne Bay, the cooling was 3 C and 2 C, respectively. The surface cooling decreased landward, and stopped at the mouth of the Terrebonne Bay and that of the Atchafalaya Bay.

Two hours later, when the eye was 25 km southwest of the Southwest Pass, the maximum surface cooling was 1 C. The distribution of surface cooling over the inner-shelf remained similar. At landfall, the inner shelf area on both sides of the track experienced surface cooling of 2-2.5 C, while at the mouth of the Barataria Bay and off the Terrebonne Bay there was about a 1 C warming.

The near bottom water cooling along the lowest sigma level is shown in Figure 4.15. Over the inner shelf the lowest sigma level represents the bottom water, while over the deep water the associated depths were generally larger than 100 m.

At hour -4, the bottom water at the edge of shelf break off the Barataria Bay had a warming of about 0.5-1 C. There was a bottom warming for the shelf break area off the Terrebonne Bay of 1-1.5 C. The bottom warming over this area was more likely due to less surface mixing and smaller rate of warm surface water entrainment down the water column. Over the inner shelf on the left of the track, the bottom water temperature was almost unchanged, while on the right side of the track the decrease of bottom water temperate was 1 to 2 C, probably due to the hurricane-induced upwelling.

Two hours later when the eye was almost over the shelf break at the west of the Birds-foot delta there was a warming over the shelf break off the Barataria Bay of about 1-2 C. The bottom temperature over the inner shelf on the left side of the track was still unchanged. At landfall till the next two hours, the Birds-foot delta area experienced a maximum warming of 1C over the shelf off the Terrebonne and Atchafalaya Bays.

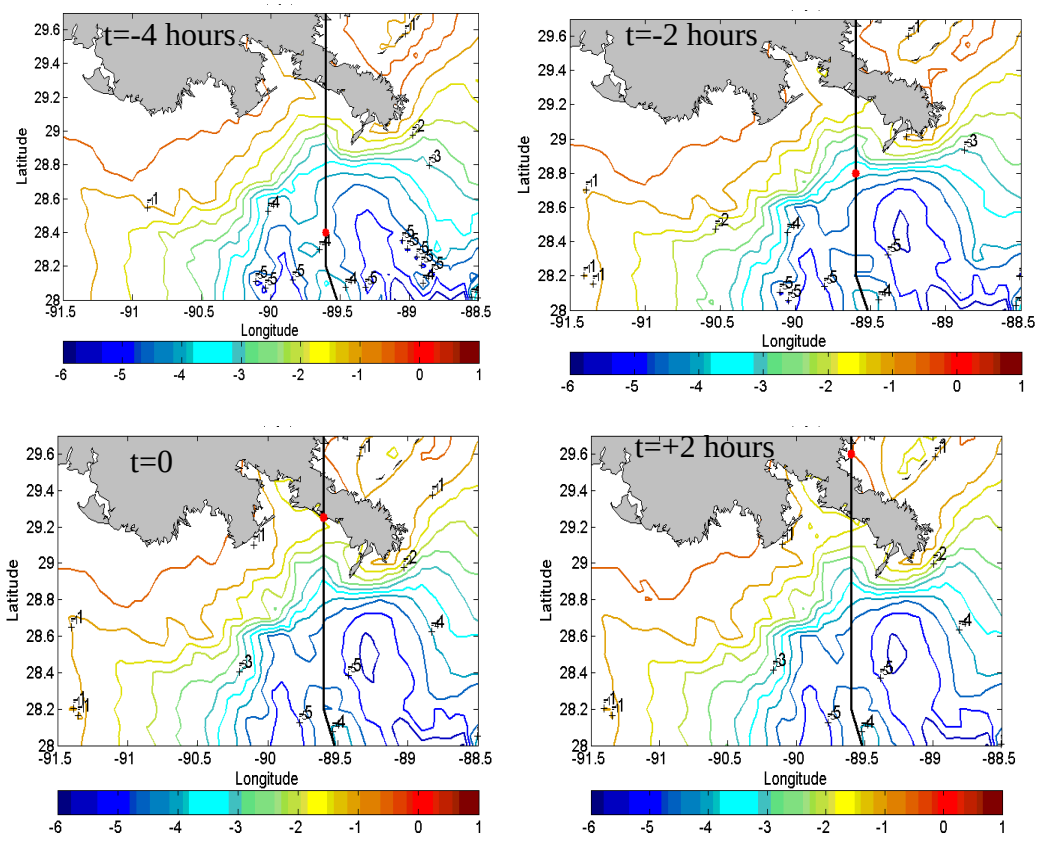

Figure 4.14: Simulated sea surface temperature cooling at different times, the solid line shows Katrina's track and red dot indicates the locations of the eye.

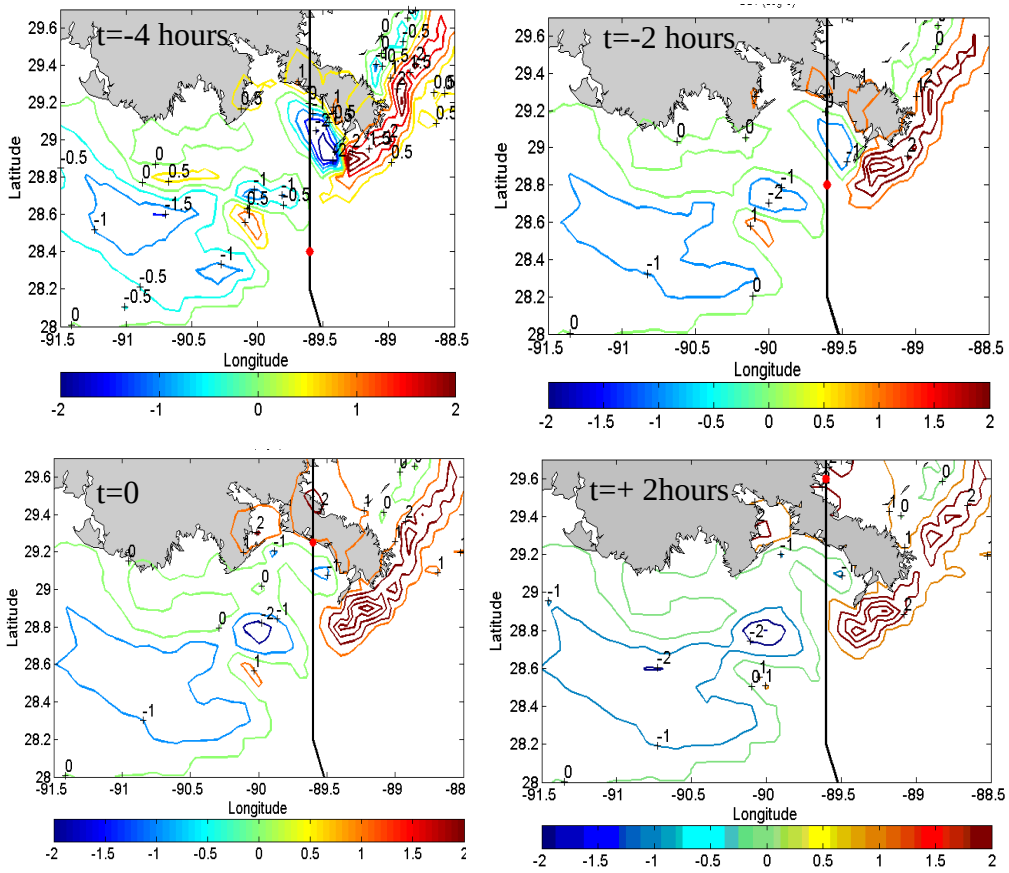

Figure 4.15: Simulated bottom temperature cooling at different times.

4.4.2 Time Series of Water Temperature

To further evaluate the evolution of the hurricane-induced temperature mixing across the water column over the Louisiana shelf, time series of vertical water temperature variations are examined at several points on both sides of the hurricane's track (Figure 4.16). For each point the temperature variations were investigated for 50 hours before and 50 hours after the time that the hurricane's eye was at the west of Southwest Pass (hereafter called CP time). Hence, positive time is after the eye passed this location, while negative time is before the eye was at this location. Point 1 is located in front of the Atchafalaya Bay where water depth is 14 m, about 200 km from Katrina's track. With such a distance, no substantial water column mixing and associated cooling is expected. Figure 4.17 shows the temperature time series at this location. The SST variations at the CP time and 50 hours after that was only 0.5 C. The minimum SST was about 30.3 C at the CP time. After 50 hours, which is almost 2 days after the landfall, the SST was about the same (30.4 C). However, the vertical temperature structure (lower panel of Figure 4.17) at this location shows more significant hurricane-induced changes. At hour -50, temperature distribution across the depth was fairly undisturbed from the initial temperature profile with SST ~ 31 C and bottom temperature 1 C cooler. Around hour -10, the turbulence and

horizontal current shear produced by the hurricane's wind, started to mix the upper water column producing a mixed layer of 7.5 meter at about the CP time with a mixed layer temperature of 30.4 C. During the next five hours, the SST decreased to 30.2 C as a result of more mixing with the colder bottom water and the MLD decreased to 5 m because of the upwelling.

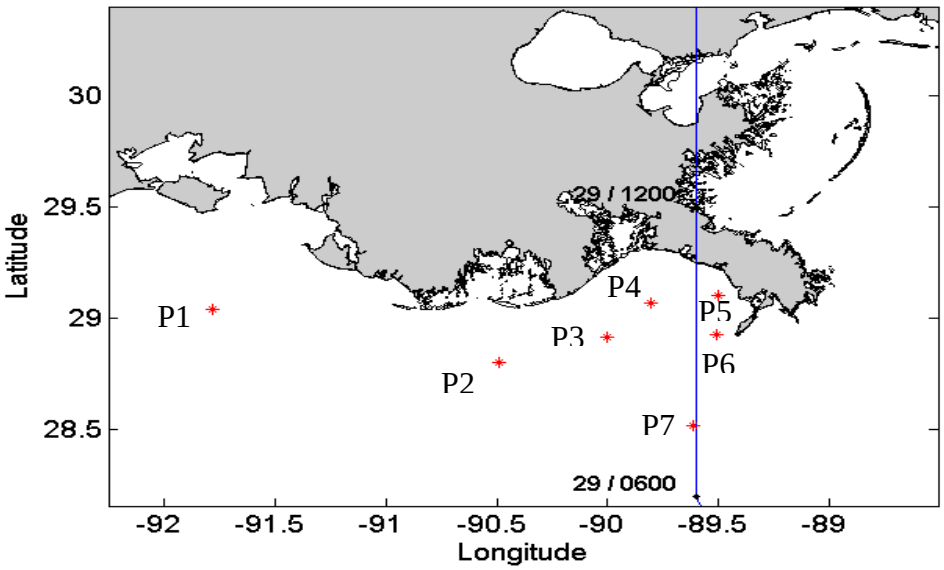

Figure 4.16: Locations of points over the Louisiana shelf selected for studying temperature time series (the blue solid line indicates hurricane's track).

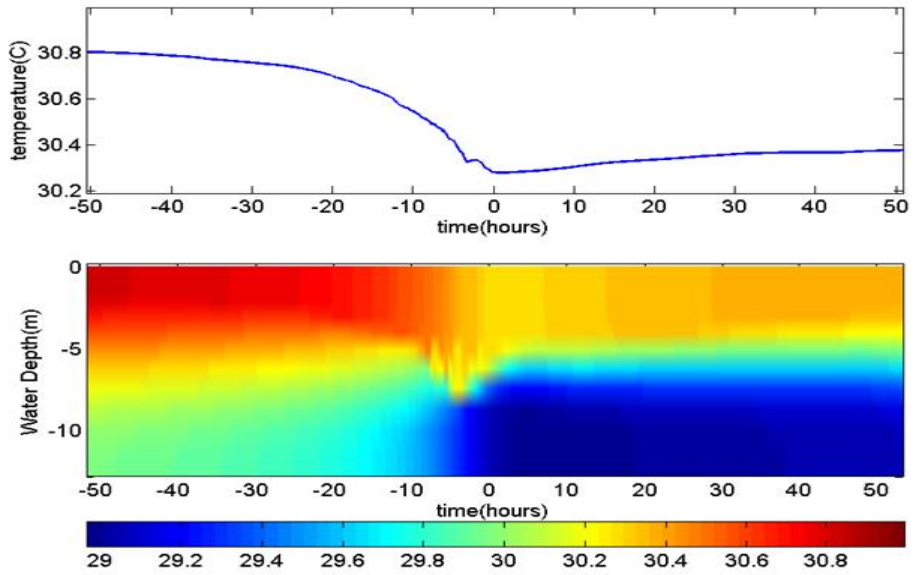

Figure 4.17: Upper panel: time variations of simulated SST at P1 for 50 hours before and 50 hours after the time that Katrina passed the closest proximity of this point, lower panel: time series of vertical temperature at this point for the same time period.

The upwelling caused cooling of the subsurface water to about 28.5-29 C and confined the mixed layer deepening for at least the next 40 hours, during which the mixed layer temperature increased to 30.4 C. Station P2 was located about 100 km (almost 3Rmw) west of the hurricane's track off the Terrebonne Bay where water depth was about 20 meter (CSI-6 station). This location was far away from the radius of maximum wind. The SST at this station (Figure 4.18, upper panel) decreased from 30.8 C at hour -50 to about 30 C at the hour -4.

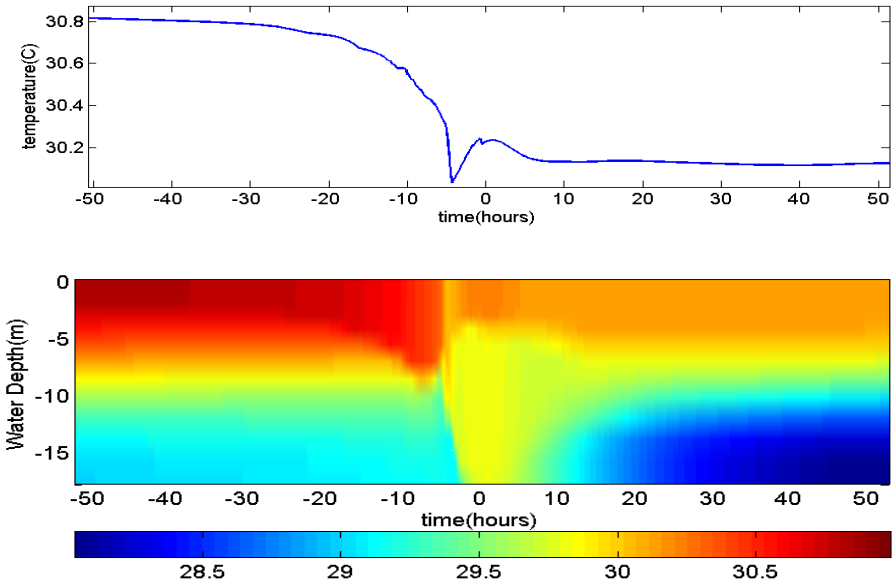

Figure 4.18: Upper panel: time variations of simulated SST at P2 for 50 hours before and 50 hours after the time that Katrina passed the closest proximity of this point, lower panel: time series of vertical temperature at this point for the same time period.

Within 4 hours, the SST increased by 0.25 C, possibly due to the advection of warmer surface waters from the western shelf regions. For the next 40 hours, the SST remained at 30.1C. The initial stratification at this location started to be affected by the hurricane winds at hour -15, when the surface warmer water began to mix with the colder water below. This turbulent entrainment caused a transient mixed layer with 15 m depth and mixed layer temperature of 29.7 C at about hour -5. After hour 10, water temperature across the depths larger than 10 m was highly affected by upwelling, reducing the minimum water temperature to 28 C. Time variations of SST and MLD at location P3 were similar (Figure 4.19). Since this point is closer to the hurricane's track, temperature response was more significant. The station is located off- the Terrebonne Bay at water depth of 33 m about 40 km west of the hurricane's track. At hour -3, the SST dropped to about 28.6 C with about 2.4 C surface cooling. Similar to station P2, this minimum was followed by a peak of 30.2 C caused by advection of warm water (Figure 4.19, upper panel).

In 10 hours, turbulent mixing decreased the SST to 29.4 C, but after the hurricane's landfall, the SST began the relaxation phase and increased to a stable value of 29.8 C at hour 50. The initial stratification was affected by the hurricane winds starting several hours before the CP time. An ephemeral mixed layer of depth 15 m and temperature of 30.2 C at CP time (Figure 4.19, lower panel) was present. During the next several hours, the MLD and temperature decreased to 12 m and 29.4 C, respectively; and 5 m and 29.8 C, respectively, during the relaxation phase (the post-storm time). Similar to stations P1 and P2, after CP time, the lower level water temperature (below~ 20 m) was affected by upwelling. Water temperature during the upwelling dropped to about 25.5 C. The coastal upwelling over the Louisiana shelf on the left side of Katrina's eye was produced by the westerly to southwesterly hurricane winds (Figure 3.4). These winds were at about the landfall and beyond. Station P4 with water depth of ~30 m was closer to the mouth of the Barataria Bay and was located northeast of P3. The distance from the hurricane's track was 25 km (note that for Katrina the radius of maximum wind was 30-35 km over the Louisiana shelf). Hence, a more significant effect of turbulence mixing was expected at this station (Figure 4.20). SST at this location decreased almost linearly from 30.5 C at hour -10 to 27.8 C at hour 5 (Figure 4.20, upper panel).

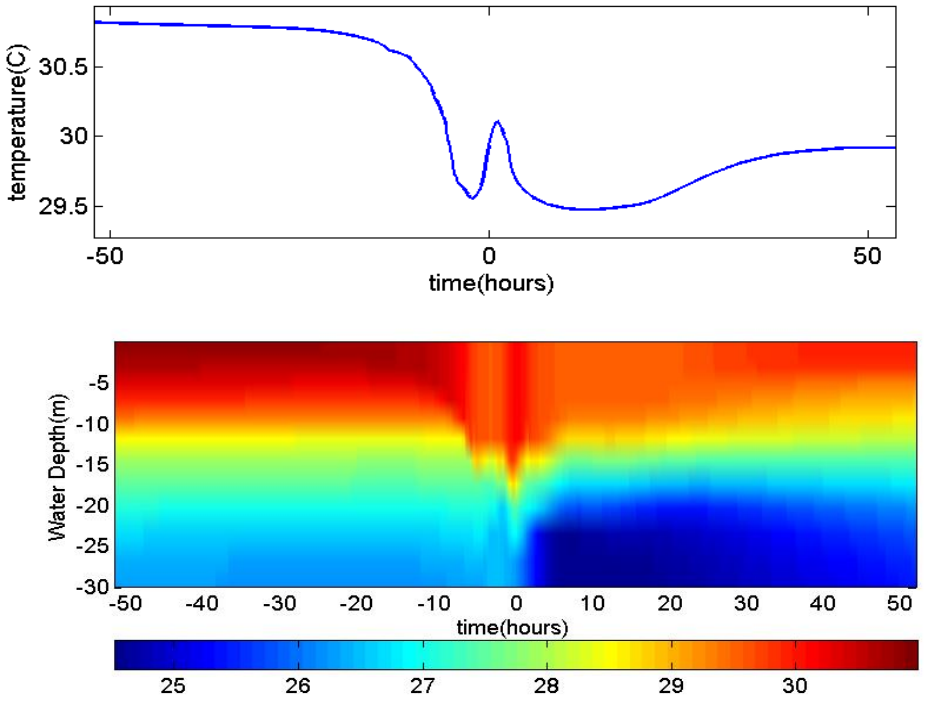

Figure 4.19: Upper panel: time variations of simulated SST at P3 for 50 hours before and 50 hours after the time that Katrina passed the closest proximity of this point, lower panel: time series of vertical temperature at this point for the same time period.

The SST rebound started right after the landfall and increased to 29.6 C at hour 50. As it is shown in Figure 4.20 (lower panel) at about hour -10, the shear entrainment mixed the surface

warm water with bottom cold water down to 25 m. This significant mixing event produced a mixed layer depth of about 20 m and temperature of about 28 C at hour 3. The mixed layer stayed almost the same for several hours until the relaxation phase started at hour 10 when the water column started to warm again. During this period, the MLD decreased from 20 m at hour 5 to a stable value of 5 m at the hour 50. The upwelling was less intense compared to other stations west of the track, probably because of the closer proximity of P4 to the coastline.

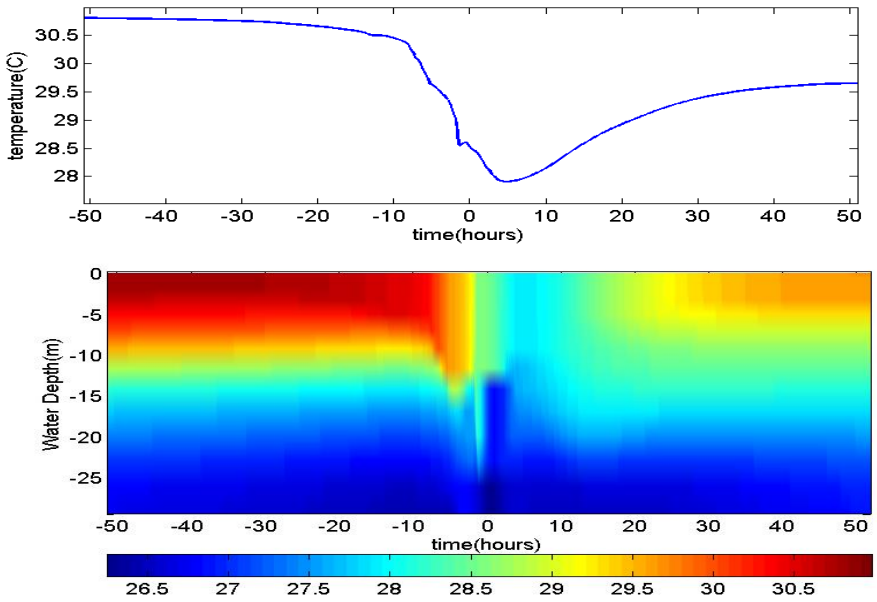

Figure 4.20: Upper panel: time variations of simulated SST at P4 for 50 hours before and 50 hours after the time that Katrina passed the closest proximity of this point, lower panel: time series of vertical temperature at this point for the same time period.

The effect of Hurricane Katrina on vertical mixing on the right side of the track was investigated by examining the time series of SST and vertical temperature structures at stations P5 and P6. It is found that the shelf response on the right side is highly affected by the geometry of the Birds-foot delta with the right forward side bias caused by the asymmetric wind of a moving hurricane. Station P5 was located northwest of the South Pass where water depth was about 11 meter and the distance from the Hurricane's track was about 10 km. The simulated SST at this location (Figure 4.21, upper panel) shows that the SST decreased from about 30.5 C at hour -10 to 28.8 C at hour 0 indicating 2 C of surface cooling from the initial SST of 30.8 C. After the hurricane passed the station, SST began to increase and reached 29.3 C in 24 hours. Afterwards, the SST continued increasing with a slower rate and reached 29.5 C at hour 50. The hurricane's effect on the stratification at this station started at about hour -22 (Figure 4.21, lower panel). At this time, a change from the initial stratification started to be visible. After about 24 hours (at hour 2), the water column was fully mixed to about 29 C. This was about 1 C lower than the initial water temperature at the bottom. It indicates the effect of cold water upwelling

and advection from the deeper shelf areas in the south. This station remained fully mixed for the next 50 hours and the temperature increased to about 29.4 C. Since station P5 is located within 1Rmw, its temperature was highly affected by the hurricane induced upwelling.

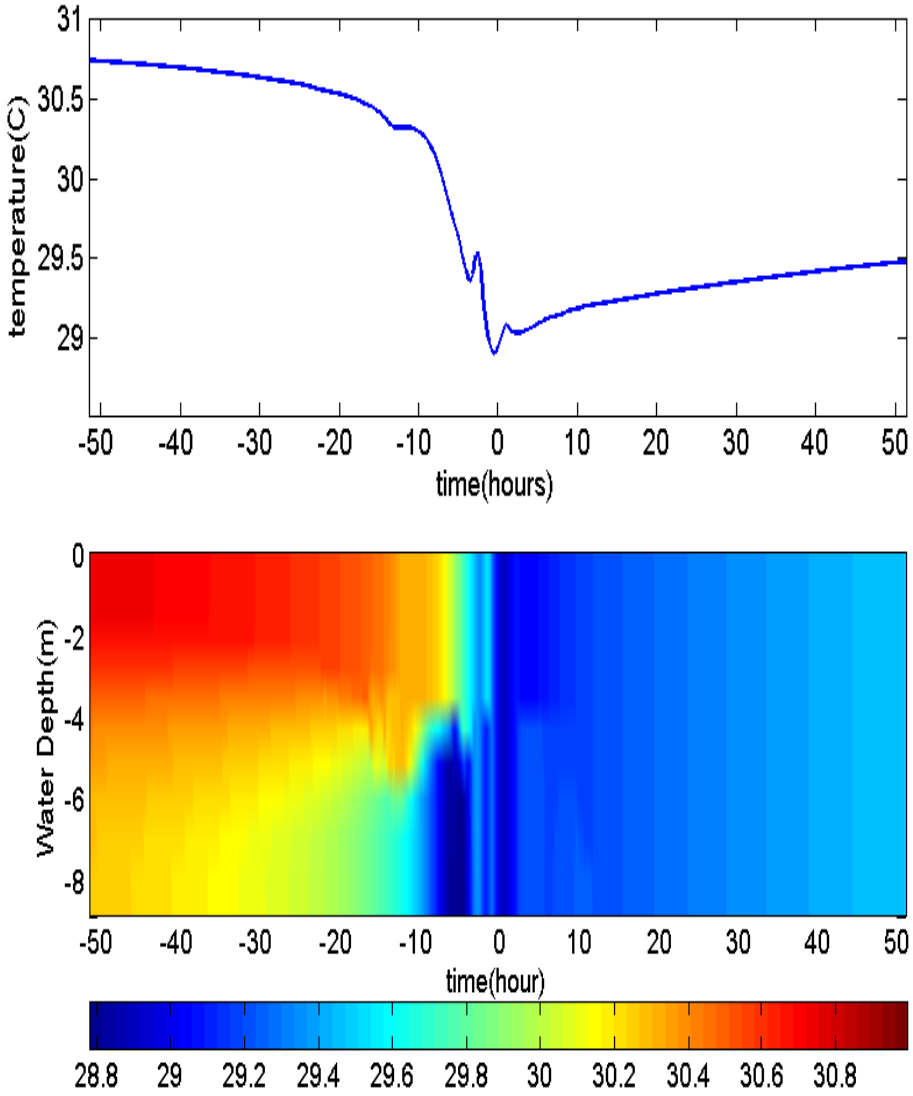

Figure 4.21: Upper panel: time variations of simulated SST at P5 for 50 hours before and 50 hours after the time that Katrina passed the closest proximity of this point, lower panel: time series of vertical temperature at this point for the same time period.

Station P6 was also on the right side of Katrina's track (Figure 4.16). It was located south of the South Pass at 30 m water and was about 10 km from the track. Katrina caused 2.5 C surface cooling at this station (Figure 4.22, upper panel). The major part of the cooling started from hour -20 when the SST was about 30.5 C. The SST decreased to about 28.5 C at hour 10 and remained the same for the next 40 hours before it started a gentle increase. The initial

stratification at this station was disturbed primary by the upwelling at about hour -10 (Figure 4.22, lower panel). This caused an increase of 2.5 C in water temperature at about 25 m.

Due to the proximity of the station to the outer shelf and deep waters, the recovery of water column temperature after the hurricane's landfall was relatively slow, as illustrated by the vertical structure at hour 50 (Figure 4.22, lower panel).

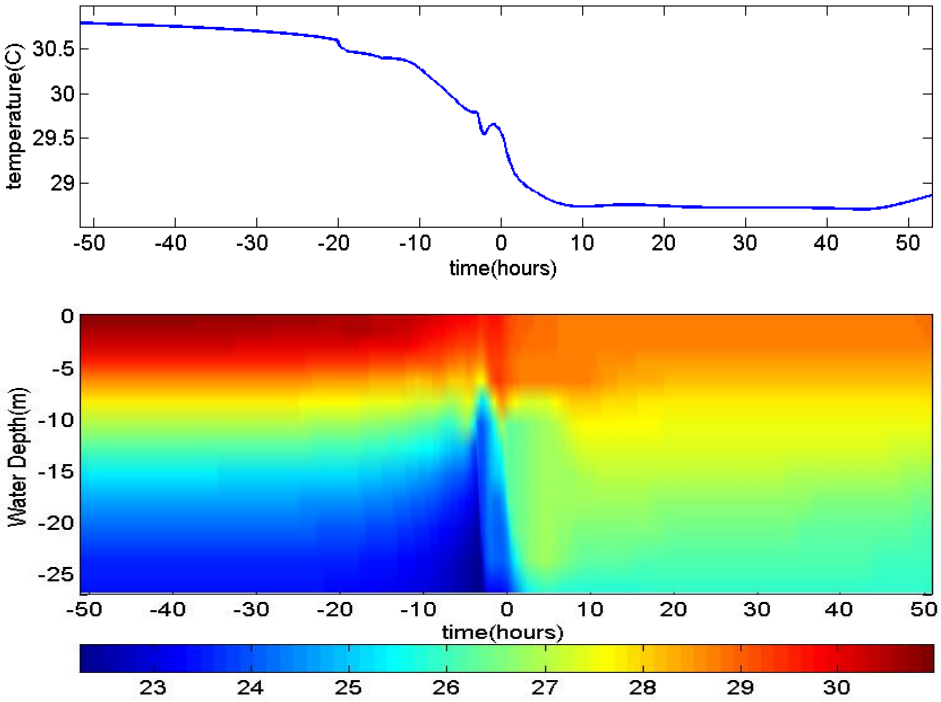

Figure 4.22: Upper panel: time variations of simulated SST at P6 for 50 hours before and 50 hours after the time that Katrina passed the closest proximity of this point, lower panel: time series of vertical temperature at this point for the same time period.

To investigate the outer shelf's response to Katrina, station P7 on the hurricane's track located 60 km southwest of the Birds-foot delta was selected. The Time series of SST and temperature structure for the upper 100 meter of water column are presented in Figure 4.23. The SST was shown to respond to the hurricane at about hour -12 (Figure 4.23, upper panel). Surface cooling induced by hurricane was more than 5 C. The largest response was produced at hour 3 when SST dropped to about 25.8 C. There was a slight increase of SST after this time. At hour 30 the SST reached 27.7 C and stayed stable for the next 24 hours. Water column stratification started to break down several hours before CP time and a mixed layer of 40 m with a temperature of 26 C was developed as a result of shear entrainment and upwelling produced over the interior region where it was less than 1 Rmw from the hurricane's center (Figure 4.23, lower panel). Due

to an intense cooling produced by the hurricane and the strong upwelling at this location almost no temperature recovery occurred after the hurricane passed.

For better understanding, a longer time series (15 days) of SST and vertical temperature structure are presented for P4 and P6 (Figures 4.24 and 4.25). At P4 both SST and stratification became stable at hour 50 and exhibited consistent patterns and values of temperature and the MLD over time. At this time the SST was still 1.2 C lower than the pre-storm SST (Figure 4.24).

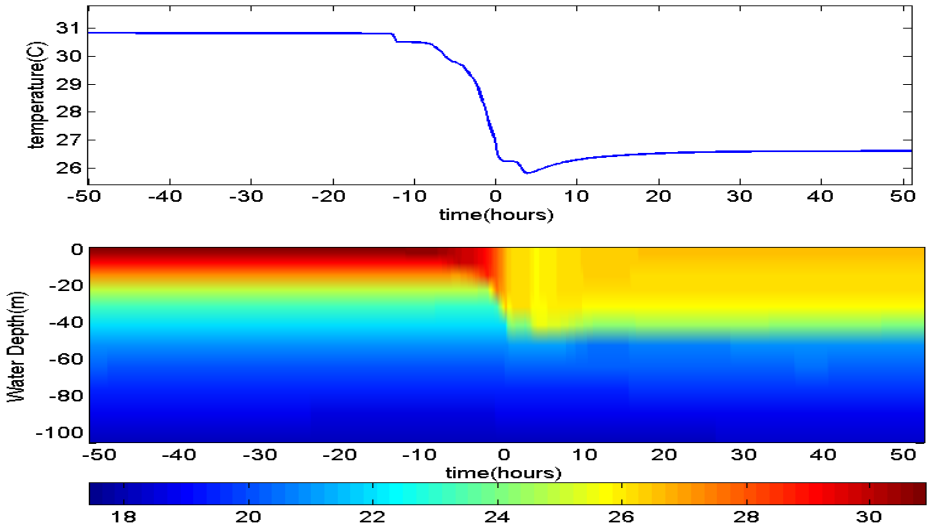

Figure 4.23: Upper panel: time variations of simulated SST at P7 for 50 hours before and 50 hours after the time that Katrina passed the closest proximity of this point, lower panel: time series of vertical temperature at this point for the same time period.

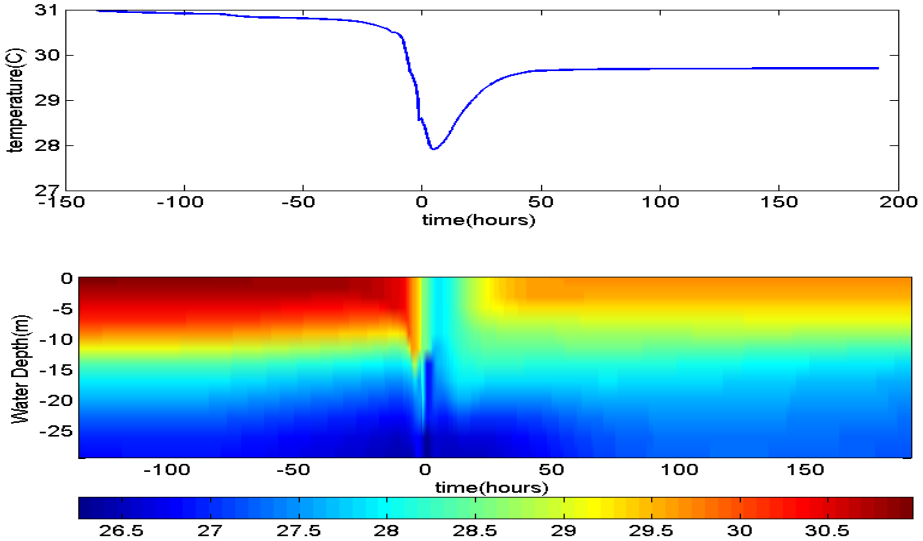

Figure 4.24: Upper panel: time variations of simulated SST at P4 for 15 days, lower panel: time series of vertical temperature at this point for the same time period.

The post-landfall temperature response at station P6 was similar to P4 (Figure 4.25). However, as mentioned before it took a longer time (longer than 50 hours after the landfall) for both SST and stratification to reach a stable condition (almost constant water temperature and MLD over time). The SST on the 9th day after the landfall was still 1.5 C lower than the initial value. The model results showed that this stable condition continued for at least two weeks after the landfall.

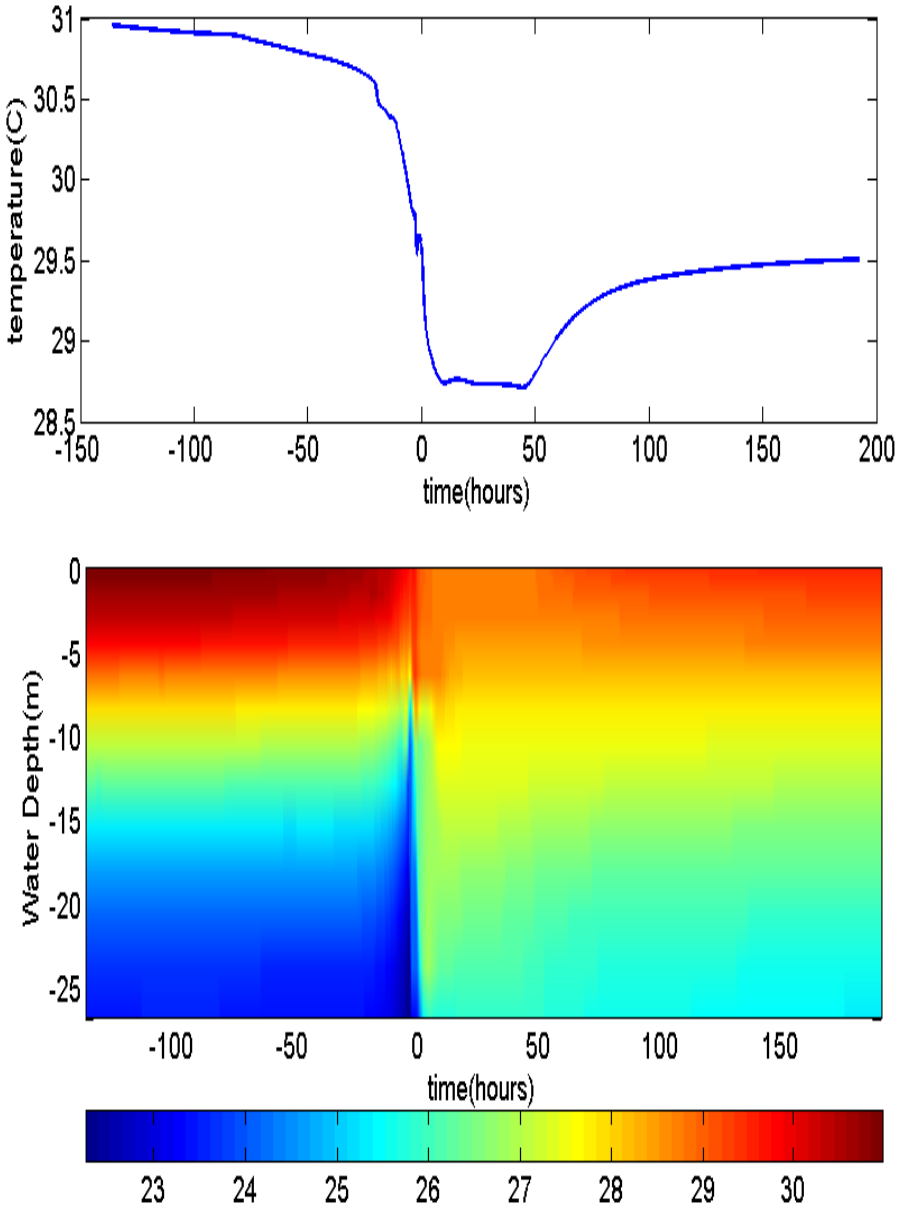

Figure 4.25: Upper panel: time variations of simulated SST at P4 for 15 days, lower panel: time series of vertical temperature at this point for the same time period.

4.4.3 Vertical Distribution of Temperature

Now we examine the vertical structures of water temperature across several north-south and east-west cross sections. Figure 4.26 shows locations of three east-west sections (EW1-EW3).

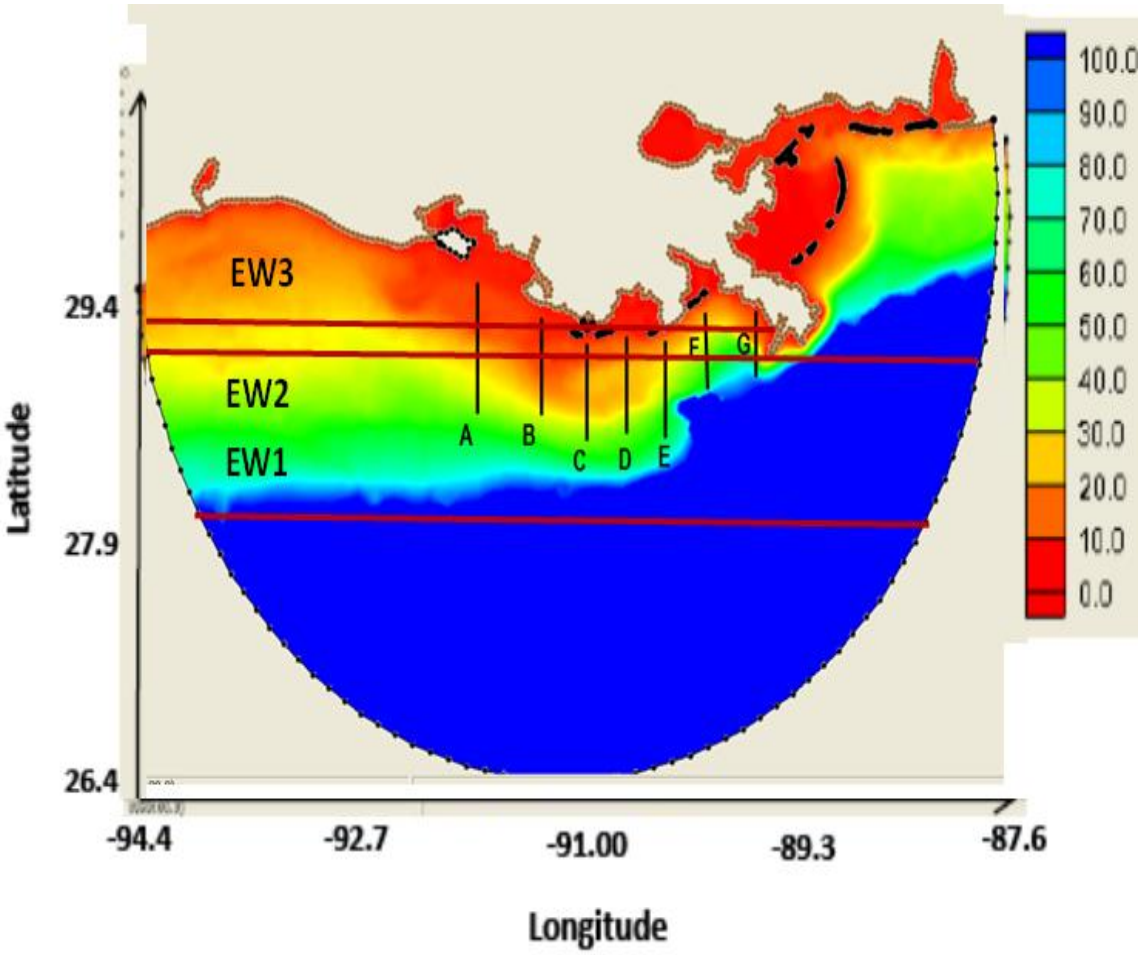

Figure 4.26: Locations of east-west sections and north-south transects selected for studying temperature structure.

In addition to the east-west sections, seven north-south transects (A-G) from the Atchafalaya Bay to the west of the Birds-foot delta were selected to examine the vertical temperature structure over the inner shelf for different times before, during and after Hurricane Katrina.

The east-west section EW1 was used to examine the response of the shelf water to Katrina. The eye crossed the section at 6:00 (UTC) on 29 August 2005. This point was located almost 100 km southwest of the Birds-foot delta. Water depths along this section are greater than 100 m.

Figure 4.27a shows the vertical structure of water temperature along this section for different times (hours -12, 0, +3). For each east-west section, the time reference is when the hurricane eye crossed the section. Hence, negative time was before the eye reached the section and positive after. The horizontal isotherms demonstrated that the outer shelf was still under the stable pre-storm stratification 12 hours before the eye crossed the section (at hour -12; Figure 4.27a).

At hour zero (the time that the eye crossed the section) the water column was significantly mixed, particularly on the right hand side of the hurricane's track. The maximum MLD was about 70 m on the right hand side at about 1Rmw from the hurricane's center, which is consistent with numerical results (e.g. Elsberry, 1976) with a MLD temperature of 25 C. Compared to the MLD just outside of the 1Rmw, the MLD under the center of hurricane was smaller (about 45-55 m) with higher mixed layer temperature (about 26-27 C) (Figure 4.27a). The MLD over the interior region was highly affected by upwelling created by divergence induced by the hurricane wind, while over the outer areas the combined downwelling and high turbulence mixing increased the MLD. Oscillations at the base of the mixed layer around the hurricane's center were the result of relatively high forward speed of the hurricane as reported by Bender (1993).

On the left hand side of the track and in the outer region, the MLD decreased from about 55 m (at about 35 km from the center) to about 25 m (at about 100 km from the center). The effect of hurricane-induced mixing was less pronounced on the left side of the track for distances larger than 150 km from the center. Three hours after the eye crossed this section the overall pattern of water column mixing was almost unchanged. However, changes can be seen in MLD and temperature on both sides of the track. On the right side there was slight increase in mixed layer temperature and the maximum MLD. On the left side, changes were more considerable. Mixed layer at this time was more developed with fewer irregularities. The location of cooling area on both sides of the track and also the location of unaffected water column was consistent with the MW-OI SST data for August 29, 2005.

At hour 6 (Figure 4.27b), the response was very similar to that at hour 3. Since the eye was located about 150 km north of the section, the depression of isotherms stopped and smoother spatial variations at the base of the mixed layer were observed. Both upwelling and downwelling started to relax as a result of the pressure gradient dissipation. Hence, the amplitude of the internal waves at the base of the mixed layer and at the vicinity of the track decreased to about 10 m. This caused a decrease of the maximum MLD on the right and an increase in the interior. Temperature structure at hour 24 (Figure 4.27b) showed a substantial dissipation of oscillations at the base of the mixed layer adjacent to the hurricane's track. The maximum MLD decreased to about 55 m and the vertical isotherms on the left of the track started to tilt as a sign of re-stratification. At day 9 after the eye crossed the section, the isotherm became relatively horizontal in water depths greater than 40 m (Figure 4.27b). The mixed layer depth on the right

side of the track was significantly decreased, although the SST (26.5 C) was still substantially smaller than the initial SST (31 C).

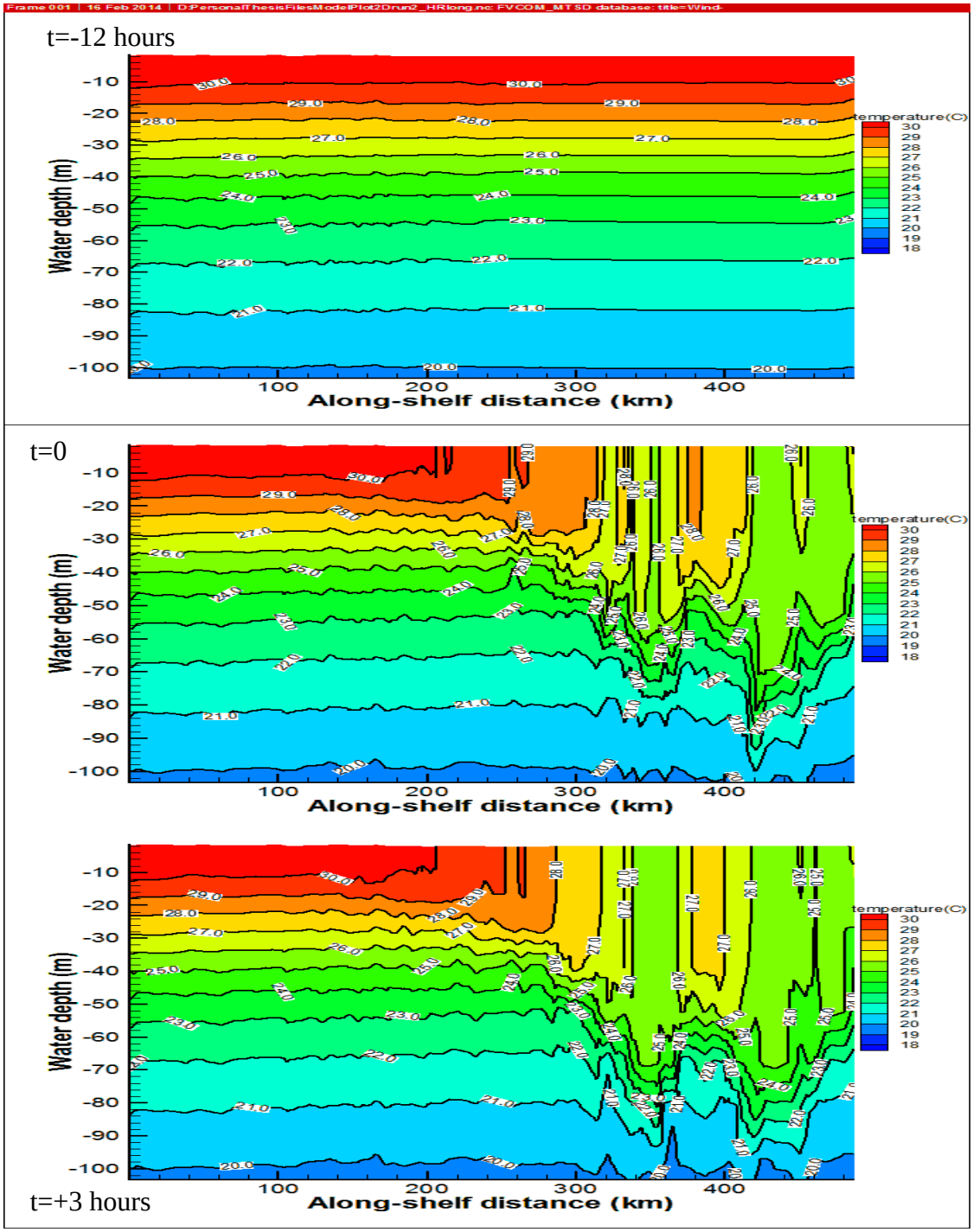

Figure 4.27a: Variations of simulated water temperature across section EW1 for different times.

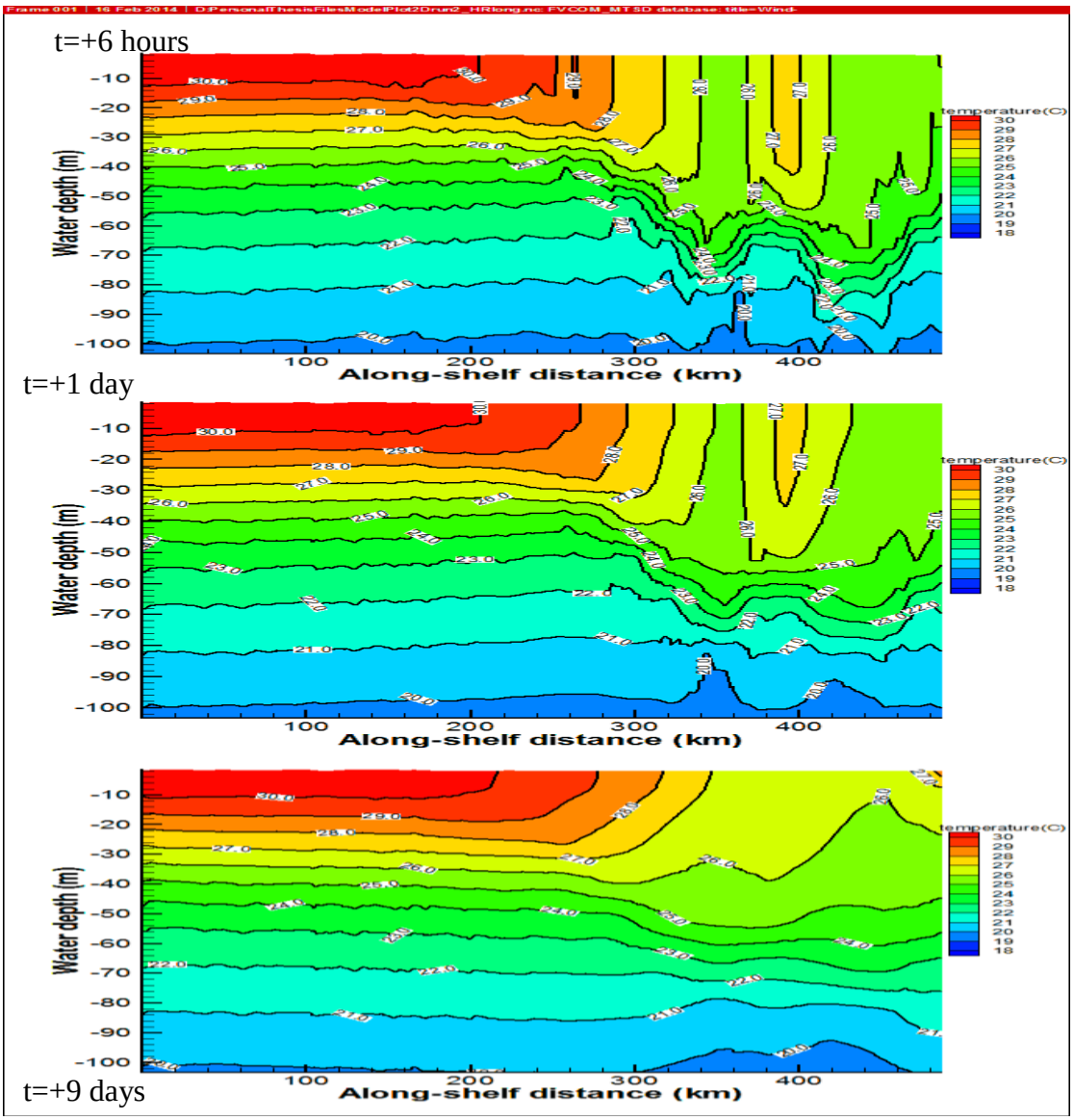

Figure 4.27b: Variations of simulated water temperature across section EW1 for different times.

Section EW2 crossed latitude 28.8, south of the Birds-foot delta, almost at the shelf break. Similar to section EW1, temperature variations were examined from the time that the eye crossed the section. At hour -12, the initial stratification was almost intact (Figure 4.28a). At hour zero, intense mixing was produced under the eye and on the right of the track similar to section EW1. The maximum MLD was ~65 m with water temperature of 25 C and was observed at about 40 km from the eye which was about 1Rmw. Under the eye, the MLD was about 50 meter as a result of smaller turbulence mixing and the hurricane-induced upwelling.

The amplitude of oscillations produced at the base of the mixed layer and the right side of the track was about 10 meter. These oscillations dissipated when hit the bottom of the shelf and produced a complex pattern of temperature variations across the lower water column off the

Barataria and the Terrebonne Bays (Figure 4.28a). The MLD and mixed layer temperature produced as a result of the turbulence mixing were about 35 m and 28 C, respectively, off the Barataria Bay. These values changed almost linearly to about 20 m and 30 C, respectively off the Terrebonne Bay. No significant mixing was produced west of this area along section EW2. The main feature of the temperature structure across this section at hour 3 was the formation of distinct mixing zones with different temperatures as functions of the distance from where the eye crossed the section.

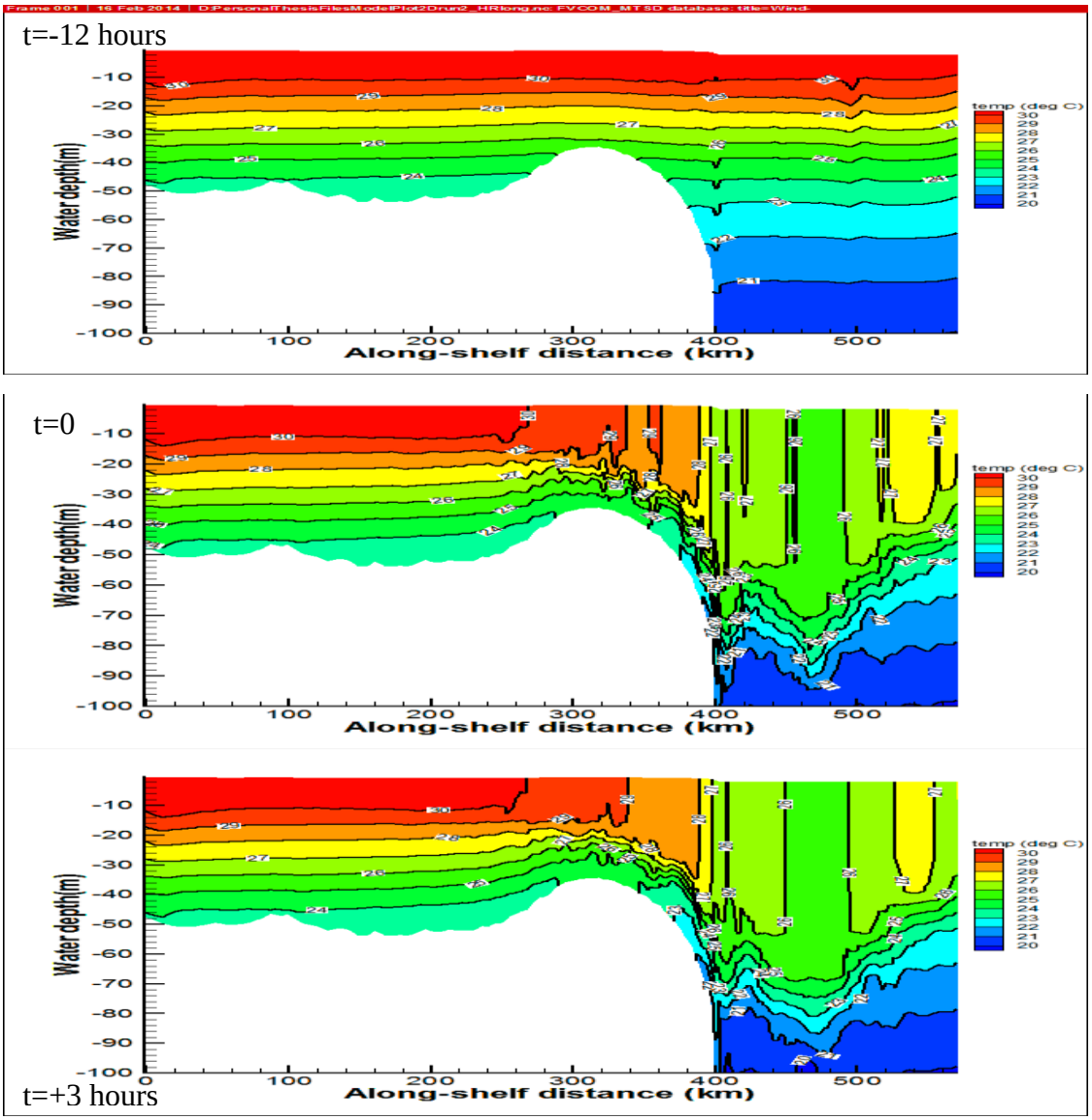

Figure 4.28a: Variations of simulated water temperature across section EW2 for different times.

A zone of maximum mixing similar to time zero was present at 40-80 km on the right side. Another zone of substantial mixing with smaller MLD (about 50 m) was under the eye's

location and a third one on the right side of the maximum MLD. The mixing region over the shelf west of the track can also be divided to different zones with decreasing MLD westward. These temperature and patterns lasted at least to hour 6 (Figure 4.28b). Eighteen hours later (hour 24), the stratification in the shelf water west of the Barataria Bay and off Terrebonne and Barataria Bays started to recover. For mixed zones on the right of the track, the pattern stayed the same with slightly reduced MLD. A completely stratified water column off the Barataria Bay was the most distinct feature of temperature distribution along EW2 on the beginning of day 9 after the eye crossed the section.

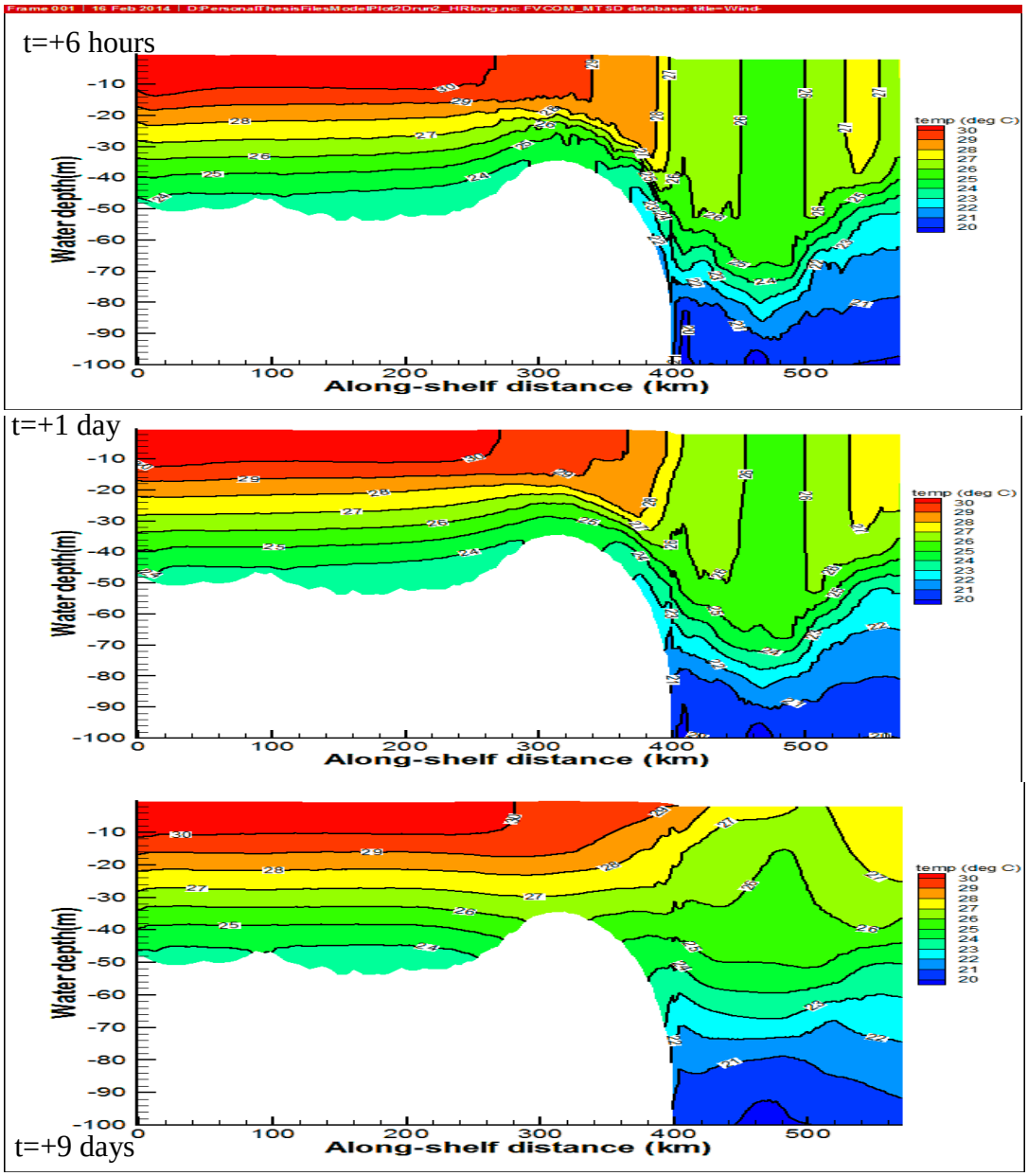

Figure 4.28b: Variations of simulated water temperature across section EW2 for different times.

More details about the temperature response of the inner shelf to Katrina are examined along section EW3. The section was extended from the Southwest Pass to the west including the inner shelf waters outside of the Barataria and Terrebonne Bays and mid-shelf waters outside of the Atchafalaya Bay (Figure 4.26). Temperature response along this section is presented in Figure 4.29a and Figure 4.29b. Similar to sections EW1 and EW2 at hour -12 the initial shelf-wide stratification was almost intact. When the eye crossed the sections (time zero) the deeper regions west of the Birds-foot delta and off the Barataria Bay were significantly affected by the hurricane-induced mixing. A maximum MLD of 40 m and temperature of 27.5 C was produced on the right side of the track, but 30 m 28 C under the eye. The oscillations at the base of the mixed layer were confined by the bottom, similar to section EW2, producing a complex temperature structure near the bottom. The effect of hurricane mixing west of the Terrebonne Bay was not pronounced.

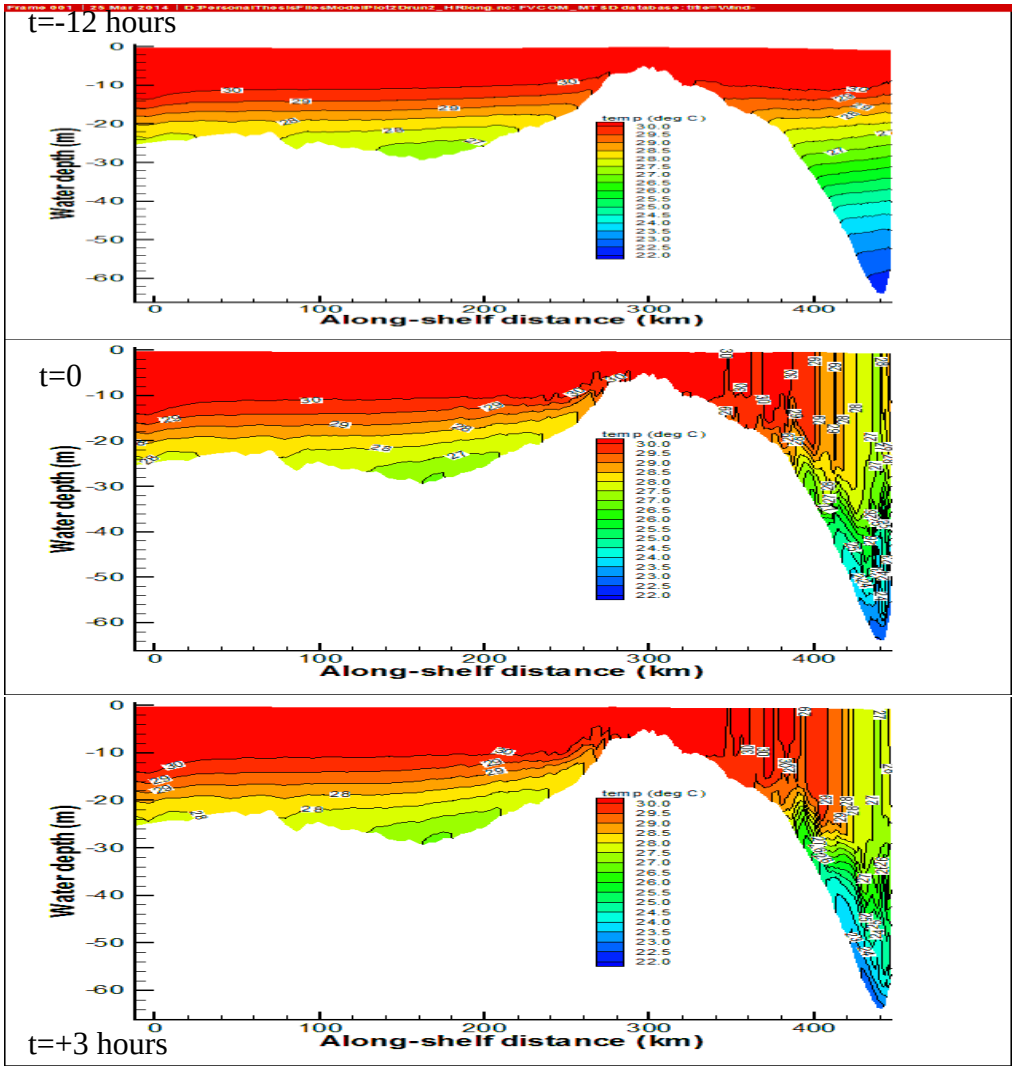

Figure 4.29a: Variations of simulated water temperature across section EW3 for different times.

The MLD over this area was smaller than 5-10 m. Deeper than 10 m, the initial stratification remained. However, as a result of the pressure gradient induced by the remote wind, the isotherms sloped westward. A substantial mitigation of mixing was produced on the left side of the track 3 hours later. At this time the MLD left of the track and the mouth of Terrebonne Bay started to decrease with an increase in temperature. The average water temperature over this area was 29.5 C. The recovery of stratification started from the right side of the track. At hour 6 the dissipation trend of mixing and shelf re-stratification continued. The overall temperature distribution pattern was similar to hour 3, but the reduction of MLD was more pronounced. The location of the maximum MLD did not change but its magnitude decreased to about 30 m and the temperature increased to about 28 C. At the base of mixed layer along the track, the oscillations were smoother and a stratified layer between the surface mixed layer and the bottom cold water was formed. By hour 24 the mixed layer almost disappeared.

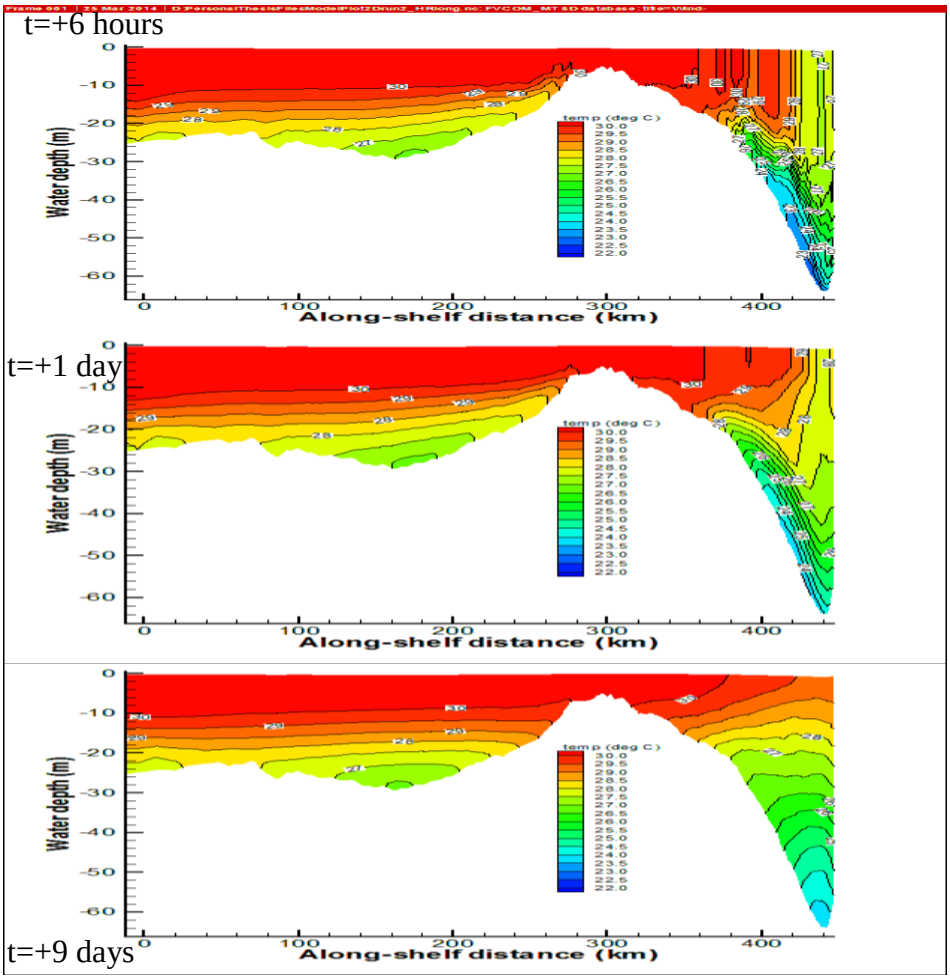

Figure 4.29b: Variations of simulated water temperature across section EW3 for different times.

The vertical profile of temperature at day 9 showed a complete stratification over the shelf water west of the Terrebonne Bay and less stratified to the east (the area which was directly

affected by the hurricane wind). More model results for temperature variations across sections EW1 and EW2 at different times are presented in appendix A. Similar to the east-west sections, the temperature response along the north-south transects is presented for 6 different times i.e. hours -12, 0, 3, 6, 24, and +196 (or 9 days).

4.4.3.1 Transect A

This transect was about 220 km on the left side of the hurricane's track. No significant temperature response was seen across this transect (Figure 4.30) and the stratification was not significantly affected by the hurricane. The initially leveled isotherms sloped toward the shore due to the hurricane offshore wind starting at hour -12. At hour zero small oscillations were seen along the isotherms for the upper 20 m. The oscillations caused a concave pattern of isotherms when they met the bottom. The shoreward inclination of isotherms existed even on day 9.

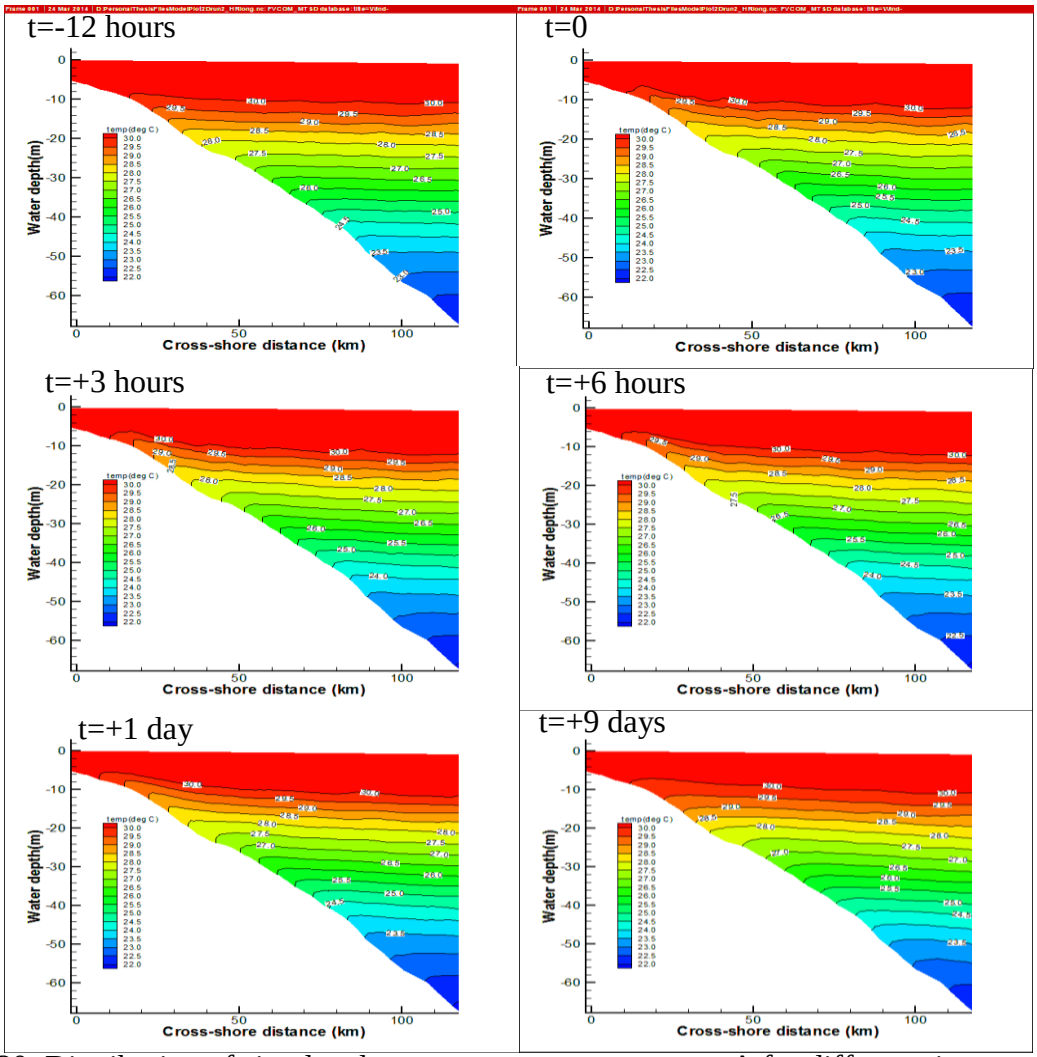

Figure 4.30: Distribution of simulated temperature across transect A for different times.

4.4.3.2 Transect B

This transect was between the Atchafalaya and Terrebonne Bays, about 180 km west of the track. Similar to transect A, the initial isotherms were inclined toward the shore at hour -12 (Figure 4.31). At hour zero, large amplitude oscillations were introduced to the isotherms in the upper 10 m, causing an average of 7 m MLD. The oscillations decreased in amplitude with increasing depth and disappeared at about 40 m. The isotherm below a 20 m upper layer was inclined more toward the shore, indicating an upwelling of colder water.

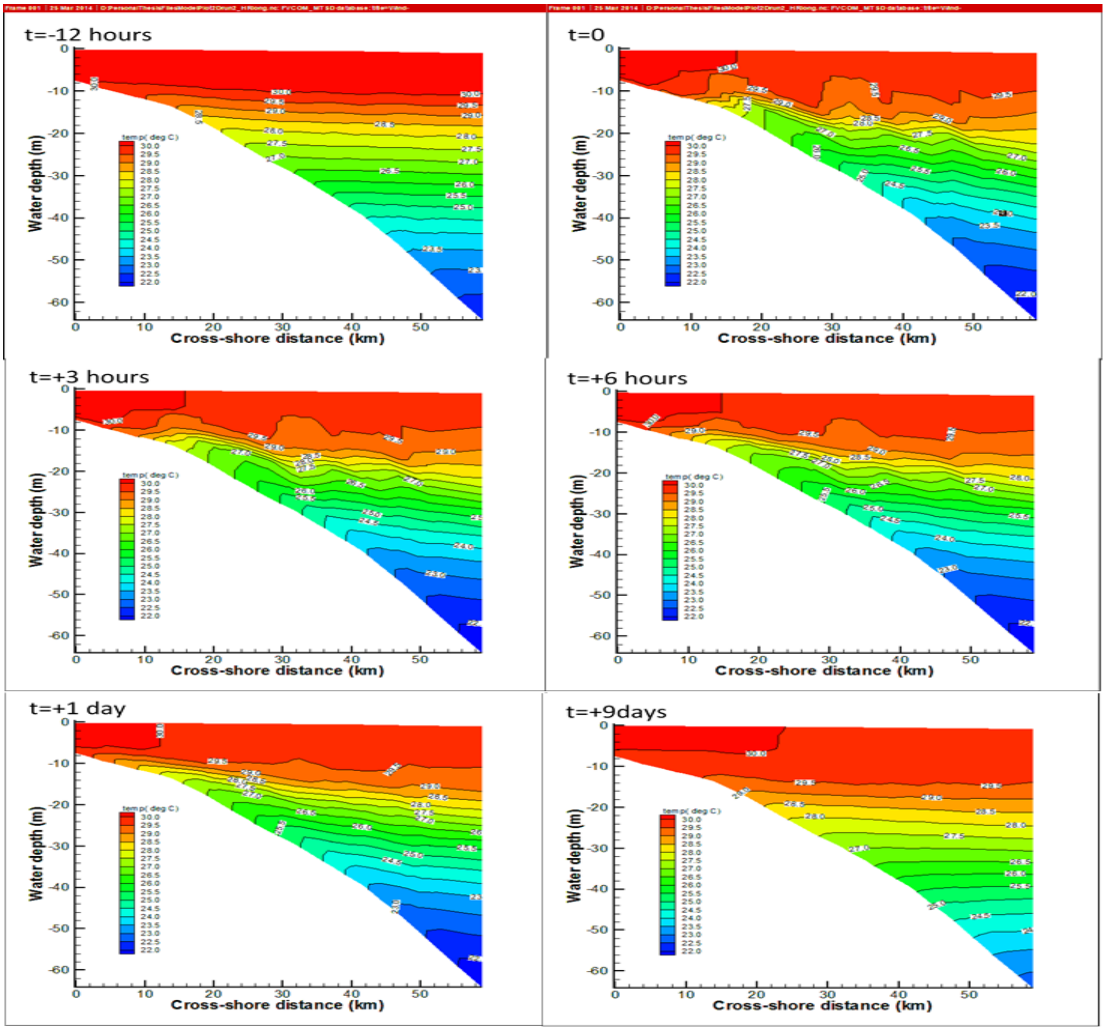

Figure 4.31: Distribution of simulated temperature across transect B for different times.

As the eye approached the shore within the next 3-6 hours more disturbances were produced where isotherms met the bottom and deep water upwelling progressed more toward the shore. The maximum MLD during this time period was about 12 m in the middle of the transect. At hour 24 the shoreward slope of the isotherms remained the same. However, most oscillations

along the isotherms were dissipated and the cold, upwelled water receded compared to that at hour 6. The isotherms were almost horizontal on day 9.

4.4.3.3 Transect C

Transect C is located west of the Terrebonne Bay, and 150 km from the hurricane's track. The stratification at this transects at hour -12 was still pretty much the same as the initial condition (Figure 4.32). When the eye approached the middle of the transect, the MLD at the offshore end of the transect (water depth of about 60 m) was 23 m with a 28.5 C water temperature. The upper 20 m was almost well mixed. Below 20 m, a zone of oscillatory temperature was produced, separating the surface mixed layer from the cold, upwelled waters.

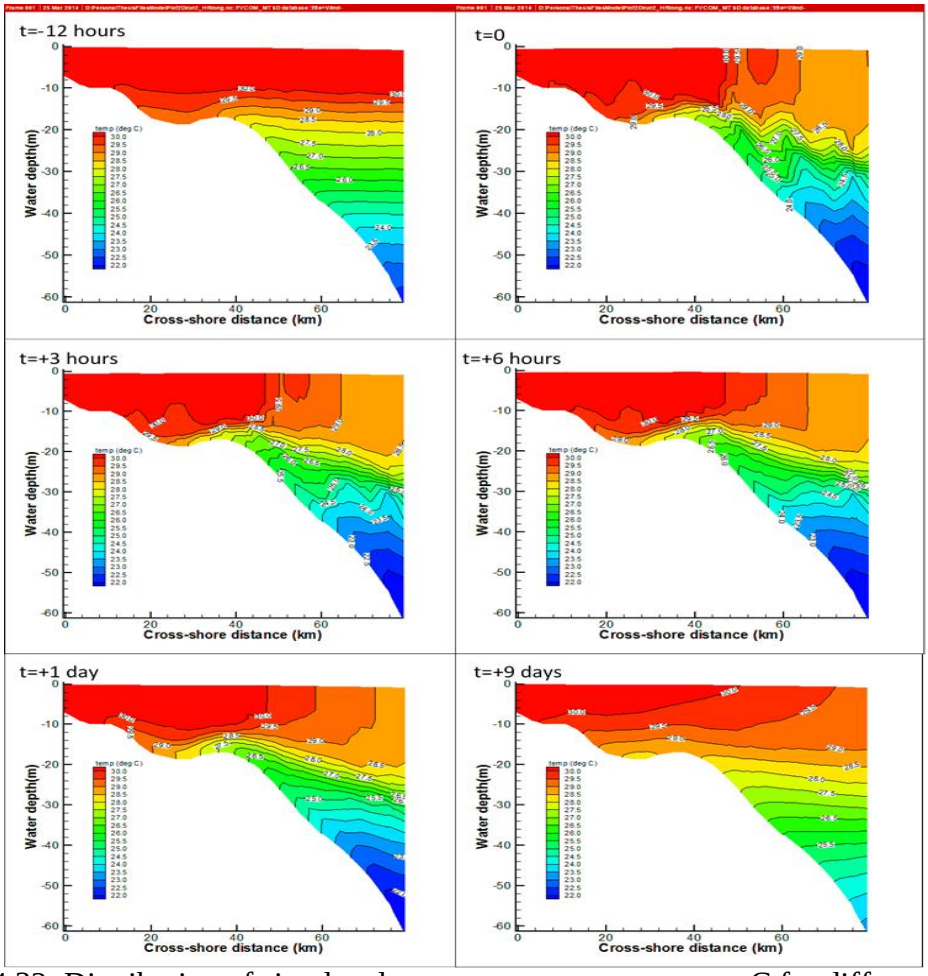

Figure 4.32: Distribution of simulated temperature across transect C for different times.

Temperature oscillations were observed in waters as deep as 45 m. The upwelling affected the shoreward part of the section. Similar patterns were observed at hours 3 and 6. However, oscillations at the base of the mixed layer were smoother and the effect of upwelling was more pronounced. On day 1, the surface mixed layer had already started to shrink. The

upwelling effect in the mid-shelf waters was still pronounced and mid-depth isotherms were smooth. Nine days after the eye past the middle of the transect, water column below 20 m was almost stratified, while the upper 20 m was partially stratified. Contrary to transects A and B, the slope of the isotherm for the upper water column was offshore ward, suggesting a pressure gradient from the outer shelf toward the inner shelf.

4.4.3.4 Transect D

Transect D, about 100 km on the left of the Katrina's track, in front of the Terrebonne Bay. Very small oscillations were produced along the isotherms for the upper 20 m water column at hour -12 (Figure 4.33).

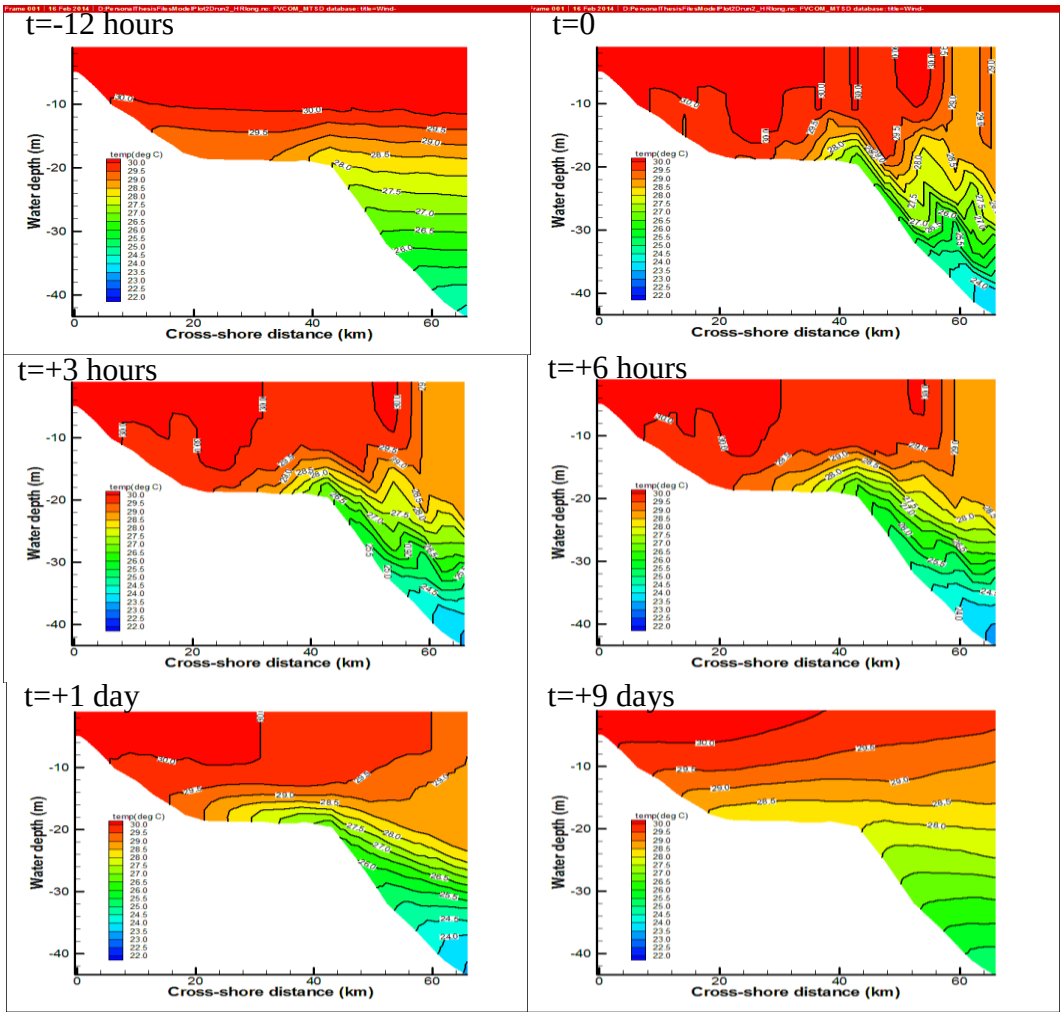

Figure 4.33: Distribution of simulated temperature across transect D for different times.

The lower layer zone had a complex pattern of temperature oscillations that caused cold water intrusion from offshore landward. The MLD at the offshore end of this transect had a maximum value of 21 m. At hour 3 the surface mixed layer was well developed. The maximum

MLD at the offshore end was more uniform. The MLD at the mid-shelf (~20 m) was about 15 m. A similar pattern was observed at hour 6 with smoother mid-depth oscillations. Eighteen hours later (hour 24), the re-stratification was pronounced and across the upper 20 m, the hurricane-induced mixed layer was vanishing. Below 20 m, a significant stratification was established. The isotherms sloped shoreward, while for the upper part the isotherms were inclined offshore ward.

4.4.3.5 Transect E

Transect E was between the Terrebonne and Barataria Bays. Although, before the hurricane reached the inner shelf the vertical temperature structure was almost intact from the initial stratification, the offshore-ward inclination of isotherms at depth 32-40 m showed a weak downwelling caused by the wind of the hurricane from offshore (Figure 4.34).

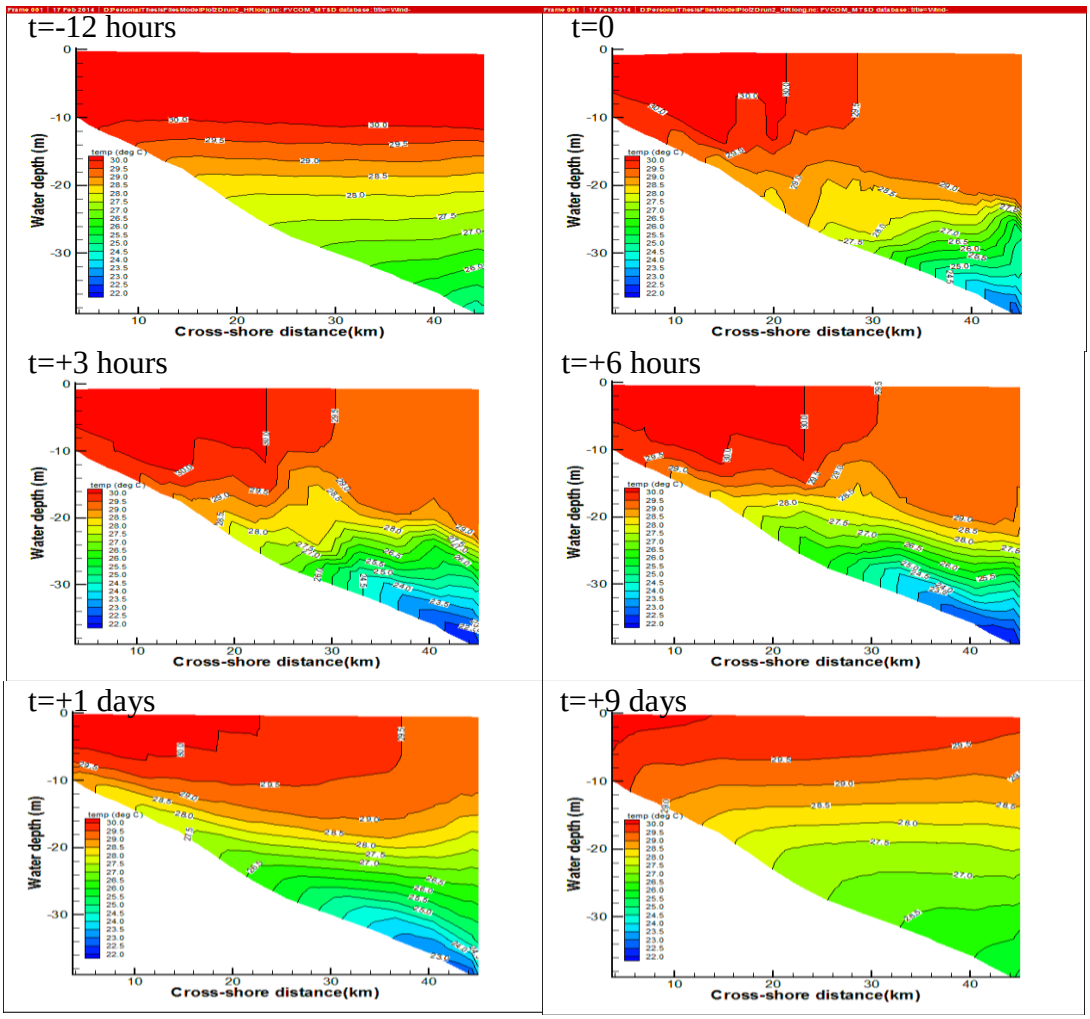

Figure 4.34: Distribution of simulated temperature across transect E for different times.

The maximum MLD at the end of transect at time zero was about 25 m in a water of about 40 m. At this time, the upper water column from the mid-shelf to the coast was still at the

initial phase of mixing. Below 25 m, there was a zone of high vertical temperature gradient and temperature oscillations at the base of mixed layer. The average slope of isotherms at these levels was still offshore ward indicating that the response was still controlled by downwelling. At the lowest water column, a colder water zone suggested an upwelling. The upwelling lasted during the next 3-6 hours. At hour 24, the water was shown having a partial re-stratification, especially for depth greater than 15 m. The upwelling was receding down slope and the surface mixed layer was replaced by a stratified layer. A moderate stratification was observed on day 9 with more inclined isotherms in the upper 10 m. This demonstrates that even after 9 days the initial stratification was not recovered.

4.4.3.6 Transect F

This transect was selected 20 km left of the hurricane's track, in front of the Barataria Bay. The initial stratification was broken at time zero when the maximum MLD was about 45 m at the offshore edge of the transect (Figure 4.35).

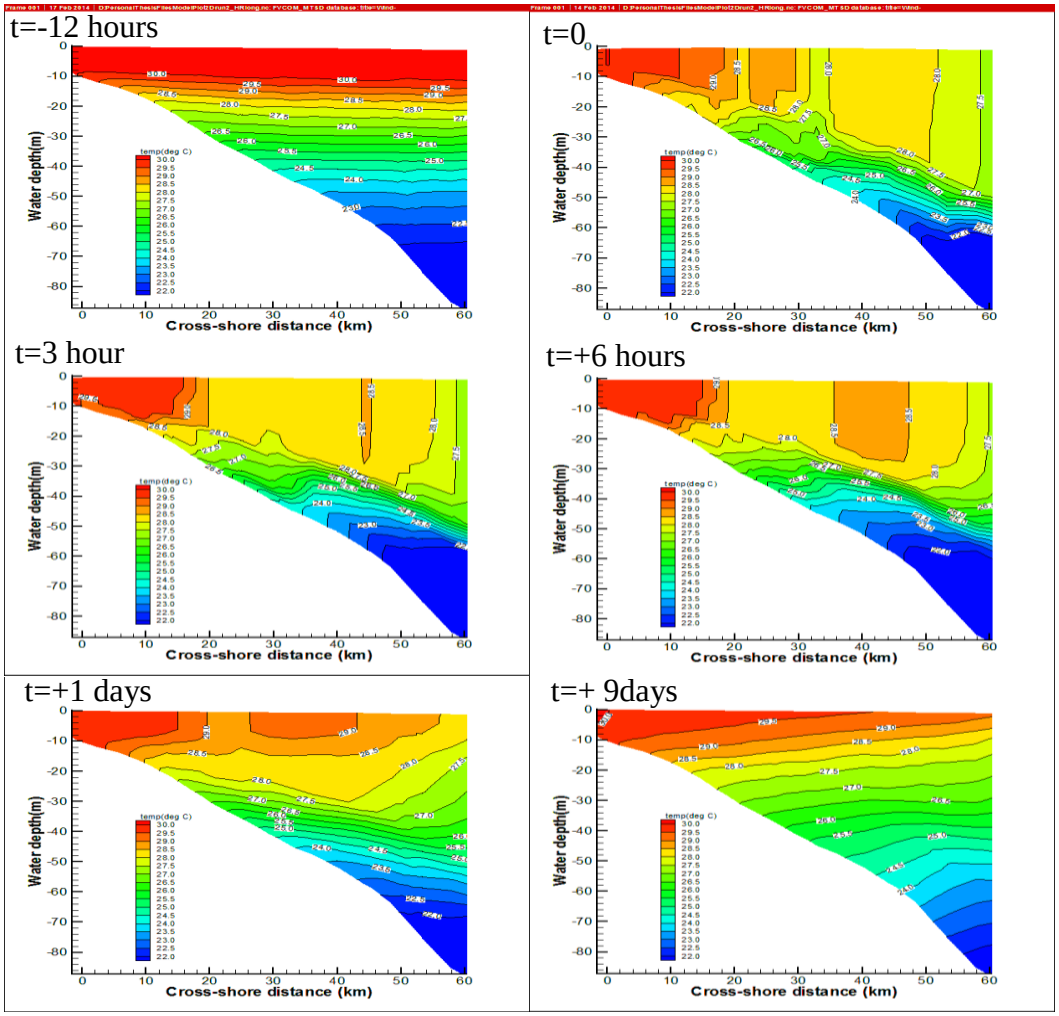

Figure 4.35: Distribution of simulated temperature across transect F for different times.

This substantial mixing was due to the intense hurricane wind within the 1Rmw. The MLD decreased linearly to about 10 meters at 15 meter water, while the mixed layer temperature decreased from 27.5 C at the offshore edge to about 29.5 C at depth of 15 meters. At depth greater than 50 m, the upwelling was pronounced. Between the surface mixed layer and the bottom upwelled water there was an intense temperature gradient. As the eye reached the latitude of the upper transect (at hour 3) the mixed layer temperature along the transect was already uniform. At hour 6 the maximum MLD decreased to about 35 m and the upwelled water started to decrease the MLD at the mid-shelf. At day 1 the surface water was still mixed with a MLD of about 10 m. At depth greater than 25 m, the upwelling started to recede but the isotherms were still inclined shoreward. Isotherms between 15 m and 30 m showed onshore and offshore slopes, respectively.

4.4.3.7 Transect G

Transect G was on the left of the Southwest Pass and 10 km of the right side of the track. At this location a remarkable effect of the hurricane wind on stratification was seen. At time zero (Figure 4.36), the MLD reached its maximum value of 55 m at the offshore end of the transect in 90 m water.

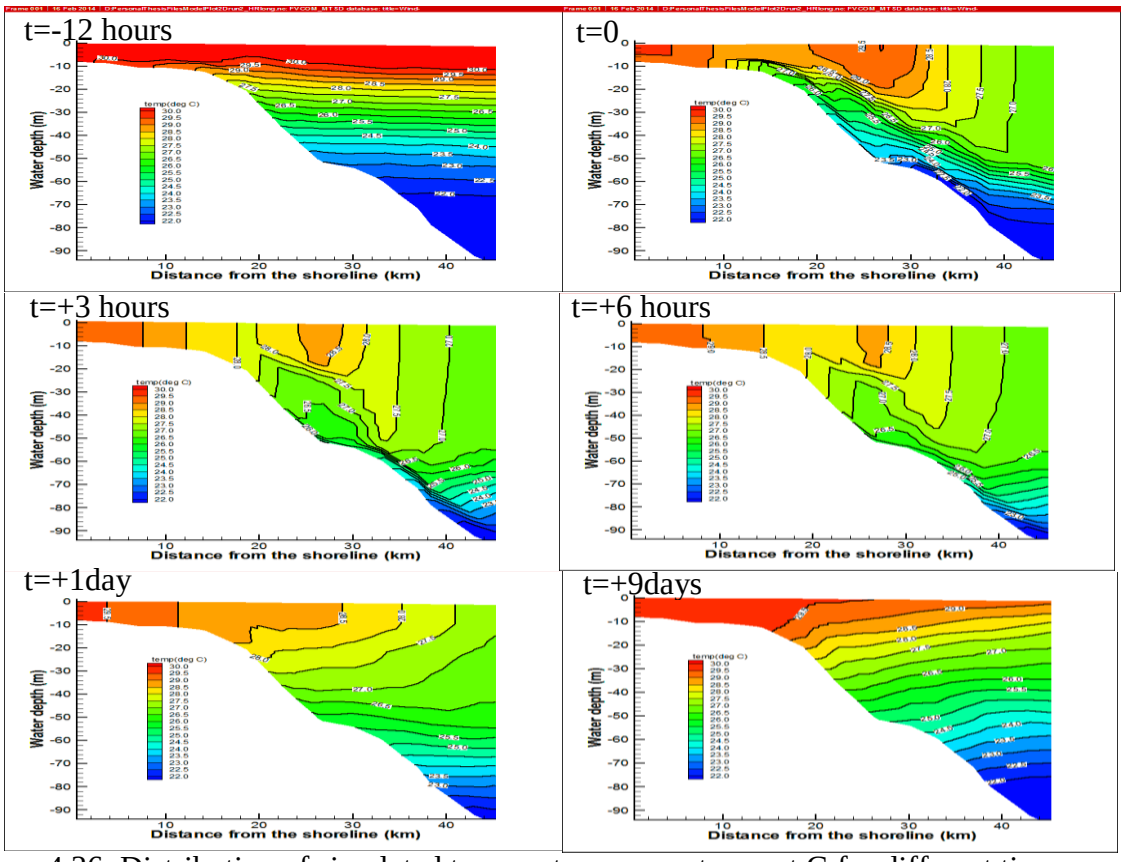

Figure 4.36: Distribution of simulated temperature across transect G for different times.

Strong upwelling was produced under the mixed layer, transporting cold water to the coastal areas up to 10 m. At hour 3, turbulence mixing dominated the upwelling and most parts of the transect were mixed. The MLD at this time varied between 60 m at the offshore end to 10 m at the on shore end of the transect. Due to intense vertical shear induced by the hurricane, the water column within 25 m was fully mixed. The mixed layer temperature varied between 26 C and 29 C. The fast deepening of the mixed layer interrupted the upwelling at 55 m. The pattern at hour 6 was similar to that at hour 3. Mixing was still dominant in the upper 12 m at the end of day 1 when the coastal areas less than 12 m were fully mixed. The stratification in waters deeper than 50 m was re-developed. Similar to transect F, at the end of day 9, the stratification was affected by the cross shelf gradient. More model results for temperature variations across north-south transect at different times are presented in appendix B.

4.4.4 Mixed Layer Depth

Variations of the MLD over the inner and outer Louisiana shelves were calculated using model results. A criterion for determining the mixed layer was applied following Montegut et al (2004). Base on this criterion if the temperature difference was less than 0.2 C, the water column was assumed to be mixed. The MLD maps are presented at four different times including hours -4, -2, 0, and 2 where time 0 is the landfall time (Figure 4.37).

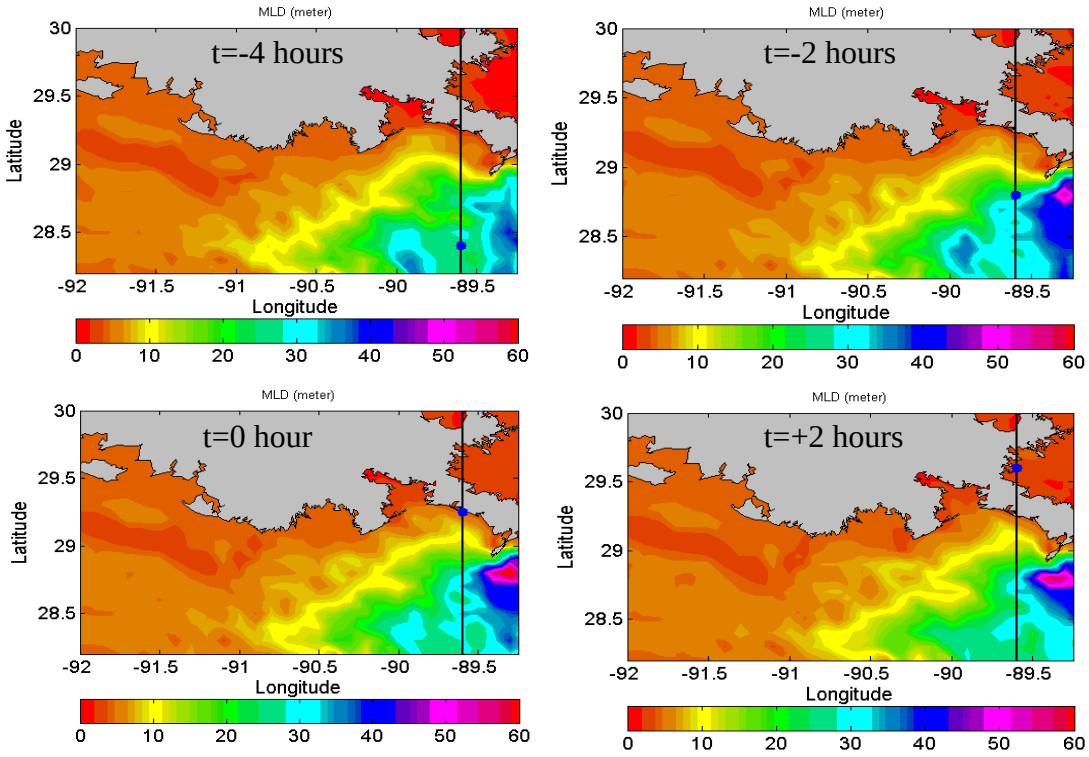

Figure 4.37: Variations of simulated MLD over the Louisiana shelf at different times.

At hour -4, the maximum MLD over the deep water on the right side of the track was about 40 m. An extensive area with MLD of about 20-25 m was observed on the left side of the track. The effect of the hurricane on the deepening of the mixed layer was pronounced off the Barataria Bay midway between the shelf break and the Bay's mouth. The deepening extended to the west off the Terrebonne Bay near the shelf break where the MLD was about 10 m. Over the rest of the inner shelf the MLD was about 5 m. At the time of landfall, more area over the inner shelf east of the Atchafalaya Bay was affected by the MLD deepening. The deepening also occurred in front of the Baratria Bay and west of the Birds-foot delta.

4.5 Discussion

4.5.1 Mixing Mechanism over the Louisiana Shelf

Study of water temperature response across the east-west sections and north-south transects indicated that during the hurricane, the water column properties were affected by both turbulence mixing and upwelling/downwelling depending on the relative locations with respect to the eye and shelf bathymetry and geometry. Turbulence mixing is the dominant force across the water column at locations within 1 to 1.5Rmw from the eye (Keen and Glen, 1999), while at the interior area with radius less than 1Rmw, upwelling depresses the mixed layer induced by turbulence mixing (Elsbery et al., 1967). The interaction between turbulence mixing and upwelling was examined for different transects over the Louisiana shelf. For most transects, especially those located east of the Terrebonne Bay, both mechanisms were significant in affecting the temperature structure in the water column. A very simple conceptual model of water column mixing induced by Katrina over the inner-shelf is presented in Figure 4.38.

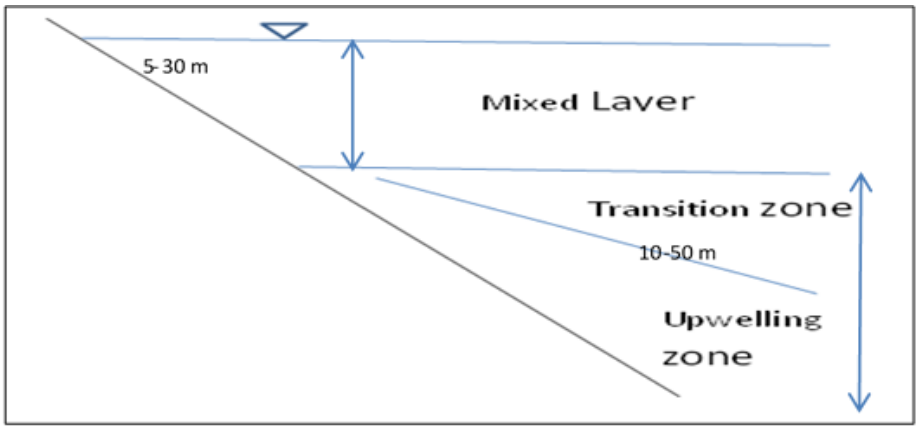

Figure 4.38: A schematic of water column mixing over the Louisiana shelf during Katrina.

The surface mixed layer was produced by turbulence mixing for the upper half of the water column, while the lower part of the water column was affected by upwelling. A transition zone of oscillatory temperature existed between these two zones. These oscillations caused mixed layer deepening when turbulence mixing was strong, upwelling was suppressed and large

mixed layer depths resulted. However, in the absence of strong turbulence mixing the oscillations dissipated with the progression of upwelling. To determine the dominant mechanism over the Louisiana shelf during Hurricane Katrina, the gradient Richardson number and buoyancy frequency (equation 1-1, Figures 4.39-4.45) are presented for the mid-water depths at different locations on the shelf. Although substantial declines (up to 75%) in the buoyancy frequency off the Atchafalaya and Terrebonne Bays (stations P1 and P2) occurred several hours before landfall, the resulted gradient Richardson number was about 2 which was larger than 0.25 for a fully mixed water column. It suggests that turbulence mixing at these two locations was not enough to mix the upper water column. It suggests that turbulence mixing at these two locations was not enough to mix the upper water column. The abrupt increase of buoyancy frequency for these stations indicated that the cooling by upwelling increased the density gradient over the uplifted thermocline.

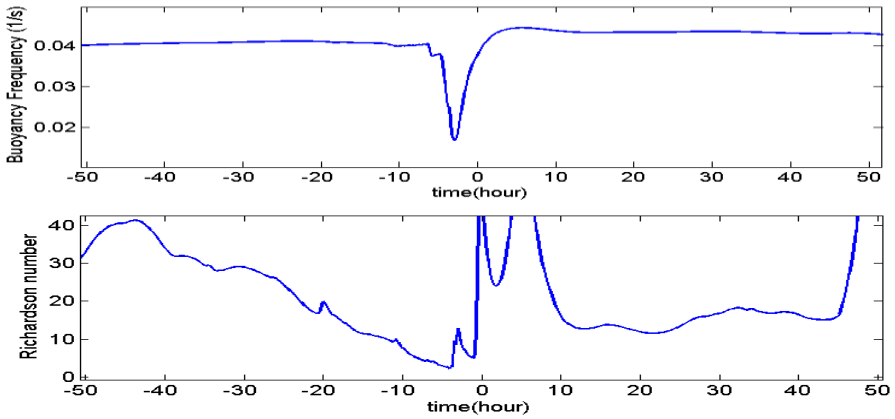

Figure 4.39: Time series of Buoyancy frequency (upper panel) and Richardson number (lower panel) at station P1.

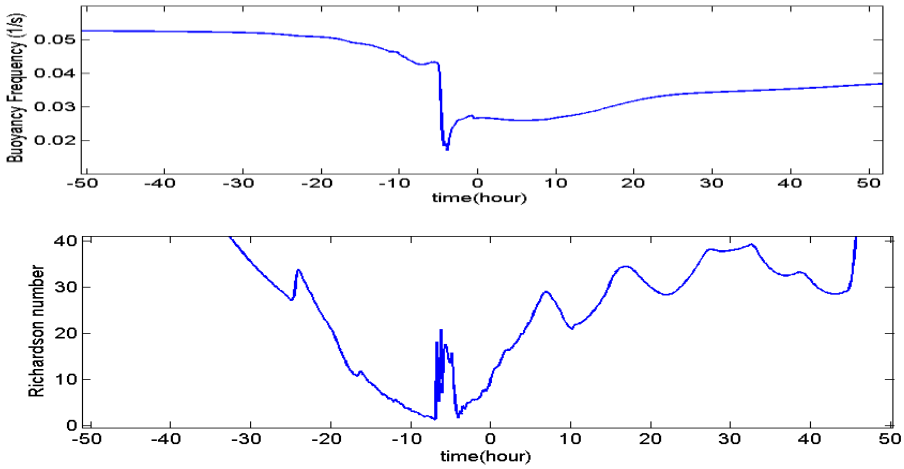

Figure 4.40: Time series of Buoyancy frequency (upper panel.) and Richardson number (lower panel) at station P2.

The very small gradient Richardson number at stations P3 and P4 for several times before and after the CP time showed the mixed water column at these two locations at least from the surface to mid-depth. This was consistent for these locations.

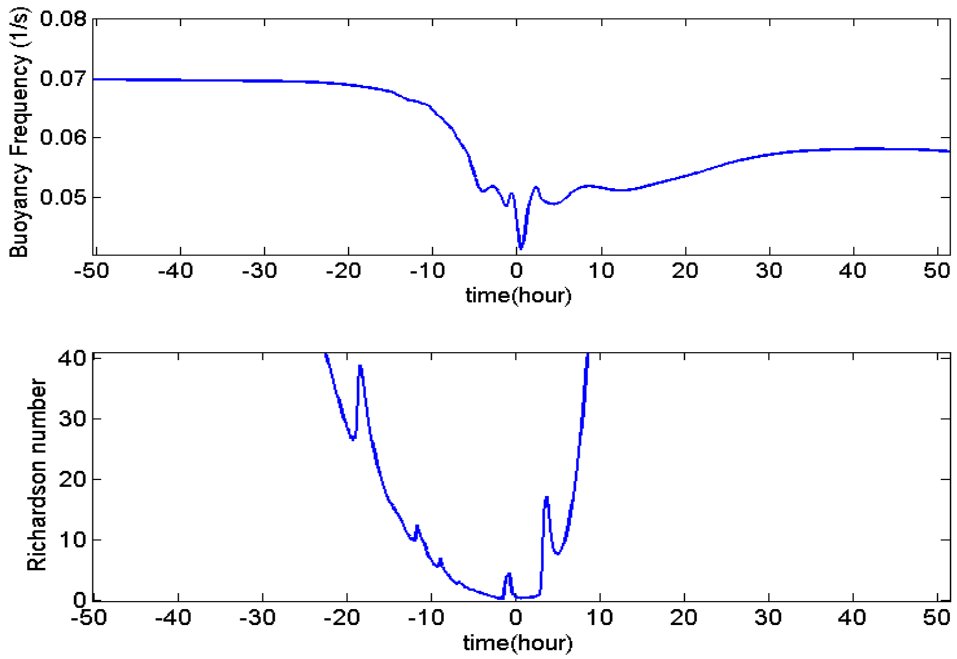

Figure 4.41: Time series of Buoyancy frequency (upper panel) and Richardson number (lower panel) at station P3.

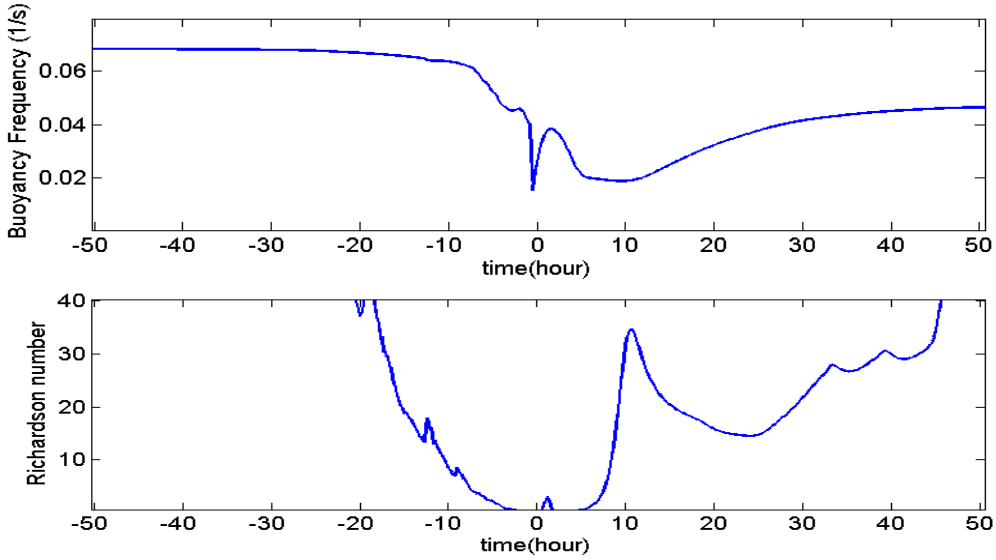

Figure 4.42: Time series of Buoyancy frequency (upper panel) and Richardson number (lower pa nel) at station P4.

The maximum effect of turbulence mixing was identified at station P5 on the right side of the track and west of the delta, where both the Richardson number and buoyancy frequency approached zero almost at CP time and water column stayed mixed at least for the next two days. This area was confined between the eye and the Birds-foot delta, hence a very intense surface current (up to 3.5 m/s) produced a strong vertical shear that fully mixed the water column and dominated the cooling effect of advected water from the shelf break to this area.

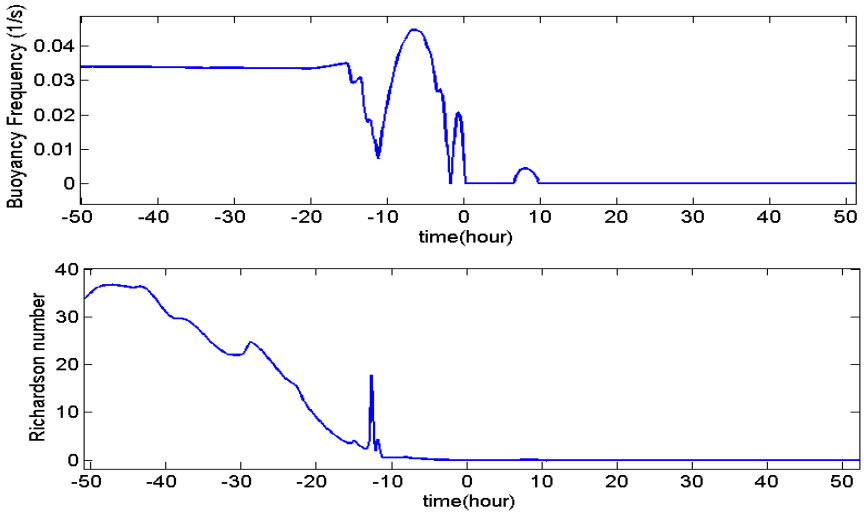

Figure 4.43: Time series of Buoyancy frequency (upper panel) and Richardson number (lower panel) at station P5.

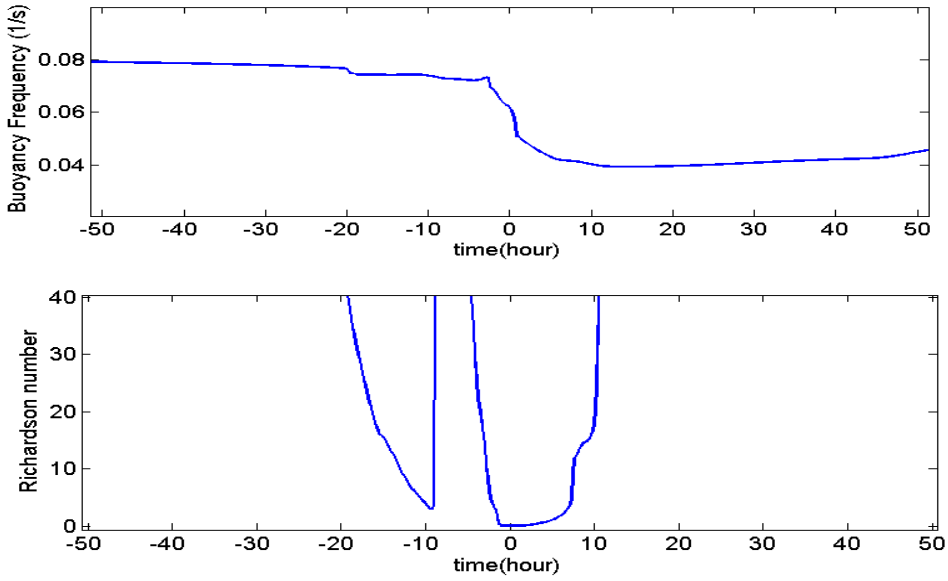

Figure 4.44: Time series of Buoyancy frequency (upper panel) and Richardson number (lower panel) at station P6.

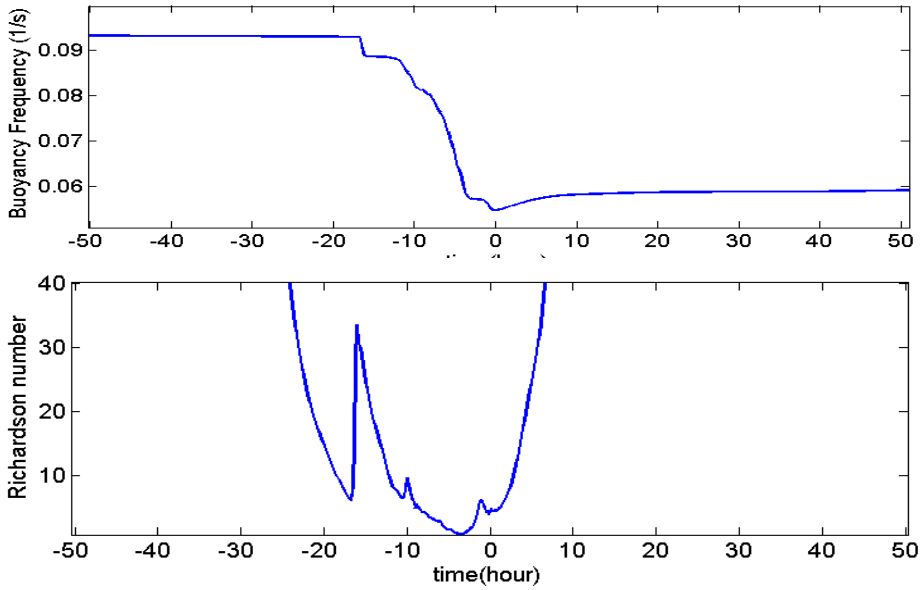

Figure 4.45: Time series of Buoyancy frequency (upper panel) and Richardson number (lower panel) at station P7.

4.5.2 The Effect of Coastal Geometry/Bottom Friction

The temperature response to a moving hurricane over the deep water is well-documented (e.g. Elsbery et al., 1967; Price, 1981; Bender, 1993; Ginis, 2002; Pan and Sun, 2012). Due to the absence of coastal and bed boundaries only the interaction between the atmospheric boundary layer and water column is required to be considered to define the response characteristics. In this regard, the spatialy variations of the mixed layer were determined using both analytical and numerical models. The studies showed the maximum MLD generally occurs on the right side of the track at the distance 1-1.5Rmw from the track (Elsbery et al., 1967; Price, 1981). Upwelling was identified as a dominant feature for the area within 1Rmw from the hurricane's center, while for the exterior area downwelling had a more significant footprint (Leiper, 1966; Elsbery et al., 1967; Martin, 1982). The interaction with the coastal geometry and the bottom boundary layer produces a more complicated response to a moving hurricane. The temperature cooling induced by Katrina at the surface over the deep water followed the general pattern as described above. Surface cooling rate decreased as the hurricane approached the shelf break. At the shelf break the cooling intensity substantially decreased, hence even at hour that the eye was hovering over the inner shelf surface, cooling was only significant in the vicinity of the track and over the other parts of inner shelf especially west of the Barataria Bay surface cooling was less than 1 C. It suggests that the internal waves contributed to deepening the mixed layer were dissipated when they met the bathymetry at the shelf break. Furthermore, the cross shelf slope intensified the upwelling signal over the inner shelf that can prevent mixed layer deepening (as examined for transects E and F). The Birds-foot delta highly affected currents and temperature response of the shelf waters confined between delta and the hurricane's track. Strong currents and vertical sheer

were identified over this area. This produced a fully mixed water column and very small Richardson numbers during the time that Katrina was translating the inner shelf.

4.5.3 Shelf re-Stratification Mechanism

After the turbulence mixing at the water surface is removed (several hours after the eye pass over specific location or after landfall) the re-stratification processes come into action and decreased the mixed layer depth until the initial stratification is reached. Over deep water, two main re-stratification forces are solar heat flux and baroclinic instability (Hosegood et al., 2008; Mei and Pasquero, 2011). Solar insolation mostly affects the stratification over the upper part of the mixed layer up to depth 25 m (Mei and Pasquero, 2011; Haney et al., 2012). Baroclinic instability is a result of vertical variations of water density caused by turbulence mixing. Furthermore, lateral gradients of water density could cause re-stratification (Hosegood et al., 2008).

Investigation of temperature variations across east-west sections and north-south transects showed that post-storm temperature recovery and shelf re-stratification starts several hours after the hurricane's landfall showing a substantial re-stratification after 1 day. Vertical temperature profiles across the transects, especially those located east of the Atchafalaya Bay, were affected by two different forces. The upper part of the water column was mixed by the hurricane-induced surface turbulence and vertical shear, while the produced pressure gradient, caused upwelling across the lower part of the water column. Offshore-ward currents were generated within the surface mixed layer on the right side of the track and a compensative shore-ward current was dominated within the lower water column. On the right side of the track, current directions across both upper and lower parts were reversed. After the hurricane force was removed, currents started a geostrophic balance phase that caused south-eastward current over the inner-shelf. Similar post-storm surface currents and their associated deep water reverse circulations were reported by Keen and Glen (1999) for Hurricane Andrew (1992) and by Mitchel et al. (2007) for Hurricane Ivan. While the pressure gradient produced as a result of vertical and horizontal variations of water density triggered the re-stratification, the offshore-ward advection associated with the geostrophic currents re-distributed isotherms and sloped them toward offshore. Current vectors rotated clockwise under the geostrophic balance and directed southward at about 3 days after landfall. This current lasted for several days and made more contribution in advection of surface water offshore-ward and re-shaping the isotherm toward a re-stratified shelf. The general pattern of re-stratifying isotherms across a transect over the Louisiana shelf after Katrina's landfall is presented in Figure 4.46.

Although, a well-developed shelf-wide thermal stratification was achieved at 10 days after landfall, isotherms were still inclined offshore-ward and SST was about 1C less than the initial value. Simulations for longer times after the landfall show that even after 20 days isotherms were still tilted. This suggests that solar insolation plays an important role in re-stratifying the shelf. The effect of solar heating on stratifying the Louisiana shelf was simulated

(chapter 6) and it was shown that the summertime solar insolation significantly stratifies the shelf and increases SST up to 1 C after almost two weeks.

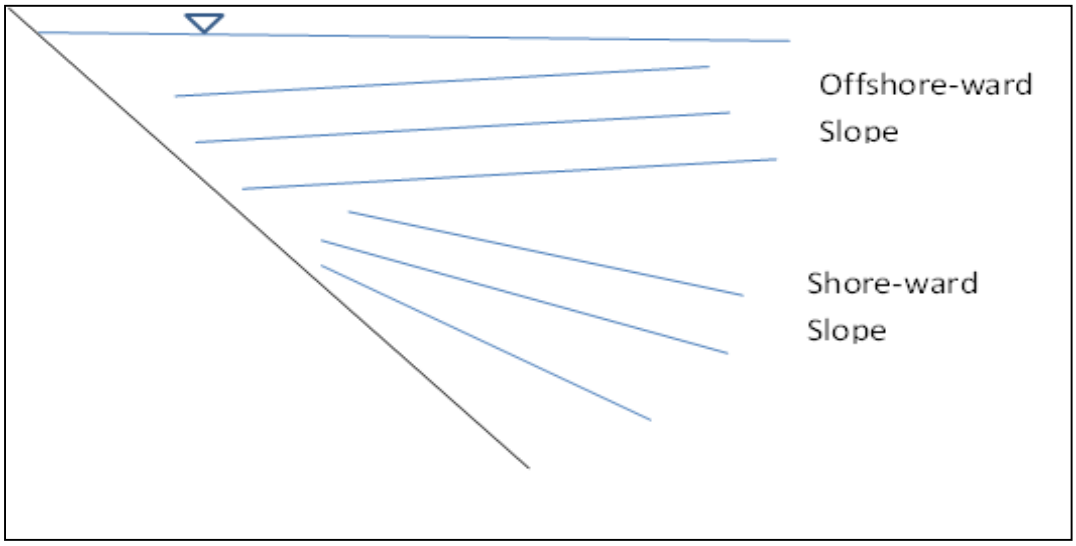

Figure 4.46: Typical distribution of isotherms across the water column during the re-stratification phase.

4.5.4 Comparing with Fall Storms

Simulation of Katrina's induced mixing over the Louisiana shelf showed that the hurricane induced mixing was transient and disappeared in several hours to a few days after landfall. Furthermore, the rapid decreasing of wind speed with increasing distance from the eye, limits the mixing area to the inner region with radius of 1-1.5 Rmw. This suggests that hurricanes' contribution in breaking down of the summertime shelf-wide stratification is temporally and spatially limited. As shown in Chapter 2, over the Louisiana shelf, wind stress during the summertime is substantially smaller than other seasons (Also see Wiseman et al., 1997). This leads to a persistant stratification and lack of water column re-oxygenation (Rabalais et al., 1994; Wiseman et al., 1997; Wang and Justic., 2009). Tropical storms and hurricanes are important mixing events during summer (DiMego, 1976). However, low occurence frequency and the stochastic nature of these events as well as the ephemeral behaviour of the associated mixing limits their effect in breaking down the summertime stable stratification over longer time periods. The wind stress increases significantly during fall (Chapter 2).

The late September corresponds to initiation of cold front outbreaks. Cold fronts are reported as the main mixing event that break down the stable summertime stratificatione over the Louisiana shelf (Rabalais et al., 1994; Wiseman et al., 1997). Wind speed a cold front passage can reach over 25 m/s over the shelf (Georgiou et al., 2005) which is able to produce strong

mixing shelfwide. In addition to high wind speeds associated with cold fronts. In comparison to tropical storms and hurricanes, cold fronts occure more frequently (every 3-7 days) from October to April (Roberts et al.,1991). Furthurmore, the direction of winds associated with cold fronts is relatively persistant and changes only between northeasterly and northwesterly while spread over more extensive areas over the shelf (Roberts et al.,1991). Hence, their cumulative impact on coastal environment is more pronounced than the tropical storms (Moeller et al., 1993). The main cummulative effect of a sequence of cold fronts on water column mixing can be weakening the strength of temperature and salinity stratification which makes the mixing process easier for the next coming cold front. The mixing effect of fall storms for October 2009 was simulated and some sample reults were presented in Appendix C. Results demonstrate the gradual but persistent deepening of the mixed layer during a one month period of fall storm outbreak.

4.6 Summary and Conclusions

In this chapter the simulation of water column mixing and re-stratification over the Louisiana shelf with the passage of Hurricane Katrina was discussed. The initial temperature and salinity profiles were based on climatological data for August from NOAA. The climatological temperature profiles were modified by using available temperature data measured using AVHRR (SST) and at two different depths (for CSI6). Satellite SST data were used to compare with the model output SST at the Louisiana shelf break. The data were also used to estimate MLD based on an analytical approach (Equation 4.1) and were successfully utilized to evaluate the simulated MLDs. Results were examined to represent temporal and spatial characteristics of mixing and re-stratification over the inner shelf. Since Katrina translated the inner shelf just west of the Birds-food delta, the mixing in most of the area between the shelf waters off the Barataria Bay and the Birds-foot delta were affected. The MLDs over this area were 10-30 m; while in the area west of the Barataria Bay the MLDs were 10 m or less. The hurricane-induced upwelling significantly affected the bottom temperature over the shelf from several hours before the hurricane reached the shelf to several days after that. West of Terrebonne Bay, the typical response of the water column was represented by a simple model including a mixed upper water column, upwelling dominated lower water column and transition zone in the middle containing dissipating oscillations at the base of mixed layer.

The shelf response to Hurricane Katrina was highly controlled by shelf bathymetry and geometry. Deep water oscillations of temperature were dissipated as they approach the bottom at the shelf break. The intense currents (up to 3 m/s) and vertical shears fully mixed the water column west of the Birds-foot delta. The main post-storm re-stratification mechanism over the inner shelf were vertical density gradients, lateral density gradients, and offshore pressure gradient produced by upwelling across the shelf. Since the solar insolation was not included in the simulations, the upper water column stratification and the SST did not return to their respective initial conditions even 10 days after landfall. Simulation of stratification induced by

the summertime solar radiation (Chapter 5) demonstrated that solar radiation significantly contributes to formation of the water column stratification and increased SST by 1 C or more.

Comparison of the resulted MLDs during and after Katrina with the maximum probable hypoxic zone over the shelf showed that the mixing over the hypoxic zone west of the Terrebonne bay can re-oxygenate the mid and bottom waters for several hours during Katrina. However, since the mixing was ephemeral and damped quickly after the landfall, the re-oxygenation appeared to be limited in time.

CHAPTER 5: NUMERICAL EXPERIMENT OF STRATIFICATION INDUCED BY SOLAR HEATING OVER THE LOUISIANA SHELF

5.1 Introduction

Studying hurricane induced temperature changes across the water column in Chapter 4 showed that just several hours after the landfall, re-stratification of water column started and after about 10 days, strong temperature stratification developed. However, isotherms were still inclined and the stratification was not recovered to the pre-storm condition even after 14 days. It was hypothesized that the reason could be caused by the neglecting of solar heating. In this chapter, the effect of solar heating on the shelf water temperature is simulated for the summer non-hurricane time to show the development of stratification.

The effect of solar heating on water column temperature is included as a heat source term in the model heat balance equation. The approach has been used by many to study the effect of atmospheric heat budget on the water column stratification and mixing during a hurricane (for example, Elsberry et al., 1976; Price, 1981; Bender et al., 1993; Zedler et al., 2002). Chen et al. (2003) presented a detailed overview of shelf heat budget and stratification under the effect of diurnal solar heating. They used different components of radiation to calculate the net heat flux as one of the inputs to the model to study stratification and circulation over the Georges Bank in the Gulf of Maine, using the ECOM-Si model. The attenuation of different wavelengths in the water column was different between the coastal and ocean waters. They controlled the selected approach by comparing the simulated sea surface temperature (SST) with the satellite SST. The simulation results showed a diurnal fluctuation of SST with approximately 1C difference between day and night temperatures, while the general trend showed an increase of SST during the simulations. In the present study we use the same approach, outlined in the study of Chen et al. (2003). The effect of diurnal solar heating on stratification is simulated and based on available data of dissolved oxygen concentration over the shelf; the role of the solar-induced stratification on bottom water hypoxia is investigated.

5.2 Numerical Model

To study the effect of solar heating on shelf stratification, an approach similar to that of Chen et al. (2003) has been followed. Solar radiation components have been introduced to FVCOM. The main equations solved by the model are momentum, continuity, salt transport, and heat transport and density equations. The equations representing heat and salt transport and density contribution are:

$$\frac{\partial T}{\partial t} + u\frac{\partial T}{\partial x} + v\frac{\partial T}{\partial y} + w\frac{\partial T}{\partial z} = \frac{\partial}{\partial z}\left(K_h \frac{\partial T}{\partial z}\right) + F_T \quad (5.1)$$

$$\frac{\partial S}{\partial t} + u\frac{\partial S}{\partial x} + v\frac{\partial S}{\partial y} + w\frac{\partial S}{\partial z} = \frac{\partial}{\partial z}\left(K_h \frac{\partial S}{\partial z}\right) + F_s \quad (5.2)$$

$$\rho = \rho(T, S) \quad (5.3)$$

in which T is water temperature, s is salinity, and ρ is water density. u, v, and w are current velocity components in x, y, and z directions respectively where x and y are horizontal coordinates and z represents the vertical coordinate. K_h is the vertical thermal diffusivity. and F_T and F_s represent horizontal thermal and salt diffusion terms.

Solar radiation is applied to the model equation through the surface boundary condition for temperature:

$$\frac{\partial T}{\partial z} = \frac{1}{\rho c_p K_h}[Q_n(x,y,t) - SW(x,y,\xi,t)] \quad (5.4)$$

In the above equation $Q_n(x,y,t)$ is the surface net heat flux which includes four components shortwave flux, longwave flux, sensible heat flux, and latent heat flux, $SW(x,y,t)$ is the shortwave flux at sea surface, and C_p is the specific heat of seawater.

Governing equations of flow as well as salt and heat transports are discretized using finite volumes and solved with Runge Kutta method. The computational mesh is the same as that used earlier (Figure 3.2). Figure 5.1 shows model bathymetry and the location of east-west and north-south sections selected for presenting model results.

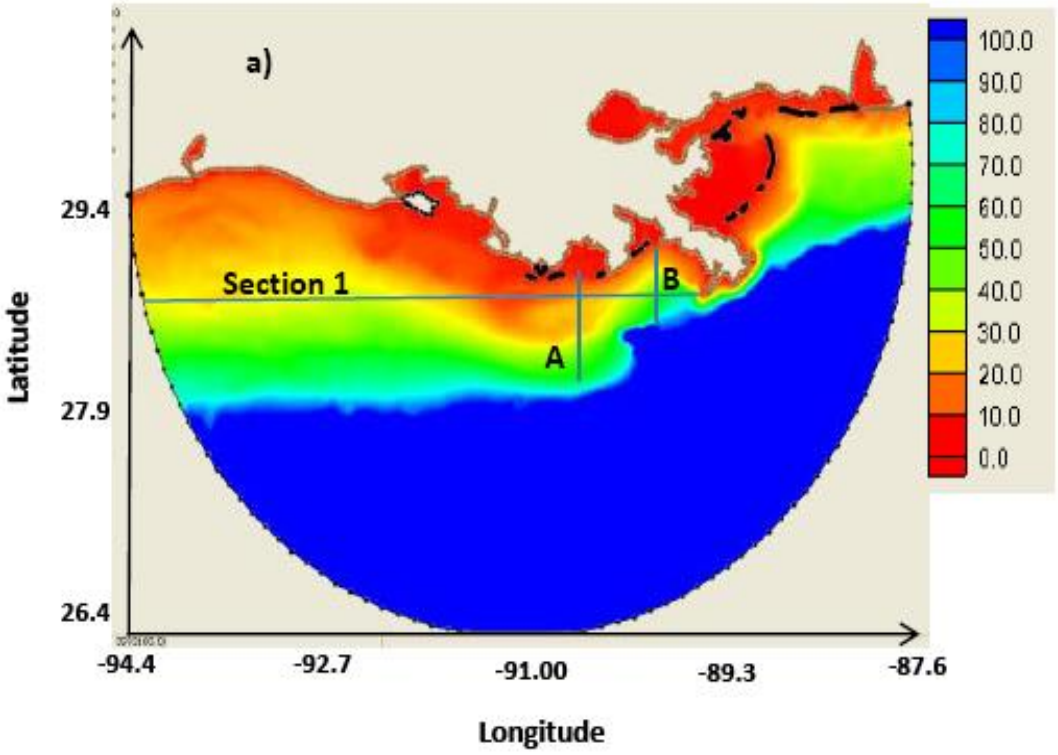

Figure 5.1: Modeling area and bathymetry, and location of sections.

5.3 Model Specification

5.3.1 Modeling Period and Data

Our simulation started in late May for several days of spin up to produce results in June because the summer related thermal stratification usually starts in June. Met-ocean data for June 2009 from the WAVCIS (www.wavcis.lsu.edu) station CSI-6, located off Terrebonne at 20 meter water depth (Stone et al., 2009) were used. The data were used for model setup and validation. Meteorological measurements including air pressure, air temperature, wind speed, and relative humidity as well as oceanographic data including sea surface temperature (SST) are used in calculating different components of input heat flux to the model (see section 5.3.2 and appendix D). SST data were also used to compare with the simulated SSTs under the effect of solar radiation. Figure 5.2 shows variations of measured SST at CSI-6 during June and July 2009. Variations of SST for a longer time period from May to December are shown in the inset. As it is shown, SST increased from May to the maximum value in August and decreased thereafter. The time series of June-July SST shows a generally increasing trend of SST with an average initial SST of about 26 C during the first few days. SST increased to a maximum of 31C by June 20 with daily fluctuations of about 1 degree. The SST stratification corresponding to this time period (from 10 to 20 June) are all oscillatory due to diurnal variation of heat flux, which continued till mid-July, when diurnal fluctuations of SST almost disappeared and SST varied following a very gentle slope. After this time, virtually no daytime heating or nighttime cooling occurred and the stratification strength during daytime and night-time was the same. The night time mitigation of stratification did not exist to assist for partial re-oxygenation in the water column, therefore severe hypoxic events are expected during this period. The disappearance of the daily variations of SST was most likely caused by cloud coverage in this time period.

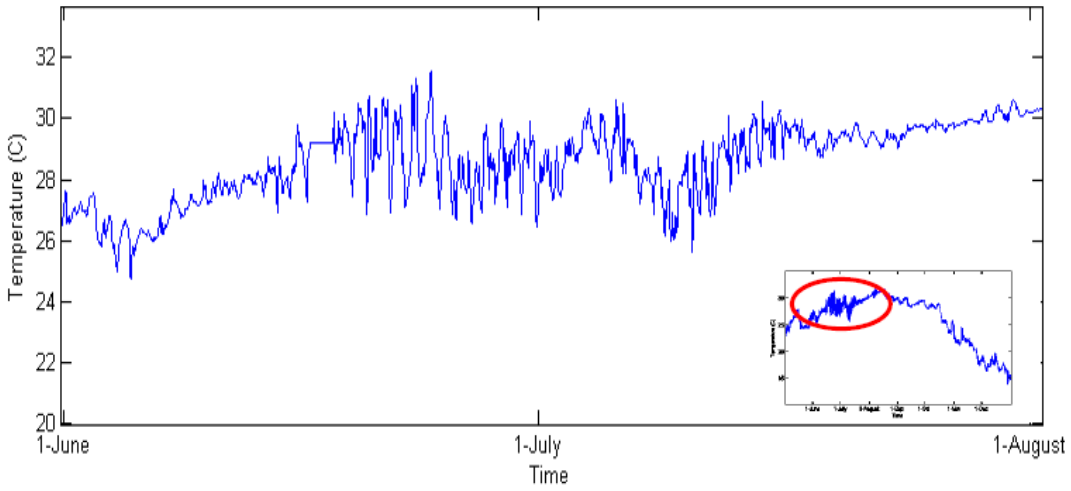

Figure 5.2: Timeseries of measured SST at the WAVCIS station CSI-6.

5.3.2 Model inputs

5.3.2.1 Heat flux

As mentioned in section 5.2, the effect of solar insolation on water temperature and density was incorporated in the model through the surface boundary condition involving two quantities: the net surface heat flux and short wave radiation flux. Although these parameters can be obtained from model outputs, low temporal resolution (time steps of 6 hour or larger) limits its use for a detailed study of diurnal shelf heating and stratification induced by solar insolation. Hence, heat flux components are calculated. Net heat flux to the water surface is the algebraic sum of for different components:

$$Q_N = Q_s + Q_{LW} + Q_L + Q_{sn} \tag{5.5}$$

in which the quantities on the right-hand side of the equation are shortwave, longwave, latent heat, and sensible heat fluxes, respectively. For each of them, the equations are presented in appendix D.

The hourly data provided an adequate temporal resolution of shortwave radiation and net heat flux. Figure 5.3 shows variations of both parameters from 1 June to 10 June 2009. The peak values show the daytime maximum insolation occurring two times between 1-4 PM.

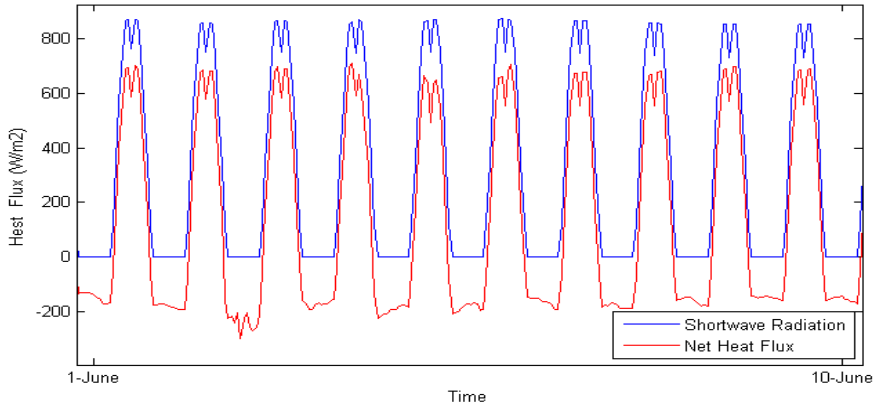

Figure 5.3: Variations of calculated short wave radiation and net surface heat flux for the first 10 days of June 2009.

Shortwave radiation is the only component of net heat flux that penetrates a layer of water column. Attenuation of shortwave flux versus water depth is presented by the following equation:

$$SW(z,t) = SW(0,t)[Re^{\frac{z}{a}} + (1-R)e^{\frac{z}{b}}] \tag{5.6}$$

where $SW(0,t)$ is the shortwave radiation at the water surface, t is time and $SW(z,t)$ is the shortwave radiation at water depth z. Parameters a and b are the attenuation lengths for longer

and shorter (waveband blue-green) wavelengths and R is the portion of shortwave flux which is associated with the long wavelengths. Appropriate values for *a*, *b*, and *R* should be considered based on the clarity of water over the modeling area. Paulson and Simpson (1977) suggested for coastal waters *R=0.78, a=1.4, and b=7.9*. In our study, a sensitivity analysis was implemented on each parameter to obtain the optimal agreement with SST measurements. The final applied values were consistent with Chen et al. (2003).

5.3.2.2 Wind Data

Although the main objective of this study is to determine the effect of solar heating on stratification, in order to evaluate the model performance and simulate the real conditions, effect of wind and the associated mixing should be considered. Wind data for June 2009 were obtained from CSI-6 and reduced to the standard level of 10 meters. The average wind speed during this month was less than 6 m/s and rarely reached 10 m/s (Figure 5.4). This implies a weak wind effect on mixing over the shelf.

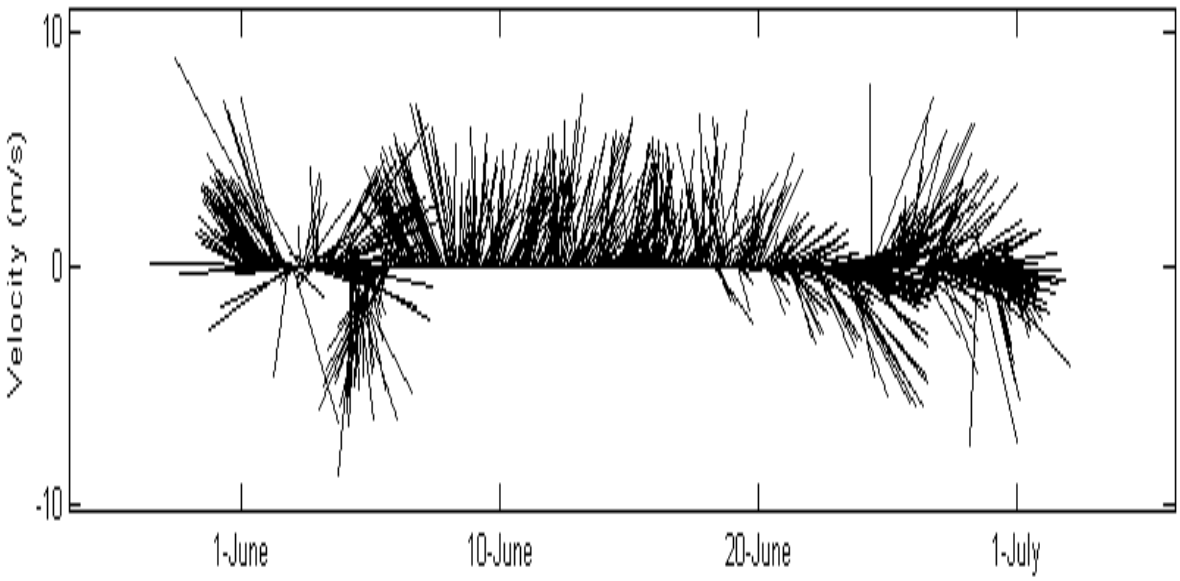

Figure 5.4: Timeseries of measured wind at CSI-6 during June 2009.

5.3.2.3 Initial Temperature Profile

For the real case simulation, the initial temperature profile over the shelf is required. Due to a lack of measurements for temperature profiles for initial conditions of the model, the climatological profile for May over the Louisiana shelf from NOAA was used. However, using the climatological profile can cause some inaccuracies. Since the data represent the average conditions for the water column temperature structure, the simulated temperatures could be larger or smaller than the reality depending on the solar insolation intensity for the simulation year in comparison to its long-term average.

5.4 Simulation Results

5.4.1 Model Evaluation

A one-month simulation of hydrodynamics and heat transport during June 2009 was performed. Results for SST were compared to field measurements at CSI-6. An optimal agreement was resulted for the case using the short/long wave attenuation lengths suggested by Chen et al. (2003) (Figure 5.5). The trend of variations of SST from 25.5 to 30 C for the time period from 5 June to 20 June was reproduced well.

Daily fluctuations of temperature were more or less in phase showing the mid-day temperature peak and night-time minimum. The simulated timeseries of SST was de-trended to show the fluctuations associated with diurnal variations of solar insolation. The resultant timeseries of daily temperature fluctuations (Figure 5.5) shows a maximum day-night temperature difference of 0.9 C with an average of 0.5 C for the first 20 days of June 2009.

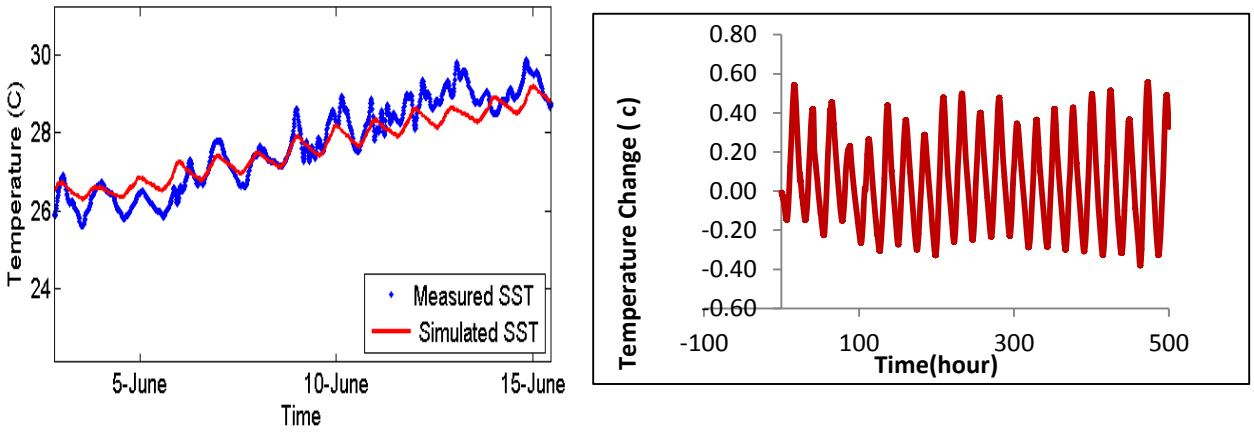

Figure 5.5: left) Comparison of simulated and measured SST at the location of CSI-6 station, right) day-night fluctuations of SST extracted from simulated SST.

5.4.2 Sea Surface Temperature

As shown above, diurnal variations of solar insolation induce similar SST fluctuations. However, the spatial variations of SST are more complicated due to the complex shelf bathymetry and variations of circulation pattern over the shelf. Figure 5.6 presents simulated SST over the study area for different times (local time) on 15 July including nighttime radiation minimum and daytime radiation peak. Shelf-wide SST map at 12:00 AM local time shows that simulated SST over the shelf area off the Barataria and Terrebonne Bays is uniform and is about 26.5 C. Over the shallow shelf off the Atchafalaya Bay, SST is higher (27.4 C) which can be partly due to the smaller depths and advection of warm water from outer shelf to this area. At this time, SST over the deep waters off the Birds-food delta is higher (28 C) compared to the inner-shelf waters. Three hours later at 3:00 AM several hours after the intense daytime solar

insulation, SST distribution off the Barataria and Terrebonne Bays is similar to 12:00 AM, but SST off the Atchafalaya Bay and the Birds-foot delta decreased to about 27 and 27.1 C, respectively. At 12:00 PM , the daytime increase of solar insolation, cause SST to increase off the Atchafalaya Bay to about 28 C and off the Birds-foot delta to about 28.2 C. Temperature distribution over the shelf just west of the Birds-foot delta is similar to other two time steps, but temperature increased to about 26.8 C. Corresponding to the peak of insolation at 3:00 PM , SST over the shelf west of the Birds-foot delta increased to 27-27.2 C and similar SST in other areas over the shelf occurred.

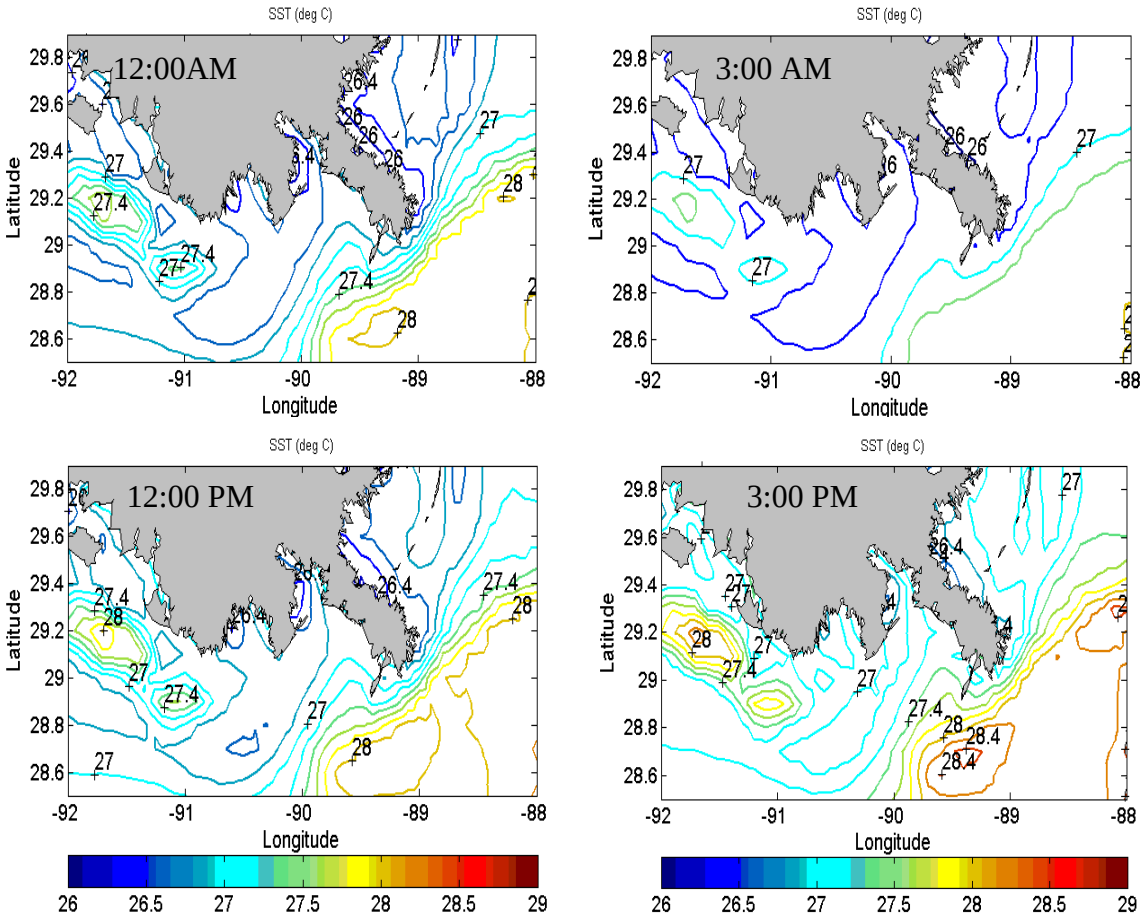

Figure 5.6: Shelf-wide variations of simulated SST on 15 June at different times (local time).

5.4.3 Vertical Distribution of Temperature

Increase of SST as a result of solar insolation causes development of temperature stratification. Furthermore, temperature difference during day and night time produces differences in water column stratification between day and night. The general behavior of induced shelf stratification based on simulation results is presented along an east-west cross-

section (Section 1 in Figure 5.1). The section extends from the South-west Pass to Sabine Bank which is about 400 km west of the Birds-foot delta representing vertical variations of simulated temperature for the inner-shelf region. Figure 5.7 shows the variations of temperature across this section for two different times at 15 June (almost 15 days after the SST started to increase). Figure 5.7, a. represents conditions for 12:00 AM Although an initially surface mixed water column was assumed for inner shelf waters, solar heating induced stratification along the shelf except for a shallow region of 30-50 km width (water depth less than 10 meters) located west of the Terrebonne Bay over which the water column is well mixed. However, the upper part of the water column (upper 7 meters) for all points along the section remained well mixed. Water temperature in the water column increased from the initial value of 25 C, the largest temperature which is about 27 C occurred just west of Birds-foot delta off Barataria Bay as well as over the shallow region west of the Terrebonne Bay with well mixed water column.

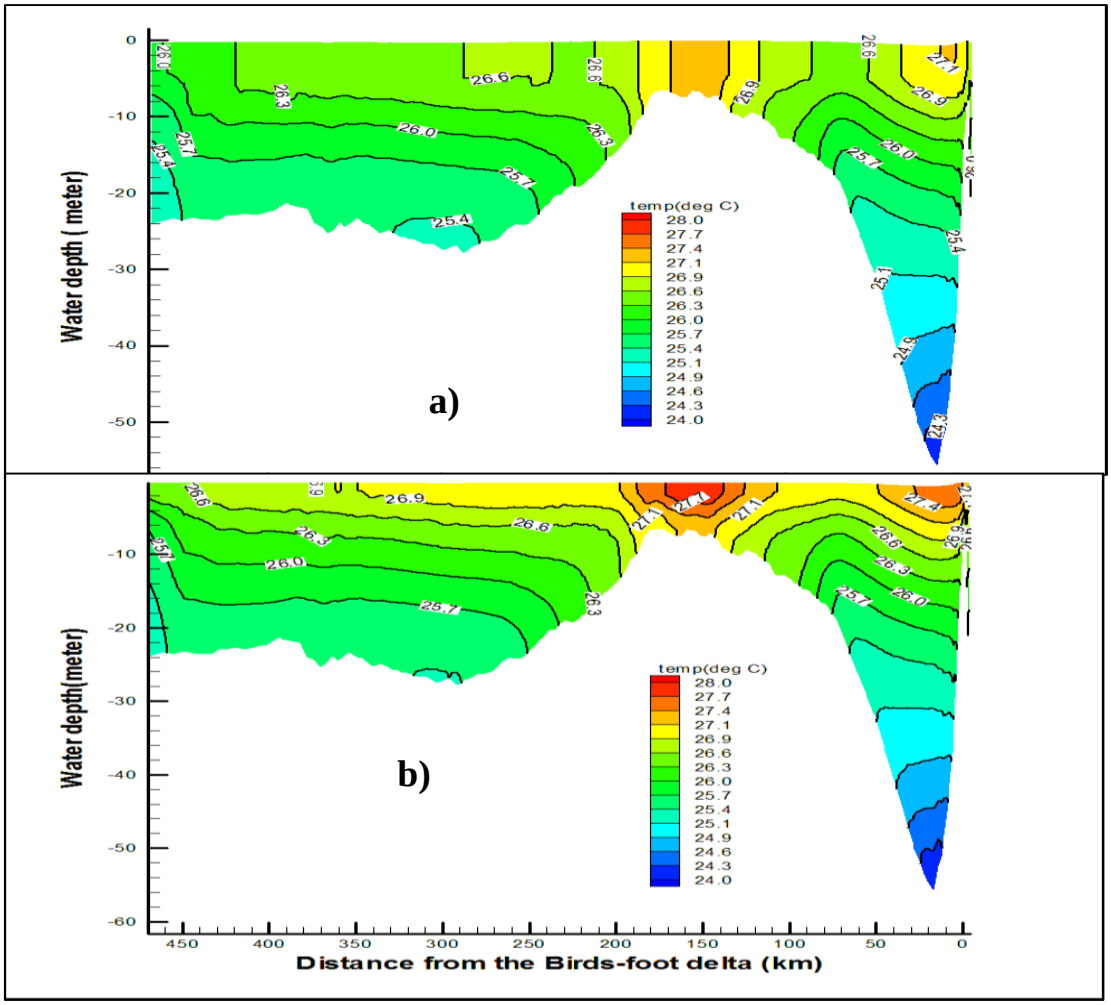

Figure 5.7: a) Night time and b) Day time distributions of temperature along an east-west section (section 5.1).

Temperature in the afternoon (3:00 PM local time, Figure 5.7, b.) after the maximum solar insolation had a much stronger stratification with the maximum SST of 28 C comparing with the night time. The shallow region of mixed water column at night time stratifies at 3 PM and isotherms get closer in both eastern and western side demonstrating stronger stratification.

For other days during the simulation period, the daytime and nighttime stratification patterns are similar. Temperature distribution at depths larger than 10 meters remained the same at day and night, consistent with the attenuation depth assumed for short wavelength radiation. For both times, isotherms were moved upward in the shelf area between the Terrebonne and Barataria Bays demonstrating the occurrence of upwelling a resulted from the south-westerly winds.

The diurnal evolution of the water column stratification was examined (Figure 5.8) for transect A on the shelf in front of the Terrebonne Bay (Figure 5.1 for location). Water temperature was presented at four different times staring from 15 June 12:00 AM for the shelf waters up to 50 meters. At night (Figure 5.8, a.) the mixed layer depth for the shoreward region of the transect (depths smaller than 20 meters) was 7-10 meters while SST was about 26.3 C. For the deeper region, mixed layer depth is smaller (less than 5 meters) and SST was about 27 C. Three hours later, at 3:00 AM (Figure 5.8, b.) the overall pattern of temperature distributions in both shallower and deeper water were similar.

However, the mixed layer depth in the shallower region decreased to about 5 meters or less and the associated SST increased to 26.6 C. At 12:00 PM (Figure 5.8, c.) when there was a substantial increase in solar radiation compared to that of morning time, over the major part of the shallow shelf, isotherms shifted upward resulting mixed layer depths smaller than 5 meters. SST over the shallow area increased to 26.9 C, while the deeper locations had SST of 27 C.

The most developed and strongest stratification was at 3:00 PM (Figure 5.8, d.) when shallower to deep waters, stratification developed. The SST increased to 27 C. Isotherms were closer to each other compared to other times demonstrating larger temperature gradient in the vertical and stronger stratification at this time. Coastal upwelling caused by south-westerly winds moved the isotherms upward. The upwelling at 3:00 PM almost reached the surface.

Development of the stratification during night and day times was compared for transect B west of the Birds-foot delta in front of the Barataria Bay (Figure 5.9). The transect extends to around 60 meters depth over an area with a steeper bed slope compared to transect A. The difference between the thermal stratification for night and day was more or less similar to that of transects A. Figure 5.9, a. shows the simulation results for water temperature on 15 June at 12:00 AM. At this time a well-established stratified layer developed beneath the mixing depth of 5-10 meters. SST was 26.9-27 C along the transect. Similar to transect A, at 3:00 PM (Figure 5.9, b.), the stratification was stronger compared to night time.

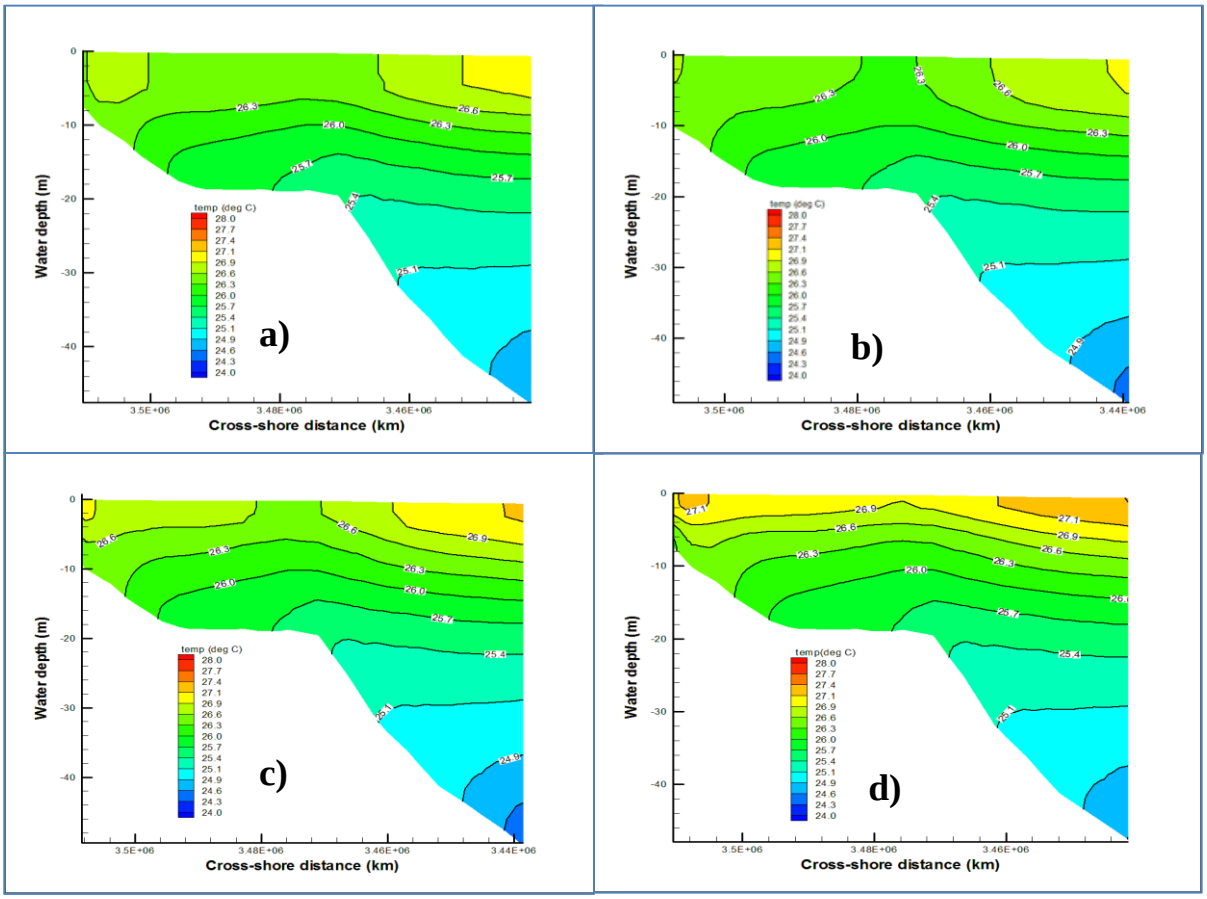

Figure 5.8: Time-evolution of stratification across transect A for 15 June 2008 at different times.

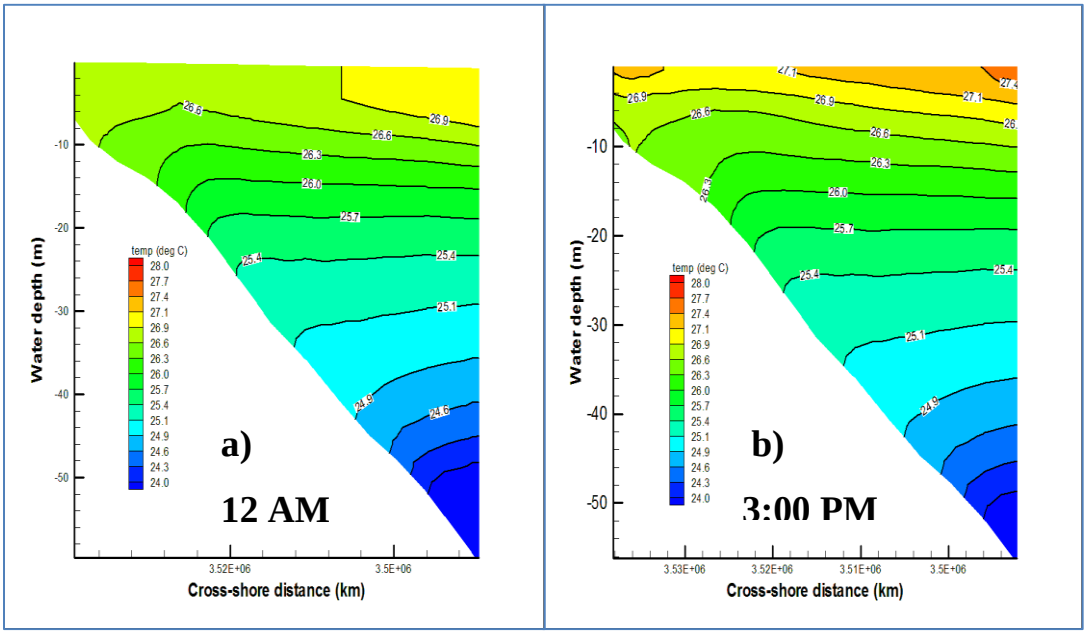

Figure 5.9: Simulated temperature across transect B in 15 July for two different times.

5.4.3 Representing Stratification Based on Gradient Richardson Number

The vertical temperature distribution along the east-west and cross-shore transects qualitatively showed that the strength of stratification increased on both diurnal and monthly time scales. To quantify this conclusion, buoyancy frequency and gradient Richardson number are examined (equation 1-1). Variations of temperature in the water column cause density to change and thereby buoyancy frequency changes. Since SST oscillates diurnally, similar variations for surface water density and the gradient Richardson number across the water column are expected. Figure 5.10, a. shows results for time variation of water density at the surface and mid-depth (depth of 10 meters from the surface) at a point off Terrebonne Bay at about 20 meters depth. Surface and mid-depth waters were selected to calculate the Richardson Number.

The current velocity beneath the mid-depth changes direction and decreases the value of current shear. The decreasing trend of density is consistent with the increasing trend of water temperature during the simulation period. Surface water density follows similar diurnal variations of SST. No fluctuations are present in the bottom water density. Between 5 June and 10 June and during night-time, surface water density increases to about the mid-depth density due to the night-time minimum heating, but after 10 June the difference of densities increased as a result of faster heating of the surface water compared to the mid-water. Note that the mid-depth density experiences a drop caused by the mixing event of 4 June.

Vertical gradient of water density were quantified to obtain buoyancy frequency (Figure 5.10, b.). Time variations of this parameter are similar to SST and surface density at both monthly and diurnal scales. Before 5 June, buoyancy frequency experienced a general declining trend as a results of mixing induced by northerly winds. After this date, buoyancy effect increased as shelf waters were exposed to solar heating for longer times. The strength of stratification is quantified based on the gradient Richardson number. Vertical gradient of current components were calculated based on the circulation model results for wind-induced currents. Since wind speed at the time was generally weak (less than 7 m/s), its impact is small. The resulted Richardson number is therefore large showing the dominant effect of buoyancy. Figure 5.10, c. shows the time series of the calculated Richardson number for this point. The time variation of Richardson number has an increasing trend especially during June (Figure 5.10, c.). The small values of Richardson number prior to 5 June show the effect of wind mixing events. Variations of buoyancy frequency and Richardson number elsewhere over the shelf are similar.

A contrast behavior was observed when the simulation was completed for a 1-month effect of fall winds (including four different cold fronts and no solar heating) during October 2009 (Figure 5.11). Buoyancy frequency as well as the Richardson number continuously decreased as a result of mixing wind events during this time. The decreasing trend of the Richardson number showed that water column was continuously mixed and more uniform vertical distributions of temperature/salinity were the results.

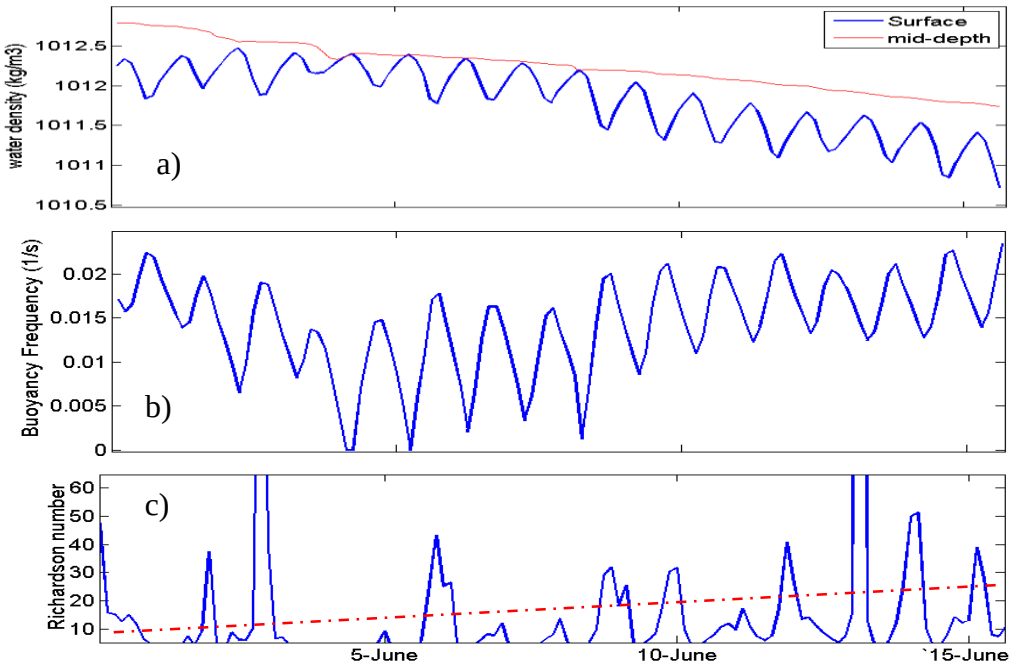

Figure 5.10: Time variations of a) simulated water density, b) calculated buoyancy frequency, c) calculated Richardson number during simulation period (dashed line shows the trend of the Richardson number variations).

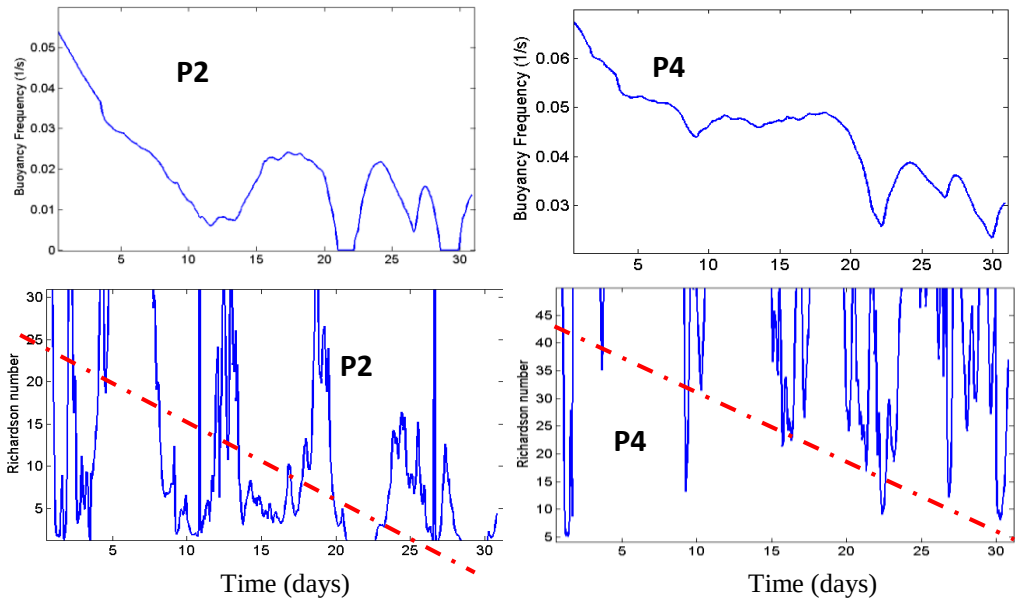

Figure 5.11: Variations of Buoyancy frequency and the Richardson number across the water column during 1 month of simulation during October 2009 for stations P2 and P4. The red dash line shows the l trend of the Richardson number variations during simulation. Locations of P2 and P4 are according to Figure 4.16.

5.5 Effect of Diurnal Heating on Bottom Oxygen

Summertime depletion of bottom water oxygen over the Louisiana shelf occurs as a result of enhanced biological processes and the strengthening of water column stratification. Our simulation results showed that stratification becomes stronger as a result of summertime solar insolation. Hence, it is expected that bottom water oxygen concentration decreases during June 2009 as the stratified water column blocks bottom water re-oxygenation. Time series of dissolved oxygen concentration at the bottom of CSI-6 (Figure 5.12, a.) during June 2009 confirms this. Oxygen concentration was about 4 mg/l on the first day of June 2009, followed by a decline. On 4 June, under northerly winds, the dissolved oxygen concentration changed from 2 mg/l to about 4 mg/l. From this time due to the reinforcement of stratification, oxygen concentration started a longer term decline, depleting the bottom oxygen to less than 1 mg/l. Variations of bottom oxygen concentration are consistent with that of the simulated SST and the associated buoyancy frequency (implying that the wind-induced mixing was not significant). The consistency was also examined for measurements at CSI-6 during summer 2005 (Figure 5.12, b.). Time series of bottom oxygen concentration during July 2005 had an average of 4 mg/l for the first 20 days when the average SST was 29 C. Increasing SST to greater than 30 C caused stronger water column stratification. Hence, oxygen concentration started to decline from 20 June and decreased to about 1.6 mg/l on 3 August. During August, SST increased to 31 C, producing an even stronger stratification and consequently oxygen concentration was almost depleted completely. This anoxic bottom water persisted on the shelf by the middle of the last week of August 2009 until the mixing produced by Hurricane Katrina broke down the stratification and re-oxygenated the bottom water.

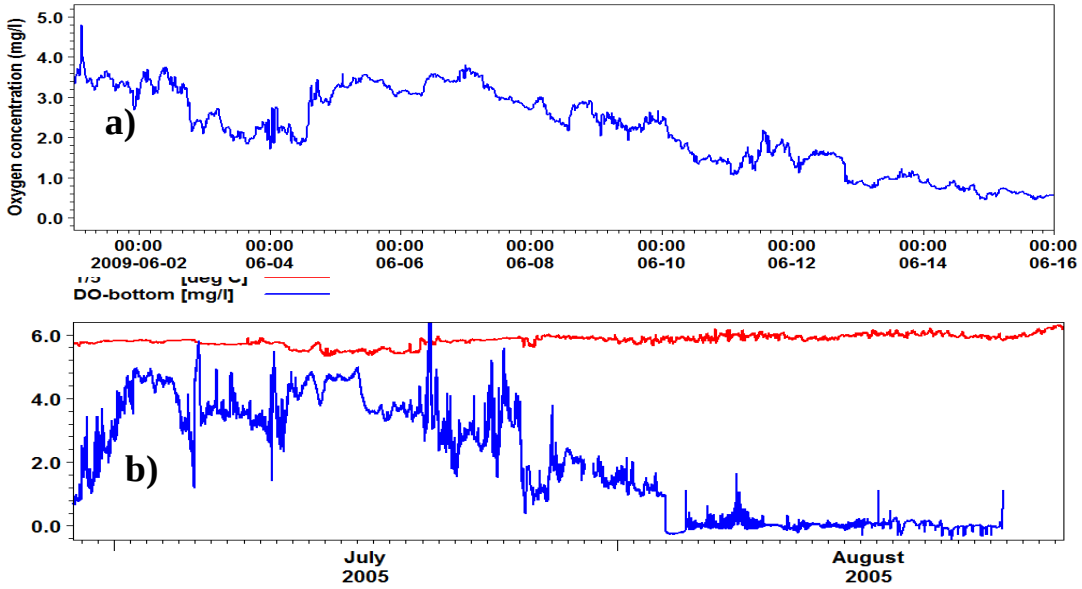

Figure 5.12: a) measured BWOC from 1-15 June2009 at station CSI-6, b) Measure SST and BWOC for July and August 2005.

5.6 Summary and Conclusion

Development of stratification as a result of the summertime increase of solar radiation over Louisiana shelf and its implication for triggering bottom water hypoxia was studied using FVCOM. SST over the shelf west of the Birds-foot Delta increased from 25 C on 1 June 2009 to about 28.5 C on 20 June. In addition to the diurnal variation of solar radiation, SST increased steadily within the month. The steady increase of the top layer water temperature caused the enhancement of stratification. As a result, the stratification was wide spread on the shelf west of the Birds-foot delta. It was stronger during the daytime and weaker during the night-time. Also, it was stronger over the shelf area between the Birds-foot delta and off the west of the Terrebonne Bay. This is the area with the most severe hypoxic events over the Louisiana shelf. Examining the pattern at different times demonstrated the effect of advection from the outer to the inner shelf as a result of northward currents produced by southerly to southwesterly winds.

Analysis showed that the buoyancy frequency followed the same increasing trend of SST in the absence of significant mixings. The Richardson number exhibited an increase after the initial mixing over the shelf. Stratification was consistent with the measured bottom water dissolved oxygen during the simulation period. Oxygen concentration increased with increasing SST when no substantial mixing existed.

CHAPTER 6: SUMMARY

6.1 Introduction

In the present research, hurricane induced mixing and post hurricane re-stratification was examined using model experiments. Hurricane Katrina was chosen as an example. Different aspects of wind induced mixing and its impact on the stratification over the Louisiana shelf were studied through numerical modeling using FVCOM. The mechanisms of mixing through the water column and subsequent re-stratification after the hurricane were investigated. This chapter summarizes the major findings and discusses potential future research.

6.2 Highlights

6.2.1 Approach

Using FVCOM, numerical experiments were performed to study the impact of hurricanes on water column stratification. The experiments considered various scenarios with different sets of forcing conditions. Some field data were used in the model validation. Firstly, the model was successfully tested for tidal currents to demonstrate the satisfactory model performance of long wave transformation from the boundary. The model was also tuned for a combination of wind and tide induced currents with properly imposed wind friction coefficient and vertical eddy viscosity.

Secondly, FVCOM was used for simulations of hurricane induced currents and temperature distribution. The hydrodynamics and temperature field were evaluated and validated using some hydrodynamics and temperature data. Model performance was also demonstrated for the solar heating over the shelf during the summertime non-hurricane conditions.

6.2.2 Data

Various data were used for model setup and validation, calibration, and evaluation. A hydrodynamic model for tidal current was evaluated using tidal predictions from NOAA, while modeling of tidal and wind-induced currents were assessed using current data from WAVCIS stations (www.wavcis.lsu.edu). Some current velocity and water level data obtained at the WAVCIS stations CSI-3, CSI-5, and CSI-6 before and during the passage of Hurricane Katrina were used to evaluate the hydrodynamic model.

In addition to the hydrodynamics data, meteorological data were used to drive the model. The hurricane wind field was evaluated over the inner Louisiana shelf using data measured at stations CSI-6 and CSI-5. Met-ocean data from CSI-6 were used for calculating different components of solar insolation for the non-hurricane summertime conditions. As it is seen, met-ocean data measured at WAVCIS station is critical in providing data over the Louisiana shelf.

6.2.3 Results

The following summarizes each chapter:

Chapter 2:

In this chapter the effect of seasonal hydrodynamics on the formation and breaking down of the seasonal stratification over the Louisiana shelf was investigated by comparing measured current data at stations located on both sides of the Birds-foot delta during summer and fall. The main results from this study are as follows:

- A substantial decline in wind stress in the summer determined the formation of a stable seasonal stratification.
- Compared to the summer, the current velocity profiles exhibit a greater vertical shear in the fall, especially for stations on the west side of the Birds-foot delta.
- The summertime current induced mixing was at least one order of magnitude greater on the eastern side of the delta presumably due to the shallow water there.
- Weaker current on the west side of the delta leads to the formation of a more persistent seasonal stratification coincides with the seasonal hypoxic zone in this region.

Chapter 3:

The simulation of hydrodynamics under Hurricane Katrina was presented. An analytical model tuned by *in situ* measurements of wind speed and direction was used to generate the hurricane wind field. Wind stress at the water surface was estimated considering the decreasing of drag coefficient for wind speed greater than 28-30 m/s. Different initial shelf stratifications and various background vertical eddy viscosities were examined. By comparing simulation results with some measurements at the WAVCIS stations, the best parameters were determined for further modeling of the hydrodynamics involving temperature and salinity. The important results are:

- The single vortex Holland (1980) model can successfully reproduce the hurricane's wind field given wind measurements for tuning the radius of maximum wind.
- The 3-D simulated current during the hurricane is sensitive to the vertical eddy viscosity.
- By assuming a constant vertical eddy viscosity, the simulated current speed tends to result in the largest values, while applying the turbulent closure scheme results in the lower limit.
- Results from a simulation using MY 2.5 closure for the vertical turbulence are more consistent with the available hydrodynamics data measured over the inner shelf during Katrina.
- A sheared response was seen in Katrina induced currents over the Louisiana shelf, resulting in obvious return flows at the bottom.
- Shelf currents at the right side of Katrina's eye were intensified as a result of the confinement of the Birds-foot delta and the right-ward increase of the wind speed due to

the forward movement of the hurricane. Current velocity up to 3.5 m/s was observed west of the delta.

Chapter 4:

Temperature variations under Hurricane Katrina over the Louisiana shelf were simulated. Climatological temperature profiles from NOAA were modified and then used as the initial conditions for simulation. For the temperature profiles over the inner-shelf, modifications were made using some available field measurements and the AVHRR SST data. During Katrina, the only available data to evaluate model results were SSTs measured by satellite using microwave, because of cloud coverage.

The Optimally Interpolated (OI) SST data covered the deep water to the edge of the shelf break (no data over the inner shelf). The simulated SSTs using different background eddy viscosity values were compared with the OI data along the shelf break, from which the proper background eddy viscosity was determined. In addition, using an empirical equation, the hurricane-induced Mixed Layer Depth was calculated using the satellite SST and the initial temperature profile. The empirical MLD was compared with the simulated MLD along the shelf break. The subsequent modeling and analysis led to the description of the hurricane-induced mixing across the shelf as well as the re-stratification on the shelf after the landfall. The last step was comparing the hurricane mixed area with the seasonal hypoxic zone to examine the effect of mixing on hypoxia. The main conclusions are:

- The Mellor-Yamada level 2.5 turbulent closures led to the best match with field data.
- The appropriate background eddy viscosity was found to be 0.0001-0.00001 m^2/s.
- The effect of hurricane induced mixing was substantial over the shelf regions within 1.5 R_{mw} from the hurricane center.
- Mixing on the right hand side of the track was more intense due to rightward-bias and current intensification because of the presence of the Birds-foot delta.
- The hurricane induced mixing was ephemeral and re-stratification started several hours after the landfall.
- A conceptual diagram for the shelf water during the hurricane mixing phase includes: a surface mixed layer, a bottom upwelling zone, and a transition layer containing damping internal waves at the base of the mixed layer.
- A day after landfall, the lower water column was significantly stratified. Ten days after the landfall, the water column was almost completely stratified, but did not recover to the pre-storm condition of stratification. The isotherms sloped offshore-ward as a result of the pressure gradient produced by a density difference.
- During the re-stratification along a typical transect on the shelf, the isotherms within the upper half of the water column sloped offshore-ward as a result of cross-shelf pressure gradient, while in the lower part, the isotherms sloped toward the shore which is driven by coastal upwelling.

- The computation of a complete recovery of temperature profiles to the pre-hurricane distribution needs the inclusion of solar heat flux in the numerical simulations.
- Hurricane induced mixing overlaps the seasonal hypoxic zone over the Louisiana shelf.

Chapter 5:

The effect of summertime diurnal solar heating on the stratification over the Louisiana shelf was addressed by numerical simulations of shelf heating under the effect of solar insolation. Solar insolation included four different components: shortwave radiation, long wave radiation, sensible heat and latent heat fluxes which were calculated using measurements of met-ocean parameters at CSI-6. The temporal variations of SST over the shelf were evaluated using measurements at CSI-6. The major results are:

- Solar heating components from empirical and analytical formula as model input provided reasonable energy source for the shelf heating.
- Starting from June 1st, the mid-summer solar heating increases SST over the shelf up to as much as 1 C by mid-June.
- The partially mixed water in March 2009 became completely stratified after 20 days of solar heating effect.
- The daily SST variation was about 1 C, while the water temperature variations significantly decrease as the water depth increases.
- The increase of SST during the summer is a result of increasing solar heating, which is negatively correlated with the bottom water oxygen concentration.

6.3 Suggestion for Future Research

More studies based on the present work can be considered as outlined for future studies below:

1- More field data of temperature and salinity are needed for more accurate model calibration and experimentation. A detailed calibration of the background eddy viscosity using field data of temperature and salinity with a high temporal resolution is needed.

2- In the present simulation, the effect of solar insolation during and after the hurricane was omitted. Although solar heating is not significant during the hurricane, it can play an important role after the passage of the hurricane in shelf re-stratification. The study of the post-storm re-stratification can be improved by inclusion of solar insolation to the model.

3- The hurricane wind field used in the present study was obtained based on an analytical model. More realistic wind field with inclusion of background non-hurricane wind for remote areas from the hurricane center can offer more realistic simulations. An option for this wind field can be combining the H*WIND hurricane wind field with NCEP reanalysis data.

4- Oscillations of temperature or salinity observed at the base of the mixed layer (through both east-west and north-south cross-sections) need to be studied thoroughly to determine the internal wave propagation over deep and shallow shelves during hurricane events.

REFERENCES

Allahdadi, M. N., Jose, F. and Patin, C. 2013. Seasonal hydrodynamics along the Louisiana Coast: Implications for hypoxia spreading. *Journal of Coastal Research,* 29**,** 1092-1100.

Allahdadi, M. N, Jose, F, Stone, G. W. and D'Sa, E. J. 2011. The fate of sediment plumes discharged from the Mississippi and Atchafalaya Rivers: An integrated observation and modeling study for the Louisiana Shelf, USA. Coastal Sediments, Miami, Fl, pp. 2212–2225.

Ardhuin, F. and Jenkins, A. D. 2006. On the interaction of surface waves and upper ocean turbulence. *Journal of Physical Oceanography,* 36**,** 551-557.

Belabbasi, L. 2006. Examination of the relationship of river water to occurrences of bottom water with reduced oxygen concentrations in the northern Gulf of Mexico. College Station, Texas: Texas A&M University, Ph.D. thesis, 119 p.

Bender, M. A., Ginis, I. and Kurihara, Y. 1993. Numerical Simulations of Tropical Cyclone-Ocean Interaction with a High-Resolution Coupled Model. *Journal of Geophysical Research-Atmospheres,* 98**,** 23245-23263.

Bingham, F. M. 2007. Physical response of the coastal ocean to Hurricane Isabel near landfall. *Ocean Science,* 3**,** 159-171.

Black, P. G., D'asaro, E. A., Drennan, W. M., French, J. R., Niiler, P. P., Sanford, T. B., Terrill, E. J., Walsh, E. J. and Zhang, J. A. 2007. Air-sea exchange in hurricanes - Synthesis of observations from the coupled boundary layer air-sea transfer experiment. *Bulletin of the American Meteorological Society,* 88**,** 357-374.

Blumberg, A. F. 1977. Numerical-Model of Estuarine Circulation. *Journal of the Hydraulics Division-Asce,* 103**,** 295-310.

Blumberg, A. F. and Goodrich, D. M. 1990. Modeling of Wind-Induced Destratification in Chesapeake Bay. *Estuaries,* 13**,** 236-249.

Blumberg, A. F. and Mellor, G. L. 1983. Diagnostic and Prognostic Numerical Circulation Studies of the South-Atlantic Bight. *Journal of Geophysical Research-Oceans and Atmospheres,* 88**,** 4579-4592.

Boegman, L., Loewen M. R., Hamblin, P. F. and Culver, D. A. 2008. Vertical mixing and weak stratification over zebra mussel colonies in western Lake Erie. *Limnology and Oceanography,* 53**,** 1093-1110.

Boweden, K. F. and Hamilton, P. 1975. Some Experiments with a Numerical-Model of Circulation and Mixing in a Tidal Estuary. *Estuarine and Coastal Marine Science,* 3**,** 281-301.

Chaichitehrani, N., D'Sa, E. J., Ko, D. S., Walker, N. D., Osburn, C. L. and Chen, R. F. 2014. Colored Dissolved Organic Matter Dynamics in the Northern Gulf of Mexico from Ocean Color and Numerical Model Results. *Journal of Coastal Research* , 296, 800.

Chaichitehrani, N., D'Sa, E. J., Osburn, C. L., Bianchi, T. S. and Schaeffer. B. A. 2013. Chromophoric dissolved organic matter and dissolved organic carbon from SeaWiFS, MODIS and MERIS sensors: Case study for the northern Gulf of Mexico. *Remote Sensing*, 5:1439-1464.

Chen, C. S., Beardsley, R. C. and Cowles, G. 2006. An Unstructured Grid, Finite-Volume Coastal Ocean Model, FVCOM User Manual.

Chen, C. S., Beardsley, R. C., Franks, P. J. S. and Van Keuren, J. 2003. Influence of diurnal heating on stratification and residual circulation of Georges Bank. *Journal of Geophysical Research-Oceans,* 108.

Chen, C. S., Reid, R. O. and Nowlin, W. D. 1996. Near-inertial oscillations over the Texas Louisiana shelf. *Journal of Geophysical Research-Oceans,* 101**,** 3509-3524.

Chen, Q., Wang, L. X. and Tawes, R. 2008. Hydrodynamic Response of Northeastern Gulf of Mexico to Hurricanes. *Estuaries and Coasts,* 31**,** 1098-1116.

Chen, Q., Wang, L. X. and Zhao, H. H. 2009. Hydrodynamic Investigation of Coastal Bridge Collapse during Hurricane Katrina. *Journal of Hydraulic Engineering-Asce,* 135**,** 175-186.

Chu, P. C., Veneziano, J. M., Fan, C. W., Carron, M. J. and Liu, W. T. 2000. Response of the South China Sea to Tropical Cyclone Ernie 1996. *Journal of Geophysical Research-Oceans,* 105**,** 13991-14009.

Cochrane, J. D. and Kelly, F. J. 1986. Low-frequency circulation on the Texas-Louisiana continental-shelf. *Journal of Geophysical Research,* 91**,** 10645-10659.

Cooper, C. and Thompson, J. D. 1989a. Hurricane-Generated Currents on the Outer Continental-Shelf .1. Model Formulation and Verification. *Journal of Geophysical Research-Oceans,* 94**,** 12513-12539.

Cooper, C. and Thompson, J. D. 1989b. Hurricane-generated currents on the outer continental-shelf .2. Model Sensitivity Studies. *Journal of Geophysical Research-Oceans,* 94**,** 12540-12554.

Cotton, G. F. 1979. ARL models of global solar radiation. In: Quinlan, F.T. (Ed.), SOLMET Volume 2: Hourly Solar Radiation – Surface Meteorological Observations. National Oceanic and Atmospheric Administration, Asheville, NC, pp. 165–184.

Crout, R. L., Wiseman, W. J. and Chuang, W. S. 1984. Variability of Wind-Driven Currents, West Louisiana Inner Continental-Shelf - 1978-1979. *Contributions in Marine Science,* 27**,** 1-11.

Cushman-Roisin, B. 1981.Deepening of the wind-mixed layer: A model of the vertical structure. *Tellus,* 33, 564-582.

Davis, R. E., Deszoek, R. and Niiler, P. 1981.Variability in the upper ocean during MLLE. Part II: Modeling the mixed layer response, *Deep-Sea Research*, 28A (12), 1453 -1475.

Dietrich, J. C., Zijilema, M., Westrink, J. J., Holthuijsen, L. H., Dawson, C., Luettich, R. A., Jensen, R. E., Smith, J. M., Stelling, G. S. and Stone, G. W. 2011. Modeling hurricane waves and storm surge using integrally-coupled, scalable computations. *Coastal Engineering*, 58**,** 45-65.

DiMarco, S. F., Howard, M. K. and Reid, R. O. 2000. Seasonal variation of wind-driven diurnal current cycling on the Texas-Louisiana Continental Shelf. *Geophysical Research Letters,* 27**,** 1017-1020.

Elsberry, R. L., Fraim, T. S. and Trapnell, R. N. 1976. Mixed Layer Model of Oceanic Thermal Response to Hurricanes. *Journal of Geophysical Research-Oceans and Atmospheres,* 81**,** 1153-1162.

Galperin, B., Sukoriansky, S. and Anderson, P. S. 2007. On the critical Richardson number in stably strastified turbulence.Atmosphere Science Letters, 8, 65–69.

Glenn, S., Arnone, R., Bergmann, T., BissettI, W. P., Crowley, M., Cullen, J., Gryzmski, J., Haigvogel, D., Kouth, J., Moline, M., Oliver, M.,Orrico, C., Sherrell, R., Song, T., Weidemann, A., Chant, R. and Schofield, O. 2004. Biogeochemical impact of summertime coastal upwelling on the New Jersey Shelf. *Journal of Geophysical Research-Oceans,* 109**,** 1-15.

Goodrich, D. M., Bolcourt, W. C., Hamilton, P. and Pritchard, D. W. 1987. Wind-Induced Destratification in Chesapeake Bay. *Journal of Physical Oceanography,* 17**,** 2232-2240.

Guttman, N. B. and Matthews, J. D., 1979. Computation of extraterrestrial solar radiation, solar elevation angle and true solar time of sunrise and sunset. In: Quinlan, F.T. (Ed.), SOLMET Volume 2: Hourly Solar Radiation – Surface Meteorological Observations. National Climatic Center, US Department of Commerce, Asheville, NC, pp. 48–54.

Hagy, J. D. and Murrell, M. C. 2007. Susceptibility of a Northern Gulf of Mexico estuary to hypoxia: An analysis using box models. *Estuarine Coastal and Shelf Science,* 74**,** 239-253.

Hetland, R. D. and DiMarco S. F. 2012. Skill assessment of a hydrodynamic model of circulation over the Texas-Louisiana continental shelf. *Ocean Modelling,* 43-44**,** 64-76.

Holland, G. J. 1980. An analytic model of the wind and pressure profiles in hurricanes. *Monthly Weather Review,* 108**,** 1212-1218.

Holland, G. J., Belanger, J. I. and Fritz, A. 2010. A revised model for radial profiles of hurricane winds. *Monthly weather review,* 138(4393-4401).

Hsu, S. A. and Yan, Z. D. 1998. A note on the radius of maximum wind for hurricanes. *Journal of Coastal Research,* 14**,** 667-668.

Hu, C. M. and Muller-Karger, F. E. 2007. Response of sea surface properties to Hurricane Dennis in the eastern Gulf of Mexico. *Geophysical Research Letters,* 34.

Imberger, J. and J. C. Patterson. 1981, "A dynamic reservoir simulation model - DYRESM: 5," in Transport Models for Inland and Coastal Waters, (ed. H. B. Fischer), Academic Press, pp. 310-361.

Ivanoff, A. 1977. Oceanic absorption of solar energy. In: Kraus, E. B. (Ed.), Modelling and Prediction of the Upper Layers of the Ocean. Pergamon, New York, p. 326.

Jacob, S. D., Shay, L. K., Mariano, A. J. and Black, P. G. 2000. The 3D oceanic mixed layer response to Hurricane Gilbert. *Journal of Physical Oceanography,* 30**,** 1407-1429.

Jacob, S. D. and Shay, L. K. 2003. The role of oceanic mesoscale features on the tropical cyclone-induced mixed layer response: A case study. *Journal of Physical Oceanography,* 33**,** 649-676.

Justic, D., Rabalais, N. N. and Turner, R. E. 1996. Effects of climate change on hypoxia in coastal waters: A doubled CO2 scenario for the Northern Gulf of Mexico. *Limnology and Oceanography,* 41**,** 992-1003.

Justic, D., Rabalais, N. N. and Turner, R. E. 2003. Simulated responses of the Gulf of Mexico hypoxia to variations in climate and anthropogenic nutrient loading. *Journal of Marine Systems,* 42**,** 115-126.

Justic, D., Rabalais, N. N., Turner, R. E. and Wiseman, W. J. 1993. Seasonal coupling between river borne nutrients, net productivity, and hypoxia. *Marine Pollution Bulletin,* 26, 184–189.

Kasai, A., Yamada, T. and Takeda, H. 2007. Flow structure and hypoxia in Hiuchi-nada, Seto Inland Sea, Japan. *Estuarine Coastal and Shelf Science,* 71**,** 210-217.

Katsev, S., Crowe, S. A., Mucci, A., Sundby, B., Nomosatryo, S., Haffner, G. D. and Fowle, D. A. 2010. Mixing and its effects on biogeochemistry in the persistently stratified, deep, tropical Lake Matano, Indonesia. *Limnology and Oceanography,* 55**,** 763-776.

Keen, T. R. and Glenn, S. M. 1998. Factors influencing model skill for hindcasting shallow water currents during Hurricane Andrew. *Journal of Atmospheric and Oceanic Technology,* 15**,** 221-236.

Keen, T. R. and Glenn, S. M. 1999. Shallow water currents during hurricane Andrew. *Journal of Geophysical Research-Oceans,* 104**,** 23443-23458.

Kim, K. O., Lee, H. S., Yamashita, T. and Choi, B. H. 2008. Wave and Storm Surge Simulations for Hurricane Katrina using Coupled Process Based Models. *Ksce Journal of Civil Engineering,* 12**,** 1-8.

Knabb, R. D., Rhome, J. R. and Brown, D. P. 2005. Tropical cyclone report: Hurricane Katrina, *National Hurricane Center, NOAA*. (Available at http://www.nhc.noaa.gov/pdf/TCR-AL122005_Katrina.pdf).

Large, W. G. and Pond, S. 1981. Open Ocean Momentum Flux Measurements in Moderate to Strong Winds. *Journal of Physical Oceanography,* 11**,** 324-336.

Leipper, D. F. 1967. Observed Ocean Conditions and Hurricane Hilda 1964. *Journal of the Atmospheric Sciences,* 24**,** 182-186.

Li, M., Zhong, L. J., Boicourt, W. C., Zhang, S. L. and Zhang, D. L. 2007. Hurricane-induced destratification and restratification in a partially-mixed estuary. *Journal of Marine Research,* 65**,** 169-192.

Loewen, M. R., Ackerman, J. D. and Hamblin, P. F. 2000. Environmental implications of stratification and mixing in a shallow lake basin. *Canadian Journal of Fishery,* 64(43-57).

Ly, L. N. and Takle, E. S. 1994. A Numerical Study of the Influence of an Air Temperature-Inversion Layer and a Seawater Density-Jump Layer on the Structure of Interacting Boundary-Layers. *Boundary- Layer Meteorology,* 67**,** 327-343.

Lyons, R., Panofsky, H. A. and Wollaston, S. 1964. The crtical Richardson number and its implication for forecast problems. *Journal of Applied Meteorology* ,3,136-142.

Makin, V. K. 2003. A note on a parameterization of the sea drag. *Boundary-Layer Meteorology,* 106**,** 593-600.

Makin, V. K. 2005. A note on the drag of the sea surface at hurricane winds. *Boundary-Layer Meteorology,* 115**,** 169-176.

Martin, P. J. 1982. Mixed-layer simulation of buoy observations taken during Hurricane Eloise. *Journal of Geophysical Research-Oceans and Atmospheres,* 87**,** 409-427.

Mayer, D. A., Mofjeld, H. O. and Leaman, K. D. 1981. Near-Inertial Internal Waves Observed on the Outer Shelf in the Middle Atlantic Bight in the Wake of Hurricane Belle. *Journal of Physical Oceanography,* 11**,** 87-106.

Mellor, G. L. and Durbin, P. A. 1975.The structure and Dynamics of the Ocean Surface Mixed layer. *Journal of Physical Oceanography,* 5,718-728.

Mitchell, D. A., Teague, W. J., Jarosz, E. and Wang, D. W. 2005. Observed currents over the outer continental shelf during Hurricane Ivan. *Geophysical Research Letters,* 32.

Montegut, C. D., Madec, G., Fischer, A. S., Lazar, A. and Iudicone, D. 2004. Mixed layer depth over the global ocean: An examination of profile data and a profile-based climatology. *Journal of Geophysical Research-Oceans,* 109.

Mukai. A. Y., Westerink. J. J, Luettich Jr. R. A. and Mark, D. A. 2001. Tidal Constituent Database for Western North Atlantic, Gulf of Mexico, and Caribbean Sea, Eastcoast.

Munk, W.H. and Anderson. E. R. 1948. Notes on a theory of the thermocline. *Journal of Marine Research,* 7, 276-295.

Nezlin, N. P., Kamer, K., Hyde, J. and Stein, E. D. 2009. Dissolved oxygen dynamics in a eutrophic estuary, Upper Newport Bay, California. *Estuarine Coastal and Shelf Science,* 82**,** 139-151.

Oey, L. Y. 1995. Eddy-Forced and Wind-Forced Shelf Circulation. *Journal of Geophysical Research-Oceans,* 100**,** 8621-8637.

Paulson, C. A. and Simpson, J. J. 1977. Irradiance measurements in the upper ocean, *Journal of Physical Oceanography,* 7, 952– 956.

Pedlosky, J. (1979), Geophysical Fluid Dynamics, 2nd ed., 710 pp., Springer, New York.

Phadke, A. C., Martinoa, C. D., Cheung, K. F. and Houston, S. H. 2003. Modeling of tropical cyclone winds and waves for emergency management. *Ocean Engineering*, 4, 553-578.

Price, J. F. 1981. Upper Ocean Response to a Hurricane. *Journal of Physical Oceanography,* 11**,** 153-175.

Price, J. F., Mooers, C. N. K. and Van Leer, J. C. 1978. Observation of strorm-induced Mixed-Layer Deepening. *Journal of Physical Oceanography,* 8,582-599.

Rabalais, N. N. 1991. *Fate and effects of nearshore discharges of OCS produced waters,* New Orleans (1201 Elmwood Park Boulevard, New Orleans 70123-2394), U. S. Dept. of the Interior, Minerals Management Service, Gulf of Mexico OCS Regional Office.

Rabalais, N. N. 2002c. *Hypoxia in the Gulf of Mexico* [Online]. Available:http://www.csc.noaa.gov/products/gulfmex/html/ecosys.htm.

Rabalais, N. N., Atilla, N., Normandeau, C. and Turner, R. E. 2004. Ecosystem history of Mississippi River-influenced continental shelf revealed through preserved phytoplankton pigments. *Marine Pollution Bulletin,* 49**,** 537-547.

Rabalais, N. N., Turner, R. E. and Scavia, D. 2002a. Beyond science into policy: Gulf of Mexico hypoxia and the Mississippi River. *Bioscience,* 52**,** 129-142.

Rabalais, N. N., Turner, R. E., Sen Gupta, B. K., Boesch, D. F., Chapman, P. and Murrell, M. C. 2007.Characterization and longterm trends of hypoxia in the northern Gulf of Mexico Does the science support the Action Plan?. *Estuar. Coasts,* 30, 753–772.

Rabalais, N. N., Turner, R. E. and Wiseman, W. J. 2002b. Gulf of Mexico hypoxia, aka "The dead zone". *Annual Review of Ecology and Systematics,* 33**,** 235-263.

Rabalais, N. N., Wiseman, W. J. and Turner, R. E. 1994. Comparison of continuous records of near-bottom dissolved-oxygen from the hypoxia zone along the Louisiana coast. *Estuaries,* 17, 850–861.

Rabalais, N. N., Wiseman, W. J., Turner, R. E., Sengupta, B. K. and Dortch, Q. 1996. Nutrient changes in the Mississippi River and system responses on the adjacent continental shelf. *Estuaries,* 19**,** 386-407.

Rego, J. L. and Li, C. 2009. On the receding of storm surge along Louisiana's low-lying coast. *Journal of Coastal Research***,** 1045-1049.

Rego, J. L. and Li, C. Y. 2010a. Storm surge propagation in Galveston Bay during Hurricane Ike. *Journal of Marine Systems,* 82**,** 265-279.

Rego, J. L., Mesel, E., Stronach, J. and Habib, E. 2010b. Numerical modeling of the Mississippi-Atchafalaya Rivers' sediment transport and fate: Considerations for diversion scenarios. *Journal of Coastal Research,* 26**,** 212-229.

Renaud, M. 1986. Hypoxia in Louisiana coastal waters during 1983: implications for fisheries. *Fish. Bulletin*. 84:19-26.

Richards, K. J., XIE, S. P. and Miyama, T. 2009. Vertical Mixing in the Ocean and Its Impact on the Coupled Ocean-Atmosphere System in the Eastern Tropical Pacific. *Journal of Climate,* 22**,** 3703-3719.

Rippeth, T. P. 2005. Mixing in seasonally stratified shelf seas: a shifting paradigm. *Philosophical Transactions of the Royal Society a-Mathematical Physical and Engineering Sciences,* 363**,** 2837-2854.

Rouse, L. J., 1998. Circulation and hydrographic structure in the vicinity of the Mississippi River delta. *In*: Murray, S.P. (ed.), *An Observational Study of the Mississippi-Atchafalaya Coastal Plume:Final Report.* New Orleans: U.S. Department of the Interior, Minerals Management Service, Gulf of Mexico OCS Study MMS 98-0040, 513.

Rouse, L. J. and Coleman, J. M. 1976. Circulation observations in the Louisiana Bight using LANDSAT imagery. *Remote Sensing of Environment,* XL, 635-642.

Scavia, D., Justic, D. and Bierman, V. J. 2004. Reducing hypoxia in the Gulf of Mexico: Advice from three models. *Estuaries,* 27**,** 419-425.

Schroeder, W. W., Dinnel, S. P. and Wiseman, W. J. 1990. Salinity Stratification in a River-Dominated Estuary. *Estuaries,* 13**,** 145-154.

Siadatmousavi, S. M., Allahdadi, M. N., Chen, Q., Jose, F. and Roberts, H. H. 2012. Simulation of wave damping during a cold front over the muddy Atchafalaya shelf. *Continental Shelf Research,* 47**,** 165-177.

Simpson, J. H. and Rippeth, T. P. 1993. The Clyde Sea - a model of the seasonal cycle of stratification and mixing. *Estuarine Coastal and Shelf Science,* 37**,** 129-144.

Smith, N. P. 1975. Seasonal-variations in nearshore Circulation in Northwestern Gulf of Mexico. *Contributions in Marine Science,* 19**,** 49-65.

Smith, N. P. 1978. Low-frequency reversals of nearshore currents in Northwestern Gulf of Mexico. *Contributions in Marine Science,* 21**,** 103-115.

Speckhart, B. L. Observational analysis of shallow water response to passing hurricanes in Onslow Bay, NC in 1999, Masters Thesis, University of North Carolina Wilmington, 1–61, 2004.

Stone, G. W., Jose, F., Luo, Y., Siadatmousavi, S. M. and Gibson, W. J. 2009. A WAVCIS-based ocean observing station off Eglin Air Force Base, Fort Walton, Florida. In: Proceeding of OCEANS 2009 MTS/ IEEE (Biloxi, Mississippi, Marine Technology Society and IEEE), pp. 1–9.

Stow, C. A., Qian, S. S. and Craig, J. K. 2005. Declining threshold for hypoxia in the Gulf of Mexico. *Environmental Science & Technology,* 39**,** 716-723.

Turner, J. S. 1973. *Buoyancy Effects in Fluids.* London: Cambridge University Press, Cambridge, 367p.

Turner, R. E. and Rabalais, N. N. 1994. Coastal eutrophication near the Mississippi river delta. *Nature,* 368**,** 619-621.

Turner, R. E., Rabalais, N. N. and Justic, D. 2006. Predicting summer hypoxia in the northern Gulf of Mexico: Riverine N, P, and Si loading. *Marine Pollution Bulletin,* 52**,** 139-148.

Turner, R. E., Rabalais, N. N. and Justic, D. 2008. Gulf of Mexico hypoxia: Alternate states and a legacy. *Environmental Science & Technology,* 42**,** 2323-2327.

Van Haren, V. 2000. Properties of vertical current shear across stratificationin the North Sea, *Journal of Marine Research, 58,* 465–491.

Voorhis, A. D., Webb, D. C. and R. C. Millar. 1976. Current Structure and Mixing in the Shelf/Slope Water Front South of New England. *Journal of Geophysical Research*, Vol. 81(21), 3695-4006.

Walker, N. D. 1996. Satellite assessment of Mississippi River plume variability: causes and predictability. *Remote sensing of environment, 58*(1), 21-35.

Walker, N. D. 2005. Wind and eddy-related shelf/slope circulation processes and coastal upwelling in the Northwestern Gulf of Mexico. *Circulation in the Gulf of Mexico: Observations and Models*. Geophysical Monograph Series 161, Copyright 2005 by the American Geophysical Union.

Walker, N., Myint, S., Babin, A. and Haag, A. 2003. Advances in satellite radiometry for the surveillance of surface temperatures, ocean eddies and upwelling processes in the Gulf of Mexico using GOES-8 measurements during summer. *Geophysical Research Letters,* 30.

Walker, N. D. and Rabalais, N. N. 2006. Relationships among satellite chlorophyll a, river inputs, and hypoxia on the Louisiana continental shelf, gulf of Mexico. *Estuaries and Coasts,* 29**,** 1081-1093.

Walker, N. D., Wiseman, W. J., Rouse, L. J. and Babin, A. 2005. Effects of river discharge, wind stress, and slope eddies on circulation and the satellite-observed structure of the Mississippi River plume. *Journal of Coastal Research,* 21**,** 1228-1244.

Wang, D. P. and Oey, L. Y. 2008. Hindcast of waves and currents in Hurricane Katrina. *Bulletin of the American Meteorological Society,* 89**,** 487-+.

Wang, L. X. and Justic, D. 2009. A modeling study of the physical processes affecting the development of seasonal hypoxia over the inner Louisiana-Texas shelf: Circulation and stratification. *Continental Shelf Research,* 29**,** 1464-1476.

Washburn, L. and Gibson, C. H. 1984. Horizontal variability of temperature microstructure at the base of a mixed layer during MILE, *Journal of Geophysical Research,* 57(C3), 3507-3522.

Wiseman, W. J. JR., Bane, J. M, Murray, S. P. and Tubman, M. W. 1976. Small-scale temperature and salinity structure over the inner shelf west of the Mississippi River delta. *Memoires Societe Royale des Sciences de Lie`ge,* 6, 277–285.

Wiseman, W. J. JR., Rabalais, N. N., Turner, R. E., Dinnel, S. P. and Macnaughton, A. 1997. Seasonal and interannual variability within the Louisiana coastal current: stratification and hypoxia. *Journal of Marine Systems,* 12**,** 237-248.

Wiseman, W. J. JR., Rabalais, N. N., Turner, R. E. and Judtic, D. 2004. Hypoxia and the physics of the Louisiana coastal current. *In*: Nihoul, J. C. J.; Zavialov, P. O. and Micklin, P. P. (eds.), *Dying and Dead Seas, climatic versus anthropic causes*. Lie`ge, Belgium: NATO Advanced Research Workshop, NATO ASI Series. Kluwer Academic Publishers, Dordrecht, Netherlands, pp. 359–372.

Wiseman, W. J. JR., Turner, R. E., Kelly, F. J., Rouse, L. J., JR. and Shaw, R. F. 1986. Analysis of biological and chemical associations near a turbid coastal front during winter 1982. *Contributions in Marine Science,* 29**,** 141-151.

Wright, L. D. and Nittrouer, C. A. 1995. Dispersal of river sediments in coastal seas: Six contrasting cases. *Estuaries,* 18**,** 494-508.

Wright, L. D, Sherwood, C. R. and Sternberg, R. W. 1997. Field measurements of fair weather bottom boundary layer processes and sediment suspension on the Louisiana inner continental shelf. *Marine Geology*, 140, 329–345.

Wyrtki, K., 1965. The average annual heat balance of the North Pacific Ocean and its relation to ocean circulation. Journal of Geophysical Research 70 (18), 4547–4559.

Xie, L., Pietrafesa, L. J., Bohm, E., Zhang, C. and Li, X. 1998. Evidence and mechanism of Hurricane Fran induced cooling in the Charleston trough. *Geophysical Research Letters,* 25**,** 769-772.

Young, I. R. and Sobey, R. J. 1981. The numerical prediction of tropical cyclone wind-waves, James Cook University of North Queensland, Townville, Dept. of Civil & Systems Eng., Research Bulletin No. CS20.

Zedler, S. E., Dickey, T. D., Doney, S. C., Price, J. F., Yu, X. and Mellor, G. L. 2002. Analyses and simulations of the upper ocean's response to Hurricane Felix at the Bermuda Testbed Mooring site: 13-23 August 1995. *Journal of Geophysical Research-Oceans,* 107.

Zhang, J. L. and Steele, M. 2007. Effect of vertical mixing on the Atlantic Water layer circulation in the Arctic Ocean. *Journal of Geophysical Research-Oceans,* 112.

Zhang, X. P. 2003. Design and implementation of an ocean observing system: WAVCIS (Wave-current-surge information system) and its application to the Louisiana coast. Louisiana,Baton Rouge: Louisiana State University, Ph.D thesis.

APPENDIX A: TEMPERATURE VARIATIONS INDUCED BY HURRICANE KATRINA ACROSS THE SELECTED EAST-WEST SECTIONS AT DIFFERENT TIMES AS DESCRIBED IN SECTION 4.4.3

Times are in hour. Positive and negative singes of times are in accordance to time frames defined in section 4.4.3.

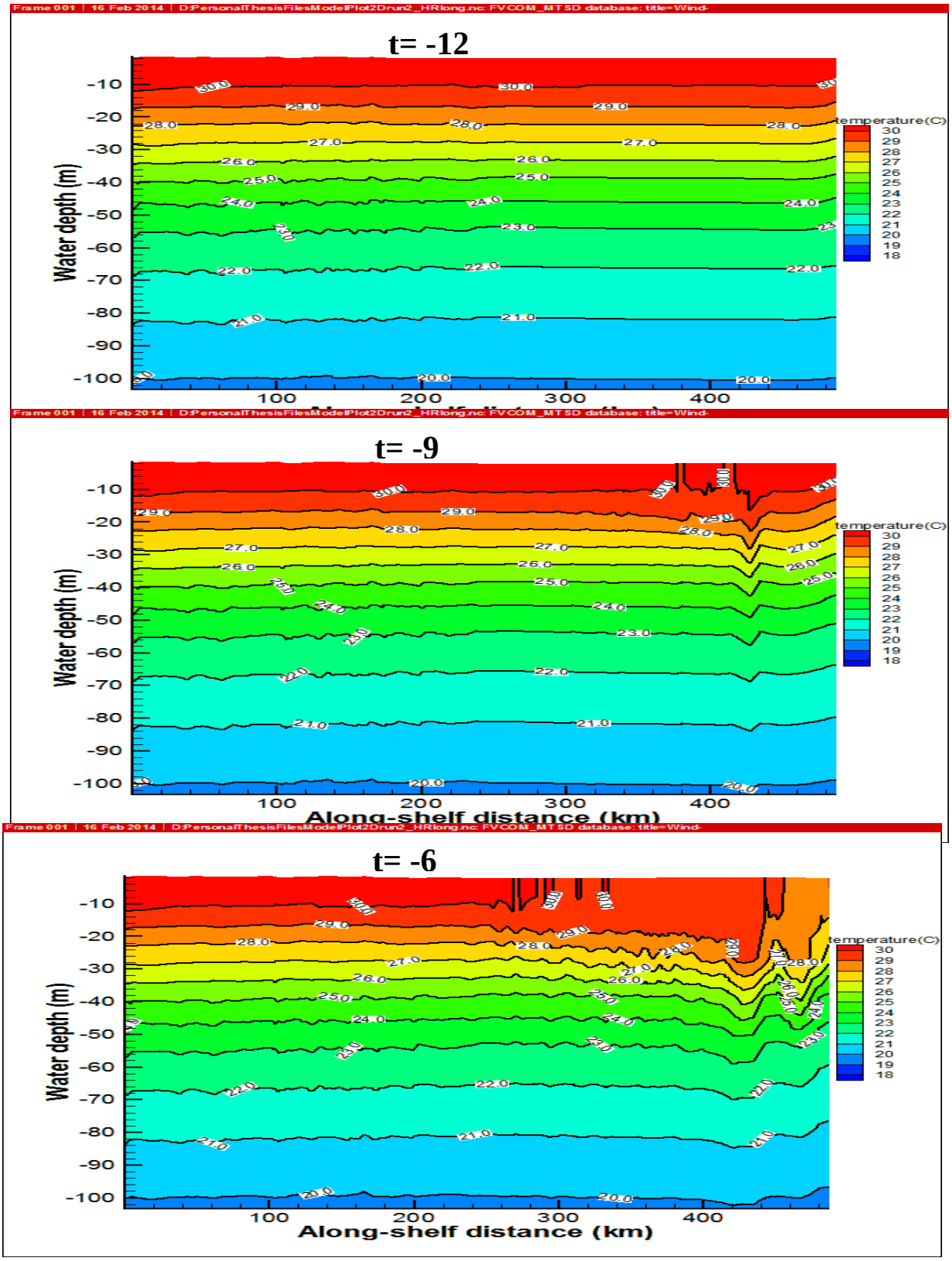
Frame 001 | 16 Feb 2014 | D:\Personal\Thesis\Files\Model\Plot2Drun2_HR\long.nc: FVCOM_MTSD database: title='Wind-
t= -12
Water depth (m)
-10
-20
-30
-40
-50
-60
-70
-80
-90
-100
100
200
300
400
temperature(C)
30
29
28
27
26
25
24
23
22
21
20
19
18
Frame 001 | 16 Feb 2014 | D:\Personal\Thesis\Files\Model\Plot2Drun2_HR\long.nc: FVCOM_MTSD database: title='Wind-
t= -9
Water depth (m)
Along-shelf distance (km)
Frame 001 | 16 Feb 2014 | D:\Personal\Thesis\Files\Model\Plot2Drun2_HR\long.nc: FVCOM_MTSD database: title='Wind-
t= -6
Water depth (m)
Along-shelf distance (km)

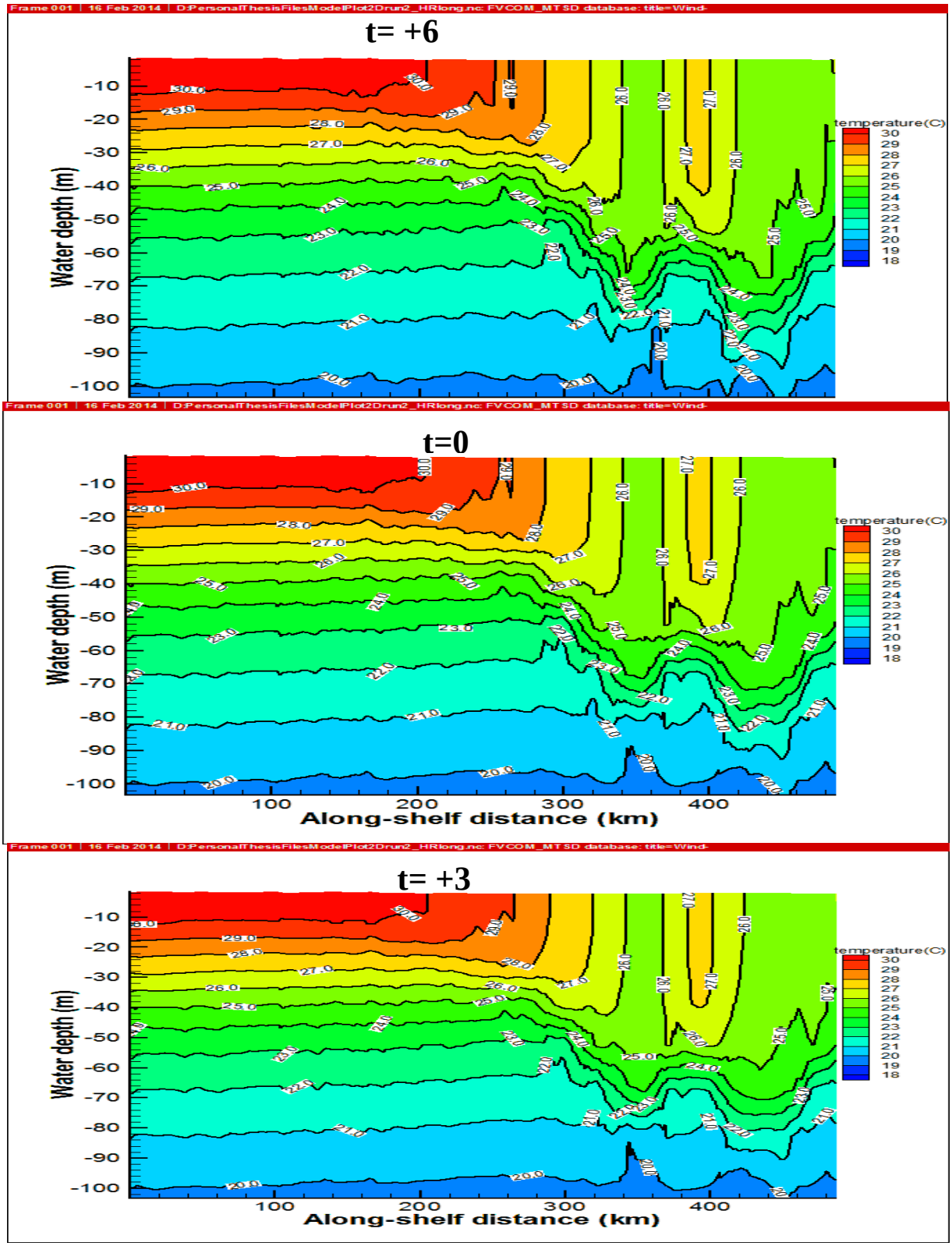
Frame 001 | 16 Feb 2014 | D:\Personal\Thesis\Files\Model\Plot2D\run2_HR\long.nc: FVCOM_MTSD database: title='Wind-
t= +6
Water depth (m)
temperature(C)
30
29
28
27
26
25
24
23
22
21
20
19
18
Frame 001 | 16 Feb 2014 | D:\Personal\Thesis\Files\Model\Plot2D\run2_HR\long.nc: FVCOM_MTSD database: title='Wind-
t=0
Water depth (m)
Along-shelf distance (km)
Frame 001 | 16 Feb 2014 | D:\Personal\Thesis\Files\Model\Plot2D\run2_HR\long.nc: FVCOM_MTSD database: title='Wind-
t= +3
Water depth (m)
Along-shelf distance (km)

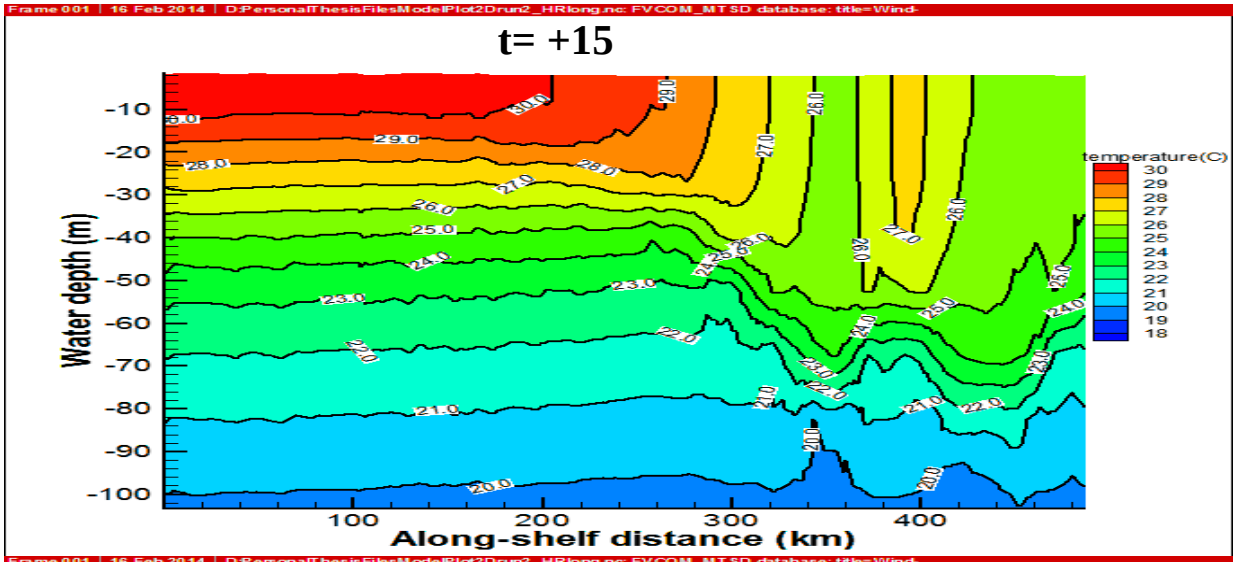
Frame 001 | 16 Feb 2014 | D:\Personal\Thesis\Files\Model\Plot2D\run2_HR\long.nc: FVCOM_MTSD database: title=Wind-
t= +15
Water depth (m)
-10
-20
-30
-40
-50
-60
-70
-80
-90
-100
100
200
300
400
Along-shelf distance (km)
temperature(C)
30
29
28
27
26
25
24
23
22
21
20
19
18

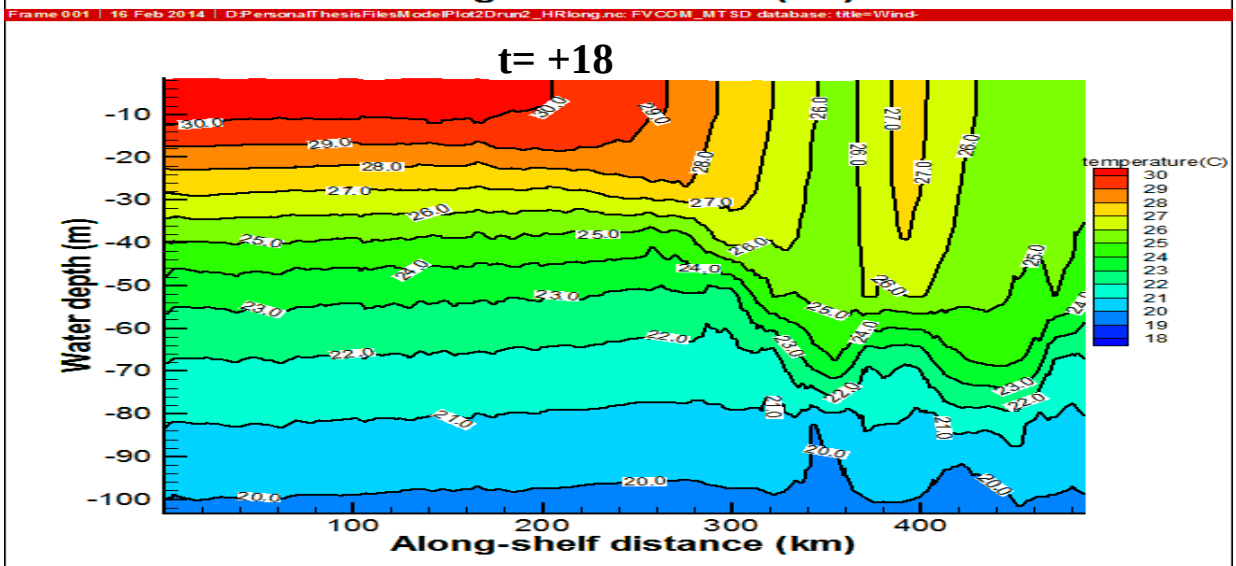
Frame 001 | 16 Feb 2014 | D:\Personal\Thesis\Files\Model\Plot2D\run2_HR\long.nc: FVCOM_MTSD database: title=Wind-
t= +18
Water depth (m)
-10
-20
-30
-40
-50
-60
-70
-80
-90
-100
100
200
300
400
Along-shelf distance (km)
temperature(C)
30
29
28
27
26
25
24
23
22
21
20
19
18

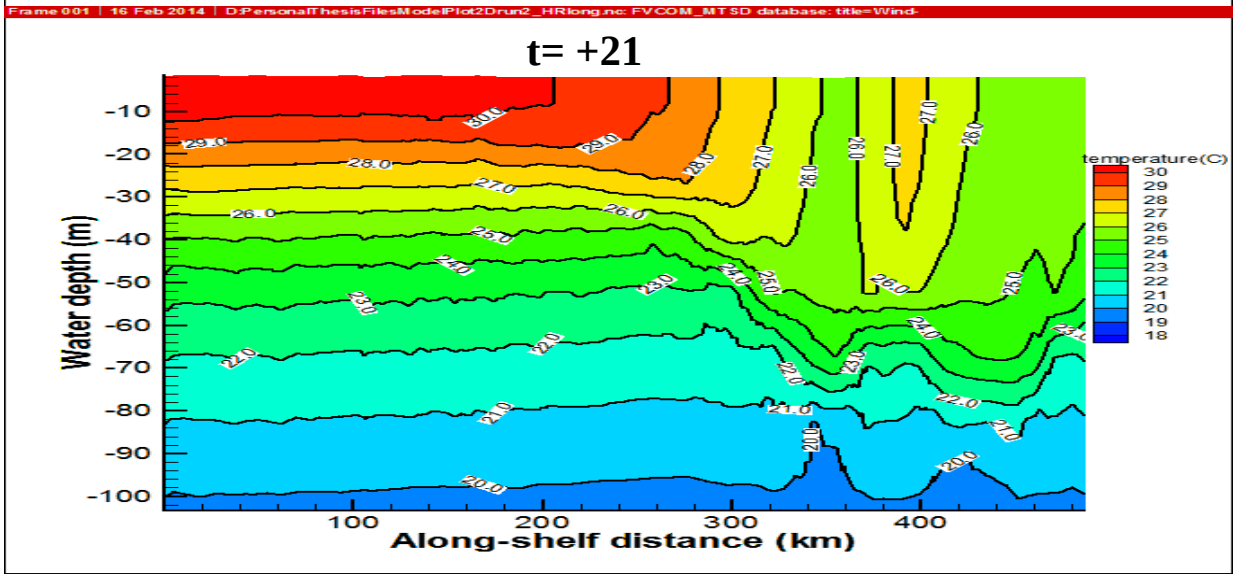
Frame 001 | 16 Feb 2014 | D:\Personal\Thesis\Files\Model\Plot2D\run2_HR\long.nc: FVCOM_MTSD database: title=Wind-
t= +21
Water depth (m)
-10
-20
-30
-40
-50
-60
-70
-80
-90
-100
100
200
300
400
Along-shelf distance (km)
temperature(C)
30
29
28
27
26
25
24
23
22
21
20
19
18

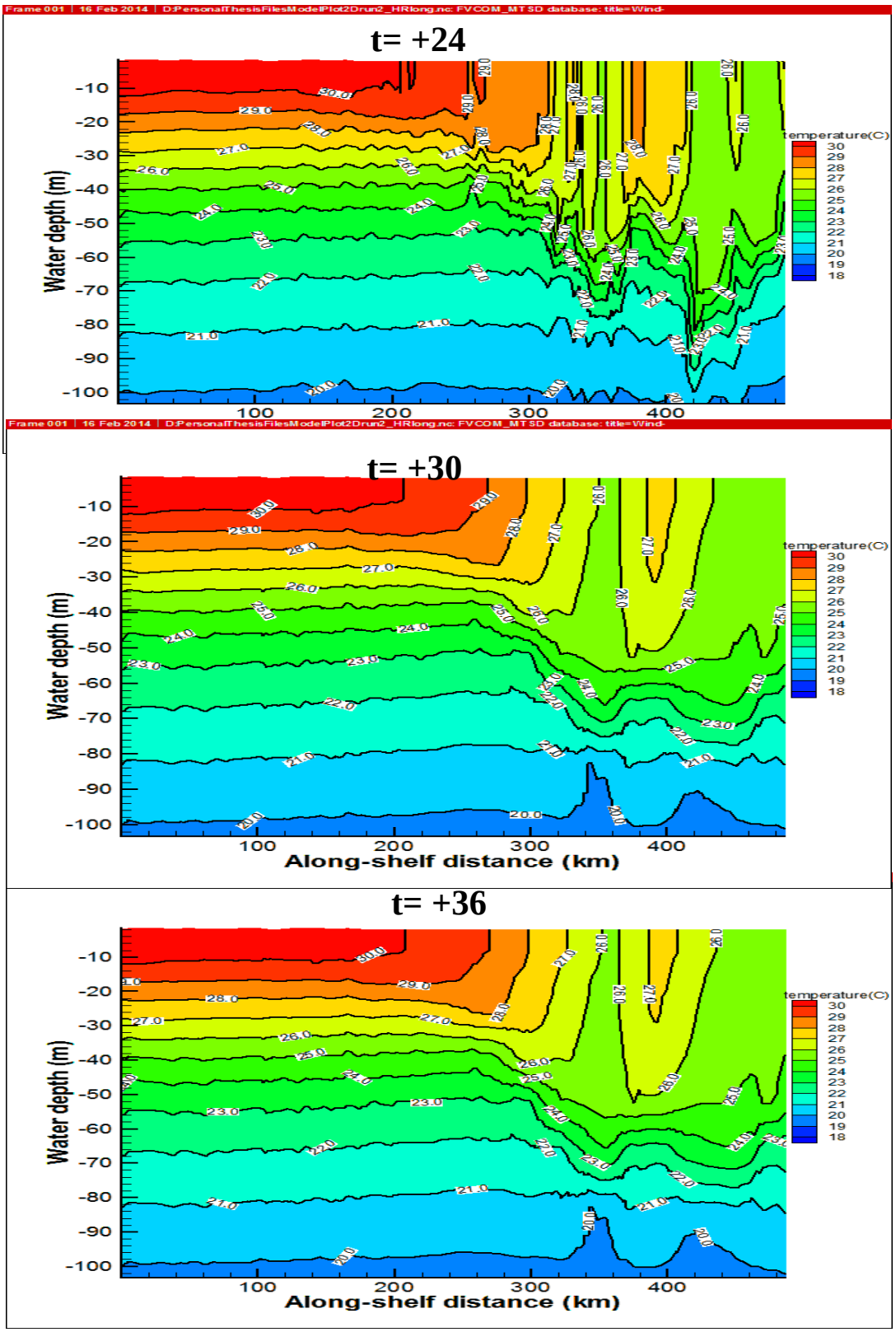
Frame 001 | 16 Feb 2014 | D:\Personal\Thesis\Files\Model\Plot2Drun2_HR\long.nc: FVCOM_MTSD database: title='Wind-
t= +24
Water depth (m)
-10
-20
-30
-40
-50
-60
-70
-80
-90
-100
100
200
300
400
temperature(C)
30
29
28
27
26
25
24
23
22
21
20
19
18
Frame 001 | 16 Feb 2014 | D:\Personal\Thesis\Files\Model\Plot2Drun2_HR\long.nc: FVCOM_MTSD database: title='Wind-
t= +30
Water depth (m)
Along-shelf distance (km)
t= +36
Water depth (m)
Along-shelf distance (km)

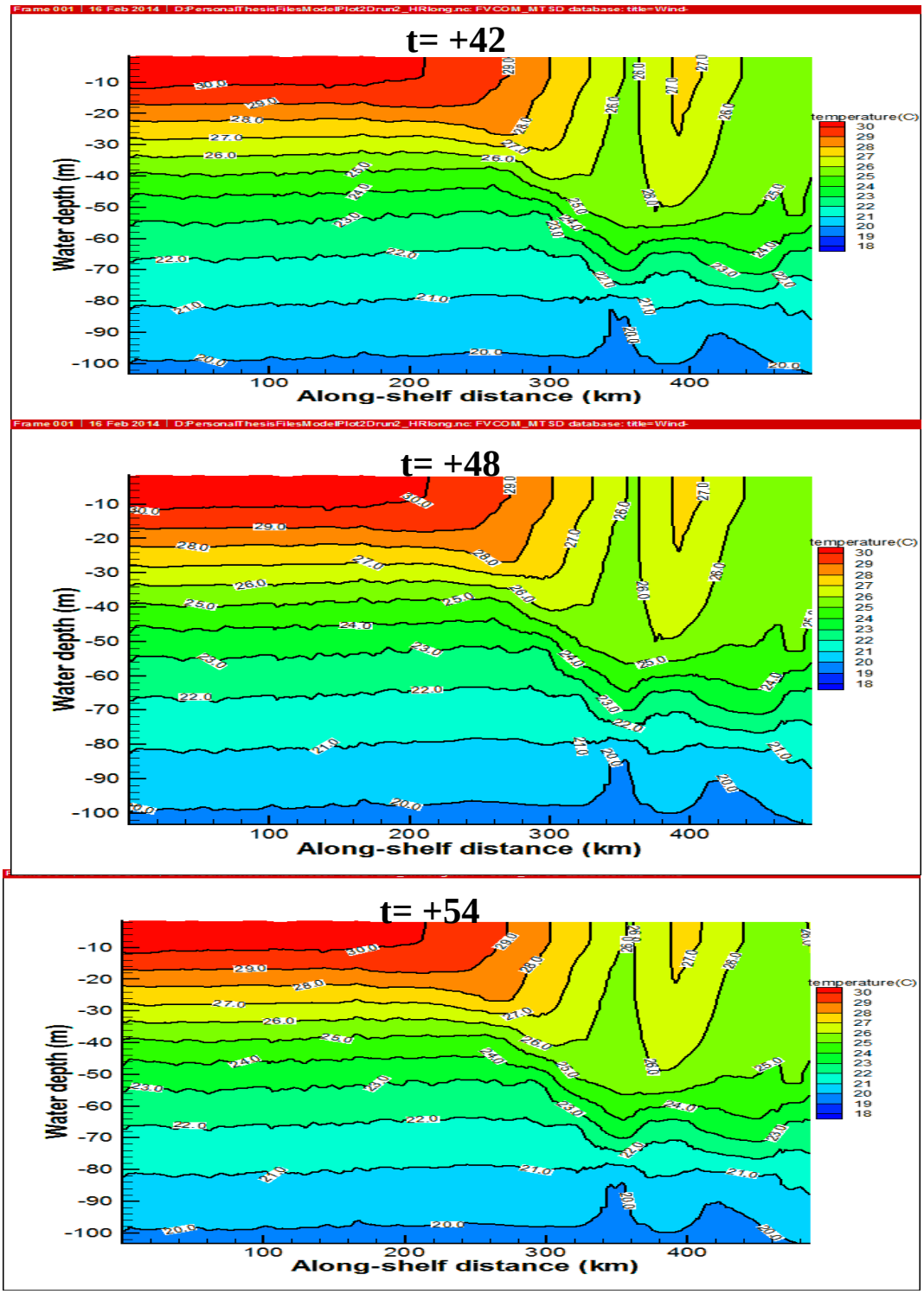
t= +42
t= +48
t= +54
Water depth (m)
Along-shelf distance (km)
temperature(C)

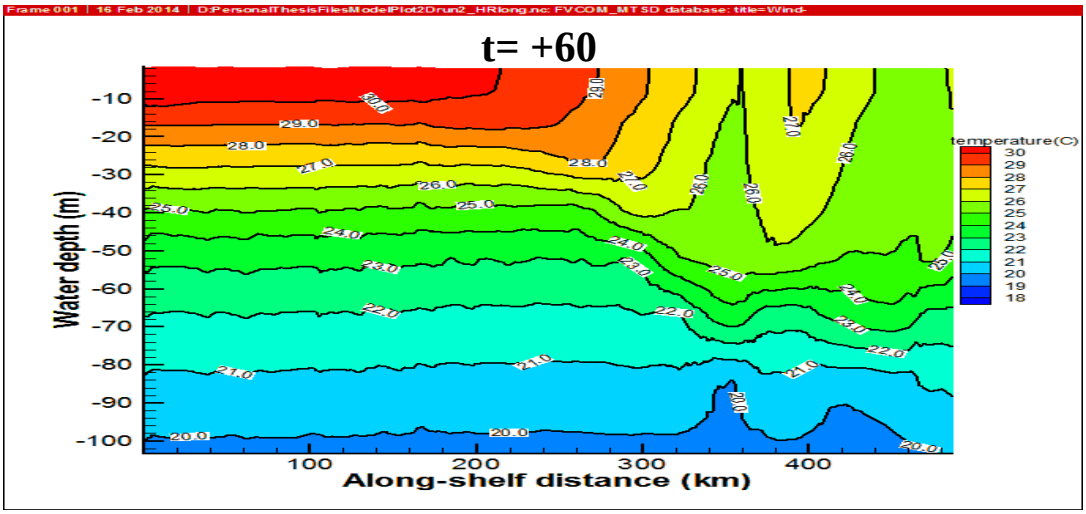
t= +60
Water depth (m)
Along-shelf distance (km)
temperature(C)

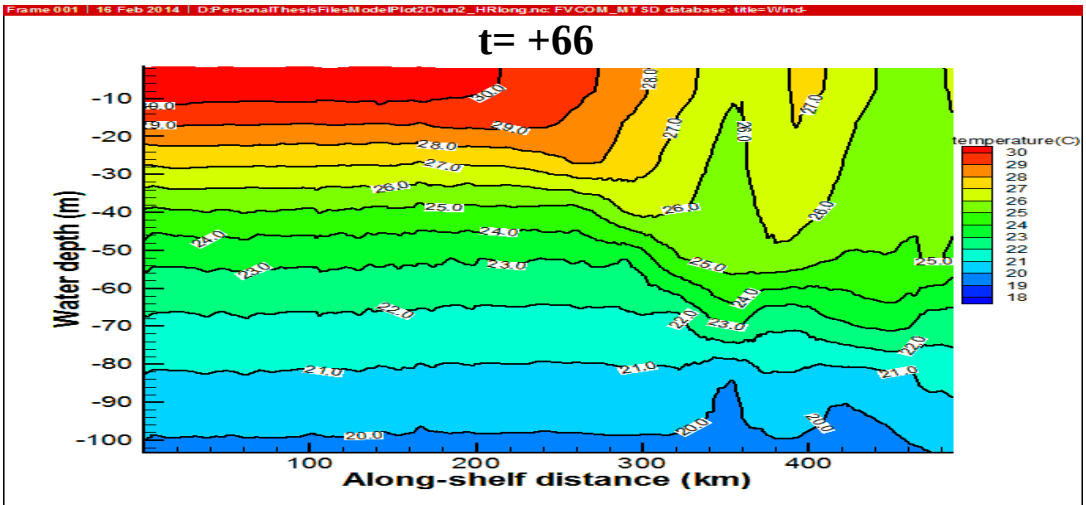
t= +66
Water depth (m)
Along-shelf distance (km)
temperature(C)

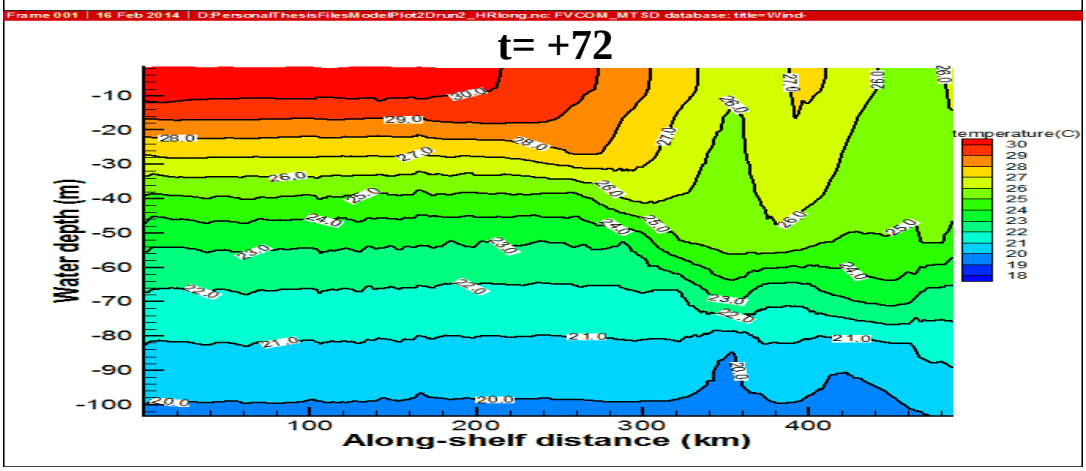
t= +72
Water depth (m)
Along-shelf distance (km)
temperature(C)

East-West section 2

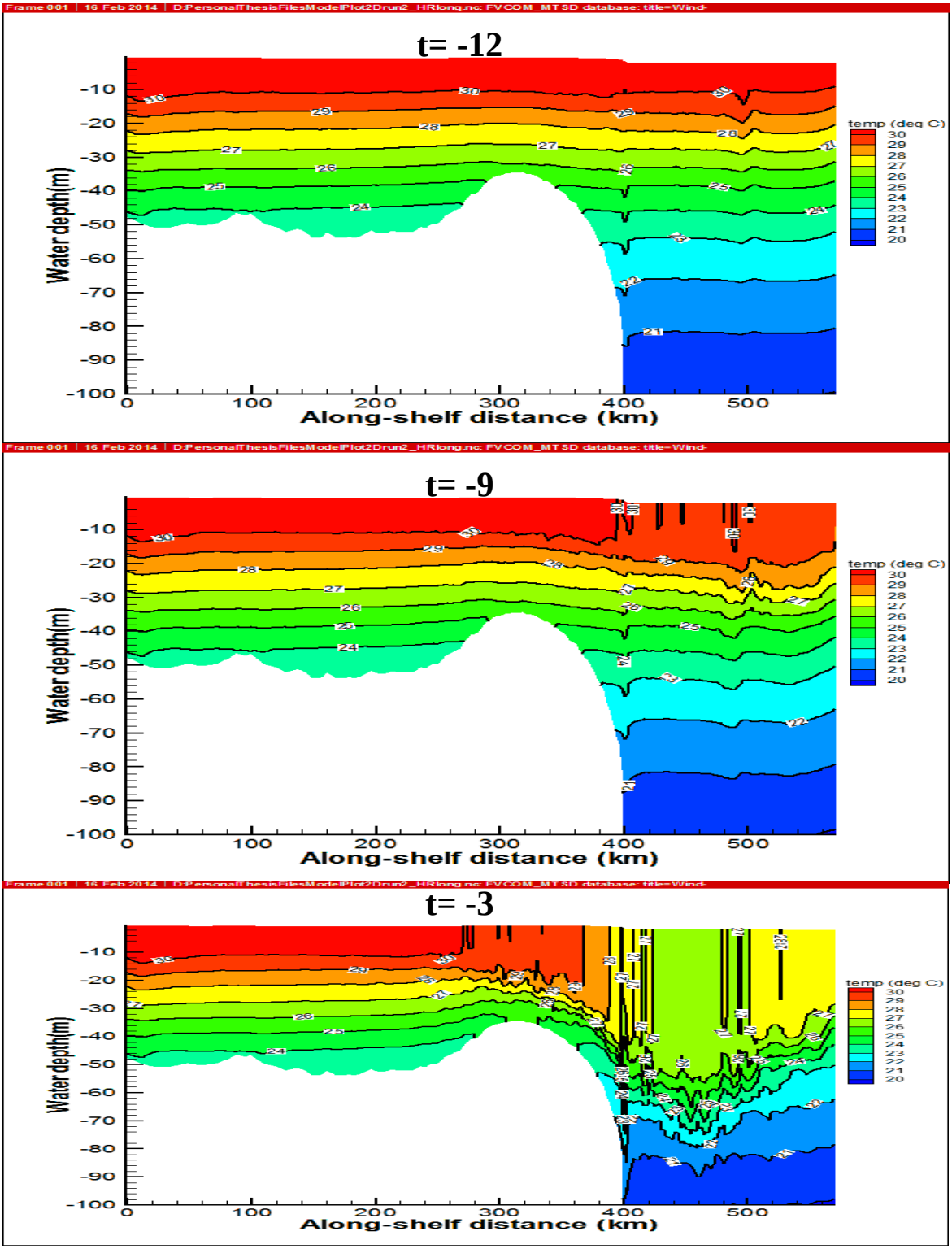

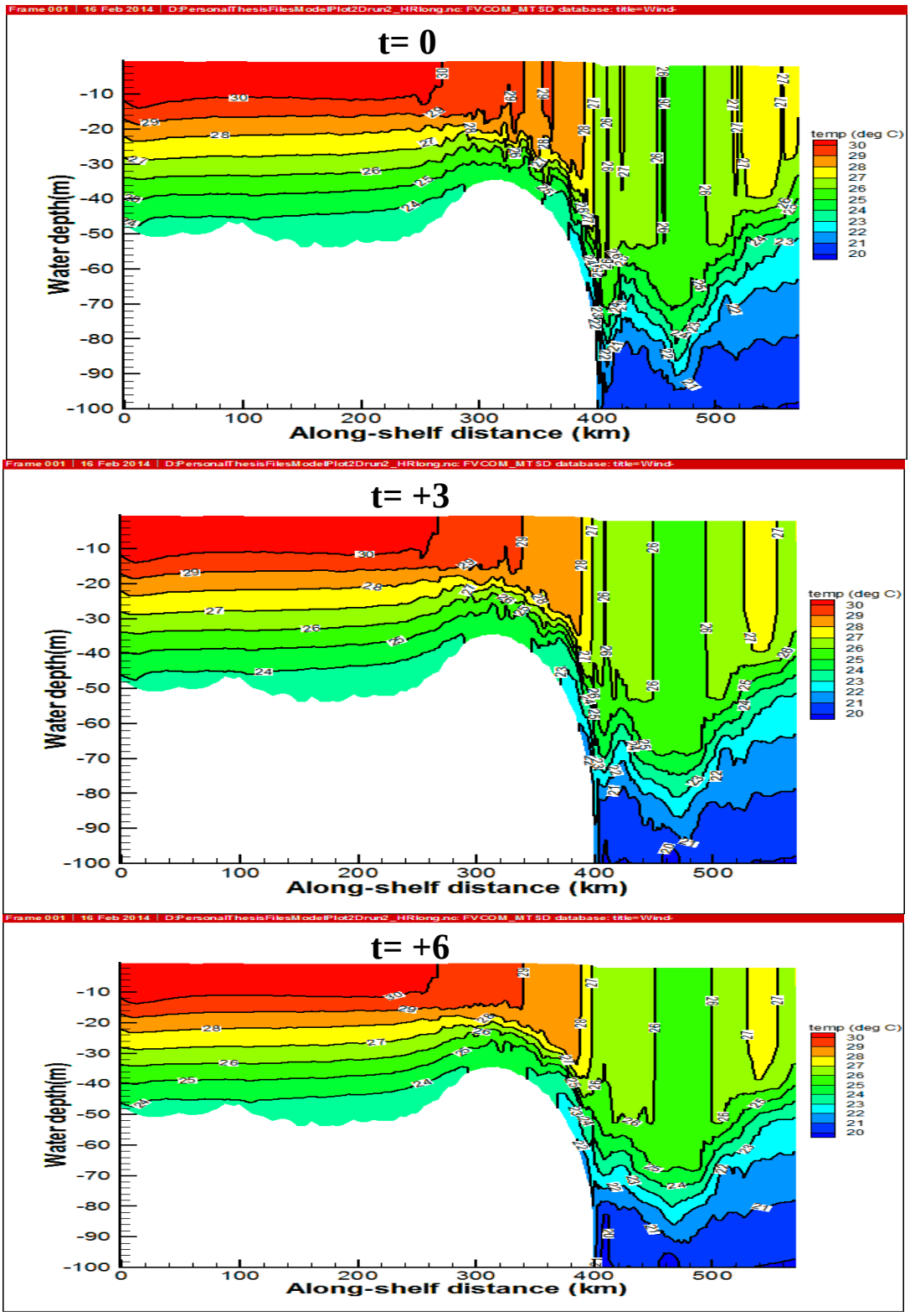
Frame 001 | 16 Feb 2014 | D:PersonalThesisFilesModelPlot2Drun2_HRlong.nc: FVCOM_MTSD database: title=Wind-
t= 0
Water depth(m)
Along-shelf distance (km)
temp (deg C)
Frame 001 | 16 Feb 2014 | D:PersonalThesisFilesModelPlot2Drun2_HRlong.nc: FVCOM_MTSD database: title=Wind-
t= +3
Water depth(m)
Along-shelf distance (km)
temp (deg C)
Frame 001 | 16 Feb 2014 | D:PersonalThesisFilesModelPlot2Drun2_HRlong.nc: FVCOM_MTSD database: title=Wind-
t= +6
Water depth(m)
Along-shelf distance (km)
temp (deg C)

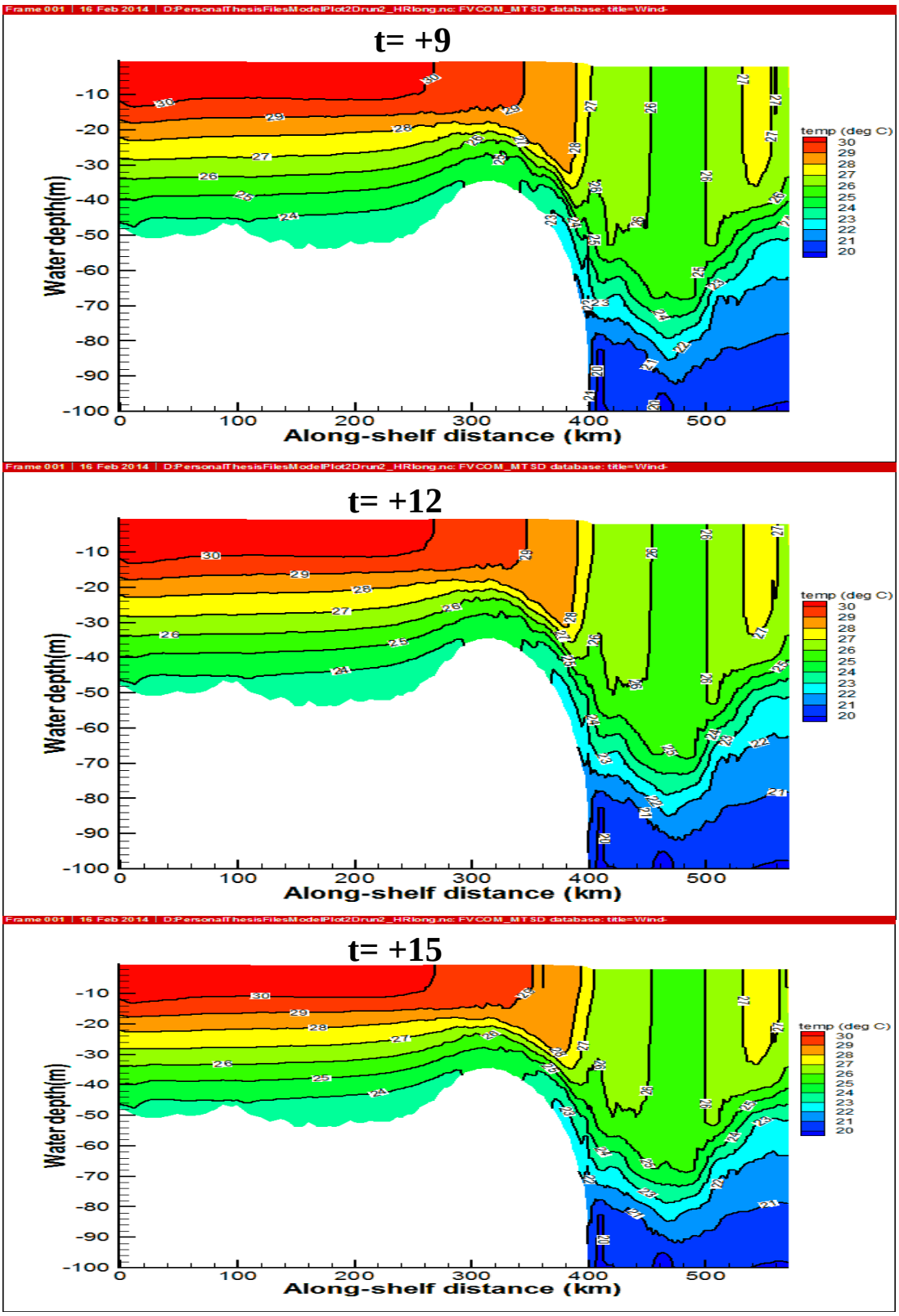
Frame 001 | 16 Feb 2014 | D:PersonalThesisFilesModelPlot2Drun2_HRlong.nc: FVCOM_MTSD database: title=Wind-
t= +9
Water depth(m)
Along-shelf distance (km)
temp (deg C)
30
29
28
27
26
25
24
23
22
21
20
Frame 001 | 16 Feb 2014 | D:PersonalThesisFilesModelPlot2Drun2_HRlong.nc: FVCOM_MTSD database: title=Wind-
t= +12
Water depth(m)
Along-shelf distance (km)
temp (deg C)
Frame 001 | 16 Feb 2014 | D:PersonalThesisFilesModelPlot2Drun2_HRlong.nc: FVCOM_MTSD database: title=Wind-
t= +15
Water depth(m)
Along-shelf distance (km)
temp (deg C)

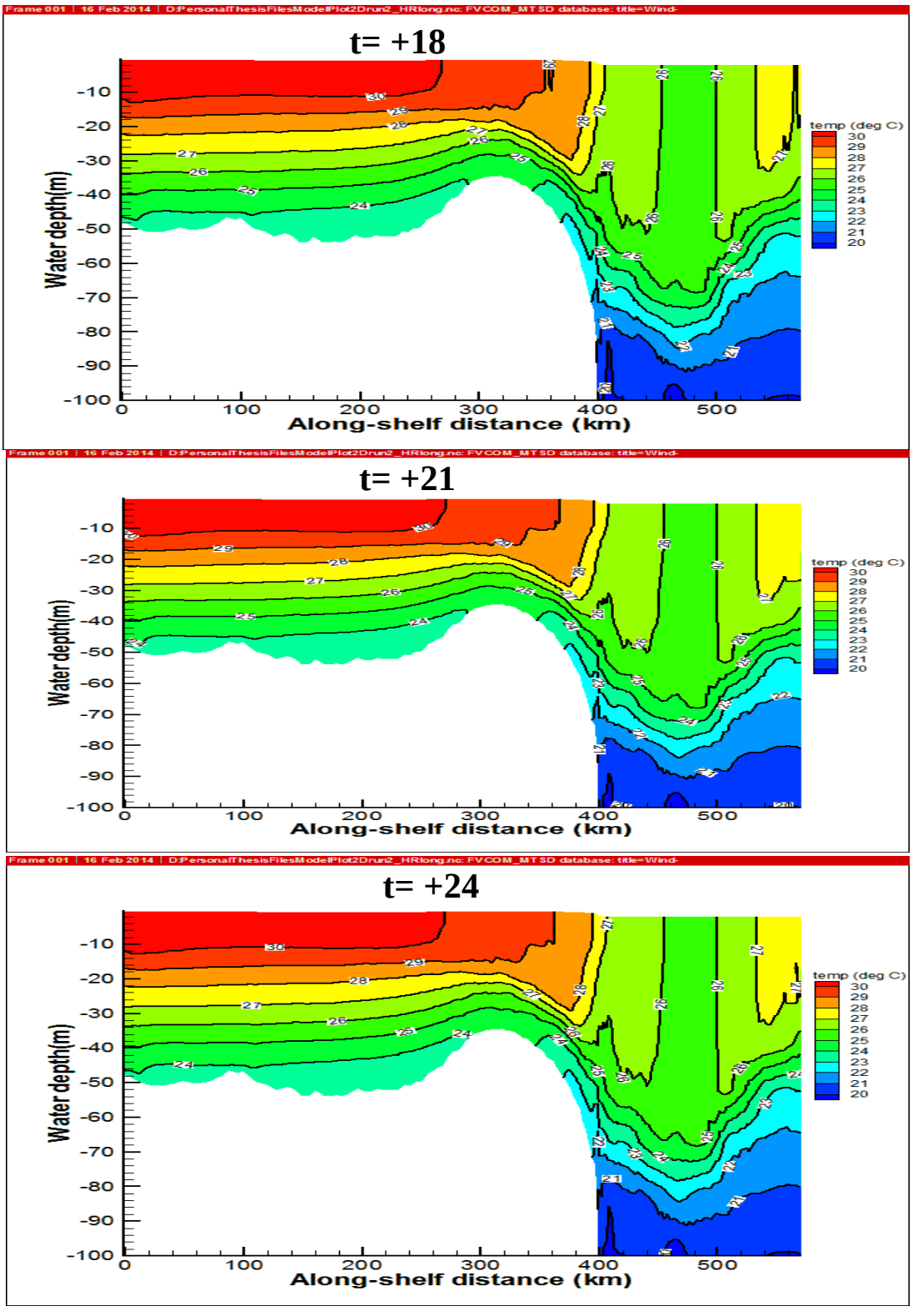
t= +18
t= +21
t= +24
Water depth(m)
Along-shelf distance (km)
temp (deg C)
30
29
28
27
26
25
24
23
22
21
20
-10
-20
-30
-40
-50
-60
-70
-80
-90
-100
0
100
200
300
400
500

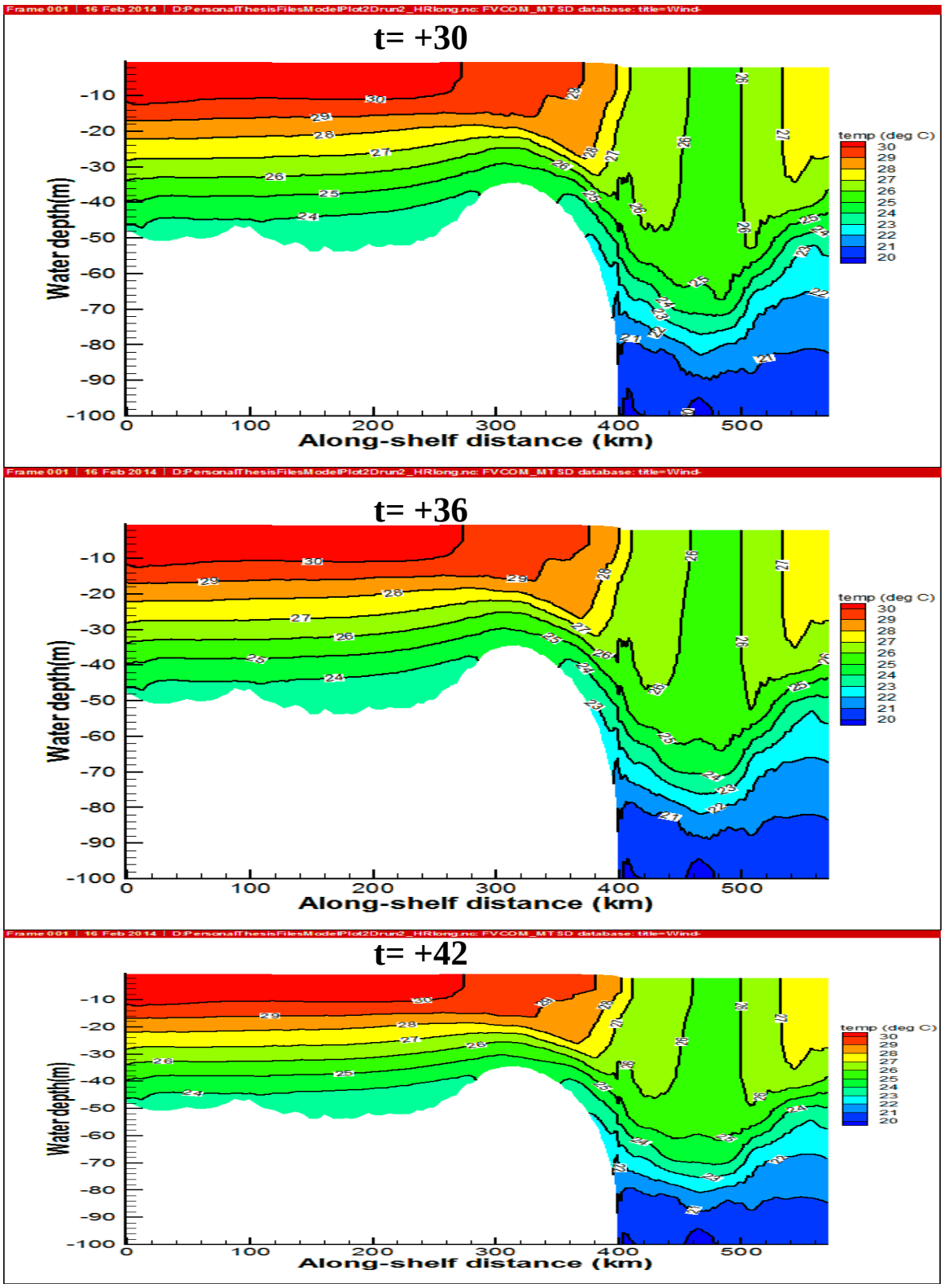
Frame 001 | 16 Feb 2014 | D:PersonalThesisFilesModelPlot2Drun2_HRlong.nc: FVCOM_MTSD database: title=Wind-
t= +30
Water depth(m)
Along-shelf distance (km)
temp (deg C)
30
29
28
27
26
25
24
23
22
21
20
Frame 001 | 16 Feb 2014 | D:PersonalThesisFilesModelPlot2Drun2_HRlong.nc: FVCOM_MTSD database: title=Wind-
t= +36
Water depth(m)
Along-shelf distance (km)
temp (deg C)
Frame 001 | 16 Feb 2014 | D:PersonalThesisFilesModelPlot2Drun2_HRlong.nc: FVCOM_MTSD database: title=Wind-
t= +42
Water depth(m)
Along-shelf distance (km)
temp (deg C)

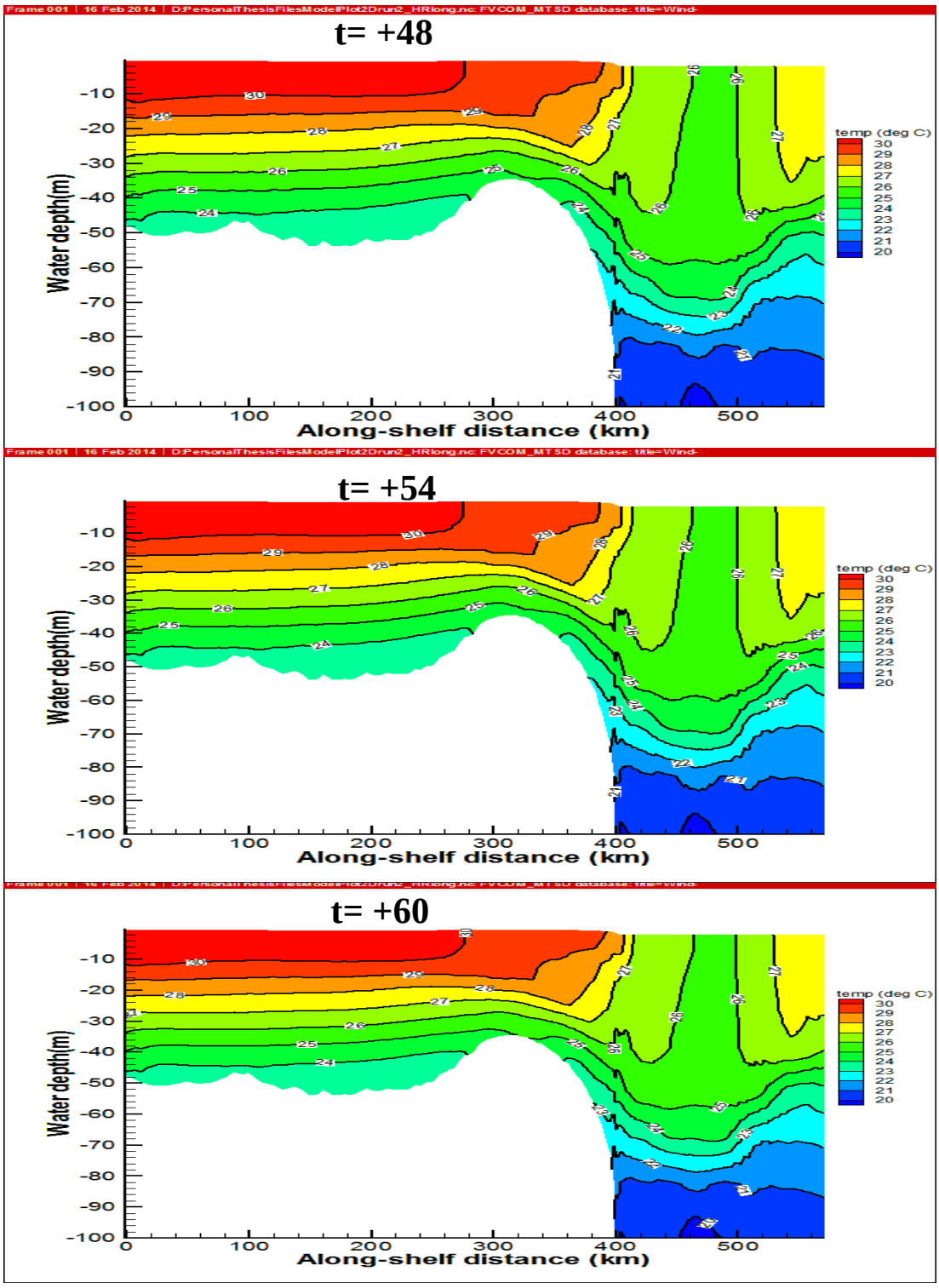
t= +48
t= +54
t= +60
Water depth(m)
Along-shelf distance (km)
temp (deg C)
30
29
28
27
26
25
24
23
22
21
20
0
100
200
300
400
500
-10
-20
-30
-40
-50
-60
-70
-80
-90
-100

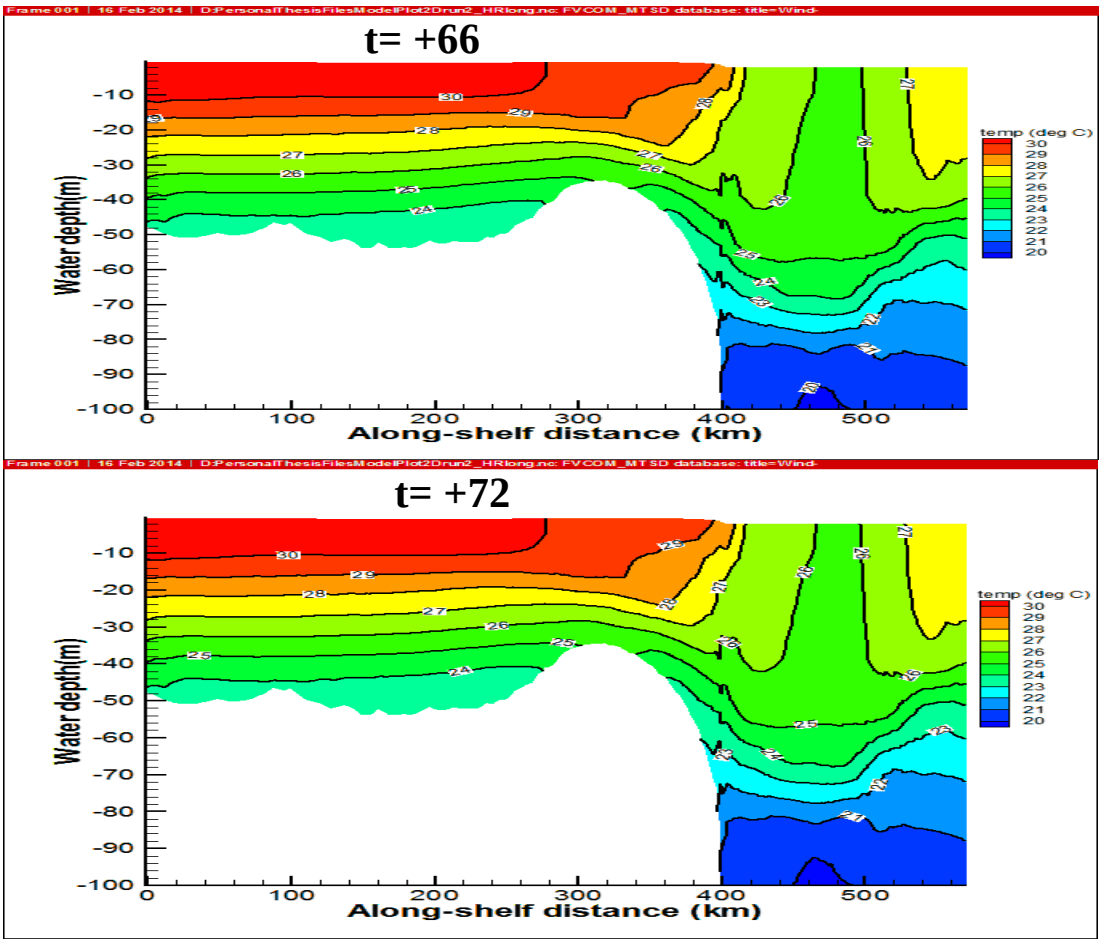
t= +66
Water depth(m)
Along-shelf distance (km)
temp (deg C)
t= +72
Water depth(m)
Along-shelf distance (km)
temp (deg C)

APPENDIX B: TEMPERATURE VARIATIONS INDUCED BY HURRICANE KATRINA ACROSS THE SELECTED NORTH-SOUTH CROSS-SECTIONS AT DIFFERENT TIMES AS DESCRIBED IN SECTION 4.4.3.

Times are in hour. Positive and negative singes of times are in accordance to time frames defined in section 4.4.3.

Cross Section D

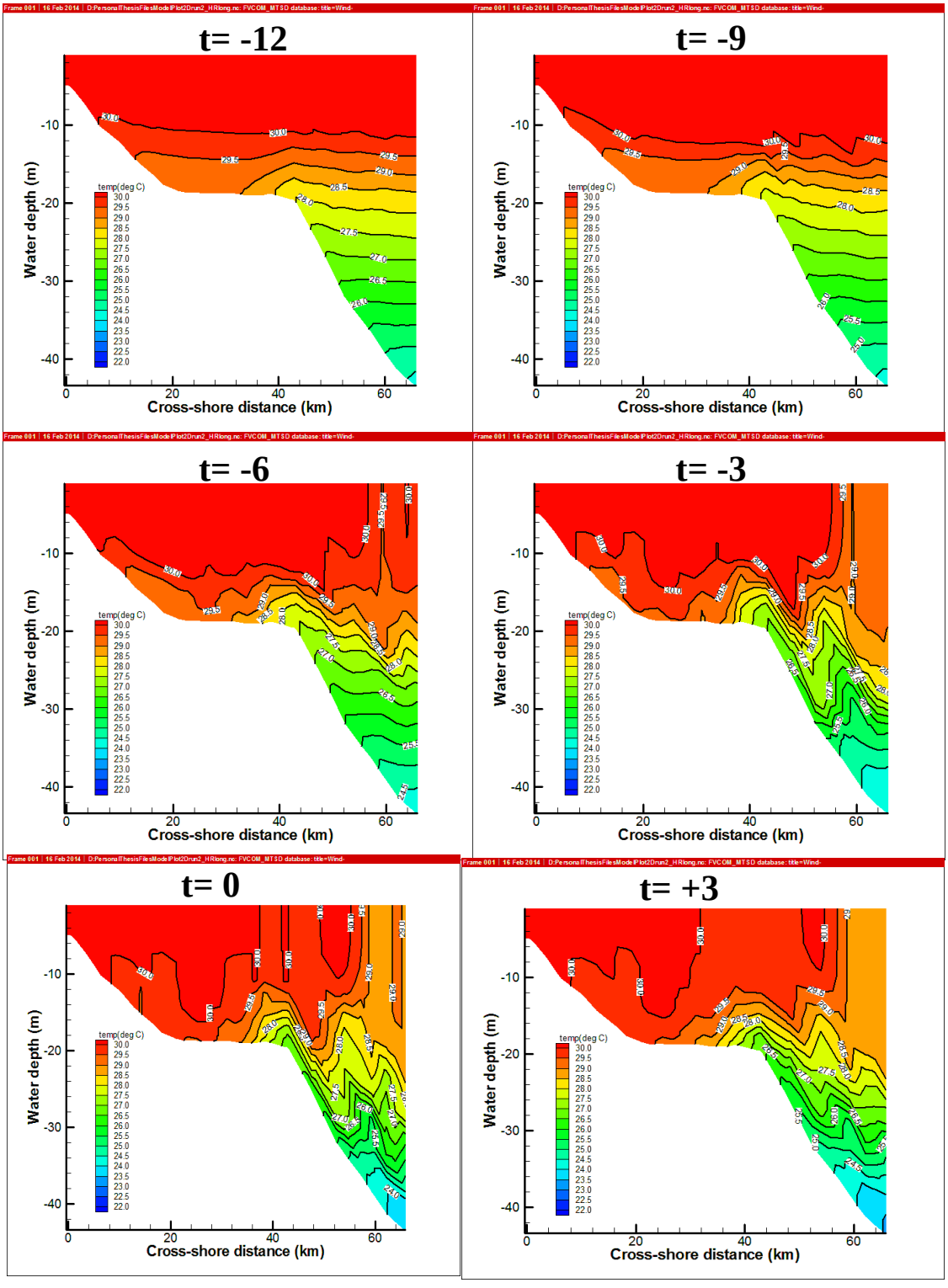

Cross Section D

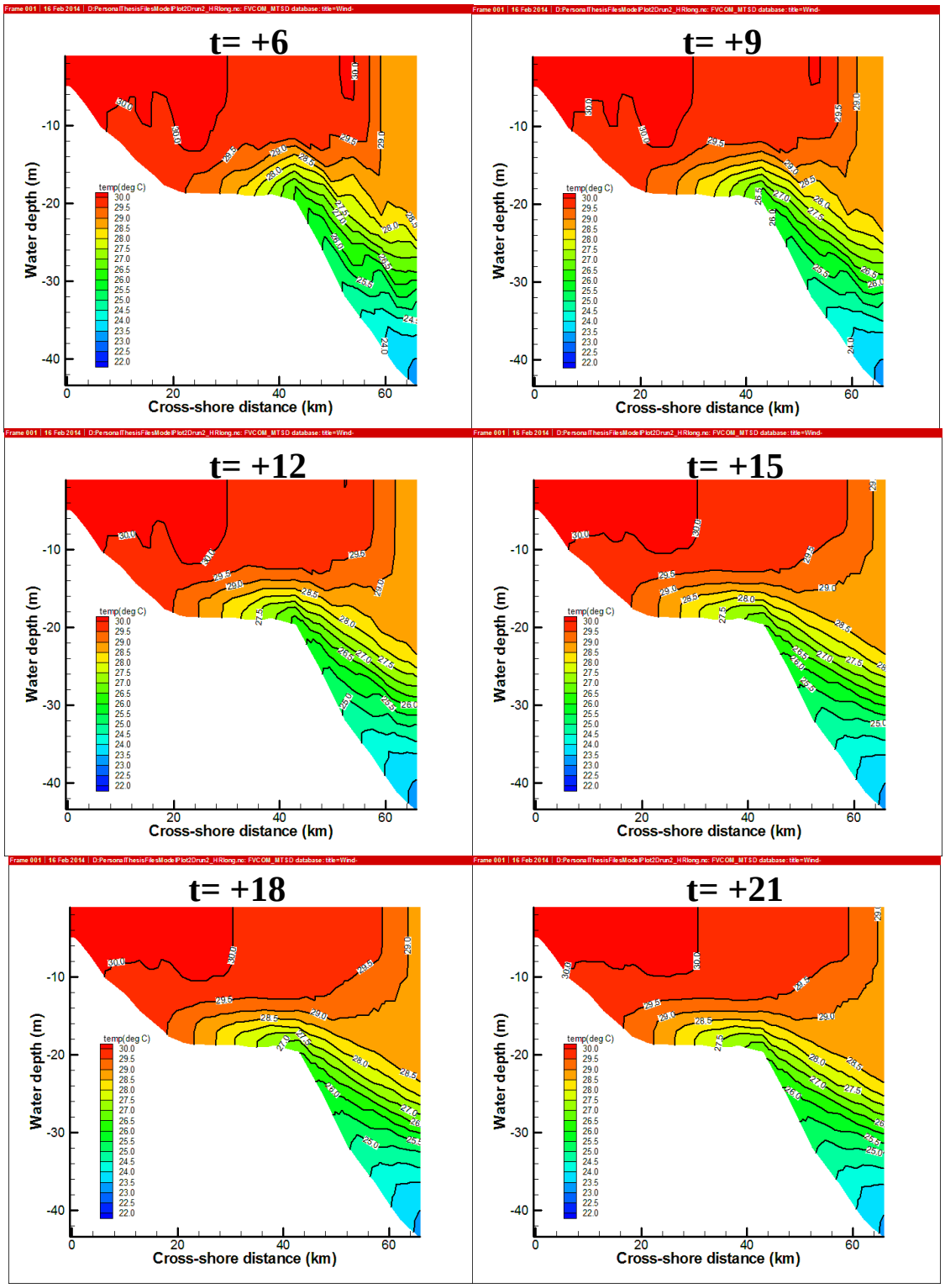

Cross Section D

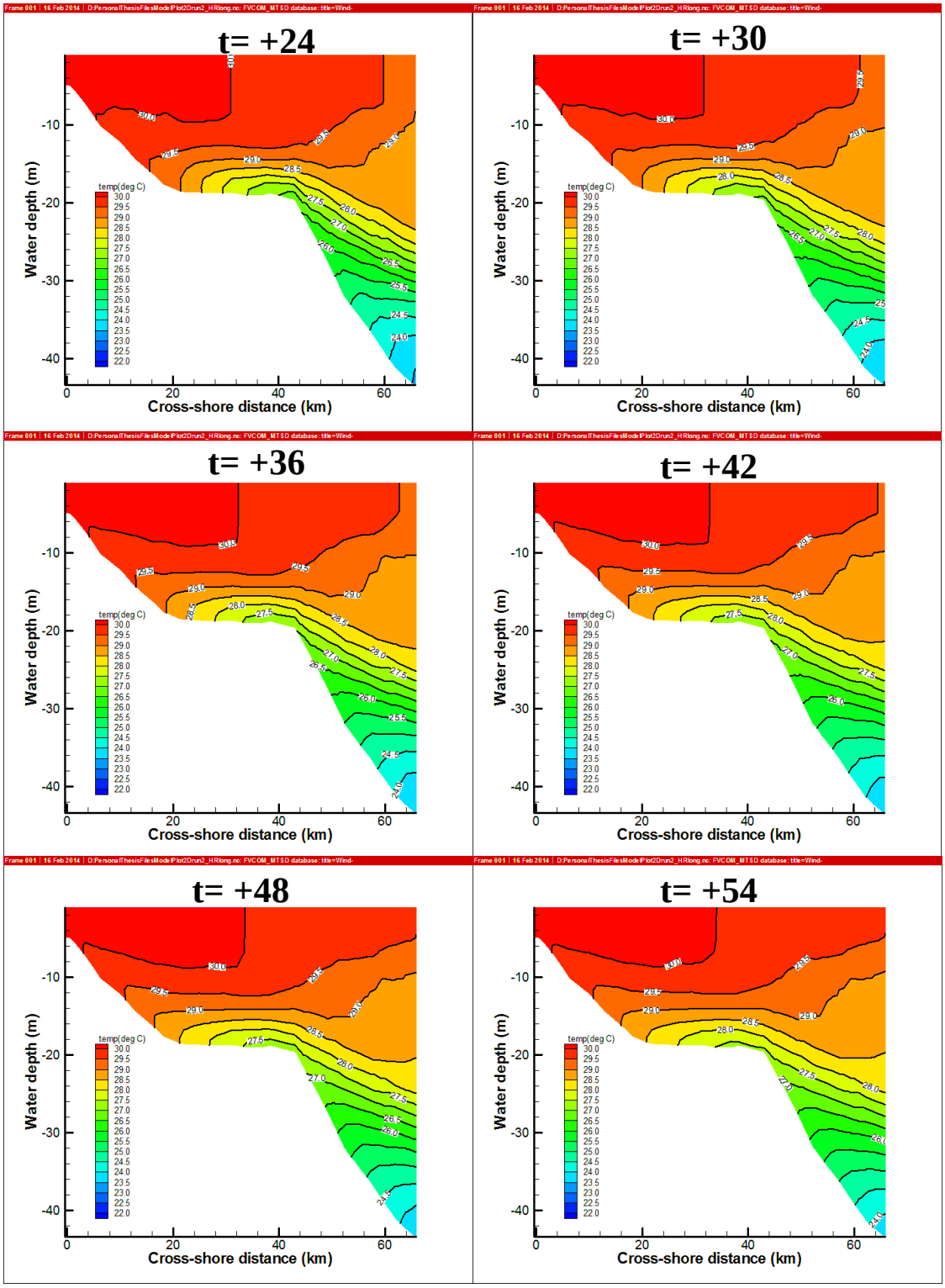

Cross Section D

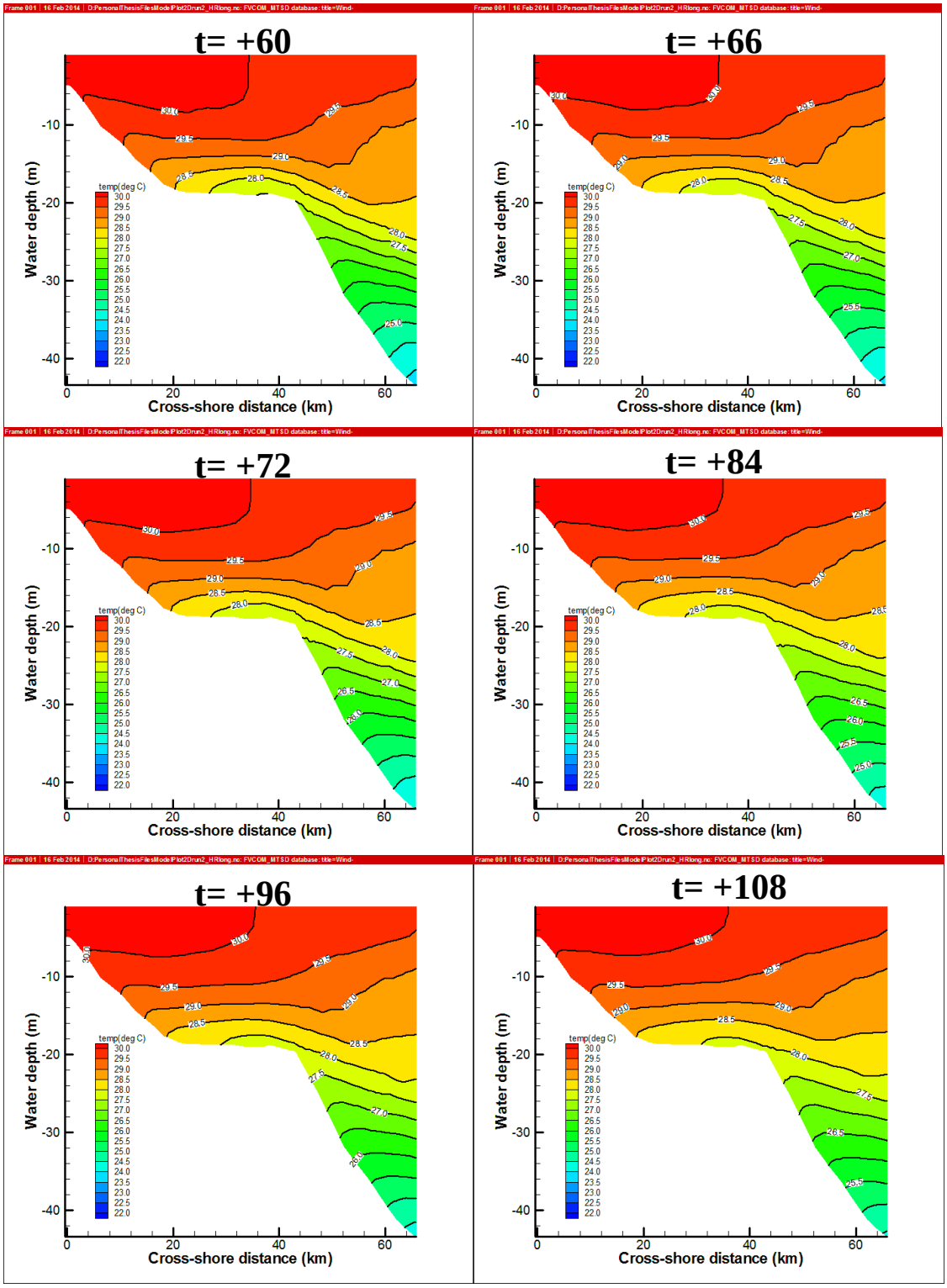

Cross Section D

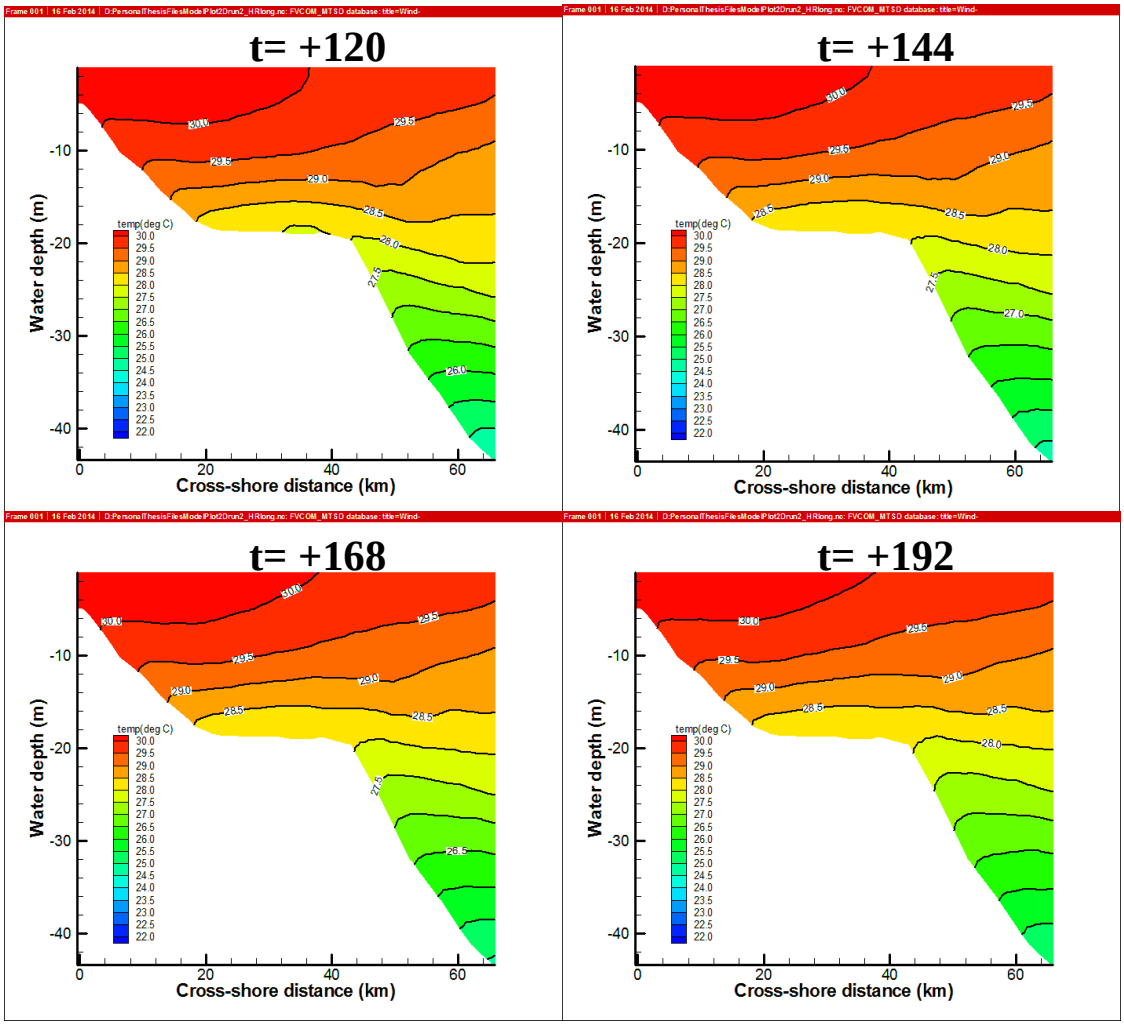

Cross Section F

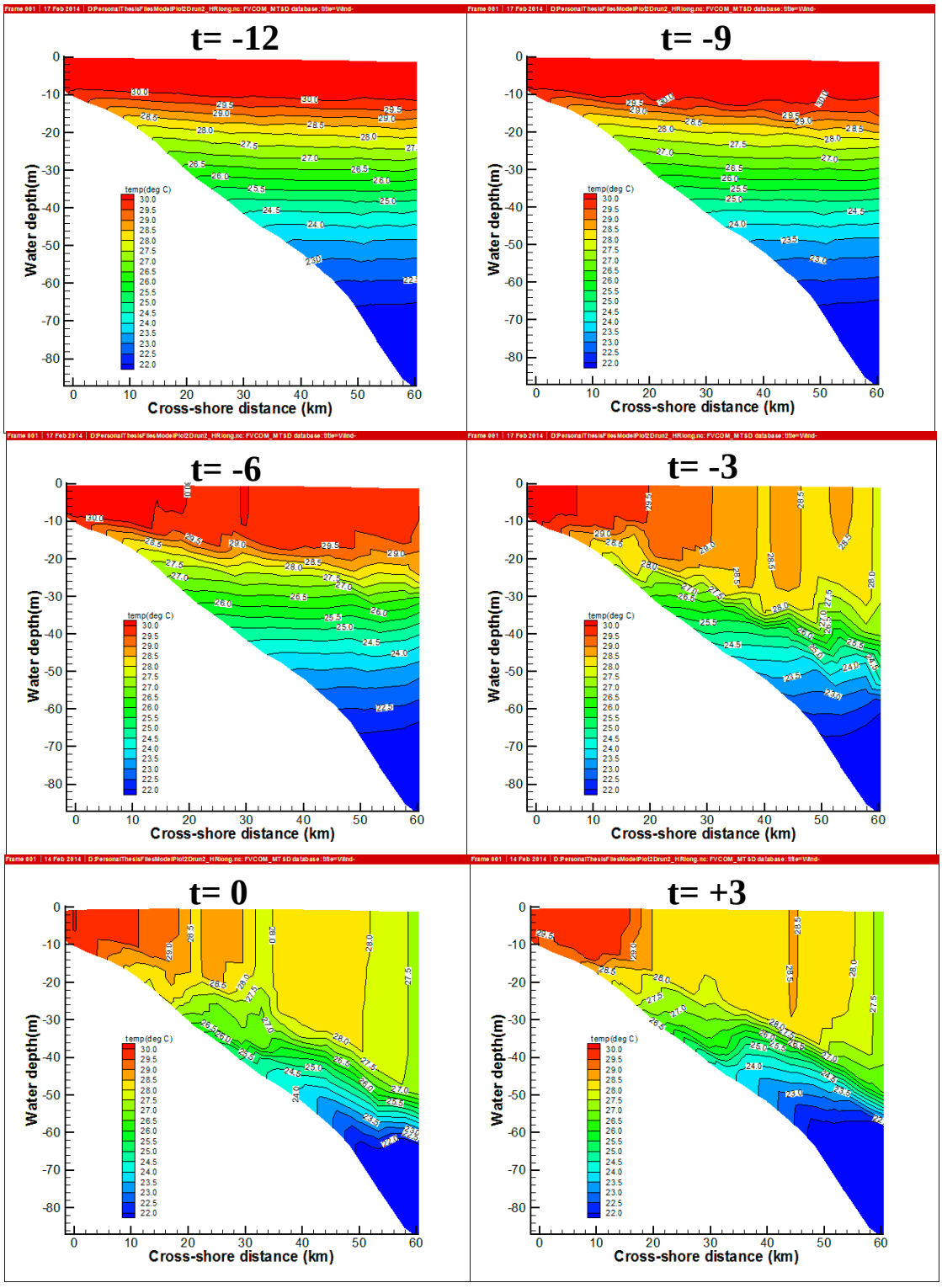

Cross Section F

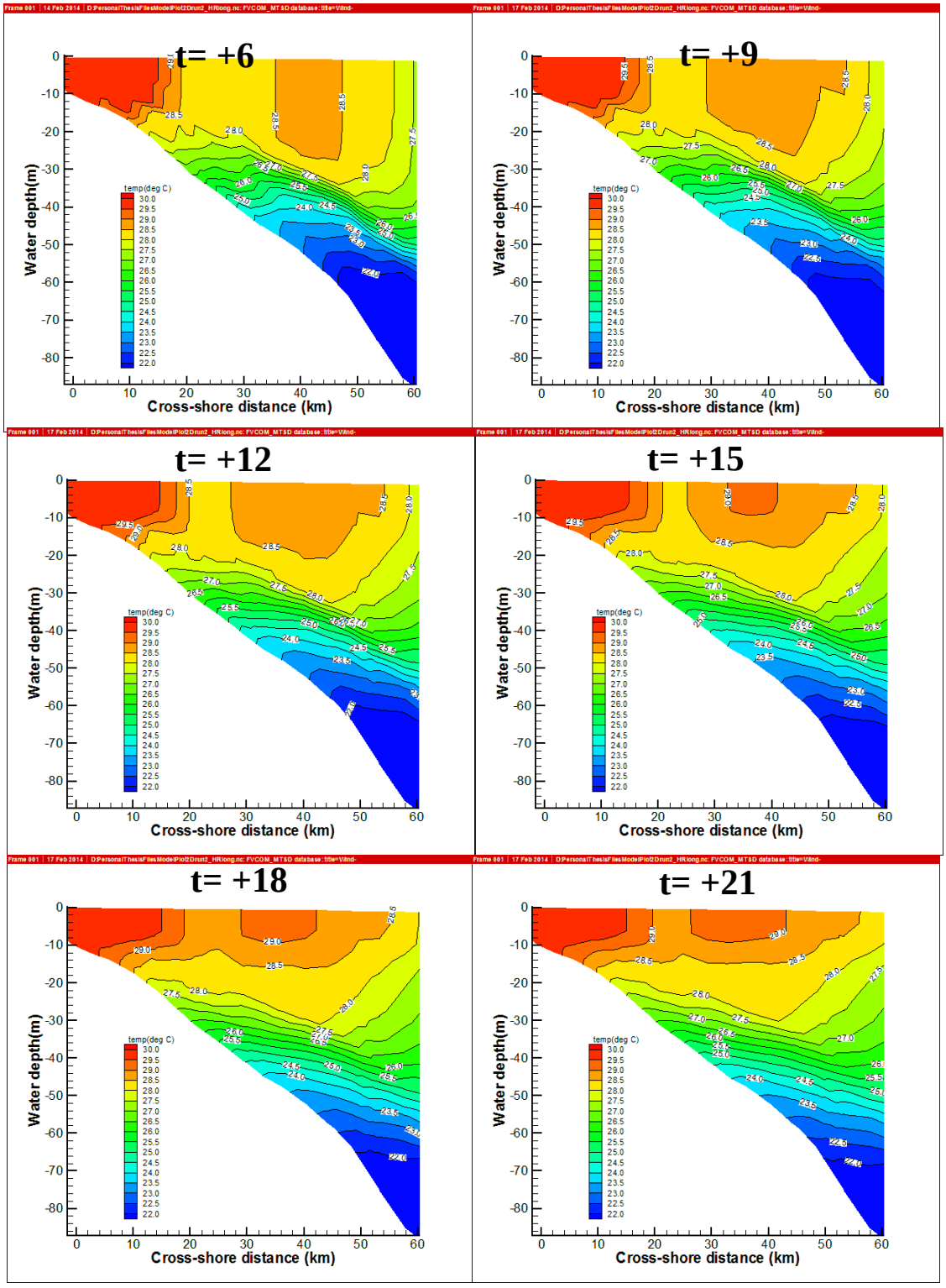

Cross Section F

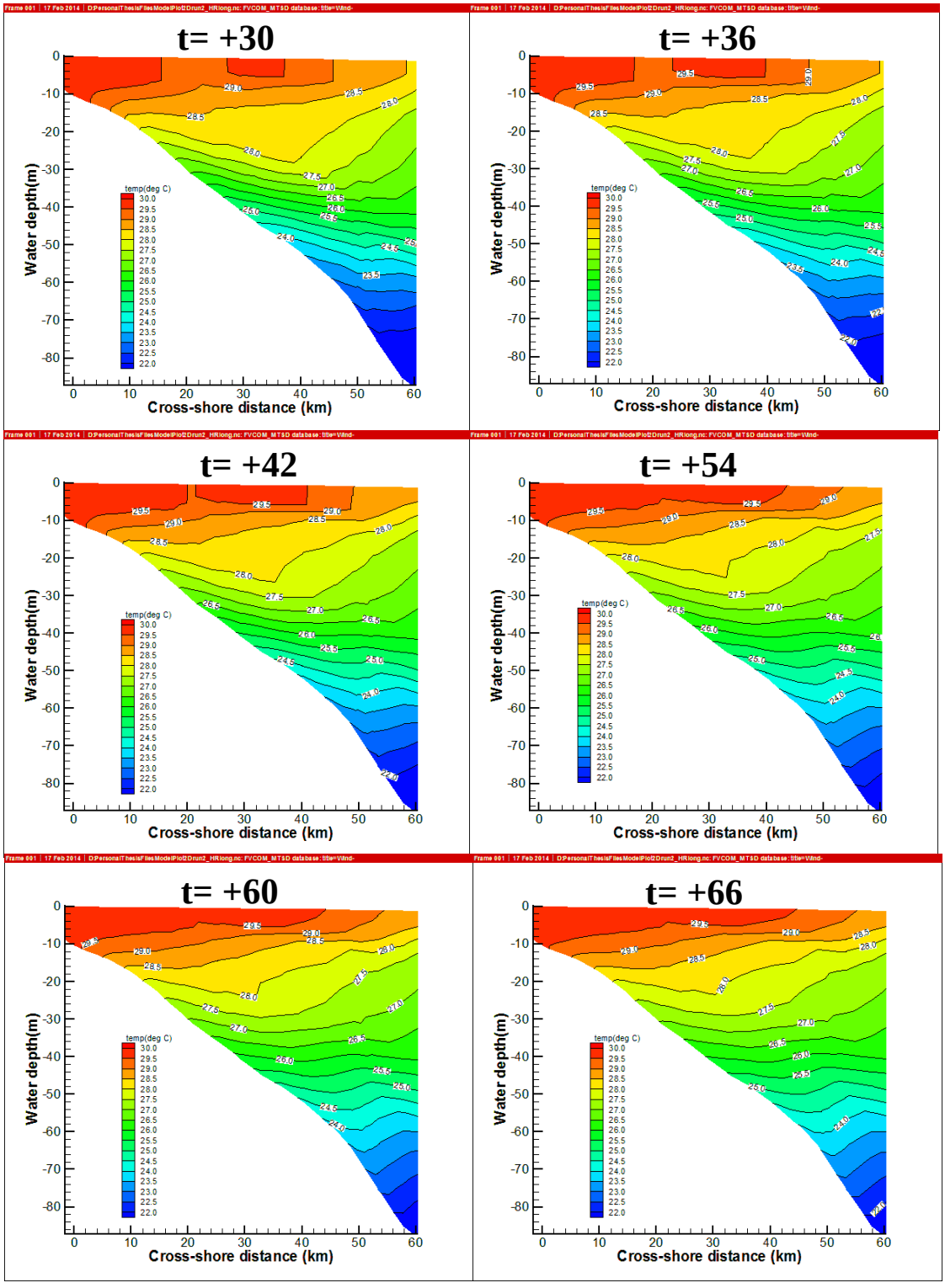

Cross Section F

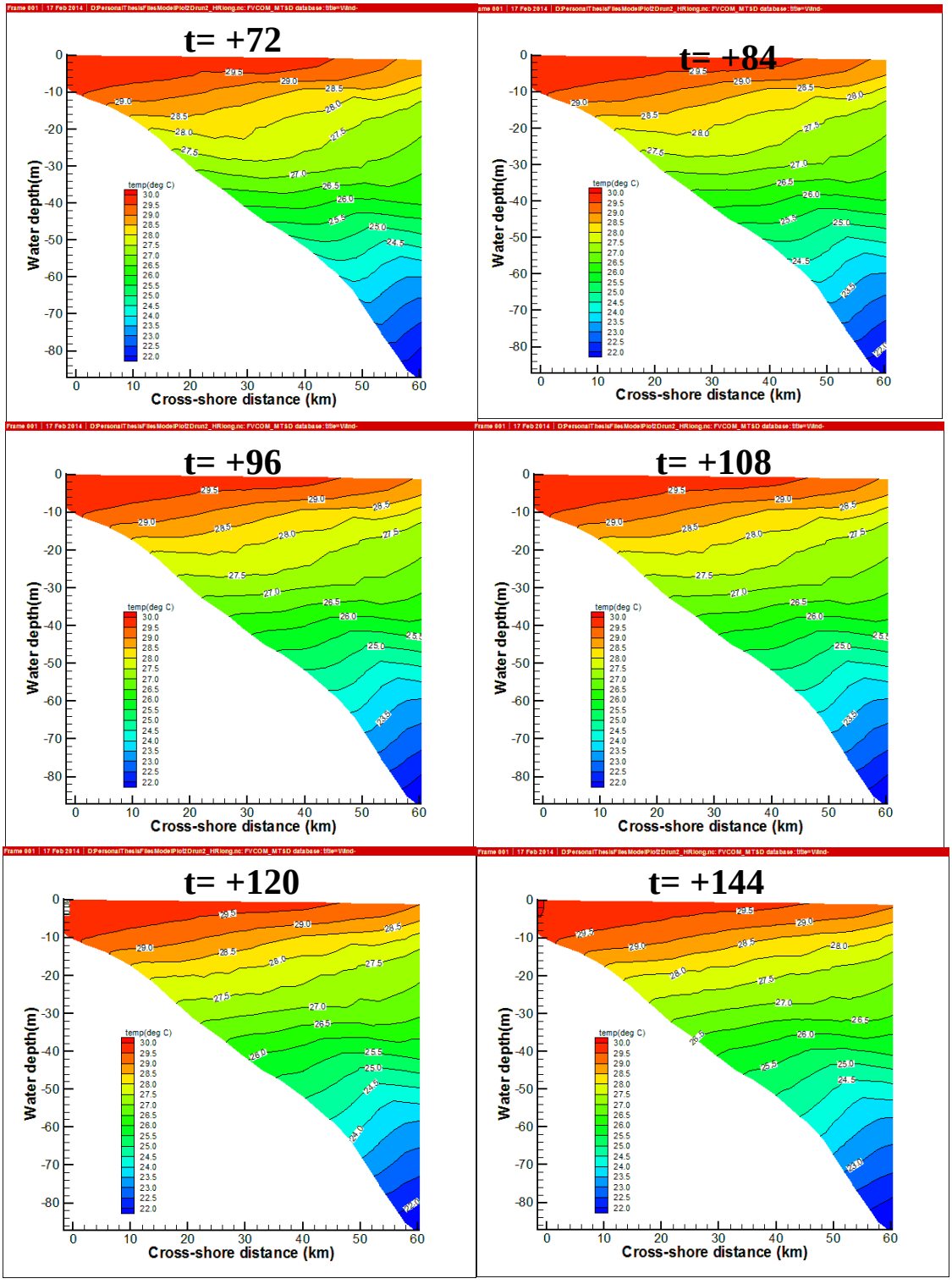

Cross Section F

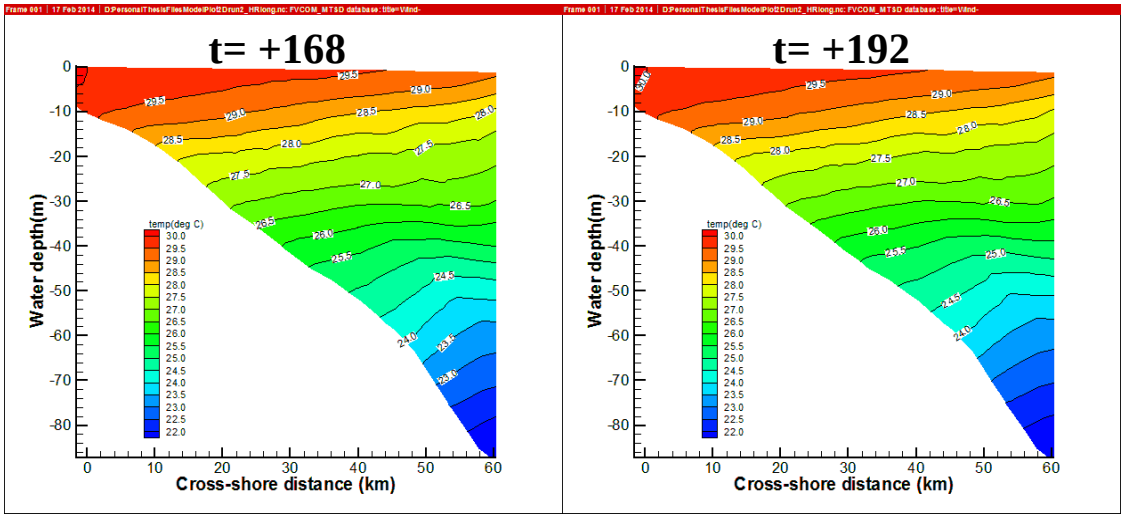

Cross Section G

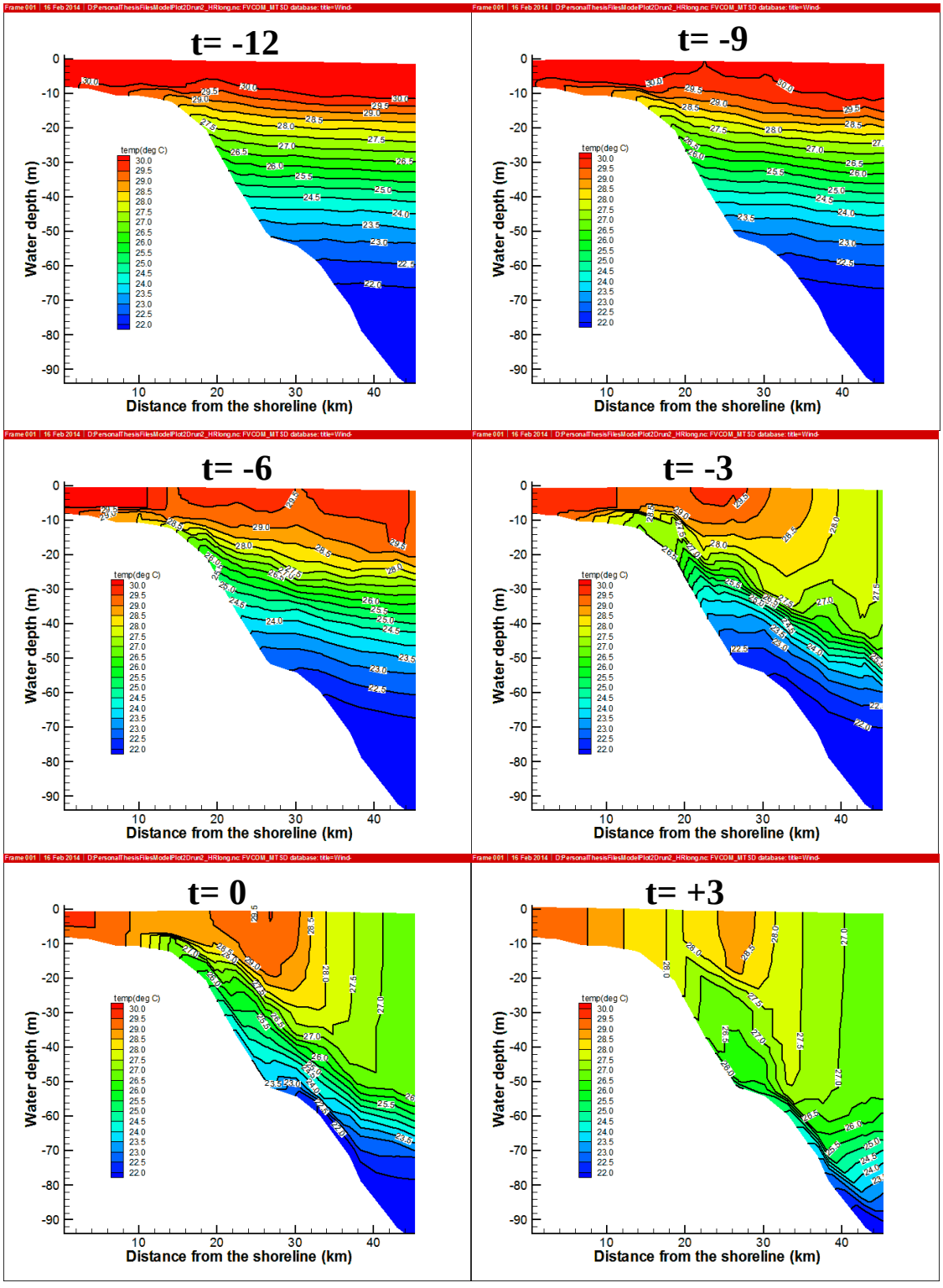

Cross Section G

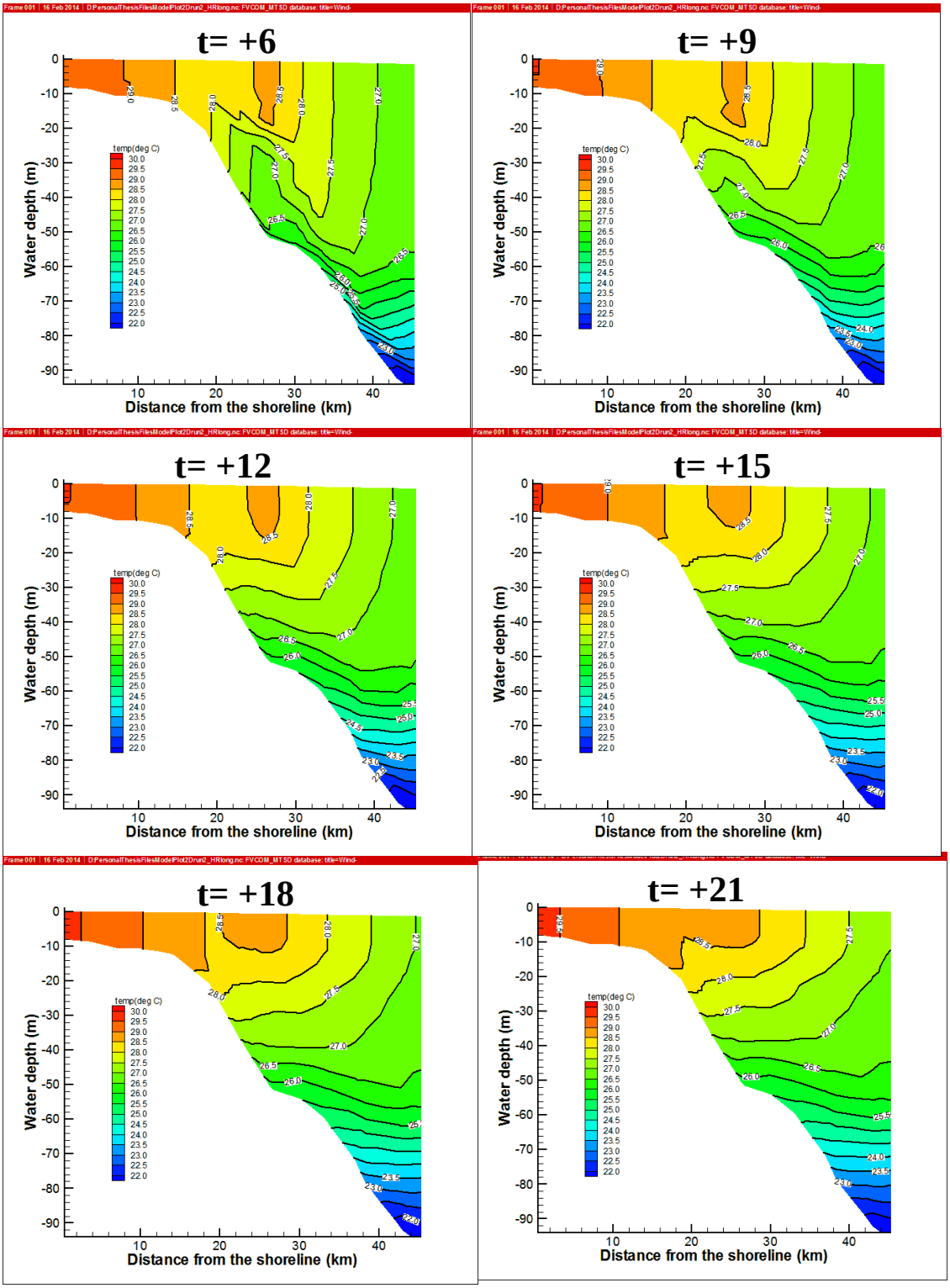

Cross Section G

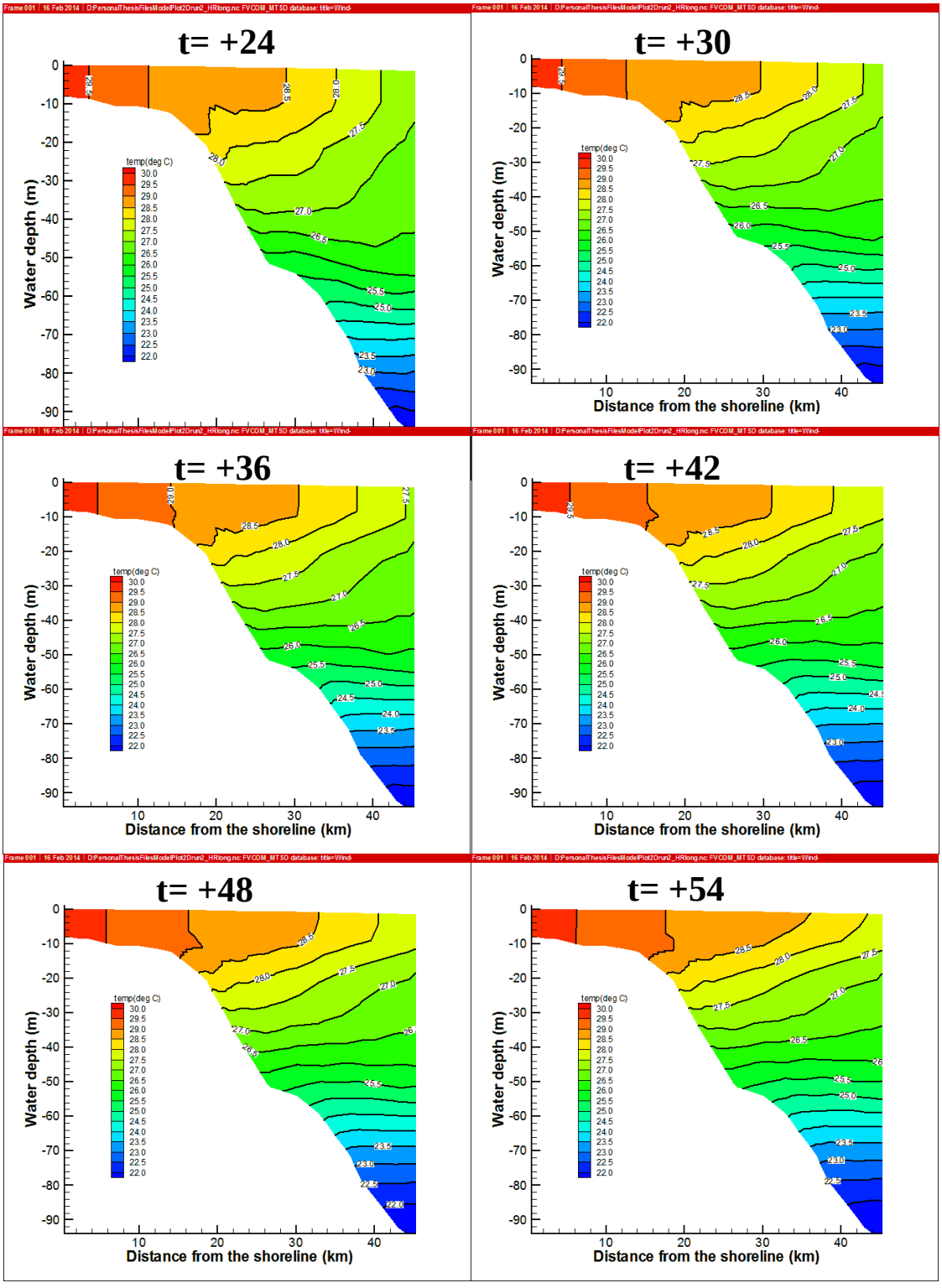

Cross Section G

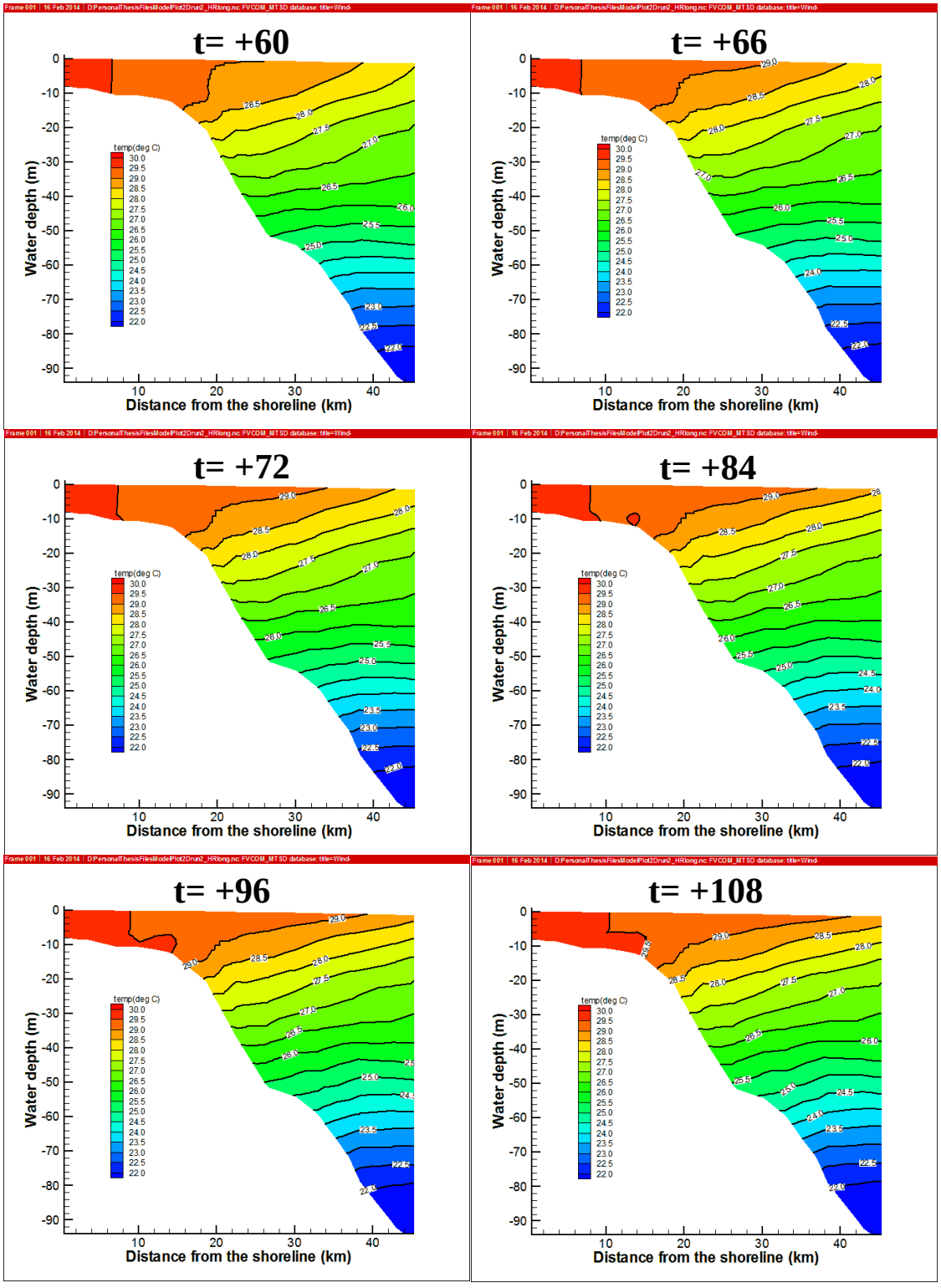

Cross Section G

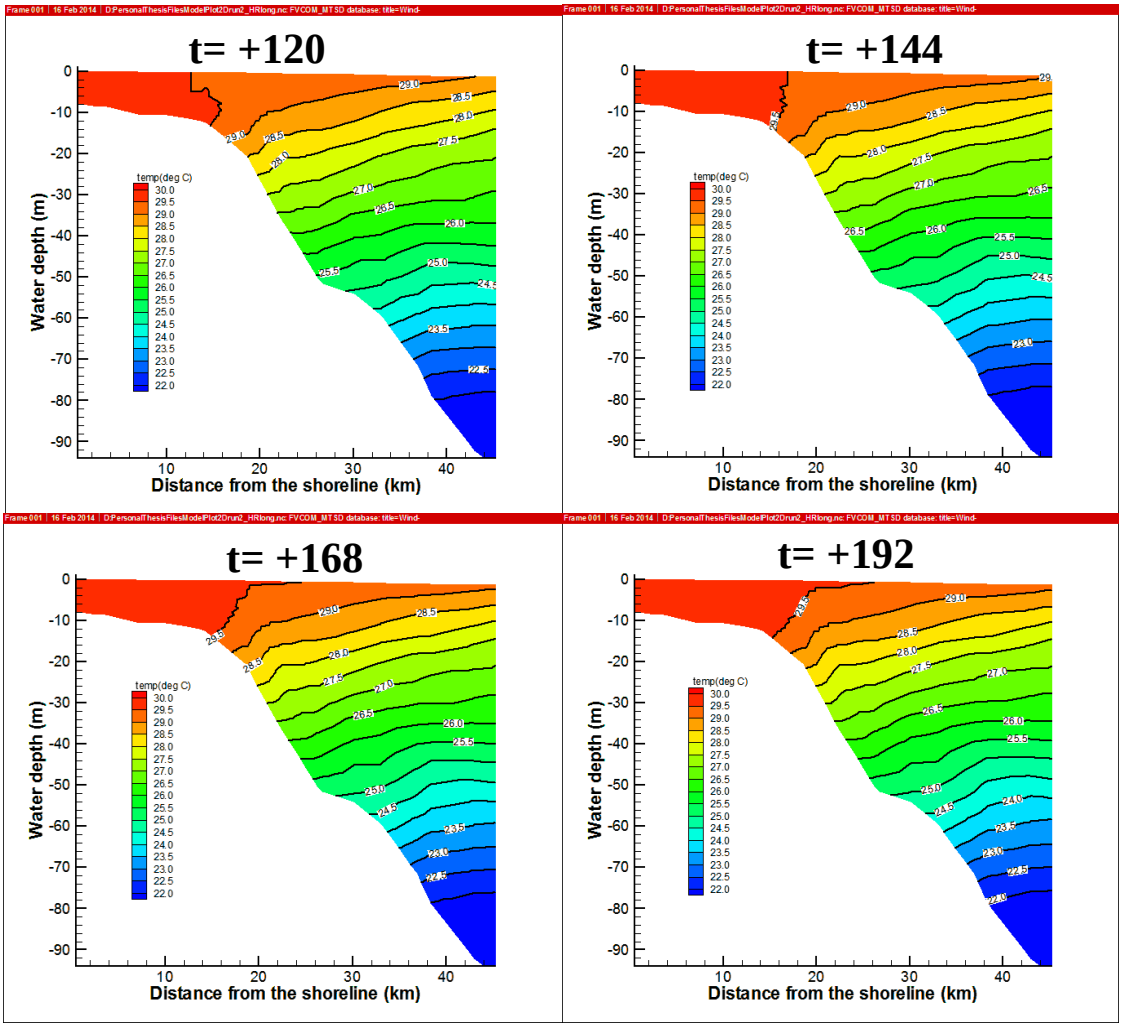

APPENDIX C: SOME MODELING RESULTS FOR FALL STORMS

The effect of fall storms on water column stratification over the Louisiana shelf was simulated for October2009 using the wind data obtained from CSI-6 applied as a uniform wind over the shelf. The model was initialized using the climatological temperature/salinity profiles prepared by NOAA for September 2009.

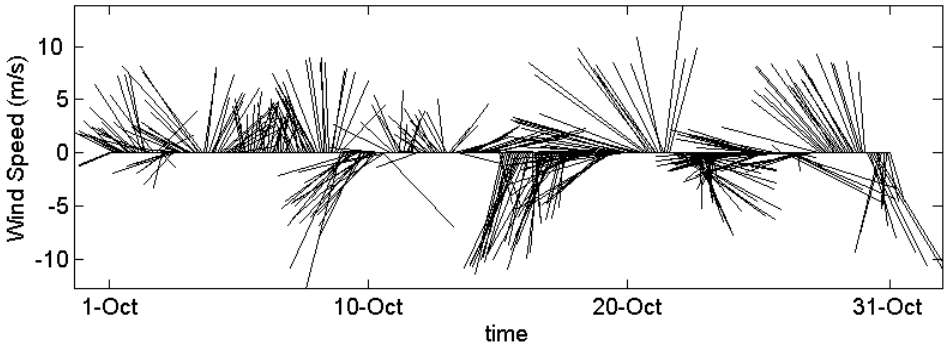

Figure C.1: Timeseries of wind vector measures at CSI-6 during September 2009.

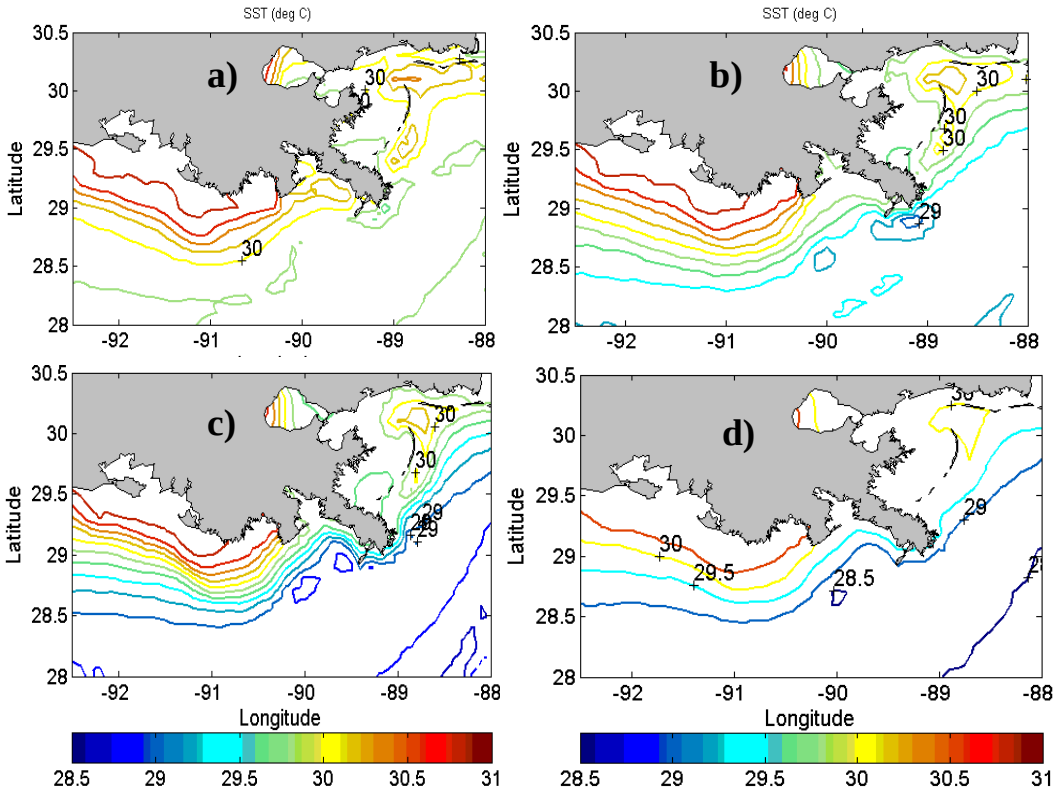

Figure C.2: Simulated SST over the Louisiana shelf on a) October 10, b) October 17, c) October 22, a) October 27.

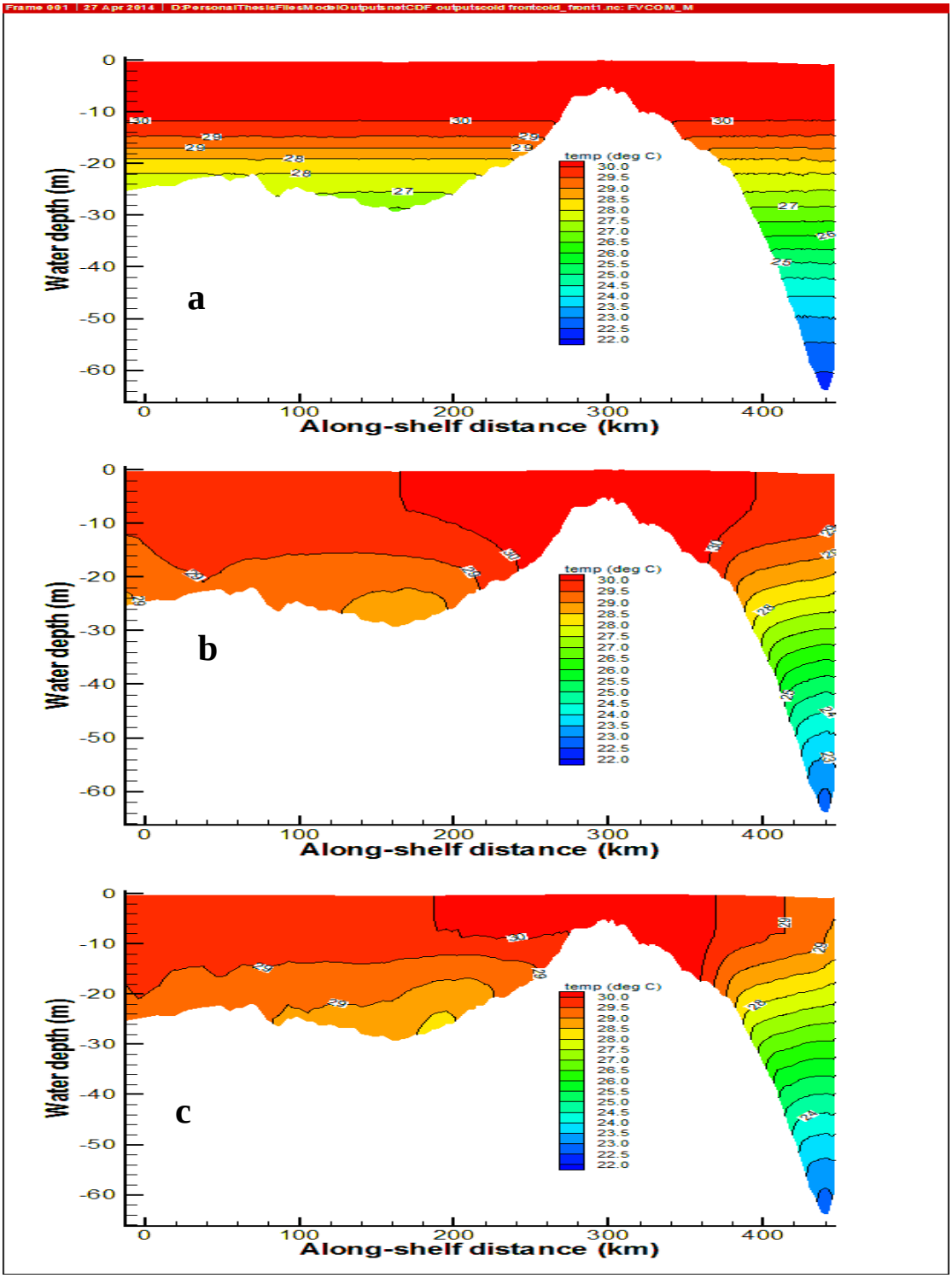

Figure C.3a: Distribution of simulated temperature across section 3 (see Figure 4.26 for location) on a) October 1, b) October 10, c) October 17.

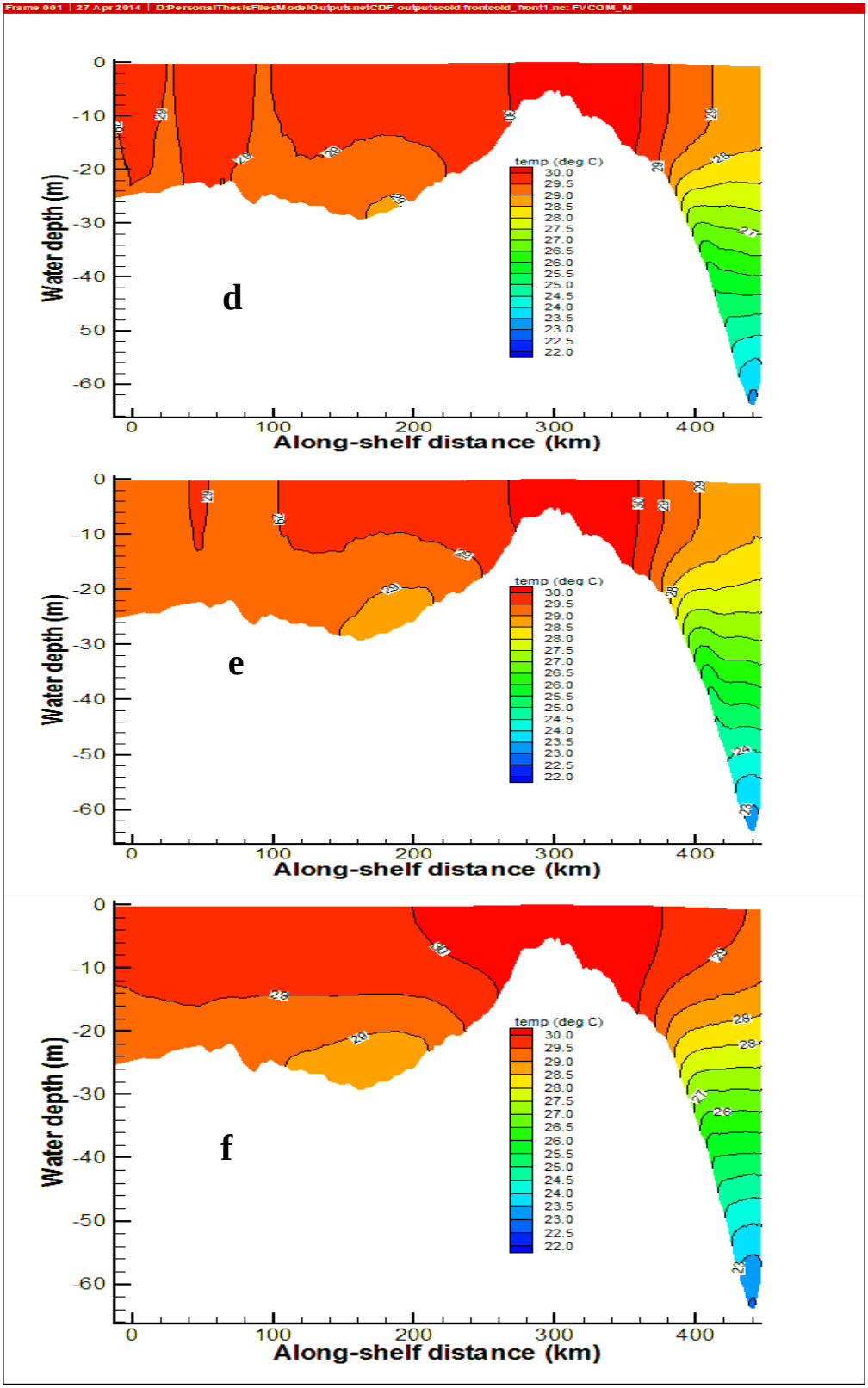

Figure C.3b: Distribution of simulated temperature across section 3 (see Figure 4.26 for location) on a) October 1, b) October 10, c) October 17.

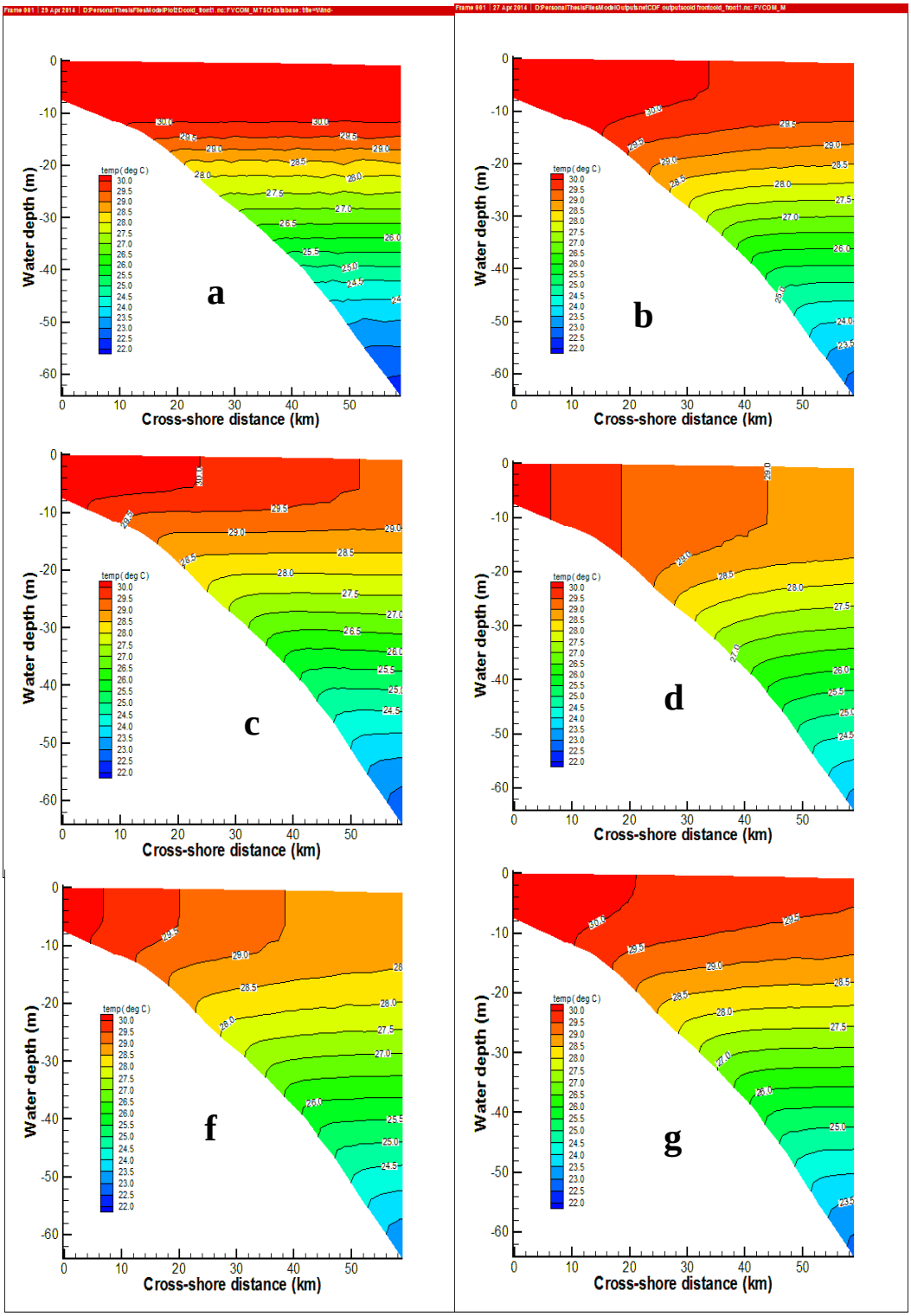

Figure C.4: Distribution of simulated temperature across transect B (see Figure 4.26 for location)a) October 1, b) October 10, c) October 17 , d) October 22, e) October 27 , f) 1-month average.

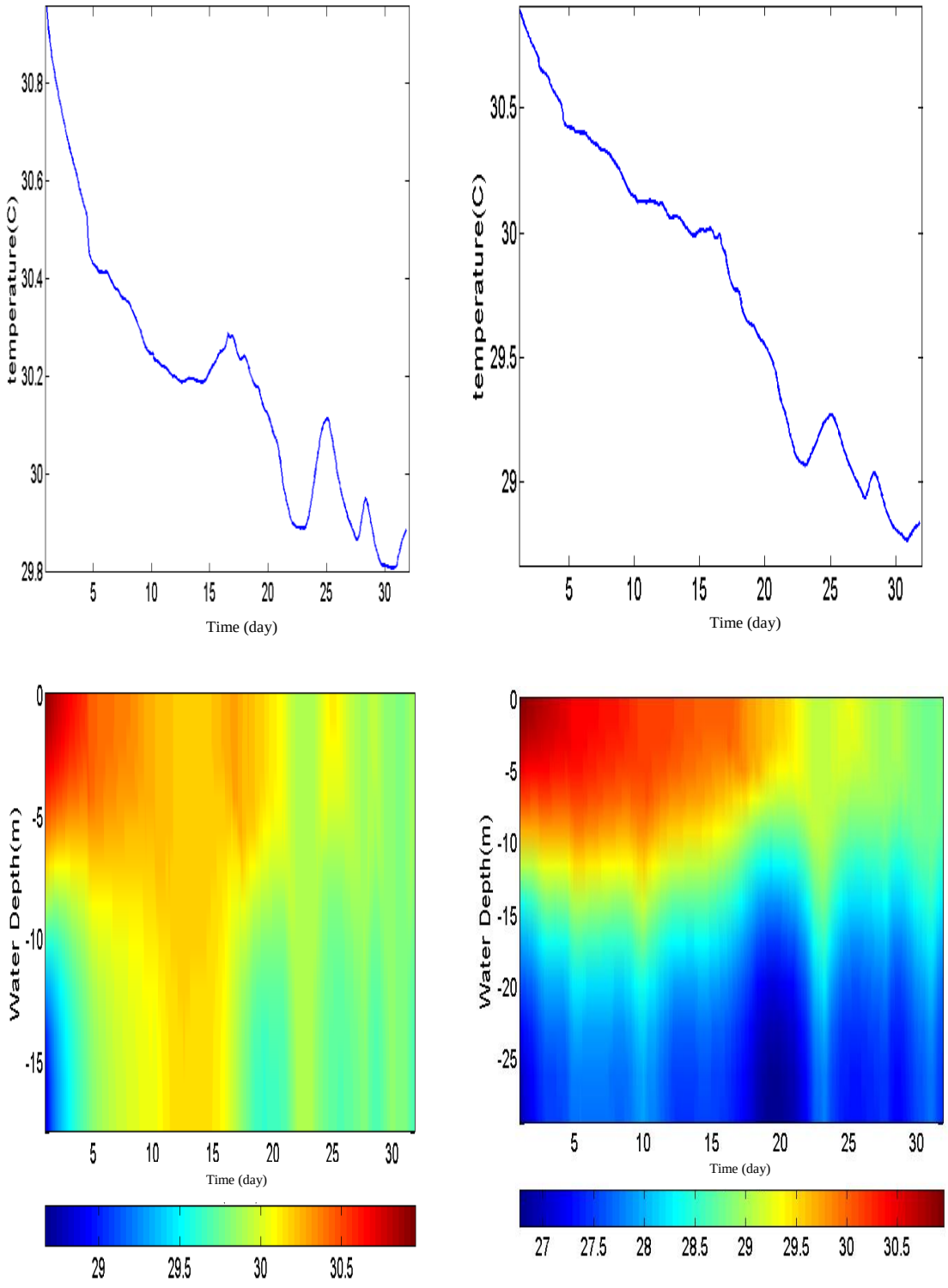

Figure C.5: Variations of SST and water temperature across the water column during 1 month of simulation during October 2009 for: left panels) station P2 and right panel) station P4. Location of stations is based on Figure 4.16.

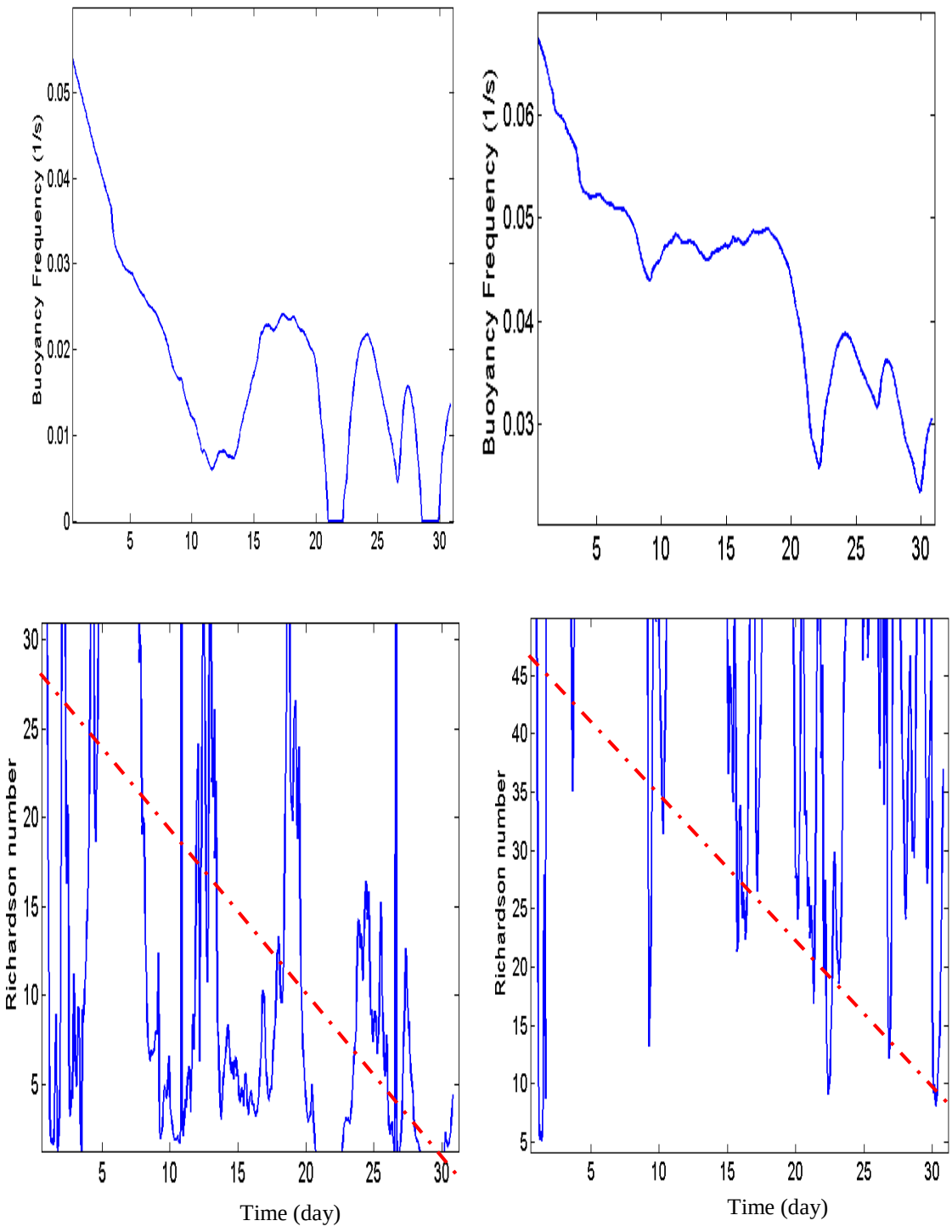

Figure C.6: Variations of Buoyancy frequency and the Richardson number across the water column during 1 month of simulation during October 2009 for: left panels) station P2 and right panel) station P4. The red dash line shows the l trend of the Richardson number variations during simulation.

APPENDIX D: FORMULATION OF DIFFERENT SURFACE HEAT COMPONENTS

(All parameters are described in Table D.1)

Shortwave Radiation: Relationships presented by Guttman and Matthews (1979), Ivanoff (1977) and Cotton (1979) was used to calculate shortwave radiation flux:

$$Q_{\circ}= \frac{Scos^2 Z}{(\cos Z+2.7)e\times10^{-5}+1.085\cos Z+0.10} \quad (D.1)$$

The cosine of the zenith angle is computed using the formula:

$$\cos Z = \sin\phi \sin\delta + \cos\phi \cos\delta \cos HA \quad (D.2)$$

The declination is $\delta = 23.44^{\circ} \times \cos\left[(172 - day\ of\ year) \times 2\pi/365\right]$, and the hour angle is $HA = (12\ hours - solar\ time) \times \pi/12$. The correction for cloudiness is given by

$$SW\downarrow = Q_{\circ}(1 - 0.6c^3) \quad (D.3)$$

The cloud correction is optional since some sources of radiation contain it already.

Longwave Radiation: The clear sky formula for incoming longwave radiation is given by Wyrtki (1965):

$$F\downarrow = \sigma T_a^4\{1 - 0.261 \exp\ [-7.77 \times 10^{-4}(273 - T_a)^2]\} \quad (D.4)$$

While the cloud correction is given by:

$$LW\downarrow = (1 + 0.275c)\ F\downarrow \quad (D.5)$$

Sensible heat: The sensible heat is given by the standard aerodynamic formula (Imberger and Patterson, 1981):

$$H\downarrow = \rho_a c_p C_H V_{wg}\left(T_{a-}T_{sfc}\right) \quad (D.6)$$

Latent Heat: The latent heat depends on the vapor pressure and the saturation vapor pressure given by Imberger and Patterson (1981):

$$e = 611 \times 10^{a(T_d - 273.16)/(T_d - b)} \quad (D.7)$$

$$e_s = 611 \times 10^{a(T_{\varepsilon fc} - 273.16)/(T_{\varepsilon fc} - b)} \quad (D.8)$$

The vapor pressures are used to compute specific humidity according to:

$$q_{10m} = \frac{\epsilon e}{p-(1-\epsilon)e} \quad (D.9)$$

$$q_s = \frac{\epsilon e_s}{p-(1-\epsilon)e_s} \quad (D.10)$$

The latent heat is also given 0.622 by a standard aerodynamic formula:

$$LE\downarrow = \rho_a L C_E V_{wg}(q_{10m} - q_s) \quad (D.11)$$

Table D.1: Parameters used for formulation of surface heat components.

Variable	Value	Description
$(\boldsymbol{a}, \boldsymbol{b})$	(9.5, 7.66)	vapor pressure constants over ice
$(\boldsymbol{a}, \boldsymbol{b})$	(7.5, 35.86)	vapor pressure constants over water
C		cloud cover fraction
C_E	1.75×10^{-3}	transfer coefficient for latent heat
C_H	1.75×10^{-3}	transfer coefficient for sensible heat
c_p	1004 J kg^{-1} K^{-1}	specific heat of dry air
Δ		declination
E		vapor pressure in pascals
e_s		saturation vapor pressure
E	0.622	ratio of molecular weight of water to dry air
HA		hour angle
L	2.5×10^{6} Jkg^{-1}	latent heat of vaporization
L	2.834×10^{6} J kg^{-1}	latent heat of sublimation
Φ		latitude
$Q_\circ$		incoming radiation for cloudless skies
q_s		surface specific humidity
q_{10m}		10 meter specific humidity
ρ_a		air density
S	1353 W m^{-2}	solar constant
Σ	5.67×10^{-8} W m^{-2} K^{-4}	Stefan-Boltzmann constant
T_a		air temperature
T_d		dew point temperature
T_{sfc}		surface temperature of the water/ice/snow
V_{wg}		geostrophic wind speed
Z		solar zenith angle

APPENDIX E: COVER PAGE OF JOURNAL OF COASTAL RESEARCH PAPER

Journal of Coastal Research	00	0	000–000	West Palm Beach, Florida	Month 0000

Seasonal Hydrodynamics along the Louisiana Coast: Implications for Hypoxia Spreading

Mohammad Nabi Allahdadi, Felix Jose*, and Cecily Patin

Coastal Studies Institute
Department of Oceanography and Coastal Science
Howe–Russell Geoscience Complex
Louisiana State University
Baton Rouge, LA 70803, U.S.A.
mallah1@lsu.edu

www.cerf-jcr.org

www.JCRonline.org

ABSTRACT

Allahdadi, M.N.; Jose, F., and Patin, C., 0000. Seasonal hydrodynamics along the Louisiana coast: implications for hypoxia spreading. *Journal of Coastal Research,* 00(0), 000–000. West Palm Beach (Florida), ISSN 0749-0208.

Summer and fall inner-shelf flow characteristics, including the vertical current structure, obtained from three WAVCIS (WAVE-Current-surge Information System) stations off the Louisiana coast were analyzed to delineate the hydrodynamic conditions that contribute to the formation of seasonal hypoxia at each station location. Two of the WAVCIS data stations used for analysis are located west of the Mississippi bird-foot delta, whereas the third is located east of the delta. Relatively small vertical gradients in the horizontal velocity current (*i.e.*, u and v velocity components) were observed during summer (2009) for both CSI-6 and CSI-9 stations, which are located well inside the hypoxia-prone zone west of the delta. In contrast, the summertime vertical gradient of horizontal current at CSI-16 (located east of the delta) was significantly higher than that of western stations. Significant differences in the vertical gradient of flow velocities along with contrast in water column density gradient during the summer culminated in a strong stratification, which is considered the main physical requirement for the formation of hypoxia. A computed criteria based on the Richardson number also pointed to higher potential for stratification at both stations west of the delta, whereas the water column east of the delta still remained subject to vertical mixing. Furthermore, summertime current fields at CSI-6 and CSI-9 were significantly less compared with CSI-16, suggesting less reoxygenation driven by advection from surrounding waters. These conditions may exacerbate hypoxia.

ADDITIONAL INDEX WORDS: *Louisiana shelf, shelf currents, stratification, advection flux, depth gradient, reoxygenation.*

INTRODUCTION

The northern Gulf of Mexico is exposed to the second largest seasonal hypoxic zone (less than 2 ppm dissolved oxygen) in the world (Rabalais, Turner, and Wiseman, 2002). A host of factors contribute to the formation of hypoxia in this region, including seasonal discharge of enormous volumes of fresh water from the Mississippi and Atchafalaya rivers and excessive nutrient loading of the shelf, particularly nitrogen and phosphorous, sourced from upstream runoff of fertilizers, urban sewage, erosion, and deforestation (Rabalais, Turner, and Wiseman, 2002). The situation is further exacerbated by the seasonal reversal of wind and, thereby, the coastal current (Cochrane and Kelly, 1986). The microtidal Louisiana coast, having a maximum tidal range of ~40 cm (Wright, Sherwood, and Sternberg, 1997) when exposed to stagnant wind and wave forcing during summer, becomes an isolated waterbody with limited mixing and exchange with the surroundings (Wiseman *et al.*, 1997). The factors contributing to the seasonal formation of hypoxia can be divided into physical and biochemical components (Justic *et al.*, 1993; Rabalais, Turner, and Scavia, 2002; Rabalais, Turner, and Wiseman, 2002; Wiseman *et al.*, 1997, 2004). Wiseman *et al.* (1997) noticed that Mississippi River flooding in early spring coincides with a perceptible decline in atmospheric activity, causing water column stratification. Increased solar heating and sunshine, together with the high nutrient loading from the Mississippi River, provide favorable conditions for phytoplankton bloom during early spring. This seasonally fixed organic carbon sinks in a short period of time, eventually leading to the depletion of bottom-water oxygen during summer months as it is oxidized (Wiseman *et al.*, 1997). In fact, biochemical factors cause eutrophication, and physical factors cause water column stratification, and the interaction between these two results in hypoxia (Belabbassi, 2006).

For some upwelling systems, the strength of physical forces (mostly wind) causes severe hypoxic events. For instance, along the New Jersey shelf, persistent summertime upwelling due to southwesterly winds produces hypoxia, as upwelling delivers

DOI: 10.2112/JCOASTRES-D-11-00122.1 received 10 July 2011; accepted in revision February 11, 2012.

* Present address: Department of Marine and Ecological Sciences, Florida Gulf Coast University, Fort Myers, FL 33965-6565, U.S.A.

Published Pre-print online 16 July 2012.

APPENDIX F: LETTER OF PERMISSION; JOURNAL OF COASTAL RESEARCH

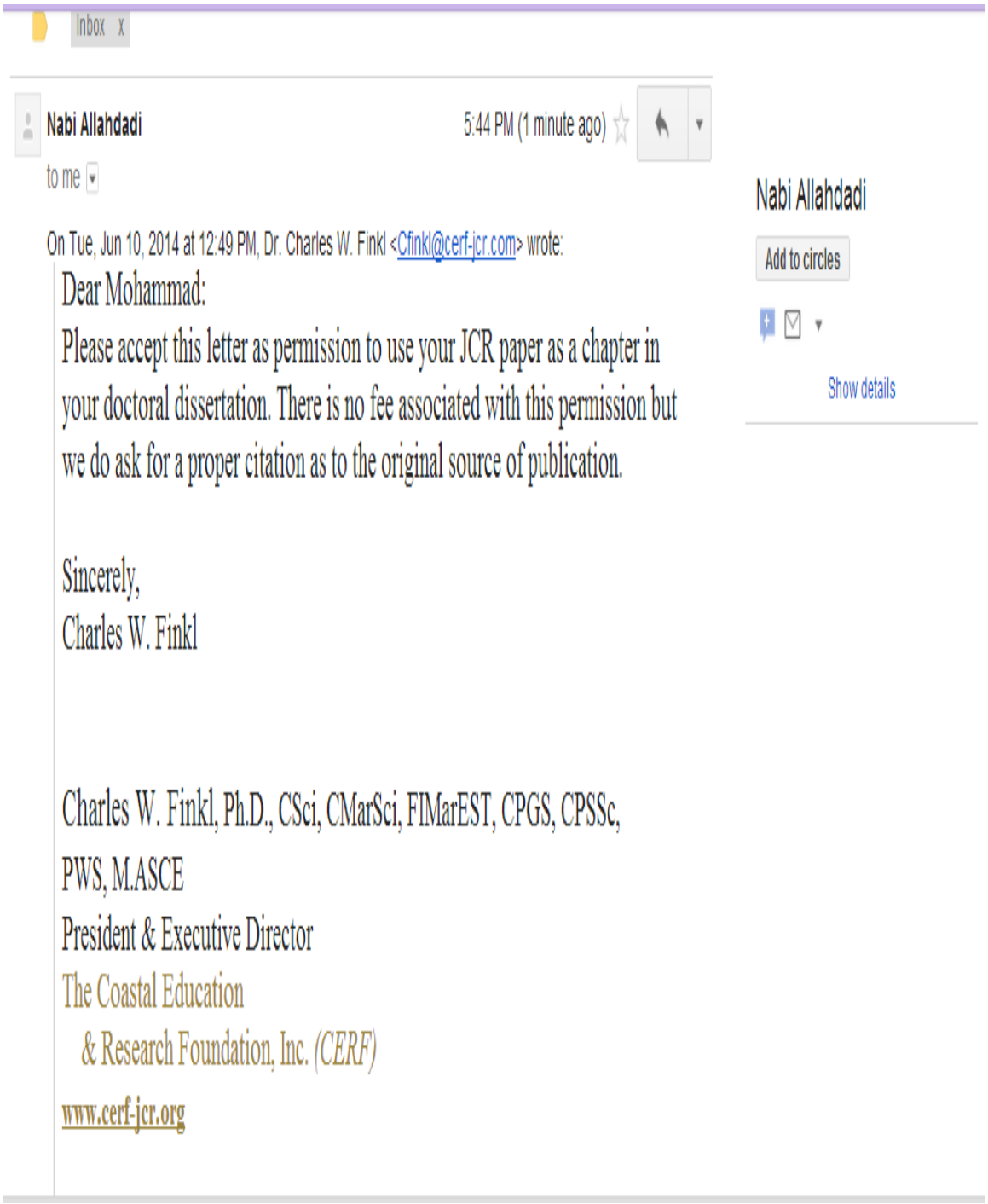

Inbox x

Nabi Allahdadi 5:44 PM (1 minute ago)

to me

On Tue, Jun 10, 2014 at 12:49 PM, Dr. Charles W. Finkl <Cfinkl@cerf-jcr.com> wrote:

Dear Mohammad:

Please accept this letter as permission to use your JCR paper as a chapter in your doctoral dissertation. There is no fee associated with this permission but we do ask for a proper citation as to the original source of publication.

Sincerely,
Charles W. Finkl

Charles W. Finkl, Ph.D., CSci, CMarSci, FIMarEST, CPGS, CPSSc, PWS, M.ASCE
President & Executive Director
The Coastal Education & Research Foundation, Inc. *(CERF)*
www.cerf-jcr.org

Nabi Allahdadi

Add to circles

Show details

VITA

Mohammadnabi Allahdai was born in Zahedan, Iran. He entered the *University of Shiraz* in September 1994 and received his Bachelor degree in Civil Engineering in August 1998. In September 1998, Nabi started his masters in Hydraulic Structures in Civil and Environmental Engineering Department at *University of Tehran*, and completed the program in February 2001. During his masters he worked under the supervision of Dr. Peyman Badiee on evaluation of wave prediction models in the Persian Gulf using numerical model Mike21-OSW. After completing his master studies, Nabi started working as a water resource/coastal engineering researcher and was involved in several national projects with numerical simulations of riverine and coastal applications. In May 2009 he joined *Louisiana State University*, Department of Oceanography as a Ph.D student under the supervision of the late Dr. Gregory Stone, when he started working on numerical simulations of hydrodynamics and sediment transport over the Louisiana shelf for about two years. After, Dr. Stone passed away in February 2011, Nabi started a new research supported by Dr. Chunyan Li, aiming at the effect of hurricanes on shelf mixing using a numerical model. Since that time he has been working on numerical simulations of hydrodynamics and ocean temperature evolution over the Louisiana shelf using FVCOM.

.